Activation of NRF2 Pathways in Glaucoma

By

Sarah Aymen Naguib

Dissertation

Submitted to the Faculty of the

Graduate School of Vanderbilt University

In partial fulfillment of the requirements

For the degree of

DOCTOR OF PHILOSOPHY

In

Neuroscience

May 13, 2022

Approved:

Tonia S. Rex, PhD (mentor)

David J. Calkins, PhD (committee chair)

Fiona E. Harrison, PhD

Sabine Fuhrmann, PhD

To my grandpa: Thank you for fostering in me a desire to learn since a young age and for instilling in me a love for science. Thank you for being the first PhD I looked up to.

To my Dad: Thank you for being the best role model I could have ever asked for. Thank you or the endless sacrifices you made throughout your life to provide Hannah, Mark and I with an amazing education in the U.S. Thank you for always being someone I could look up to. I am so proud to be your daughter.

To my Mom: Thank you for always believing in me, being there for me and pushing me to never give up. Thank you for all the time and energy you poured into supporting me throughout the last few years. I couldn't have made it without your listening ears.

To my husband, Dylan: I wouldn't be here without you. Thank you for accompanying me on this journey to becoming Dr. Naguib in more ways than I can even put into words. Thank you for believing in me, thank you for listening to me, thank you for loving me so well. You are the best partner I could have ever imagined. I love you.

ACKNOWLEDGEMENTS

This work was supported by DoD W81XWH-15-1-0096 (TR), DoD W81XWH-17-2-0055 (TR), NEI R01 EY022349 (TR, DC), NEI R01 EY017427 (DC), NEI U24 EY029893 (TR), NEI U24 EY029903 (DC), Potocsnak Discovery Grant in Regenerative Medicine, Ayers Foundation Regenerative Visual Neuroscience Pilot Grant, Ret. Maj. General Stephen L. Jones, MD Fund, Stein Innovation Award (DC), Stanley Cohen Innovation Fund (DC), NEI P30EY008126 (VVRC), T32 EY021833 (VVRC) and Research Prevent Blindness, Inc Unrestricted Funds (VEI). The funding sources had no involvement in the study design, or collection, analysis, or interpretation of the data. The authors confirm that there are no known conflicts of interest associated with this publication and there has been no significant financial support for this work that could have influenced its outcome.

First, I'd like to thank my incredible PhD advisor, Dr. Tonia Rex. Dr. Rex, thank you for always being there for me as a support system and someone I could talk science with. Your open door meant a lot in the highest of highs and the lowest of lows in graduate school. Thank you for always looking out for opportunities for me to grow and learn as a scientist—through collaborations, learning new techniques, meeting new people, etc. Thank you for pushing me by asking the tough questions, helping me prepare for anything from my qualifying exam to my job talks and for believing me that I could handle a lot more than I thought I could. Thank you for allowing me to pursue my interests within my projects to explore questions that we hadn't initially sought out to answer. You are a role model and someone who I aspire to be as a PI one day. Thank you for everything.

Thank you also to my amazing committee members. Dr. Calkins, thank you for checking in on me and having difficult conversations with me. Thank you for pushing me to succeed and believing in me. Thank you for all your advice along the way these last few years. Dr. Harrison, thank you for being always asking questions in VBI Forum and our committee meetings and thank you for continuing to be a mentor/collaborator since I rotated in your lab. Dr. Fuhrmann, thank you for helping me to think outside of the box when it came to my project and for asking insightful questions in my committee meetings.

There are so many people who I worked with in the Vanderbilt Eye Institute—without each and every one of you, I wouldn't be here. First, Jon Backstrom. Jon, thank you for answering all my questions about molecular biology when I came into the lab and knew absolutely nothing. Thank you for your patience with me. Thank you for asking tough questions and providing really helpful input on my projects. And, of course, thank you for generating the plasmids that I used throughout my dissertation. I hope to know 1/3 as much as you do one day. Elisabeth, thank you for all your support in maintaining the mouse colony, helping me with hundreds of microbead and intravitreal injections and for keeping the lab together. Thank you also for being a friend and keeping me sane over the last couple of years. To the rest of the lab: it has been a pleasure to work with you all over the last few years. Thank you for letting me bother you all with questions, laughing with me, and for supporting me in numerous ways I can't even think of. To Brian, thank you for all your help with placing orders and bringing a lot of laughs to the floor. To Andrew and Joe, thank you for all the laughs, the science conversations, the happy hours and the fun we've had over the last couple of years. You both made my time as a graduate student more fun than I expected and always helped me answering questions or being a support system when I needed it. To all those on the floor who I've talked to and haven't named—thank

you for the constant snacks in the breakroom, the fun conversations in the microscope room and for all your random reagents and science questions I've asked for along the way. My project wouldn't be possible without you all.

To all the people who I have collaborated with, this project would not be possible without you. Purnima, thank you for your endless efforts in sectioning my optic nerves and eyes. I have learned so much from you and I definitely wouldn't be able to accomplish my IHC, optic nerve counts, etc. without your hard work. For Carli in the Duvall lab, thank you for all your help in making the different variations of microparticles that I used throughout my dissertation. Thank you for all of our science conversations and for always being on top of things. Dr. Duvall, thank you for your expertise in planning all of the PLGA or PPSES projects.

To my friends I've made in Nashville who have become my second family: I literally wouldn't be here without you. When I moved here, I didn't know basically anyone and now, I can look back with lifelong friends. Thank you all for the laughs, the tears, the science talk, the travels, the workouts, the coffee dates, the happy hours, the girls' nights and the countless adventures in the in-between. I cannot imagine how I would have survived graduate school without the family that I have formed here in Nashville. I can't wait to see what each and every one of you do in your future careers. I am so proud of all of you. To Veronika: thank you for being my best friend, my therapist, my shoulder to cry on, one of the funniest people I've ever met and the most motivated peer I've ever had. Thank you for always having my back, thank you for pushing me to never give up and thank you for understanding me in a way that I didn't know was possible. Thank you for befriending me when I really needed it in the fall of first year of graduate school—had you not done that, I don't even know where I would be.

Thank you to my family. Mom and Dad, thank you for always believing in me and for setting me up for success my entire childhood to get me to this point. Thank you for instilling in me the importance of education and hard work. Thank you for sacrificing so much for me before you ever knew I would be your daughter. Dad, thank you for showing me what hard work means and for being the role model I could always look up to when things were challenging. I hope to be 1/10 as successful as you one day. Mom, thank you for always picking up the phone when I needed it. Thank you for listening to my problems when you always have a million other things you could be doing. Thank you for giving me advice, thank you for encouraging me to rest, thank you for our hours and hours that we spent on FaceTime and on the phone. Thank you for being the best mom I could have ever asked for—I hope one day that I can be 1/100 as great of a parent as you are. Thank you for loving me unconditionally. Hannah and Mark, thank you for always making me laugh and pretending to listen when I talk about science. Your humor has always been appreciated.

Last but definitely not least, to Dylan, my husband. My dissertation would mean nothing had it not been for you and all your support. Thank you for being my cheerleader, my support system, my shoulder to cry on, my tech support and my best friend. Thank you for never giving up on me and for dealing with me when I was under stress. It's impossible to imagine what life would look like without you in it and I definitely know that I wouldn't have been able to make it this far in graduate school without you. You are the best thing that has ever happened to me.

TABLE OF CONTENTS

LIST OF TABLES

Table Page

LIST OF FIGURES

CHAPTER 1

Introduction

1.1 Layers of the Retina

The retina is about 0.5mm thick in humans and lines the back of the eye. All vertebrate retinas are composed of three layers of neuron cell bodies and two layers of synapses. There are three types of excitatory, glutamatergic neurons in the retina that work together in a feed-forward circuit: photoreceptors, bipolar cells, and retinal ganglion cells (RGCs). In the outer retina, synaptic transmission occurs first from photoreceptors to bipolar cells. In the inner retina, synaptic transmission occurs from the bipolar cells to the RGCs (Kolb, 2012). There are two main classes of interneurons that are largely GABAergic that help to modulate this excitatory signaling in both the outer and inner retina—in the outer retina, horizontal cells modulate the photoreceptor-bipolar cell connection; in the inner retina, amacrine cells modulate the bipolar cells-RGC connection. There are also three main classes of glia within the retina that work together to support each of these classes of neurons—astrocytes, Müller glia and microglia (Jäkel & Dimou, 2017; Kolb, 2012). Each of these types of glia contribute to homeostasis while also responding to insult, injury, or disease and will be discussed in greater detail in the following section.

On one end of the retina is the outer limiting membrane, which forms a barrier between the subretinal space. This is where the photoreceptors project to the retinal pigment epithelial (RPE) layer behind the retina. The RPE is responsible for nourishing the retina via its attachment to the choroid. This layer is also extremely important for absorbing scattered light such to decrease potential radiation onto the retina and decrease downstream oxidative stress.

Additionally, the RPE comprises the blood-retinal barrier where there are tight junctions that control which ions, nutrients, etc. can enter the retina (Strauss, 2005; Yang et al., 2021). There are several other functions for the RPE, which will not be discussed in this dissertation. On the other end of the retina is the inner limiting membrane, where the inner part of the retina borders the vitreous humor (Li et al., 2020; Nickells, 2002).

There are structural differences between the central and the peripheral regions of the retina. The central retina is considerably thicker than the peripheral retina, primarily due to more densely-packed photoreceptors and their respective bipolar and ganglion cells. In humans, the more densely-packed photoreceptors are primarily cones while the peripheral retina is predominately rods (Kolb, 2007, 2012; Li et al., 2020).

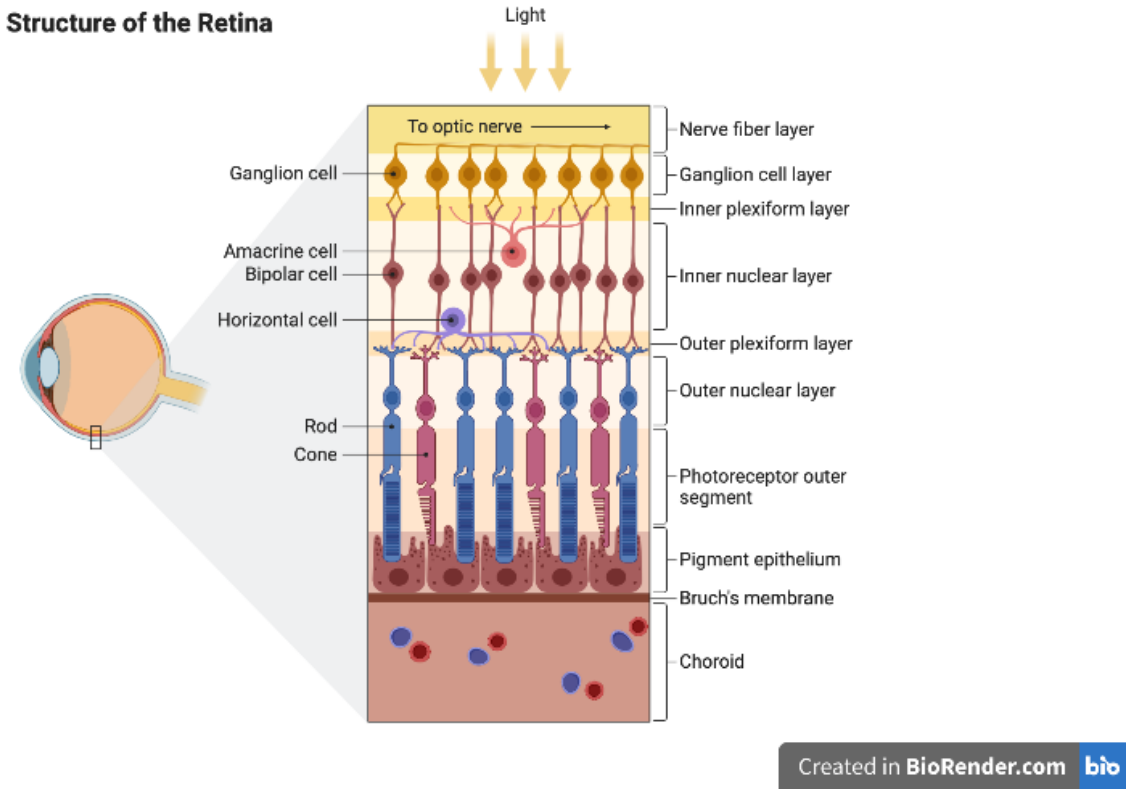

Figure 1.1 Anatomy of the human retina.

1.2 Retinal Ganglion Cell Background

Considering that RGCs are the primary cell type in the retina that is affected by glaucoma pathology, it is important to understand their morphology and physiology. RGCs are structurally similar to other neurons in that they have three main parts—the dendrites, the soma, and the axons. The dendrites of the neurons collect information from surrounding neurons, the soma is responsible for integrating this information from surrounding neurons, and the axon then relays that information to other neurons. Ganglion cells are the final output of neurons in the retina and are responsible for relaying information from the retina to the brain. By the time that visual information reaches the RGCs, a lot of pre-processing has already been done by the photoreceptors and the bipolar cells in the vertical pathway as well as from photoreceptor to horizontal cell to bipolar cell to amacrine cell to RGC in the lateral pathway (Kim et al., 2021; Oliveira-Valença et al., 2020). The optic nerve then packs all the axons of the RGCs in a bundle and passes the information to the next relay station in the brain, which changes based on which species we are discussing. Two of these brain visual centers are the lateral geniculate nucleus and the superior colliculus, among others such as the suprachiasmatic nucleus. The location of where the axons of particular RGC axons end up depends on their "trigger features" that they encode. "Trigger features" refers to the fact that different RGCs are selectively tuned to detect features such as color, size, direction and speed of motion (Kolb, 2012).

All the neurons in the retina function without myelination of their axons. RGCs are special in the sense that as their axons exit the retina, they become myelinated past the optic nerve head in the retrolaminar zone. The lack of myelination while in the retina is really important for light to hit these cells in the back of the eye during phototransduction. However, because RGCs are critical to the processing and transmitting the visual information from the

retina to the brain, which is a very metabolically demanding process, the myelination of their axons is really important for increasing efficiency (Calkins, 2012; Crish et al., 2010; Kolb, 2012). The fact that RGC axons are myelinated in one region and unmyelinated in another creates a sharp energy gradient that makes them particularly susceptible to oxidative stress, as will be discussed in later sections of this chapter.

RGCs attempt to make up for the lack of efficiency in their unmyelinated portion by having a high density of mitochondria in this region. In response to signals such as increased calcium influx or an increased local demand of ATP, mitochondria can be trafficked in both anterograde and retrograde directions. There are a variety of conditions that inhibit mitochondrial trafficking including increased cytochrome C and oxidative stress as well as increased mitochondrial permeability. Several of these consequences are found in animal models of glaucoma (Ito & Di Polo, 2017; Osborne & Del Olmo-Aguado, 2013; Tezel, 2006).

Additionally, RGCs have a very characteristic morphology in comparison to other neurons in the retina and the CNS. RGC axons are extraordinarily long in comparison to the axons of photoreceptors and bipolar cells: their axons are up to 50 times longer than photoreceptor axons and are also half as thick. The relatively thin size of RGC axons is important for energy consumption as well as action potential production but there are also consequences to the axons being so thin (Calkins, 2012; Crish et al., 2010).

There is a very high membrane-to-axoplasm ratio in RGCs, which creates a big difference in available sites for calcium influx and the ability to buffer this calcium accumulation. Calcium accumulation has been studied in multiple neurodegenerative diseases as a cause of oxidative stress. Changes in the intracellular calcium concentration of a cell control important physiological functions in neurons such as neurotransmitter release and gene

expression (Duncan et al., 2010). These aforementioned calcium changes are mediated either by calcium influx through voltage-gated plasma membrane calcium channels or release from intracellular stores (Gleichmann & Mattson, 2011; Mallick et al., 2016). Both age-related and pathological changes in calcium signaling have been implicated in several neurodegenerative disorders including glaucoma (Duncan et al., 2010; Gleicmann and Mattson, 2011; Payne et al., 2013). Upcoming studies are targeting abnormal calcium signaling as a drug target for glaucoma and other related diseases (Calkins, 2012).

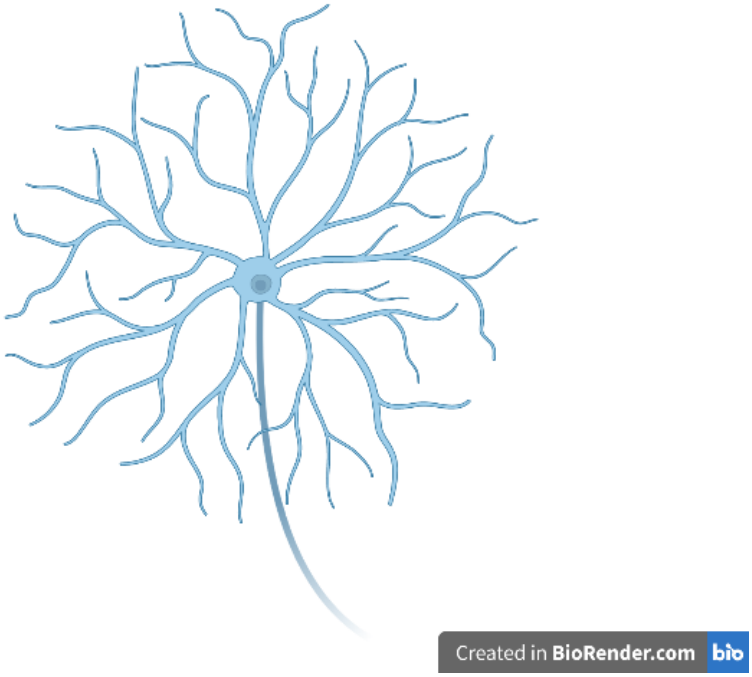

Figure 1.2 Structure of a retinal ganglion cell.

1.3 Glial cells of the Retina

The word “glia” comes from the Greek language meaning glue, implying that these cells are responsible for holding together the nervous system in some way. This is an accurate name for these cells, as both the central and peripheral nervous systems rely heavily on glial cells in

order to support neurons (Jakel et al., 2017). The major difference between glial cells and neurons is that neurons directly participate in synaptic interactions via the propagation of action potentials, whereas glial cells cannot electrochemically communicate with each other or with neurons in this way. Glial cells are responsible for supporting neurons and help define synaptic contacts and the signaling abilities between neurons. Glial cells outnumber neurons at a ratio of at least 3:1 and have complex processes that extend from their cell bodies (Barres, 2008). Though they have many complex processes, these structures are not axons or dendrites that are characteristic of neuronal structure. There are numerous functions of glial cells including maintaining the ionic milieu of neurons, modulating signal propagation, maintaining synaptic action by controlling the uptake of neurotransmitters, providing a scaffold for neuronal development, and preventing/aiding in recovery from neuronal injury. Glial cells also protect the blood-retina barrier, which is evident by their activation in the peripapillary chorio-retinal response to stress or injury (Barres, 2008; Vecino et al., 2016). In general, glial cells are highly plastic, meaning that they are able to quickly respond and adapt to homeostatic imbalances by changing their morphology and expression of different cell markers (Jakel et al., 2017; Ripps et al., 1985). This advanced adaptability is extremely important in defining glial cells as the support system of the retina.

There are four main types of glial cells in the developed retina. Astrocytes, which are restricted to the retina and the optic nerve, are named after their star-like projections with elaborate processes (Kolb, 2017). They work to maintain the chemical environment of neuronal signaling. Oligodendrocytes are responsible for myelinating neurons, allowing to conduct action potentials in the most efficient way possible using saltatory conduction. Müller glia are responsible for many functions, including potassium homeostasis and providing the retina with

structural support. Lastly, microglial cells are the resident immune cells of the retina, and are responsible for removing debris during normal cell turnover and after neuronal injury.

Astrocytes constitute the major cell type exhibiting homeostatic interactions with retinal ganglion cells, which makes them a promising target for therapy in glaucoma. They can be used as indicators of retinal stress and injury (Eng et al., 1985; Eng et al., 1994). Astrocytes can also sense neurotransmitter release from nearby neurons because they express neurotransmitter receptors themselves (Allen & Lyons, 2018). Additionally, they can release gliotransmitters that modulate synaptic transmission, although they do not conduct neurotransmission themselves.

During periods of trauma, astrocytes can increase in number, a process termed astrogliosis. Whether the role of astrogliosis is beneficial or detrimental is up for debate (Varela et al., 1997; Morgan, 2000). Astrocytes are defined as reactive based on their morphology, including enlarged soma and thickened and elongated processes (Prasanna et al., 2011). Studies also show that the orientation of astrocytic processes may be indicative of the reversibility of astrogliosis, which could depend on how acute/chronic the stimulus is, and how focal or global the insult is (Morgan, 2000; Hernandez et al., 2008). Increased inflammation and recruitment of immune cells from astrogliosis can ultimately contribute to RGC degeneration and death, which has been shown in several models of glaucoma.

The second main type of glial cells in the retina is microglia. Microglia are the resident immune cells of the brain that play an essential role in the innate immune response. These cells are extremely important because the retina needs protection from toxins and pathogens. They also work with astrocytes and Müller glia to regulate glucose, ions, and neurotransmitter transport (Wang et al., 2017). Microglia have the ability to survey the environment, seek out damage, and phagocytose anything in the immediate area that is dangerous. They have

multidimensional activation states in CNS diseases and injuries, such that these cells can have beneficial or detrimental roles depending on the context. Given their roles in phagocytosis, microglia have important roles such as immune surveillance and clearance of damaged tissue and other debris from the surrounding areas of neurons (Wei et al., 2018).

Oligodendrocytes are the myelinating cells of the central nervous system, generated from oligodendrocyte progenitor cells. The myelin sheath is an extension of the oligodendrocyte plasma membrane that wraps around the nerve axons in a concentric way. This process of myelination is an extremely complex process that is tightly regulated. Myelination is necessary for increasing efficiency of action potentials in the CNS, and while this process is important, it is not a focus of my dissertation work (Allen & Lyons, 2018; García-Bermúdez et al., 2021; Jäkel & Dimou, 2017).

The last type of glial cells in the retina are Müller glia, which are radial glial cells in the retina. These glial cells span the entire length of the retina. On one end, the outer limiting membrane of the retina contains the junctions between the photoreceptors and the Müller cells. On the other end of the retina, the inner limiting membrane contains the Müller cell end feet. The cell bodies of these glia are in the inner nuclear layer and their processes project to either the outer or inner limiting membrane (Backstrom et al., 2019; García-Bermúdez et al., 2021; Goldman, 2014; Reichenbach & Bringmann, 2013; Vecino et al., 2016a).

Müller glia help to structurally support the retina because they stretch radially along the entire thickness of the retina. These cells also have a wide range of functions that are necessary to the health of the rest of the neurons in the retina. Some of these functions include, but are not limited to: breaking down glycogen to supply end-products of anaerobic metabolism to fuel aerobic metabolism in neurons, getting rid of neural waste products, recycling amino acid

transmitters that have already been used, protecting neurons from excess glutamate, phagocytosing neuronal debris, synthesizing retinoic acid, and controlling homeostasis via potassium buffering (García-Bermúdez et al., 2021; Reichenbach & Bringmann, 2020; Vecino et al., 2016).

1.4 Glaucoma Background

Glaucoma is a group of optic neuropathies that is characterized by the progressive degeneration and eventual death of RGCs. The mechanism by which RGCs degenerate and die in glaucoma is not yet understood. Glaucoma currently affects over 70 million people worldwide and is the second leading cause of blindness, but is the leading cause of irreversible blindness. Every year, about 100,000 people get diagnosed with glaucoma, and about 10% of those patients are bilaterally blind. The prevalence of glaucoma is significantly higher in people of African descent or elderly populations as well as people with a family history of glaucoma, diabetes, hypertension, or myopia (Schuster et al., 2020; Wareham et al., 2021.; Weinreb et al., 2014).

The major risk factors for developing glaucoma are age, genetics, and sensitivities to increases in intraocular pressure (IOP). Currently, the only modifiable risk factor for treatment of glaucoma is IOP, which will be discussed in detail later (Heijl et al., 2002; Nickells et al., 2012). Ultimately, these IOP-dependent treatments are not sufficient as there are patients with normal tension glaucoma, who do not have elevated IOP, but do have glaucomatous pathology (Killer & Pircher, 2018; Mallick et al., 2016). Additionally, as we will discuss later, there are also patients with elevated IOP who do not respond well to IOP-lowering treatments and continue to progress to neurodegeneration. Therefore, in the field, there is an urgent need to develop better treatments for glaucoma that target RGC survival and prolong disease progression.

1.5 Genetics of Glaucoma

While glaucoma cannot be linked to a single causal gene, there are a few that stand out as relevant for disease. The first reported locus for primary open-angle glaucoma is *GLC1A,* which is located on chromosome 1 (Weinreb et al., 2014). The relevant gene at this locus is *MYOC,* which is responsible for encoding the protein, myocilin. Mutations in *MYOC* usually occur in the juvenile or early adult forms of primary open-angle glaucoma and are characterized by very high increases in IOP. In adults with primary open-angle glaucoma, the prevalence of *MYOC* mutations is only about 3-5%. Carriers of these disease-associated mutations develop the glaucoma phenotype in about 90% of cases (Tamm et al., 2002). While the exact role of the myocilin protein in glaucoma pathogenesis has not yet been elucidated, it is likely that these mutations alter the myocilin protein such that intraocular pressure can no longer be regulated. Myocilin mutations have been shown to be involved with deficits in protein trafficking and can result in an accumulation of misfolded proteins, possibly contributing to increased IOP (Johnson et al., 2000).

Another gene that has been linked to glaucoma is the *OPTN* gene. Interestingly enough, people with this gene have normal levels of IOP (Minegishi, 2016). *OPTN* is involved in many critical cellular functions including but not limited to vesicle transport, autophagy, and NF-KB regulation (Sarfarazi et al., 2003). As personalized medicine continues to improve, these GWAS findings will become increasingly more helpful in understanding the disease.

1.6 Types of Glaucoma

Glaucoma is commonly known as the “silent thief of sight” because there is a lack of symptoms in the most common type of glaucoma, primary open angle glaucoma. In these

patients, the disease remains asymptomatic until it is severe, which likely means that there are even more people who have glaucoma than are even accounted for. Population surveys suggest that only 10 to 50% of people with glaucoma are aware that they have it. There are two main types of glaucoma—primary open angle glaucoma and primary closed angle of glaucoma. Primary open angle glaucoma, as previously mentioned, accounts for roughly 80% of glaucoma patients (Stein et al., 2021; Tham et al., 2014; Weinreb et al., 2014). However, it is important to note that primary closed angle glaucoma is more severe and accounts for the majority of patients with the most severe vision loss. Primary open angle glaucoma is often a diagnosis of exclusion because, in these patients, there is no apparent preceding ocular or systemic causes to this disease. The diagnosis of primary open angle glaucoma largely depends on a normal gonioscopic appearance of the anterior chamber of the eye, glaucomatous optic disk cupping and damage, and peripheral visual field loss. Often times, patients with primary open-angle glaucoma have increased resistance to aqueous humor outflow through the trabecular meshwork (Lee & Higginbotham, 2005; Weinreb et al., 2014).

On the other hand, primary closed angle glaucoma is usually diagnosed due to dramatic signs and symptoms that eventually can lead to the aforementioned irreversible blindness phenotype. Primary closed angle glaucoma accounts for about 10% of glaucoma patients in the United States and is substantially more common among women, elderly patients, Asians, and people with hyperopia or a family history of glaucoma. This type of glaucoma occurs because aqueous humor cannot properly flow through the pupil into the anterior chamber of the eye. In these patients, there is increased pressure behind the iris, due to the buildup of aqueous humor, which results in an occluded anterior chamber angle (Khazaeni & Khazaeni, 2022; Weinreb et al., 2014). The symptoms of primary closed-angle glaucoma can include severe ocular pain,

redness, blurred vision, seeing halos around lights, headaches, and associated nausea and vomiting. Unfortunately, there are many patients who experience the nausea and vomiting and their diagnosis is often mistaken for a condition that is purely gastrointestinal. Primary closed-angle glaucoma is usually a bilateral disease, such that there is an increased risk if the disease is present in one eye that the other eye will also develop angle-closure. In these situations, there are prophylactic treatments that can be done. This disease is diagnosed through an eye examination and medications for these patients must be administered immediately following diagnosis (Lee & Higginbotham, 2005; Schuster et al., 2020).

Secondary forms of glaucoma are caused by a variety of ocular diseases or systemic diseases such as uveitis, inflammation, and any neovascular disease. The secondary forms of glaucoma are much less common than the primary forms of the disease. Some of the types of secondary glaucoma include inflammatory glaucoma, pigmentary glaucoma, neovascular glaucoma, traumatic glaucoma, and pseudo-exfoliative glaucoma. These types of glaucoma can also be caused by intraocular surgeries such as cataract or retina surgery (Crish et al., 2010; Lee & Higginbotham, 2005; Weinreb et al., 2014).

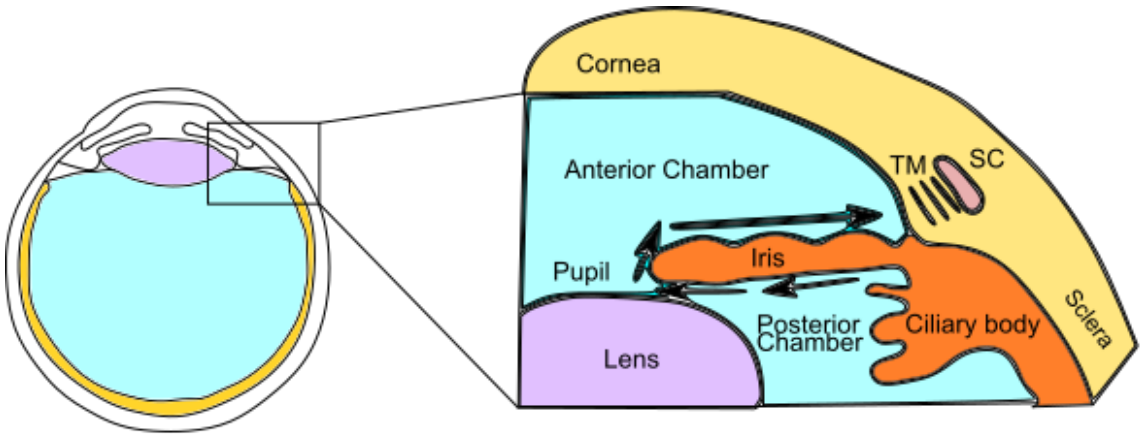

Figure 1.3 Outflow of aqueous humor in the human eye.

1.7 Intraocular Pressure and its Relationship to Glaucoma

Although we do not yet understand the pathogenesis of glaucoma, we do know that intraocular pressure (IOP) can be related to RGC death. Additionally, IOP is the only treatable risk factor of the disease, meaning IOP is the independent variable in the majority of animal models to study glaucoma (Chen et al., 2011). Other risk factors, such as genetics, have been previously discussed in the thesis.

Intraocular pressure is determined by the secretion of aqueous humor from the ciliary body and drainage through the trabecular meshwork and the uveoscleral outflow pathway. Elevated IOP can occur when outflow is blocked, causing mechanical stress and strain on the lamina cribrosa and adjacent tissues in the posterior part of the eye. This stress and strain can result in compression, deformation, and disruption of axonal transport, disrupting retrograde delivery of important trophic factors to RGCs from the lateral geniculate nucleus in the brain (Heijl et al., 2002; Jayaram, 2020). This disrupted axonal transport occurs relatively early in glaucoma pathology in many experimental models of glaucoma, which will be discussed later.

There are also patients who exhibit normal intraocular pressure, a condition known as normal tension glaucoma. There are a variety of theories as to what the pathology is behind normal tension glaucoma. It is possible that normal tension glaucoma is caused by local or general dysregulation of vasculature or by abnormal circulation of cerebrospinal fluid which results in damage to the optic nerve. Ultimately, the lower tolerance of normal IOP in these patients still results in mechanical damage that is seen in other glaucoma patients. Interestingly, in some normal tension glaucoma patients, the same treatments to lower IOP in patients with other types of glaucoma can be effective, which again points to a very complicated relationship

between glaucoma pathology and IOP (Killer & Pircher, 2018; Mallick et al., 2016; Weinreb et al., 2014a).

The majority of studies examining the mechanical damage that occurs in normal tension glaucoma patients focuses on a structure in the eye known as the lamina cribrosa. This mesh-like structure is extremely important in the pathway between the axons in the eye and the axons that exit via the optic nerve. These transitional axons are dependent on nutrients and oxygen from the capillaries within the lamina cribrosa (Quigley & Addicks, 1981). The lamina cribrosa is vulnerable to mechanical damage because it is only 1/3rd as thick as the sclera, and its load-bearing connective tissue components are only 40% of the tissue volume in the laminar region of the optic nerve head. This structure is responsible for providing physical support to the optic nerve head and must allow an opening for axons to leave the retina and enter the brain, leaving it vulnerable to different types of damage depending on the type of glaucoma the patient has (Burgoyne et al., 2005; Quigley et al., 1983; Quigley & Addicks, 1981; Weinreb et al., 2014).

1.8 Current Standards of Treatment for Glaucoma

Unfortunately, the treatments available for glaucoma can slow progressive degeneration but cannot reverse symptom progression or cure the disease. Each patient has to be considered and treated individually according to their susceptibility to optic nerve damage, visual field loss, response to medications/surgery, and personal preferences. Treatment for glaucoma should be directed at decreasing IOP and fixing whatever the underlying cause of glaucoma is, if possible.

Conventional treatment for glaucoma usually starts with topical medications in the form of eyedrops. ß-blockers or topical prostaglandin analogs are usually where treatments start, especially since these medications have very few adverse effects and only need to be used once a

day. The disadvantages of ß -blockers and prostaglandins include ocular irritation, allergic conjunctivitis, respiratory failure, bradycardia, cardiac failure, depression, increased pigmentation of the iris, hypertrichosis of eyelashes, intraocular inflammation, and impotence (M Almasieh et al., 2010; Durães et al., 2018). The second-line of treatments usually include topical carbonic anhydrase inhibitors. These treatments have fewer systemic adverse effects, but they are more inconvenient for patients because they are needed to be administered multiple times a day and, therefore, have very low patient compliance (Kimura et al., 2017a; Rusciano et al., 2017).

Most patients with primary open-angle glaucoma can be treated with the aforementioned medications. However, another therapy known as laser trabeculoplasty, is also an option for patients with primary open-angle glaucoma. In this procedure, the surgeon uses a laser beam to open clogged channels within the trabecular meshwork. Other procedures such as a trabeculectomy removes part of the trabecular meshwork to create an opening in the sclera. Additionally, the surgeon could also insert a small tube shunt into the eye to help with fluid drainage. All these methods aim to improve aqueous humor outflow to reduce IOP (Conlon et al., 2017; Tham et al., 2014).

The definitive treatment for primary closed-angle glaucoma is a procedure known as an iridectomy, which can be performed by incisional or laser surgery. This procedure creates an opening in the iris to allow the aqueous humor to flow out between the posterior and anterior chambers of the eye. Primary closed-angle glaucoma is considered a medical emergency, so patients must have these procedures performed immediately in combination with other IOP-lowering treatments (Khazaeni & Khazaeni, 2022; Weinreb et al., 2014a).

1.9 Clinical v. Experimental Glaucoma

In order to better understand glaucoma, animal models are used to study the underlying pathology of the disease. There are a wide variety of different animal species that have been used to better study and model the disease, including monkeys, rats, mice, pigs, dogs, and cats. Some of these models are induced models of glaucoma while others are spontaneous. Using various animal models to study glaucoma pathogenesis, it has been established in the field that anterograde transport (from the retina to the brain) is disrupted first in the progression of the disease. On the other hand, retrograde transport (from the brain to the retina) is affected later on in disease pathogenesis (Bouhenni et al., 2012; Evangelho et al., 2019; Harada et al., 2019a; Ishikawa et al., 2015). The last stage of disease progression in humans, rodents, and non-human primate models of experimental glaucoma is the caspase-dependent apoptotic death of the RGC cell bodies (Nickells, 2002). Additionally, data gathered from both human and animal models of glaucoma indicate that RGC axon degeneration occurs in a distal to proximal fashion, characterizing glaucoma as a "dying back" neuropathy, where "dying back" refers to slow and progressive degeneration of neurons under stressed conditions from its terminals toward its cell bodies. The majority of animal studies aim to model primary open angle glaucoma, while there are much fewer models of primary closed angle glaucoma (Calkins, 2012b; Crish et al., 2010). Due to the nature of my research, I will be focusing primarily on rodent models of glaucoma.

It is important to note that there are some key differences in human retinal biology and rodent ocular, retinal and neurobiology, as my dissertation work has been done entirely in mice. The mouse retina is rod-dominated, so that it is specialized for vision under low-light conditions, whereas the human retina is cone-dominated and is used for color vision, details and motion (Li et al., 2020). Mice also only have two photopigments—one that is for short wavelengths of light

and one that is for medium wavelengths whereas humans have three. Mice also don't have a fovea unlike humans (Li et al., 2020; Volland et al., 2015).

Additionally, one of these key differences is the primary target for RGC axons leaving the optic nerve—in humans, the primary target is the lateral geniculate nucleus whereas in mice, the primary target is the superior colliculus. Mice have also a disproportionally larger lens than humans, meaning the anterior segments are slightly different shapes between the two species. The mouse optic nerve head also does not have collagen beams like humans' and instead has pores that are created via astrocytes. Despite these differences, mice remain a useful tool to study glaucoma (Crish et al., 2010; D. Sun et al., 2009).

There are also a lot of similarities to human and mouse biology, which make mice excellent model organisms for glaucoma studies. Mice have all of the same major classes of neurons and interneurons in their retinas as humans do. In the outer retina, it has previously been shown that both humans and mice have a higher density of photoreceptors in the center than in the periphery (Kolb, 2012; B. Li et al., 2020). In terms of IOP regulation, mice and humans have similar mechanisms to regulate aqueous humor outflow and have similar responses to IOP-lowering compounds (Weinreb et al., 2014a).

Another huge advantage of using mice as a model organism is that they can be very easily genetically manipulated. A mouse strain that expresses a point mutation in the gene for myocilin (Tyr423His) was developed in order to model primary open angle glaucoma, where a similar mutation (Tyr437His) is seen in human patients (Harada et al., 2019; Mukai et al., 2019). Myocilin has been shown to be a causative gene of glaucoma in humans (Wiggs & Pasquale, 2017). Once mice with the myocilin mutation reach 18 months of age, they display a 20% loss in RGCs in their peripheral retinas, axonal degeneration in the optic nerve, elevation of IOP at a

moderate level, and endothelial cell detachment within their trabecular meshwork. Another genetic mouse model of glaucoma involves a mutation in the collagen type 1 gene. These mice show a gradual increase in IOP as they age that corresponds with axon loss in the optic nerve (Harada et al., 2019; Quillen et al., 2020). This suggests that there is a relationship between regulation of IOP and collagen turnover. These two genetic models are used to study primary open angle glaucoma.

To study primary closed angle glaucoma or spontaneous ocular hypertension, another genetic mouse model that involves a loss of Vav2/Vav3 is used. The Vav proteins are a family of guanine nucleotide exchange factors that are responsible for activating Rho guanosine triphosphatases in a phosphorylation-dependent manner. These proteins are important in controlling cell behavior through their regulation of actin structures that are involved in migration and adhesion (Bouhenni et al., 2012; Fujikawa et al., 2010). This model results in elevated IOP and results in changes within the iridocorneal angle, leading to angle closure. The elevation of IOP follows closely with loss of RGCs in the optic nerve head.

Additionally, a very commonly used mouse model to inherited glaucoma in humans is the DBA2/J mouse strain. These mice develop elevated IOP as they age because their anterior segment develops anomalies, their iris atrophy, and their iris pigments disperse (Harada et al., 2019). The model has some challenges—there is a lot of variability within animals and, due to changes in their cornea, it can be difficult to acquire *in vivo* imaging and electrophysiology data.

In order to study normal tension glaucoma where elevated IOP is not relevant in disease pathology, two spontaneous mouse models are often used—EAAC1 KO mice and GLAST KO mice. EAAC1 and GLAST are both glutamate transport genes, the former is expressed in neurons and the latter is expressed in Müller glia in the retina (Kimura et al., 2015). Both of

these KO mice exhibit spontaneous death of their RGCs and optic nerve degeneration, without any increase in IOP. Glutamate transporters are very important in clearing glutamate from the synapse so that excitotoxicity does not occur. Additionally, glutamate that is taken up into neurons or glia is converted into glutathione. Thus, these KO mice are good models of normal tension glaucoma and show the role of glutamate excitotoxicity and oxidative stress in glaucoma pathology (Harada et al., 2019; Mallick et al., 2016).

Two inducible rat models of primary closed angle glaucoma are photocoagulation of the trabecular meshwork/episcleral vessels and episcleral vein cauterization. In the photocoagulation model, a diode laser (wavelength of 532nm) is aimed at the trabecular meshwork and episcleral vessels (Yun et al., 2014). In the episcleral vein cauterization model, the deep superior, temporal, and inferior episcleral veins are cauterized, and IOP is elevated as soon as 30 minutes after surgery (Ko et al., 2005a; Wang et al., 2010). These models both result in elevated IOP for 4 weeks after injury, as well as loss of RGC cell bodies and damage to their axons. Some of these glaucoma models have differences in how long IOP is elevated or how quickly it is elevated after injury depending on the mouse strain. While both of these models involve RGC axonal and cell body loss that reflects human glaucoma, their methods to induce ocular hypertension are quite severe and often unrealistic for what is seen in the clinic—the IOP in these models is significantly higher than what is usually seen in the clinic and is elevated very quickly after the procedure, whereas human glaucoma is often a very slow-progressing disease. In the photocoagulation model, IOP is usually elevated to around 49 +/- 6 mmHg (Yun et al., 2014) and in the episcleral vein cauterization model, IOP is usually elevated to around 45 +/- 5mmHg (Ko et al., 2005; Wang et al., 2010).

1.10 Microbead Occlusion Model of Glaucoma

For the purposes of this dissertation, we will focus primarily on the inducible microbead occlusion model (MOM) of glaucoma. One of the advantages of having an inducible model of glaucoma is that the elevation of IOP is less variable and is controlled by the experimenter to reduce the biological variability in animals (Calkins et al., 2018; Sappington et al., 2010). Several of the aforementioned models of glaucoma, many of which were also inducible, were less clinically relevant than the MOM due to the fact that their elevation of IOP was very dramatic and unstable over time. There is also potential for secondary inflammation, altered venous pressure, and ocular trauma in models where the IOP is elevated drastically and suddenly. The MOM, on the other hand, has significant advantages including but not limited to the fact that it is not technically challenging, it is reliable in producing similar IOP elevations to what is found in the clinic, there is a very low risk for animals to develop secondary injuries, and it can be temporally controlled (Calkins et al., 2018; Claes et al., 2021).

In the MOM, researchers induce ocular hypertension via the intracameral injection of polysterene fluorescent microbeads. Animals are anesthetized using isofluorane and microbeads are injected into the anterior chamber of the eye, where they are then distributed throughout the necessary drainage canals to clog aqueous humor outflow over time (Sappington et al., 2010). This model was initially used in monkeys but has since evolved to be used in rabbits, rats, and mice. In many studies, one eye is injected with the aforementioned microbeads while the other eye serves as an internal control and receives a saline injection (Lambert et al., 2019, 2020). However, recent studies have shown that the eye receiving saline should no longer be used as a control due to the fact that it is not normal itself and shares glycogen stores—among other things—with the ocular hypertensive eye (Cooper et al., 2020). Thus, in my studies, injections

are always bilateral such that a mouse is either a saline control, receiving a saline injection in both eyes, or an elevated IOP mouse, receiving microbeads in both eyes (Naguib et al., 2021).

Similar to what is seen in the clinic, axonal degeneration in the optic nerve is a hallmark of microbead-injected mice. Previous studies using cross-sections of the optic nerve in both rats and mice showed a decrease in axon density, a decrease in axon counts and an increase in the number of degenerative axons at 4 weeks post-IOP elevation in comparison to saline-injected controls (Calkins et al., 2018; Lambert et al., 2020; Sappington et al., 2010). Additionally, visual function has been measured in rats and mice at multiple timepoints following induced ocular hypertension with this model and both species show decreased amplitudes of their visual evoked potentials in comparison to saline-injected controls (Bond et al., 2016; Hines-Beard et al., 2016a).

The MOM is a well-characterized model of glaucoma in many ways. One key aspect of this model that has not yet been completely elucidated is what occurs early following IOP elevation. This model is excellent at recapitulating the fact that glaucoma is a chronic, slow-developing disease in most patients, but what occurs before week 4 post-IOP elevation is not yet fully known in this model. Previous work from Risner et al. showed that as soon as 2 weeks post-IOP elevation, RGCs have signs of dendritic pruning and interestingly, even in the cells that were pruned, there was a transient increase in excitability that only lasted for a couple of weeks (2018). These findings suggested that glaucoma involves an early axogenic response that offsets IOP-induced stressors on RGCs, but that ultimately the response is not severe until 4 weeks post-IOP elevation. These findings are incredibly important to understanding what is occurring early in pathology in this model—my thesis work sought to further understand the retina's other

endogenous responses to IOP-induced stress and figure out what glaucoma is such a slow-progressing disease.

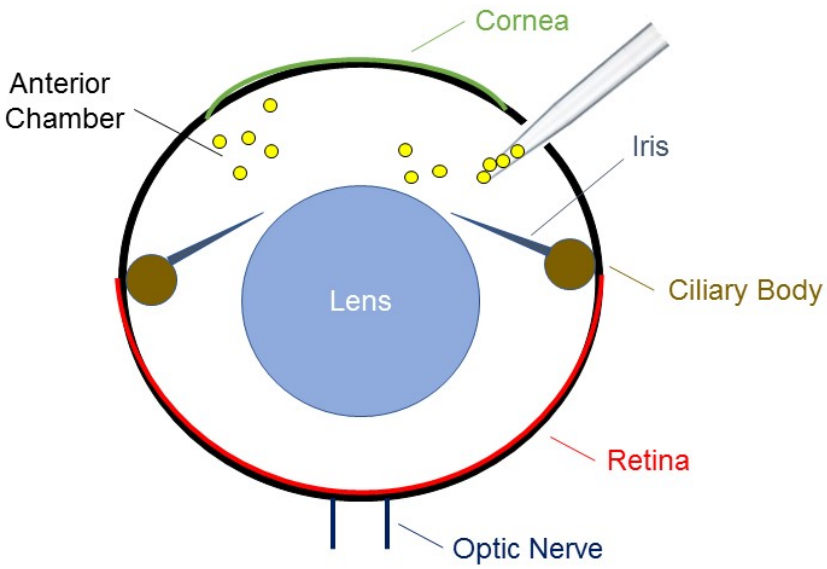

Figure 1.4 Demonstration of IOP elevation in the microbead occlusion model of glaucoma.

1.11 The Relationship between Oxidative Stress and Glaucoma

While we do not fully understand the mechanism underlying glaucoma, we do know that, along with many other neurodegenerative diseases, oxidative stress plays an important role in disease pathogenesis. Oxidative stress occurs when there is an imbalance between reactive oxygen species (ROS) and antioxidant defenses, where oxidants exceed antioxidants (Birben et al., 2012; Sharifi-Rad et al., 2020). ROS, when regulated, are normal and important for biological systems to function—oxygen's reactivity allows it to participate in high-energy electron transfers, which increase ATP generation through the process of oxidative

phosphorylation. While oxidative phosphorylation is required for organisms to survive, it renders proteins, lipids, and DNA vulnerable to attack, which will be discussed later.

ROS can be divided into free radicals and non-radicals. Free radicals can be readily generated from atomic oxygen due to the fact that it has two unpaired electrons in its outermost shell. Radicals contain an unpaired electron, meaning oxygen can function as a free radical in complexes that leave one of those valence electrons unpaired. Some ROS are generated from light, smoke, heavy metals, and other environmental sources, though the majority are produced regularly within the mitochondrial respiratory chain (Birben et al., 2012; Forman & Zhang, 2021; Pamplona & Costantini, 2011; Pizzino et al., 2017). Some common ROS include the superoxide anion, hydrogen peroxide, hydroxyl radical, and organic peroxides.

In a healthy system, the presence of ROS is balanced by a variety of antioxidant systems in place, the specifics of which will be discussed later (Sharifi-Rad et al., 2020; SIES, 1993); however, accumulation of ROS, also known as oxidative stress, can cause cell membrane damage via lipid peroxidation, alterations of protein structure and function due to oxidation, and fragmentation of RNA or DNA. Under hypoxic conditions, the mitochondrial respiratory chain can also produce nitric oxide, a kind of reactive nitrogen species (RNS). RNS then can generate other reactive species, including reactive aldehydes, which are products of excessive lipid peroxidation. Consequently, proteins and lipids are very susceptible for oxidative attack (Liguori et al., 2018; Sies et al., 2017).

Mitochondria are responsible for the regulation of both metabolic and apoptotic signaling pathways within a cell. Their major functions include generation of ATP, regulation of cellular calcium stores, balancing reactive oxygen species, and mediation of apoptosis, among many others. Within the retina, there are particularly large numbers of mitochondria present in the

RGC unmyelinated axons and in the inner segments of the photoreceptors (Bristow et al., 2002; Wang et al., 2003; Carelli et al., 2011). Most diseases that cause blindness are associated with mitochondrial dysfunctions due to RGC death (Schrier & Falk, 2011; Yu-Wai-Man et al., 2011). Lascaratos et al. demonstrated that mitochondrial genetic dysfunctions exist in primary open-angle glaucoma as well as normal-tension glaucoma (2012). This is evidenced by the fact that a maternal history of open-angle glaucoma is much more likely than a paternal history, which is in line with mitochondrial genetics (Mithcell et al., 2002). Additionally, in the clinic, lymphocytes taken from patients have been reported to have a significantly lower mean mitochondrial respiratory activity than their age-matched controls. In a study of Saudi Arabian cases of glaucoma, over half of patients had novel, nonsynonymous, potentially pathogenic changes in their mitochondrial DNA from blood samples (Abu-Amero et al., 2006). It is hypothesized that these mutations are spontaneously generated in response to oxidative stress throughout life, and could be linked to optic nerve injury in both open-angle and normal-tension glaucoma. *In vitro* studies have also shown a deficit in complex-I ATP synthesis (Abu-Amero et al., 2006; Lee et al., 2012). Diminished mitochondrial transport to neuronal processes has been implicated in Alzheimer's Disease and other neurodegenerative disorders (Chang and Reynolds, 2006; Rintoul & Reynolds, 2010).

The prevalence and incidence rates of glaucoma increase with age, and there is evidence suggesting that age-related mitochondrial dysfunction can play a role in neurodegenerative diseases, including glaucoma. As previously mentioned, increasing age is a risk factor for glaucoma. The specific relationship between mitochondrial dysfunction, mutations in mitochondrial DNA and increasing age is controversial (Kong et al., 2009; Sharifi-Rad et al., 2020). As rats age, mitochondrial ATP production and oxidative phosphorylation declines, while

ROS in neuronal tissues increases. Additionally, the number of mutations in mitochondrial DNA also increases with age; mice with certain mitochondrial DNA mutations have also shown to have a “premature aging” phenotype that includes alopecia, osteoporosis, cardiomyopathy, and shortened life span than wildtype mice (Dumanović et al., 2021; Liguori et al., 2018; Sharifi-Rad et al., 2020; Zhang et al., 2015). All in all, mitochondria play a huge role in regulating oxidative stress and apoptosis and thus, are an important player in glaucoma pathology.

The influence of oxidative stress and mitochondrial dysfunction does not only occur in experimental glaucoma, but it is also observed in the clinic. In glaucoma patients, increased levels of 8-hydroxy-2-deoxyguanosine have been found in trabecular meshwork tissues. In other studies, also using donor tissue from glaucoma patients, there is a correlation between the degree of oxidative damage and the IOP of these patients as well as visual field deficits (Moreno et al., 2004; Saccà & Izzotti, 2008). Additionally, glaucomatous human retinas and optic nerve heads have shown an upregulation of hypoxic stress-induced proteins and heat shock proteins. Many of these patient tissues, including trabecular meshwork, optic nerve head, retina, and aqueous humor, also display decreased total reactive antioxidant potential and increased antioxidant enzymatic activity of superoxide dismutases and glutathione peroxidases (Garcia-Medina et al., 2020; Zhao et al., 2016). Additionally, it has been consistently shown that glaucoma patients have decreased glutathione in their blood plasma. Mutations in genes associated with oxidative stress have also been correlated with glaucoma in patients. Mutations in CYP1B1, a member of the cytochrome P450 family, have been involved in primary congenital glaucoma. The GSTM1 enzyme is one of the major polymorphisms of GST—and has been shown to be a null genotype in glaucoma patients (Ghanem et al., 2010; Gherghel et al., 2005).

Even though ocular hypertension is not present in all patients with glaucoma, it is important to acknowledge that this pathology has been correlated with increased ROS and RGC death in many studies. Along these lines, both models of acute ocular hypertension, such as the retinal ischemia model, as well as moderate and chronic models, such as the DBA/2J model, show generation of ROS, demonstrating that elevation of IOP is associated with oxidative stress (Kimura et al., 2017; Moreno et al., 2004; Saccà & Izzotti, 2008). This phenomenon was shown in another model of ocular hypertension, in which intraocular hyaluronic injections are administered. Researchers found a significant decrease in retinal antioxidants and an increase in lipid peroxidation following increased IOP. Similarly, a study using hypertonic saline injections into rats showed a significant increase in protein carbonyl immunoreactivity after elevation of IOP, which demonstrates that oxidative modification of proteins is occurring in this model (Almasieh et al., 2013; Wang et al., 2010). Cauterization of the episcleral veins to induce IOP elevation, another common animal model of glaucoma, also shows an increase in ROS production and increased lipid peroxidation. One particularly interesting paper examined the role of hydrogen peroxide in ocular hypertension and found that perfusion of trabecular meshwork cells with this oxidant was sufficient to alter drainage of aqueous humor within the bovine anterior chamber (Ferreira et al., 2010; Arana et al., 2020; Ko et al., 2005). The aforementioned studies show that RGCs exposed to elevation in IOP are prone to oxidative stress.

1.12 Antioxidant Defenses to Oxidative Stress

Because cells will inevitably face oxidative stress, it is evolutionarily beneficial for cells to have endogenous mechanisms to reduce levels of oxidative stress. Counteracting oxidative stress is done by activating the endogenous antioxidant systems to produce antioxidant proteins.

These systems can be divided into two phases within the cell: phase I and phase II reactions(Sharifi-Rad et al., 2020; Sies et al., 2017). Phase I reactions are carried out by the cytochrome P450 enzyme system and are responsible for reducing the oxidants via redox reactions. Then, phase II reactions are responsible for the conjugation of hydrophilic molecules via antioxidant proteins, such as glutathione (GSH), coenzyme Q10, and superoxide dismutase (SOD), to name a few (Birben et al., 2012; Garcia-Medina et al., 2020). These antioxidants act in either direct or indirect manners, and, as their names imply, either directly quench ROS or synthesize and recycle other antioxidant proteins, which indirectly quenches ROS.

Many of the enzymatic antioxidant defenses have transition metals, which allow them to take on different valences as electrons are transferred from the oxidant to the antioxidant. For example, there are two forms of superoxide dismutase, which is the enzyme responsible for breaking down superoxide into hydrogen peroxide—which can then be broken down into water and oxygen by other enzymes such as catalase or glutathione peroxidase. These two forms of superoxide include a manganese form that is found within the mitochondria and the copper/zinc form, which is found in the cytosol of the cell (Izzotti et al., 2006; Ko et al., 2005).

Glutathione peroxidase's activity is dependent on the presence of another antioxidant, glutathione, in its reduced form, which acts as a hydrogen donor. Glutathione is extremely important as it is the major thiol redox buffer in cells and is involved in a variety of different antioxidant reactions (Vriend & Reiter, 2015). Specifically, it has been demonstrated in a variety of glaucoma models that astrocytes exhibit diminished glutathione levels.

There are a variety of other defenses to oxidative stress; the primary chemicals are vitamin C (ascorbate) and vitamin E (a-tocopherol). These two vitamins work together such that vitamin C is necessary to regenerate vitamin E once it has been oxidized (Hui et al., 2020).

Thioredoxin and other thiol-related compounds are also non-enzymatic defenses that the cell can use to detoxify hydrogen peroxide (Hansen, 2004).

There are also a variety of transcription factors that act as hydrogen peroxide sensors, can induce expression of antioxidant genes to combat oxidative stress, and can maintain cellular homeostasis. Some of these transcription factors include AP-1, CREB, HSF1, HIF-1a, TP53, Notch, CREB-1 and NRF2, the last of which is the focus of my dissertation research (Espinosa-Diez et al., 2015; Soriano et al., 2009; Tonelli et al., 2017).

1.13 The Relationship between Antioxidants and Glaucoma

It is likely that an increase in oxidative stress in glaucoma patients is not sufficient to drive pathogenesis; however, it is possible that these patients have a weakened antioxidant response system such that their cells cannot completely combat the oxidative stress presented. Alternatively, it could be that their genetics or sensitivities to increases in IOP combined with increased oxidative stress exacerbate existing pathology. Clinical studies have shown a decrease in antioxidants, such as glutathione, in the plasma levels of patients with glaucoma.

As previously mentioned, there are many patients that do not respond to IOP-lowering compounds to slow the progression of glaucoma. Antioxidants are becoming a strategy to protect RGCs in this disease in these patient populations. In another study with primary open-angle glaucoma patients as well as pseudoexfoliative glaucoma patients, there was an overall reduction in the total antioxidant capacity in the serum of these patients in comparison to age-matched controls (Ghanem et al., 2010). Additional studies have shown significant correlations between the degree of oxidative damage in the trabecular meshwork with increased IOP and visual field

loss (Saccà & Izzotti, 2008; Zhao et al., 2016). Some glaucoma patients in one particular study treated with vitamin C saw observably decreased IOP (Hui et al., 2020).

In mouse models, antioxidants are efficacious at reducing glaucoma pathology. In a study using the DBA2/J mouse model, animals treated with a-lipoic acid had increased RGC survival in comparison to controls. In a model using microbeads and viscoelastic injections to induce ocular hypertension, treatment with another antioxidant, tempol, reduced RGC death. Additionally, oral administration of geranylgeranylacetone, which is used as a treatment for gastric ulcers but also is an antioxidant as it inhibits apoptosis through increasing heat-shock protein 70, suppressed RGC death in the GLAST KO mice (Huang et al., 2007). Valproic acid, a drug used in the treatment of epilepsy but has also been known for its antioxidant effects, prevents glaucomatous neurodegeneration in multiple mouse models through its stimulation of the BDNF-TrkB pathway (Biermann et al., 2010; Kimura et al., 2015). This drug also has been shown to increase activities of superoxide dismutases, catalases, and glutathione peroxidases following retinal ischemia/reperfusion injury.

One of the antioxidants that has been studied is coenzyme Q10, a cofactor of the mitochondrial respiratory chain that has been shown to scavenge free radicals, decreasing reactive oxygen species. In a 12-month clinical trial, glaucoma patients were either treated with a beta blocker alone or a combinatorial therapy that included a ß-blocker but also coenzyme Q10 and vitamin E (Davis et al., 2017; Martucci & Nucci, 2019). The glaucoma patients that received the combinatorial therapy saw improved visual cortical responses as determined by visual evoked potentials and electroretinograms.

Vitamin B3 (also known as nicotinamide) has also been studied as a potential antioxidant therapy in glaucoma patients due to its ability to regulate calcium homeostasis, maintain

mitochondrial function, and regulate vasculature. Vitamin B3 has been shown to decrease RGC loss in animal models in an IOP-independent manner. In a phase III clinical trial in Australia, oral vitamin B3 had impressive preliminary findings in patients with primary open angle glaucoma (Hui et al., 2020).

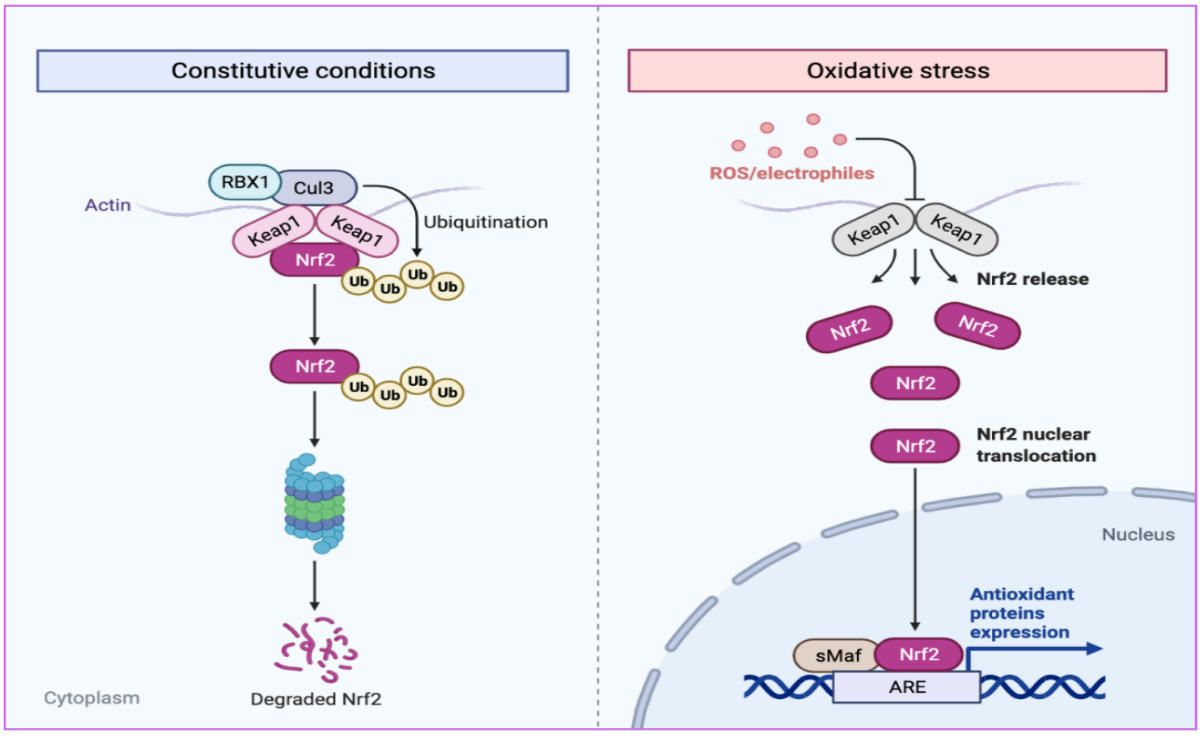

Figure 1.5 Mechanism of activation of NRF2 in constitutive conditions and oxidative stress.

1.14 NRF2, KEAP1 and the Antioxidant Response Element

The NRF2-KEAP1-ARE pathway has been shown to be the major regulator of cytoprotective responses to oxidative stress. As such, it has become a target for a variety of therapies for neurodegenerative diseases, including glaucoma, which will be discussed later. NRF2, which stands for nuclear factor E2-related factor 2, is a transcription factor that belongs to the Cap 'n' Collar family of regulatory proteins (Nguyen et al., 2009; Tonelli et al., 2018). Some of the other proteins in this family, defined by a basic leucine zipper region, include NRF1,

NRF3, Bach1, Bach2 and NF-E2. NRF2 has 7 different functional domains, known as Neh1-7. The major regulatory domain of the protein is Neh2, which is located in the N-terminus, and is involved in maintaining the protein's stability (Huang et al., 2015; Vriend & Reiter, 2015).

NRF2 has a very short half-life of less than 15 minutes as it is an unstable protein. NRF2's activity and stability are regulated primarily by its repressor protein, KEAP1 (Kelch-like ECH-associated protein 1). KEAP1 interacts with NRF2 via the ETGE and DLG motifs within the two binding sites inside its main regulator domain, Neh2, and promotes Nrf2's ubiquitylation through the cullin-3-dependent pathway (Espinosa-Diez et al., 2015; Huang et al., 2015; Vriend & Reiter, 2015). Previous studies have shown that there is a direct correlation between the amount of KEAP1 protein in the cell and the rate at which NRF2 is ubiquitylated and subsequently degraded. In short, the binding of KEAP1 to NRF2 targets NRF2 for degradation by the 26S proteosome via the ubiquitin-dependent pathway (Cuadrado et al., 2019; Raghunath et al., 2018; Xu et al., 2013).

KEAP1 can function as an oxidant-sensor via its sulfhydryl groups. In the presence of ROS, KEAP1's cysteine residues can become oxidized, leading to a conformational change that causes NRF2 dissociation and accumulation in the cytosol. NRF2's antioxidant activity is dependent on its dissociation from KEAP1 such that it is able to accumulate in the cytosol and translocate into the nucleus to bind to the ARE (Nguyen et al., 2000, 2009; Raghunath et al., 2018).

KEAP1's oxidation is not the only way that NRF2 can accumulate in the cytosol of the cell. Upstream signaling molecules such as p62 and p53-regulated p21 can interfere with the binding of NRF2 and KEAP1 and result in activation of NRF2 (Huang et al., 2015; Leung et al., 2003). Upstream signaling molecules have also been shown to phosphorylate NRF2 at the Ser40

residue, its only phosphorylation site, which can also cause it to accumulate in the cytoplasm and translocate into the nucleus to bind to the ARE. Some of these upstream signaling molecules include but are not limited to PI3K, Akt, JNK and MAPK (Bryan et al., 2013; L. Ma et al., 2015; Niture et al., 2014; Peng et al., 2019; Song et al., 2019; Sun et al., 2009; Sykiotis et al., 2011; Wang et al., 2008).

The ARE is a cis-acting enhancer that is located in the 5' flanking region of many phase II detoxification and cytoprotective genes. Upon NRF2's binding to the ARE, it interacts to form a heterodimer with small Maf proteins, a family of transcription factors. Many other transcription factors also bind to the ARE but NRF2 is the primary transcription factor responsible for the elevating expression of these antioxidant genes. The aforementioned direct and indirect antioxidant proteins necessary for a cell's response to oxidative stress are both regulated by NRF2 binding to the ARE (Nguyen et al., 2009; Schmidlin et al., 2019; Soriano et al., 2009; Vriend & Reiter, 2015). Some of genes that encode for cytoprotective proteins via the activation of the ARE include, but are not limited to, SOD, catalase, glutathione S-transferases, heme oxygenase-1, and thioredoxin reductase-1 (Banning et al., 2005; Raghunath et al., 2018; Tonelli et al., 2018). Overall, NRF2's binding to the ARE is necessary for a cell's response to oxidative stress to be at full capacity; deficiencies of NRF2, which will be discussed later, have been linked to not only increased oxidative stress but also increased neurodegeneration and cell death in models of glaucoma (Johnson et al., 2008; Nakagami, 2016; Xu et al., 2014, 2015).

1.15 NRF2 and Glaucoma

NRF2 has been shown to play an essential role in an organisms' ability to combat oxidative stress via its binding to the ARE and inducing expression of these antioxidant protein

genes. In NRF2 knockout (KO) mice, the ability of the ARE to induce transcription of cytoprotective genes is significantly impaired, which makes these mice extremely vulnerable to a wide variety of both pharmacological and environmental insults. Studies show that NRF2 KO mice are more susceptible to conditions including but not limited to cigarette smoke induced emphysema, acetaminophen hepatotoxicity, and embryonic lethality via increased oxidative stress (Harada et al., 2019; Nakagami, 2016; Nguyen et al., 2000; Xu et al., 2015). Thus, these mice are a useful tool in order to determine the role of oxidative stress in a variety of neurodegenerative disease, including glaucoma.

The NRF2-ARE pathway has been shown to mediate neuroprotection in several animal models of retinal disorders, including a few animal models that imitate glaucomatous disease pathology. One study used glaucomatous trabecular meshwork cells, which undergo increased apoptosis in response to ocular hypertension, to determine the role of NRF2 in glaucoma pathogenesis. Overexpression of NRF2 in these cells resulted in upregulation of an anti-apoptotic factor, BCL-2, as well as a down-regulation of p53 and Bax, an apoptosis regulator (Cheng et al., 2017; Wang et al., 2020). This *in vitro* study demonstrates the role of NRF2 in trabecular meshwork cells, making this transcription factor a promising target for glaucoma therapy.

In both retinal ischemia/reperfusion and optic nerve injury models of glaucoma, the administration of an NRF2 activator after injury, known as CDDO-lm, was shown to protect RGC survival (Cho et al., 2015; Espinosa-Diez et al., 2015; Li et al., 2020; Xu et al., 2015). Another study showed that delivery of VPA and α-lipoic acid, neuroprotective agents, decrease ROS generation via the activation of the NRF2/HO-1 pathway (Inman et al., 2013). Thus, activation of the NRF2 pathway in response to multiple optic nerve injury models results in

neuroprotection, indicating the importance of this transcription factor in regulating oxidative stress from injury.

While NRF2 activation results in RGC protection in animal models of glaucoma, it is also important to examine the consequences of a system lacking normal amounts of NRF2. One study showed that depletion of NRF2 enhanced RGC death that had been induced by optic nerve injury. Similarly, NRF2 KO mice show an exaggeration of oxidative stress markers as well as increased capillary and neuronal degeneration. These KO mice show significantly increased RGC death following optic nerve injury in comparison to control mice, which also show RGC death after injury (Fujita et al., 2017; M. Wang et al., 2020). Genetic replacement with NRF2 in these NRF2 KO mice is able to decrease RGC death (Fujita et al., 2017). In a nerve crush model, NRF2 deficient mice also showed increased RGC death, which suggests that the absence of NRF2 is sufficient to enhance the existing death in these cells (Himori et al., 2013; Xiong et al., 2015).

All of the aforementioned findings show a correlation between the activation of NRF2 and neuroprotection as well as a correlation between RGC death from various injury models and a depletion of NRF2. These studies further demonstrate that NRF2 is a promising therapeutic target for glaucomatous neurodegeneration, and its exact role in disease pathogenesis must be elucidated.

1.16 Neuroprotection in Glaucoma

As of now, the only treatments for glaucoma revolve around lowering IOP. As previously mentioned, there many patients with elevated IOP who do not respond to IOP-lowering treatments as well as patients with normal tension glaucoma, whose IOP is not elevated.

Neuroprotective treatments in glaucoma refer to treatments that do not involve lowering IOP and instead, seek to protect RGCs from glaucomatous pathology or delay existing neurodegeneration.

One of the commonly used neuroprotective agents against glaucoma is brimonidine. Brimonidine is an alpha-2 adrenergic agonist that works to lower the IOP of glaucoma patients. Previous studies have shown that this drug can protect RGCs from somatic, axonal and dendritic degeneration in a variety of models, including NMDA-induced neurotoxicity, ischemia/reperfusion, ocular hypertension, optic nerve crush and optic neuritis. Several of these studies also showed that these effects were independent of IOP, showing that brimonidine has promise to treat patients who do not have ocular hypertension concurrently with their glaucomatous pathology (Doozandeh & Yazdani, 2016; Mallick et al., 2016). There are several possible mechanisms by which brimonidine could be having its neuroprotective effects, including but not limited to its ability to activate neurotrophic factors, modulate blood vessel dilation and construction, inhibit glutamate, and downregulate apoptosis factors. Specifically, studies have shown that brimonidine increases the transcription of brain-derived neurotrophic factor (BDNF) and fibroblast growth factor (FGF) as well as their respective receptors. These factors have been shown to regulate various cellular functions, including but not limited to neuronal growth, plasticity, differentiation, and survival (Cantor, 2006; Doozandeh & Yazdani, 2016). Additionally, brimonidine has been shown to not only protect the retina following injury in a dose-dependent and a time-dependent manner, but it has also been shown to assist with neuronal regeneration following injury. In the well-characterized rat episcleral vein cauterization model of glaucoma, continuous subcutaneous delivery of brimonidine significantly improved RGC survival and morphology as well as reduced axonal transport deficits (Lambert et al., 2011). Brimonidine has been shown to be effective in glaucoma patients, as well, showing that it

is a promising therapeutic that needs to be further studied. In a study where 99 low-pressure glaucoma patients were treated with brimonidine, the incident of visual field progression was significantly lower in comparison to the other patients treated with another IOP-lowering drug, timolol. A large portion of the patients in this study, however, were lost to follow-up of the study or had allergies to the drug, which may have skewed the study's findings (Cantor, 2006; Doozandeh & Yazdani, 2016; Oh et al., 2019; Sun et al., 2017). More investigation is needed to better understand brimonidine's effects as a neuroprotective in glaucoma patients.

Another promising neuroprotective in glaucoma is stem cell therapy using both mesenchymal stromal cells or human embryonic stem cells. Mesenchymal stromal cells (MSCs) have been implicated in glaucoma neuroprotection in several studies using animal models and post-mortem human tissue (Naik et al., 2020; Vasudevan et al., 2011; Weinreb & Levin, 1999). It is important to note that MSC treatment has its shortcomings—MSCs are delivered via intravitreal injections, which can have adverse effects including but not limited to reactive gliosis, vitreous clumping, and epiretinal membrane thickening. Human embryonic stem cells (hESCs) are pluripotent cells that have the ability to differentiate into all 3 embryonic layers. Previous preclinical studies using monkey eyes showed that successful integration of hESCs can be used to mediate light responses in the host's retina. Of course, this technology also has its own pitfalls, especially because the use of hESCs have been ethically controversial (Chamling et al., 2016; Doozandeh & Yazdani, 2016; Johnson et al., 2011). Nevertheless, there are at least three clinical trials that are currently underway that are investigating the role of stem cells in glaucoma. These studies should hopefully increase understanding of the practical applications of stem cell therapy in glaucoma.

Neurotrophins, including the aforementioned BDNF, have been also implicated as potential neuroprotectives in glaucoma patients (Chitranshi et al., 2018; Foldvari & Chen, 2016). One study reported decreased BDNF in early glaucoma and suggested that BDNF could be used as a potential biomarker for detecting early disease (Oddone et al., 2017). Administration of BDNF as well as other trophic factors in combination (such as neurturin, glial derived neurotrophic factor) showed enhanced RGC survival. Additionally, ciliary neurotrophic factor (CNTF) is being explored in a phase II clinical trial. In this study, CNTF is administered via an implantable polymeric device that is given via an intravitreal injection. The way that the device encases CNTF allows for RPE cells to sustained release of CNTF to the RGCs (Shpak et al., 2017). There is also another neuroprotective agent, recombinant human nerve growth factor (rhNGF), that is being studied in a phase 1b clinical trial as a neuroprotective agent in glaucoma patients. This particular treatment is already FDA approved to treat neurotrophic keratitis (Chitranshi et al., 2018; Vasudevan et al., 2011).

Another neuroprotective agent with promising efficacy is memantine, which is a non-competitive NMDA antagonist with anti-glutamate excitotoxicity effects (Doozandeh & Yazdani, 2016; Weinreb et al., 2018). This drug has been previously used in moderate to severe Alzheimer's Disease but recent studies have also shown that it can protect against RGC loss in monkey experimental glaucoma. While there was a clinical trial that made it to phase III for memantine as a therapeutic for glaucoma patients, ultimately, the drug did not show any significant effects.

Calcium channel blockers (CCBs) have also been implicated in glaucoma neuroprotection because they can prevent calcium-mediated apoptosis and can also improve ocular blood flow (Doozandeh & Yazdani, 2016; Duncan et al., 2010; Mallick et al., 2016). Two

particular CCBs are brovincamine and nilvadipine, which both can permeate the blood-brain barrier and can increase CNS blood flow without affecting the rest of the body. Clinical trials have shown therapeutic efficacy in both of these drugs—patients with normal tension glaucoma that were treated with either of these CCBs had a delay in progression of their visual field deficits in comparison to controls. It is important to note, however, that the increase in ocular blood flow caused by treatment of CCBs can actually result in an acute increase in IOP in some patients (Araie et al., 2016; Duncan et al., 2010).

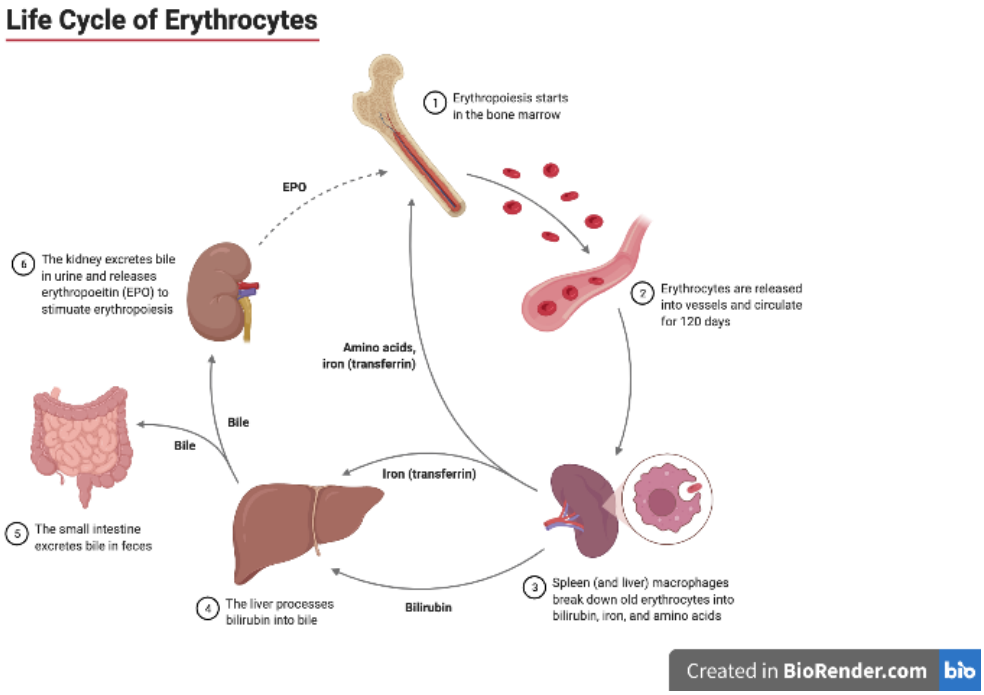

Figure 1.6 Life cycle of erythrocytes.

1.17 EPO as a Neuroprotective for Glaucoma

Erythropoietin (EPO) is a 165 amino acid glycoprotein. EPO is a cytokine that belongs to the type 1 superfamily, and a hormone that is produced by the kidney in adults, but is produced by the liver during development. Its main role is to induce proliferation, differentiation, and

maturation of red blood cells (erythrocytes) both in embryos and adults (Peng et al., 2020; Suresh et al., 2020; Tsiftsoglou & Kalyuzhny, 2021). It is also secreted in response to cellular hypoxia and stimulates red blood cell production in the bone marrow to ameliorate for this. Low levels of EPO are constantly being secreted as a compensatory mechanism for normal turnover of red blood cells (Peng et al., 2020; Rey et al., 2019; Subiras et al., 2012).

The binding of EPO to its receptor, EpoR, results in a conformational change that yields autophosphorylation by JAK-2. EPO then induces phosphorylation on tyrosine residues of the receptor, creating a binding site for other proteins during amplification of the signaling cascade that will follow (Bunn, 2013; Subiras et al., 2012; Tsiftsoglou & Kalyuzhny, 2021). Some of the many pathways that are activated by EpoR include but are not limited to STAT-1, STAT-3, STAT-5, PI3K, MAPK and PKC (Cao et al., 2010; Guillard et al., 2003; Jiang et al., 1998; Myklebust et al., 2002; Shi et al., 2010; Tóthová et al., 2021; Tsuji-Takayama et al., 2006; Von Lindern et al., 2000; Wu et al., 2018). Activation of these pathways then lead to the regulation of cell cycle via AKT. The exact signaling pathways that are activated differ depending on the disease/injury or cell type of interest and thus, EPO is known for its pleiotropic effects. EpoR has been found in several non-erythroid tissues, including but not limited to heart, muscles, central and peripheral nervous systems and muscles (Hernández et al., 2017; Peng et al., 2020; Tsiftsoglou & Kalyuzhny, 2021). Ultimately, however, there are issues with non-specific EpoR antibodies, which makes it difficult to confirm some of these findings.

Thus far, the primary clinical use for EPO treatment has been in anemic patients—specifically those with conditions like chronic renal failure. There are also several clinical trials using EPO for the treatment of optic neuritis, amyotrophic lateral sclerosis, spinal cord injury, and traumatic brain injury (Al-Sarraf et al., 2018; Ponce et al., 2013; Rey et al., 2019). EPO has

also been shown to activate HIF-1, which is also activated by other pro-inflammatory markers such as TNFa, IL1b or lipopolysaccharides. The activation of HIF-1 is particularly interesting for neuroprotective purposes since many neurodegenerative diseases, including glaucoma, have a very important pro-inflammatory component (Bunn, 2013; Zakharova et al., 2018).

EPO is also known for its neuroprotective effects because activation of the EpoR can inhibit several pro-apoptotic proteins including p53 and cytochrome C. EpoR has also been found to be expressed throughout the CNS, suggesting EPO could easily target cells within the nervous system. Several studies have shown EPO's neuroprotection *in vitro.* In one study, PC12 cells were treated with EPO and were protected against cell death when dosed prior to exposure to amyloid beta peptide (Koriyama et al., 2010). *In vivo,* rats pre-treated with EPO before inducing ischemia via a middle cerebral artery occlusion model showed a decrease in necrotic tissue as well as decreased edema. In another study, either pre-treatment or post-treatment with EPO prevented neuronal damage in a model of global cerebral ischemia. Interestingly, EPO's protection in this particular study was contingent upon phosphorylation of Akt but not PI3K (Al-Sarraf et al., 2018; Jeong et al., 2017; Rey et al., 2019; Subiras et al., 2012).

In the retina, EPO treatment has been shown to protect both RGCs and photoreceptors from various types of insults/injury. RGCs are protected following EPO treatment in a model of optic nerve crush-induced cell death. Additionally, in a model of glaucomatous degeneration, systemic EPO treatment protected RGCs (Wang et al., 2012; Zhong et al., 2007). A subretinal injection of EPO was sufficient to protect photoreceptors from the retinal degeneration slow phenotype in mice. Additionally, EPO treatment protected photoreceptors in a light-damage model for rats (Rex et al., 2009; Sullivan et al., 2011).

Previous studies have used local delivery of EPO via subretinal or intravitreal injections and have proven successful (Aghdam et al., 2016; Rex et al., 2009; Rey et al., 2019; Shirley Ding et al., 2016; Xu et al., 2012). Of course, direct delivery of EPO into the eye only requires such a low dose and won't induce an increase in hematocrit due to the fact that the protein is not being delivered systemically. With regard to systemic delivery of EPO, because it is endogenous to the CNS, it has the ability to cross the blood brain barrier and the blood retina barrier and therefore can access the optic nerve for additional neuroprotection. Systemic delivery of EPO has its own advantages, too—it will prevent any further degeneration or inflammation into the eye that would be needed with multiple intravitreal or subretinal injections (Bricker-Anthony et al., 2017; Hernández et al., 2017; Subiras et al., 2012; Sullivan et al., 2011).

EPO has been difficult to utilize as a neuroprotective agent because of its extremely short half life in humans, lasting only about 5-6 hours *in vivo*. Additionally, EpoR trafficking is inefficient such that only 10% of the receptor is actually available on the cell surface so that EPO can even bind to it in the first place (Aghdam et al., 2016; Bunn, 2013; Suresh et al., 2020). The reason for this inefficiency is the fact that transport of EpoR requires the N-terminal portion of JAK-2 to bind to the cytoplasmic region of the ER so that the protein can be properly folded and sorted to the cell surface (Shi et al., 2010). Additionally, if EPO is administered consistently, it can cause increases in hematocrit, which can be detrimental (McCarty et al., 2001; Suresh et al., 2020).

1.18 EPO-R76E

Our lab and others have previously published using viral deliveries of a mutant form of EPO, EPO-R76E. EPO-R76E was a mutation created in our lab by mutating a single amino acid

from an arginine to a glutamate at the 76th position in the active form of the protein. This mutation is equally neuroprotective as wildtype EPO without the increase in hematocrit. The first use of this mutated form of EPO was tested in mouse model of photoreceptor death (Sullivan et al., 2011).

Gene therapy using EPO-R76E has also provided extensive protection in multiple models of glaucoma as well as other neurodegenerative disease models (Bond et al., 2016; Bricker-Anthony et al., 2017; DeJulius et al., 2021; Hines-Beard et al., 2016; Sullivan et al., 2011). Many gene therapy studies employ adeno-associated viruses, which are small, non-enveloped viruses that are nonpathogenic. Recombinant AAV gene therapy involves the removal of two viral genes and then the gene of interest is inserted between the inverted terminal repeats. Their genome is linear, single-stranded DNA. rAAVs are nontoxic and have the ability to transduce cells in a wide range of tissues including but not limited to brain, retina, muscle, liver and lungs (McCarty et al., 2001; Naso et al., 2017; Shin et al., 2012). There are several human serotypes of AAVs (1-12), with AAV2 the primary one of interest in this dissertation (Nickells et al., 2017).

rAAV.EPO-R76E has been used as a neuroprotective in multiple models of glaucoma in our lab. In the well-characterized DBA2/J model as well as in the MOM, systemic rAAV delivery of EPO-R76E was delivered at the same time as IOP was elevated. In the DBA2/J model, rAAV.EPO-R76E treatment preserved visual function, as measured by visual evoked potentials. Ultimately, this paper elucidated that systemic rAAV.EPO-R76E is a potential therapeutic target for glaucoma, as it was delivered at the onset of IOP elevation rather than prior to IOP elevation. In another study from our lab also using DBA2/J mice, systemic rAAV.EPO-R76E was delivered prior to IOP elevation/glaucomatous neurodegeneration; mice that received

rAAV.EPO-R76E had significantly decreased levels of proinflammatory cytokines and increased antioxidant proteins by the time that the mice reached 8 months of age in comparison to controls.

In the recent few years, our lab has sought to move away from systemic delivery of EPO-R76E because of its aforementioned disadvantages, and instead explore options to only deliver EPO to the necessary cells. To allow for sustained release of EPO-R76E after a single intravitreal injection, we and others have explored microparticle-mediated delivery of EPO-R76E. Previous studies have used the poly(lactic-co-glycolic acid)/poly(lactic acid) (PLGA/PLA) microparticle system in a rat model of optic nerve crush and demonstrated efficacy in protecting retinal neurons (DeJulius et al., 2021; Rong et al., 2017; Wang et al., 2012). In this model, a single injection of these microparticles sustained RGCs up to 8 weeks after injury, whereas free EPO would have had to be delivered every 2 weeks to see similar protection. We have also previously published using EPO-R76E formulated into microparticles containing PLGA in a model of blast-indirect traumatic optic neuropathy (DeJulius et al., 2021). In that study, we showed that a single intravitreal injection of these microparticles delivered intravitreally one day after injury protected against optic nerve degeneration and visual function deficits.

1.19 Conclusions and Hypotheses

All in all, glaucoma is a neurodegenerative disease with an unknown etiology that results in the degeneration and eventual death of RGCs (D. J. Calkins, 2012b; Schuster et al., 2020; Weinreb et al., 2014a). Oxidative stress plays an important role in the progression and pathology of neurodegenerative diseases including glaucoma (Ferreira et al., 2011; Saccà & Izzotti, 2008; Tezel, 2006). Additionally, ROS has been shown to be elevated early in disease progression in clinical and experimental glaucoma (Ferreira et al., 2010; Malone & Hernandez, 2007; Saccà &

Izzotti, 2008). Previous studies have shown that antioxidant treatments can be protective in multiple models of glaucoma (Chhunchha et al., 2017; Himori et al., 2013; Inman et al., 2013; Yang et al., 2016). NRF2 is a viable therapeutic target for glaucoma, as its activation leads to upregulation of antioxidant genes that can be used as a defense against increased ROS (Batliwala et al., 2017; Cheng et al., 2017; Cho et al., 2015; Fujita et al., 2017; Himori et al., 2013; Hvozda Arana et al., 2020; Wang et al., 2020; Xu et al., 2015). Sustained release of EPO has been shown to have antioxidant and neuroprotective effects in multiple models of glaucoma; specifically, EPO-R76E allows for similar neuroprotection without clinically relevant increases in hematocrit (Bond et al., 2016; Hines-Beard et al., 2016; Resende et al., 2018; Sullivan et al., 2011; Zhong et al., 2007). EPO has been shown to induce NRF2's nuclear translocation and activation (Genc et al., 2010; Wu et al., 2018; Zakharova et al., 2018).

We sought to first understand the time-course at which ROS markers can be detected in the MOM. Understanding what occurs at early timepoints following IOP elevation but prior to disease pathology would help us to identify a therapeutic window. We also hypothesized that NRF2 would be activated in the MOM prior to axon degeneration and visual function deficits present at later timepoints in disease pathology. We initially expected that NRF2 activation in the MOM would occur primarily via oxidation of its repressor protein, KEAP1, although it would be possible that NRF2 could also be activated via phosphorylation by an upstream signaling molecule including but not limited to PI3K, Akt, MAPK, or JNK. We expected that the lack of functional NRF2 using a knockout mouse would result in a diminished antioxidant response of the retina, and ultimately an exacerbated and accelerated phenotype of glaucomatous neurodegeneration. We then hypothesized that NRF2's activation would occur largely in RGCs, as they are the primary cell types affected by glaucoma pathology, although we also expected to

see some activation of NRF2 in surrounding glial cells. We estimated that overexpression of *Nrf2* would result in neuroprotection in the MOM. Lastly, we expected that upon treatment of EPO-R76E, administered via sustained-release PLGA microparticles, would result in neuroprotection of RGCs via phosphorylation and activation of NRF2.

CHAPTER 2

Retinal Oxidative Stress Activates the NRF2/ARE pathway: An Early Endogenous Protective Response to Ocular Hypertension

This chapter of my thesis is published in *Redox Biology:*

Naguib S, Backstrom JR, Gil M, Calkins DJ, Rex TS. Retinal oxidative stress activates the NRF2/ARE pathway: An early endogenous protective response to ocular hypertension. Redox Biol. 2021 Jun;42:101883. doi: 10.1016/j.redox.2021.101883. Epub 2021 Jan 29. PMID: 33579667; PMCID: PMC8113046.

2.1 Abstract

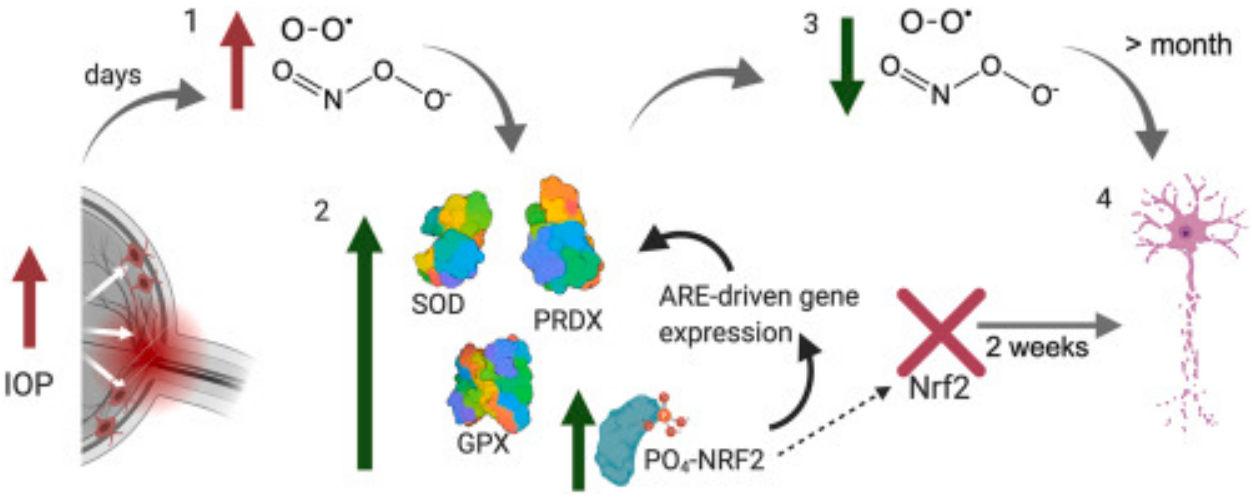

Figure 2.1 Graphical abstract

Oxidative stress contributes to degeneration of retinal ganglion cells and their axons in glaucoma, a leading cause of irreversible blindness worldwide through sensitivity to intraocular pressure (IOP). Here, we investigated early elevations in reactive oxygen species (ROS) and a role for the NRF2-KEAP1-ARE endogenous antioxidant response pathway using microbead occlusion to elevate IOP in mice. ROS levels peaked in the retina at 1- and 2-wks following IOP

elevation and remained elevated out to 5 weeks. Phosphorylation of NRF2 and antioxidant gene transcription and protein levels increased concomitantly at 2-wks after IOP elevation, along with phosphorylation of PI3K and AKT. Inhibiting PI3K or AKT signaling prevented NRF2 phosphorylation and reduced transcription of antioxidant-regulated genes. Ocular hypertensive mice lacking Nrf2 had elevated ROS and a diminished increase in antioxidant gene expression. They also exhibited earlier axon degeneration and loss of visual function. In conclusion, the Nrf2-Keap1-ARE pathway is endogenously activated early in glaucoma due to phosphorylation of NRF2 by the PI3K/AKT pathway and serves to slow the onset of axon degeneration and vision loss in glaucoma. These data suggest that exogenous activation of this pathway might further slow glaucomatous neurodegeneration.

2.2 Introduction

Glaucoma is a group of chronic optic neuropathies characterized by progressive degeneration of retinal ganglion cells (RGCs) and their axons, which transmit visual information to the brain via the optic nerve. Glaucoma is the leading cause of irreversible blindness worldwide and is characterized by age-related sensitivity to intraocular pressure (IOP; Calkins & Horner, 2012; Killer & Pircher, 2018; Weinreb et al., 2014). Current treatments for glaucoma aim to reduce IOP through medical or surgical intervention. Although this is relatively effective, many patients continue to experience vision loss despite these treatments (Goldberg, 2003; Killer & Pircher, 2018; Weinreb et al., 2014a). Our goal is to better understand the molecular mechanisms underlying RGC degeneration and death in glaucoma in order to identify targeted therapies to protect these neurons.

RGCs and their axons are vulnerable to oxidative stress for a variety of reasons including, but not limited to, the lack of myelination along part of the axon resulting in increased metabolic demand, which is compensated for by a larger number of mitochondria (Calkins, 2012; Chrysostomou et al. , 2013; Ko, et al., 2005; Morgan, 2012; Osborne & Del Olmo-Aguado, 2013; Tezel, 2006). Oxidative stress contributes to glaucoma pathogenesis in both animal models of the disease and in patients (Calkins, 2012; Tezel, 2006; Inman et al., 2013; Yang et al., 2016; Zhao et al., 2016). Treatment with the antioxidant a-lipoic acid reduced RGC degeneration and improved axon function in an inherited model of glaucoma (DBA2/J) (Inman et al., 2013), and treatment with valproic acid preserved RGCs in excitatory amino acid transporter 1 knockout mice (GLAST KO), which are often used as a model of normal tension glaucoma (Kimura et al., 2015, 2017a).

The retina responds endogenously to reactive oxygen species (ROS) via multiple mechanisms. For example, the retina increases expression of heat shock proteins and the anti-apoptotic Bcl-2 and Bcl-x genes in response to elevated ROS (Chaudhary et al., 1999; W. Huang et al., 2007; Levin et al., 1997). Hypoxia inducible factor-1□ (HIF-1□) and Nuclear factor erythroid 2-related factor 2 (NRF2) are two transcription factors that regulate the production of antioxidant proteins (Lacher,et al., 2018; Toth & Warfel, 2017). Here we focus on the NRF2/ARE pathway. Under homeostatic conditions, NRF2 remains sequestered in the cytosol of the cell by Kelch-like ECH associated protein 1 (KEAP1), which targets NRF2 for ubiquitin-dependent degradation. Following increases in ROS, KEAP1 is oxidized and undergoes a conformational change resulting in the release of NRF2 and subsequent translocation into the nucleus (Nguyen et al., 2000; Nguyen et al., 2009; Tonelli et al., 2018; Vomhof-DeKrey & Picklo, 2012; Vriend & Reiter, 2015). Nuclear NRF2 interacts with small Maf proteins, and

binds to the antioxidant response element (ARE) to modulate transcription of antioxidant genes. NRF2 can also undergo activation and nuclear translocation via phosphorylation by upstream signaling molecules including, but not limited to, PI3K, AKT, MAPK, JNK and GSK-3b (Bryan et al., 2013; Culbreth & Aschner, 2018; Niture et al., 2014; Peng et al., 2019; Wang et al., 2008)

Nrf2 knockout (KO) mice are more susceptible to RGC death following optic nerve crush and showed an increase in oxidative stress markers after injury in comparison to their wild-type controls (Himori et al., 2013; Koriyama et al., 2010; Koriyama et al., 2013). In another study using the ischemia-reperfusion model of glaucoma, administration of an NRF2 activator was protective against RGC death. Similar findings of increased susceptibility to RGC death in Nrf2 KO mice were found in an ischemia-reperfusion model (Xu et al., 2015). Additionally, overexpression of Nrf2 following optic nerve crush in another study increased antioxidant gene expression and protected against RGC death (Fujita et al., 2017).

In this study, we report that elevation of ROS occurs early after ocular hypertension, weeks before detectable pathology or vision loss in the well-characterized microbead occlusion model of glaucoma (MOM). Further, we show that this elicits an endogenous antioxidant response mediated by NRF2 activation. Somewhat surprisingly, we show that NRF2 phosphorylation is increased; thus, the increase in ARE-driven transcripts is not due solely to oxidation of KEAP1. The increased NRF2 phosphorylation is dependent on upstream activation of PI3K or AKT. Further, the lack of Nrf2 prevents this endogenous response and results in earlier onset of axon degeneration and vision loss. Together, these data suggest that the NRF2/ARE pathway contributes to the slow onset of neurodegeneration after induction of ocular hypertension and that this pathway is a viable therapeutic target for glaucoma therapies.

2.3 Materials and Methods

2.3.1 Mice: C57Bl/6 J (Jackson Labs, Bar Harbor, ME) or B6.129X1-*Nfe2l2*^{tm1Ywk}*/J* mice (Jackson Labs, Bar Harbor, ME) were group-housed, maintained on a 12-h light-dark cycle, and provided food and water ad libitum. All experiments were approved by the Institutional Animal Care and Use Committee of Vanderbilt University. Male and female mice (2-3 months old) were used for this project.

2.3.2 Microbead Occlusion: We elevated IOP bilaterally using occlusion of the anterior chamber with 2 µl injections of 15-µm diameter FluoSpheres polystyrene microbeads (Thermo Fisher, Waltham, MA) as previously described (Sappington et al., 2010; Ward et al., 2014; Bond et al., 2016; Calkins et al., 2018). Additional mice received bilateral injections of an equivalent volume of lactated Ringer's saline solution as controls. Briefly, 1.5 mm outer diameter/1.12 mm inner diameter filamented capillary tubes (World Precision Instruments, Sarasota, FL) were pulled using a P-97 horizontal puller (Sutter Instrument Company, Novato, CA), and the resulting needles were broken using forceps to an inner diameter of ~100 µm. Microbeads were loaded and injected using a microinjection pump (World Precision Instruments, Sarasota, FL). Mice were anesthetized with isoflurane and dilated using topical 1% tropicamide ophthalmic solution (Patterson Veterinary, Devens, MA), and 2 µl (~2,000 microbeads) were injected. The needle was maintained in the injection site for 20 seconds before retraction to reduce microbead efflux. Mice were given topical 0.3% tobramycin ophthalmic solution (Patterson Veterinary, Devens, MA) following injection.

2.3.3 IOP measurements: We measured IOP immediately prior to microbead injection and biweekly thereafter using the Icare TonoLab rebound tonometer (Colonial Medical Supply, Franconia, NH) as previously described (Calkins et al., 2018; Hines-Beard et al., 2016). Mice were anesthetized using isoflurane, and 10 measurements were acquired from each eye within 2 minutes of induction of anesthesia.

2.3.4 *In vivo* electrophysiology: Mice were dark adapted overnight, dilated with 1% tropicamide for 10 minutes and anesthetized with 20/8/0.8 mg/kg ketamine/xylaxine/urethane according to previously published methodology (Naguib et al., 2019; Bernardo-Colón et al., 2018). Mice were placed on heated surface of the ERG system to maintain body temperature. Corneal electrodes with integrated stimulators (Celeris System, Diagnosys LLC, Lowell, MA) were placed on eyes that were lubricated with GenTeal drops. Subdermal platinum needle electrodes were placed in the snout and back of the head at the location of the visual cortex. A ground electrode was placed in the back of the mouse. For VEPs, mice were exposed to 50 flashes of 1Hz, 0.05 cd.s/m^2 white light with a pulse frequency of 1. For ERGs, mice were exposed to flashes of 1 Hz, 1 cd.s/m^2 white light with a pulse frequency of 1. For photopic negative ERGs (PhNR), mice were exposed to 20 continuous flashes of white light on a green background with a pulse frequency of 2. Each experimental group had 12-16 eyes. For ease of comparison, 2-week (wk) wild-type data from Figure 2.2 is reshown in Figure 2.6 to compare to Nrf2 KO mice.

2.3.5 Inhibitor Injections: A subset of mice (n=20) was intravitreally injected with a PI3K inhibitor (Wortmannin, 1ul, 10mM, every 3 days) or vehicle (DMSO). Another subset of mice

(n=20) was injected intraperitoneally with an AKT inhibitor (Ipatasertib, 20mg/kg every other day) or DMSO/saline one week after elevation of IOP.

2.3.6 Dihydroethidum Fluorescence: A dye that fluoresces in the presence of superoxide and, to a lesser extent, hydrogen peroxide, dihydroethidum (DHE), was utilized for these studies as previously described (Bernardo-Colon et al., 2018). Mice were anesthetized with 2.5% isofluorane and intravitreally injected with 1 µl (0.5uM) of DHE (ThermoFisher Scientific, Waltham, MA) diluted in phosphate-buffered saline (PBS) using a 30-gauge Hamilton syringe. Just prior to imaging, mice were anesthetized with ketamine/xylazine and eyes were dilated with 1% tropicamide. Thirty minutes after DHE injection, fluorescence was imaged on a Micron IV retinal imaging microscope (Phoenix Research Labs, Pleasanton, CA) using an FF02-475/50 nm excitation filter (Semrock, Inc. Rochester, NY) and ET620/60X emission filter (Chroma Technology Corp., Bellows Falls, VT). The average intensity of the fluorescence throughout the retina was quantified using ImageJ (Rasband, W.S., 2018). For each experimental group, 6-8 eyes were analyzed. For purposes of comparison, the 2-wk wildtype data from Figure 2.2 is reshown in Figure 2.6 to compare to Nrf2 KO mice.

2.3.7 Tissue collection: For western blots and qPCR, retinas were collected and flash frozen from mice euthanized by anesthetic overdose and cervical dislocation. For immunohistochemistry and optic nerve histology, tissue was collected and incubated in 4% paraformaldehyde for until use at 4^{o}C.

2.3.8 Protein assay: Protein concentrations were determined from 10 □l of retina homogenates with the Pierce BCA Protein Assay Kit (cat#: 23225, ThermoFisher Scientific, Waltham, MA). BSA was used as the protein standard. Absorbance was measured with the plate reader POLARstar Omega (BMG Labtech, Ortenburg, Germany).

2.3.9 Western blot: Single retinas were sonicated in lysis buffer (PBS, EDTA and Halt protease inhibitor) and centrifuged for 30 minutes at 4°C. 4x Laemmli buffer (Bio-rad, cat# 1610747) containing 2-ME was added to the samples and heated for 5 minutes at 95°C. Known amounts of protein (10-20 □g/retina) or protein ladder (cat#1610375, Bio-rad, Hercules, CA) were loaded in 4-20% polyacrylamide gels (Bio-Rad #456-1095). Proteins were transferred onto nitrocellulose using the Bio-Rad trans blot turbo transfer system. Membranes were blocked in 2% BSA in TBS overnight at 4°C. Membranes were incubated in primary antibody (NRF2, pNRF2, SOD2, β-actin, PI3K, pPI3K, Akt, pAkt, JNK, pJNK, GSK3B, pGSK3B, MAPK, pMAPK, SOD3, PRDX6, GPX1, HIF1-a, NQO-1, HO-1) at room temperature with rocking for 2 hours. β-actin was used as the loading control for all experimental groups. After washing, membranes were incubated with secondary antibody (IRDye 800CW Donkey anti-rabbit, #926-32213 or IRDye 680CW Donkey anti-mouse, #926-68022,1:5000 in 1% BSA/TBS) at room temperature for 1 hour. After washing, blots were imaged with a Bio-Rad ChemiDoc system. Band density was quantified by scanning the blot using Adobe Photoshop. Each band was selected with the same frame and set measurements were used to obtain the gray mean value for each. Band intensity measurements from protein of interest were divided by band intensity measurements of loading control (b-actin). Each experimental group had 5 retinas. For purposes of comparison, the 2-wk wild-type data in Figure 2.3 was reshown in Figure 2.6 to compare to Nrf2 KO data.

2.3.10 Co-immunoprecipitations: Single retinas were sonicated in 300 ml lysis buffer (1% SDS, 5 mM EDTA and Halt protease inhibitor) and centrifuged for 30 minutes at 4^{o}C. Supernatant was collected and placed on ice. Lysates were pre-cleared using normal serum for 1 hour on ice. 1-5 ml of antibody was added after supernatant was separated in a clean microcentrifuge tube and incubated overnight at 4^{o}C rocking. 70 ml Protein G-coupled Sepharose beads were added on ice to each sample and incubated at 4^{o}C under agitation for 4 hours. Beads were washed with lysis buffer 3 times to remove nonspecific binding. Then 50 ml of beads were eluted by using 50 ml of 2x SDS with DTT. Samples were boiled at 95^{o}C for 5 minutes and analyzed via western blot as stated above.

2.3.11 Quantitative PCR: Retinas were extracted from euthanized mice and placed immediately onto dry ice and stored at $^{-}$80^{o}C until homogenized by hand using 1.5ml-capacity pestles (cat#46C911, Grainger, Nashville, TN). RNA was extracted using a Qiagen RNeasy kit (Valencia, CA) as previously described (Hines-Beard et al., 2016). RNA concentration and purity were measured on a spectrophotometer. First-strand complementary DNA (cDNA) was synthesized from 250 ng of RNA from each sample using the Superscript III First-Strand synthesis system and oligo-dT20 primers (Invitrogen, Waltham, MA). Quantitative PCR (qPCR) was performed using Power SYBR green master mix (Applied Biosystems, Waltham, MA). All primer sequences were obtained from previous studies; we assessed the following: *Nrf2*, *Prdx6*, *Gpx1*, *Txn1*, *Hif1α*, *Sod2* and *Sod3* (see Table 2). All qPCR was performed in duplicate using an Applied Biosciences 7300 real-time PCR system (Waltham, MA). The assay was performed in triplicate on 5 retinas per condition. The amplification threshold was set using system software.

Relative changes in gene expression were determined using GAPDH as the internal control. Each experimental group had 5 retinas.

2.3.12 PCR microarray: The same cDNA used for the quantitative PCR analysis was also used in an RT2 Profiler mouse oxidative stress PCR array kit per manufacturer's instructions (Qiagen, Valencia, CA) as previously described (Hines-Beard et al., 2016). The cDNA from each group was pooled to have sufficient material for the assay. Each experimental group had 5 pooled retinas.

2.3.13 Immunohistochemistry: Eyes stored in paraformaldehyde were embedded in Tissue Freezing Medium (Electron Microscopy Sciences) overnight, and 10-µm-thick sections were collected on a cryostat. Cross sections were incubated overnight at 4°C in PBS containing 5% normal donkey serum (Millipore Sigma, #D9663, St. Louis, MO), 0.1 % Triton X-100, 0.5 % BSA, and 0.1 % sodium azide (PBTA). Retina sections were then incubated overnight at 4°C with rabbit anti-nitrotyrosine (Millipore Sigma, Burlington, MA #AB5411; 1:400) and mouse anti-NeuN (Millipore Sigma # MAB377X, 1:400) in PBTA, rinsed with PBTA, and then incubated overnight at 4°C with Alexa Fluorophore donkey secondary antibodies (ThermoFisher anti-rabbit 488 #R37118; 1:200, and anti-mouse 555 #R37118; 1:200 in PBTA. After extensive washing, sections were mounted with DAPI (ThermoFisher Scientific, Waltham, MA). Slides were imaged on a Nikon Eclipse epifluorescence microscope (Nikon, Melville, NY). All images were collected from the same retinal region with identical magnification, gain and exposure settings. Fluorescence intensity was quantified via ImageJ as previously described (Naguib et al. 2019). A rectangle was selected around the region of interest, channels were split for multiple

antibodies, threshold was adjusted, noise was de-speckled and fluorescence intensity was measured. Fluorescence intensity was normalized to saline-injected mice. Each experimental group included 5 eyes.

2.3.14 Optic nerve counts: Optic nerves were post-fixed in glutaraldehyde followed by Resin 812 embedding and Araldite 502 (cat#: 14900 and 10900 respectively, Electron Microscopy Sciences, Hatfield, PA) according to previously published protocols (Naguib et al., 2019, Bernardo-Colon et al., 2018, Hines-Beard et al., 2012). Leica EM-UC7 microtome was used to collect 1 mm thick sections of the optic nerves. Sections were then stained with 1% paraphenylenediamine and 1% toluidine blue and were imaged on a Nikon Eclipse Ni-E microscope using 100x oil immersion objective (Nikon Instruments, Melville, NY). The optic nerves were montaged into a 5 x 5 image using the Nikon Elements software to scan a large image. We used the Counting Array and Better Cell Counter plugins to ImageJ, which creates a grid of nine squares overtop the montaged optic nerve. We manually counted healthy and degenerating axons, which are color-coded by the plugins. Degenerative axon profiles were identified by dark paraphenylenediamine staining due to collapsed myelin or loose myelin (onioning) surrounding the axon. A grid was used to avoid bias, by always counting in the same squares, using a cross configuration. Twenty percent of the optic nerve cross-sectional area was counted and the total was multiplied by five to estimate total and degenerating axons within the nerve. Each experimental group included 4-5 nerves. For purposes of comparison, the 2-wk wildtype data in Figure 2.2 was reshown in Figure 2.6 to compare to Nrf2 KO mice data.

2.3.15 Data Analysis: All statistical analyses were performed using GraphPad Prism software (La Jolla, CA). A one-way ANOVA with a Bonferroni post hoc test ($a = 0.05$) was used to analyze western blot quantification, IHC fluorescence quantification, ON quantification data, and ERG/VEP latencies and amplitudes. A one-way ANOVA and Dunnett's multiple comparisons post hoc test ($a = 0.05$) were used to analyze the qPCR results. Means and standard deviation were calculated for each data set.

2.4 Results

2.4.1 Reduction in PhNR precedes axon degeneration and VEP deficits

After injection of microbeads, IOP remained elevated for the duration of the study (Figure 2.1A). When IOP began decreasing in a subset of mice, we reinjected microbeads (arrow in Figure 2.1A). IOP elevation caused a reduction in the VEP amplitude 5-wks later ($p<0.0001$, Figure 2.1B, C) in agreement with previous studies from our lab (Bond et al., 2016; Hines-Beard et al., 2016b). In comparison, the VEP amplitude was unaffected at 2-wks post-IOP elevation (Figure 2.1C). The total number of axons was decreased and the number of degenerative axons was increased in the 5-wk post-IOP elevation group in comparison to saline-injected controls ($p=0.0011$, Figure 2.1D-F), similar to our previous studies (Bond et al., 2016; Calkins et al., 2018; Hines-Beard et al., 2016). In contrast, at 2-wks post-IOP elevation, there was no evidence of axon degeneration or axon loss in the ocular hypertensive optic nerves as compared to saline controls (Figure 2.1D-F).

The VEP is recorded from the visual cortex and thus does not directly measure activity from the optic nerve. A direct measure of RGC physiological function might be more sensitive to glaucomatous changes. This is supported by recently demonstrated changes in single cell RGC

physiology at 2-wks post-IOP elevation (Risner et al., 2018). Therefore, we measured the photopic negative response (PhNR), which is a part of the cone ERG pathway. We detected a significant decrease in the PhNR amplitude at both 2-wks (n=12) and 5-wks (n=14) post-IOP elevation in comparison to saline-injected controls, $p=0.0019$ and $p<0.001$, respectively (Figure 2.1G, H). PhNR latency was unaffected at 2-wks post-IOP elevation, but was increased at 5-wks ($p=0.0441$, Figure 2.1I).

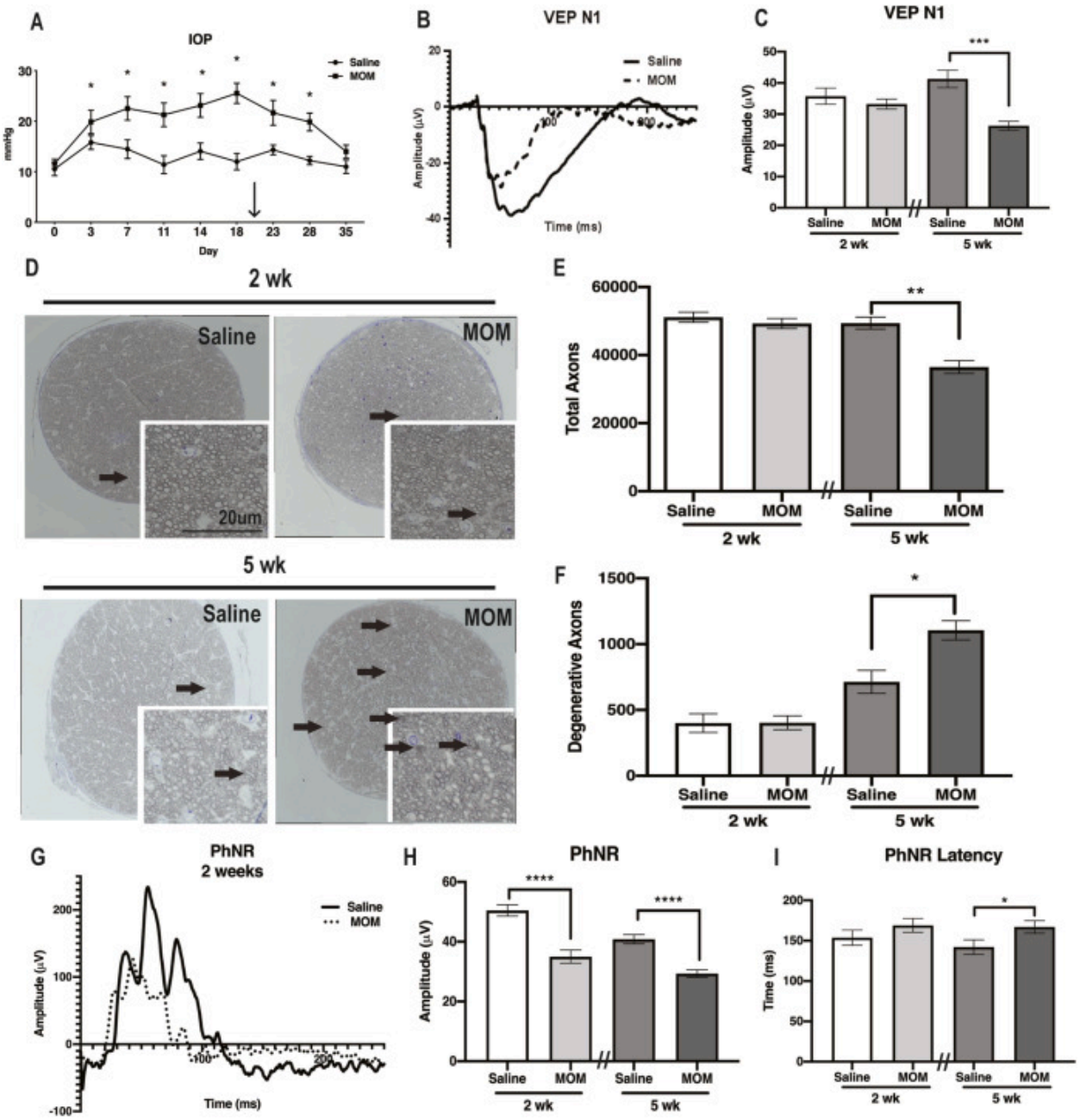

Figure 2.2. Visual function and optic nerve structure at 2- and 5-weeks post-IOP elevation. A) IOP levels over time, arrow indicates re-injection of microbeads, *p < 0.05. B) Representative VEP N1 waveforms, showing decreased amplitude in 5wk MOM-injected mice. C) Quantification of VEP N1 amplitude, ***p < 0.001. D) Representative micrographs of optic nerves, insets show higher magnification. Scale bar applies to all insets. Arrows indicate degenerative axons. E) Quantification of total axons in the optic nerves, showing a decrease only at 5 wk post-IOP elevation, **p < 0.01. F) Quantification of number of degenerative axons, showing an increase at 5 wks, *p < 0.05. G) Representative waveforms of photopic negative response (PhNR) amplitude in saline and 2-week post-IOP elevation mice. H) and I) Quantification of the PhNR amplitude and latency, showing decreases in amplitudes at both timepoints and an increase in latency at 5-wks, *p < 0.05, ****p < 0.0001.

2.4.2 Increased ROS and an endogenous retinal antioxidant response occur early in ocular hypertension

The level of retinal superoxide was increased at 1-wk (n=12) and 2-wks (n=8) post-IOP elevation in comparison to saline-injected controls, based on DHE fluorescence, $p<0.0001$ for both (Figure 2.2A, B). DHE fluorescence was elevated to a lesser extent at 3- and 4-wks post-IOP elevation (n=6 eyes/group, $p=0.0086$ and $p=0.0048$, respectively) (Figure 2.2A, B). As a further assessment of oxidative stress, we immunolabeled with nitrotyrosine (Figure 2.2C). Nitrotyrosine immunofluorescence was detected specifically within the ganglion cell layer (GCL) at all timepoints post-IOP elevation (Figure 2.2C). To determine if the anti-nitrotyrosine labeled astrocytes or neurons, we co-labeled with NeuN (Figure 2.2C, inset). Co-labeling was present indicating that nitrotyrosine was increased in the neurons of the GCL (Figure 2.2C inset). Quantification of the anti-nitrotyrosine fluorescence showed a statistically significant increase in all MOM groups compared to saline controls (n=5 eyes/group, $p<0.0001$, $F=51.6$, Figure 2.2D). Nitrotyrosine fluorescence increased significantly between 1- and 5-wks post-IOP elevation ($p=0.0015$, Figure 2.2D) but not between 2- and 5-wks.

Next, we wanted to determine if the retina endogenously responds to the increases in ROS. Using an oxidative stress PCR array, we detected increased expression of the antioxidant enzymes *Prdx6, Gpx1, Gpx2, Gpx5, Gpx6, Gpx7, Gsr, Sod1* and *Sod3* that was greatest at 2-weeks post-IOP elevation (Figure 2.2E-G). Using qPCR, we confirmed a statistically significant increase in expression for *Prdx6* ($p=0.0094$), *Sod3* ($p=0.0436$) and *Gpx1* ($p=0.0148$) as compared to saline-injected controls (Figure 2.2H). In order to determine if there was also an increase at the protein level, we performed western blot analysis for these three representative antioxidant enzymes. PRDX6 was increased at 2-wks post-IOP elevation (n=5 retinas/group,

p=0.0002, F=23.72) (Figure 2.2I, J). Both GPX1 and SOD3 were increased at both 1- and 2- wks post-IOP elevation in comparison to saline-injected controls (n=5 retinas/group, p=0.0014, F=14.44 and p=0.0013, F=11.78, respectively) (Figure 2.2I, K, L).

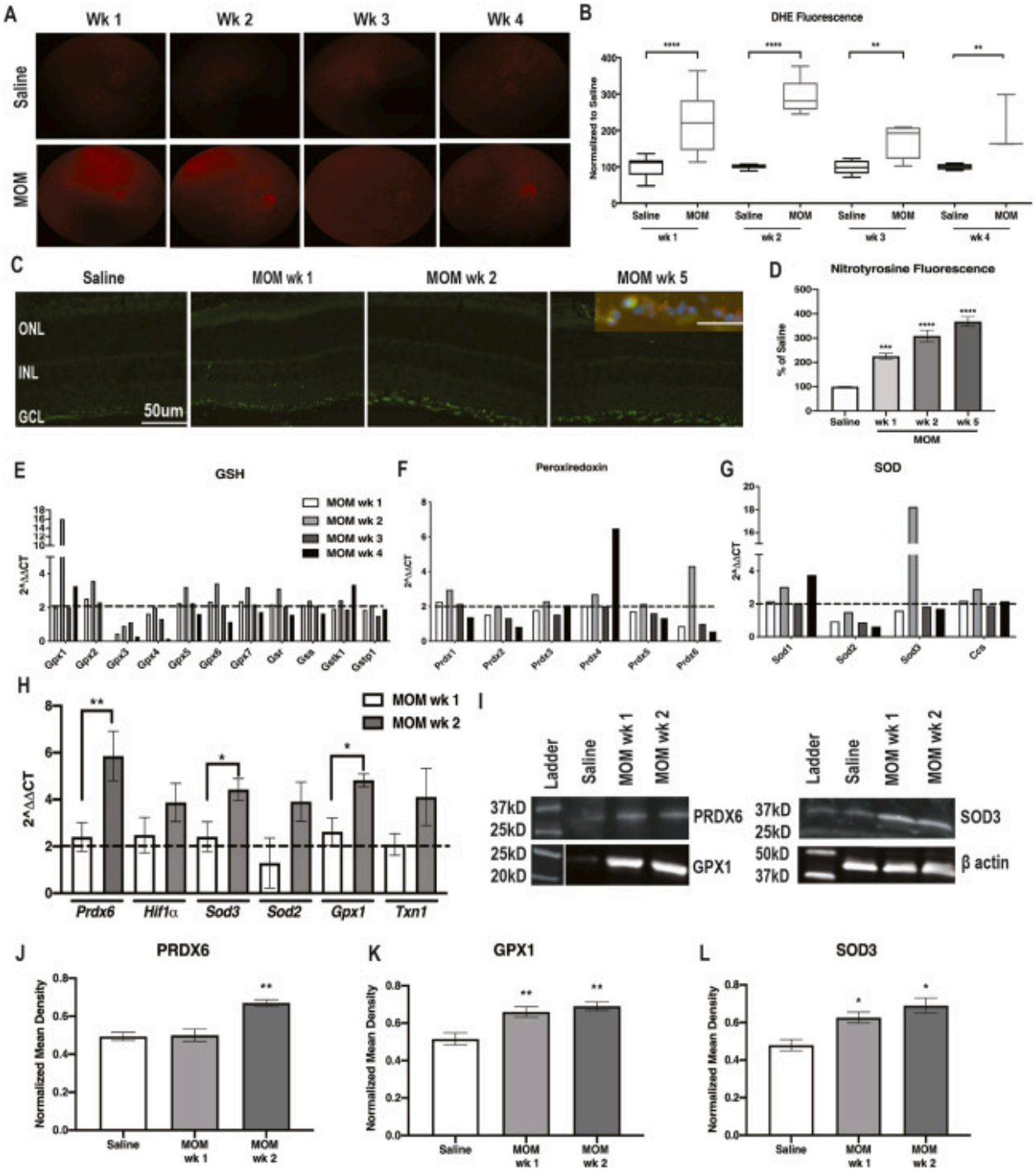

Figure 2.3. ROS and antioxidant proteins increased at 1-wk and 2-wks post-IOP elevation. A) Representative fundus images of DHE fluorescence in all groups. B) Quantification of DHE fluorescence at 1–4 wks post-IOP elevation in comparison to saline-injected controls, showing increases in the microbead injected mice at all time points, **p < 0.01, ****p < 0.0001. C) Fluorescence micrographs of retinas labeled with DAPI (blue) and nitrotyrosine (green). Inset shows double-labeling with anti-nitrotyrosine (green) and anti-NeuN (red). D) Quantification of nitrotyrosine immunofluorescence showing increases at all timepoints after IOP elevation, ***p < 0.001, ****p < 0.0001. E-G) Quantification of fold changes in PCR microarray for: E) GSH-related genes; F) Peroxiredoxin-related genes; and G) SOD-related genes. Dotted line indicates threshold for increase compared to saline. H) Confirmatory qPCR for fold change over saline in antioxidant gene transcription, *p < 0.05, **p < 0.01. I) Representative western blots for β-actin, PRDX6, SOD3 and GPX1. J-L) Quantification of PRDX6, SOD3 and GPX1, respectively, after normalization to β-actin, *p < 0.05, **p < 0.01. (For interpretation of the references to color in this figure legend, the reader is referred to the Web version of this article.)

2.4.3 NRF2 is released from KEAP1 and activated via phosphorylation

Since one of the major pathways that controls expression of these genes is the NRF2/KEAP1/ARE pathway, we next investigated activation of this pathway in ocular hypertension. Nrf2 mRNA levels trended down at 2-wks post-IOP elevation, but did not reach statistical significance (n=5 retinas/group, p=0.33; Figure 2.3A). There was also no difference in NRF2 protein levels at any timepoint assessed as compared to saline-injected controls, (n=5 retinas/group, p=0.97, F=0.0769) (Figure 2.3B, C). NRF2 can become activated either by oxidation of its repressor protein, KEAP1, which targets the protein for degradation via ubiquitination (Huang et al., 2015; Nguyen et al., 2009; Niture et al., 2014; Vriend & Reiter, 2015), or by phosphorylation of NRF2 (pNRF2). We detected a significant, transient, increase in NRF2 phosphorylation at 2-wks post-IOP elevation in comparison to all other groups (n=5 retinas/group, p<0.0001, F=23.36, Figure 2.3D, E). We used co-immunoprecipitation to assess the amount of NRF2 bound to its repressor protein, KEAP1. There was no difference in total KEAP1 protein levels in saline-injected controls or at any timepoint post-IOP elevation (n=5 retinas/group, p=0.9701, F=0.0305) (Figure 2.3F, G). In addition, the association between NRF2

and KEAP1 was decreased in the ocular hypertensive mice as compared to saline controls (p=5 retinas/co-IP; p<0.0001, F=26.72; Figure 2.3F, H). There was a slight, but statistically significant increase in association between KEAP1 and NRF2 at 2-wks than at 1-wk (p=0.0155, Figure 2.3F, H).

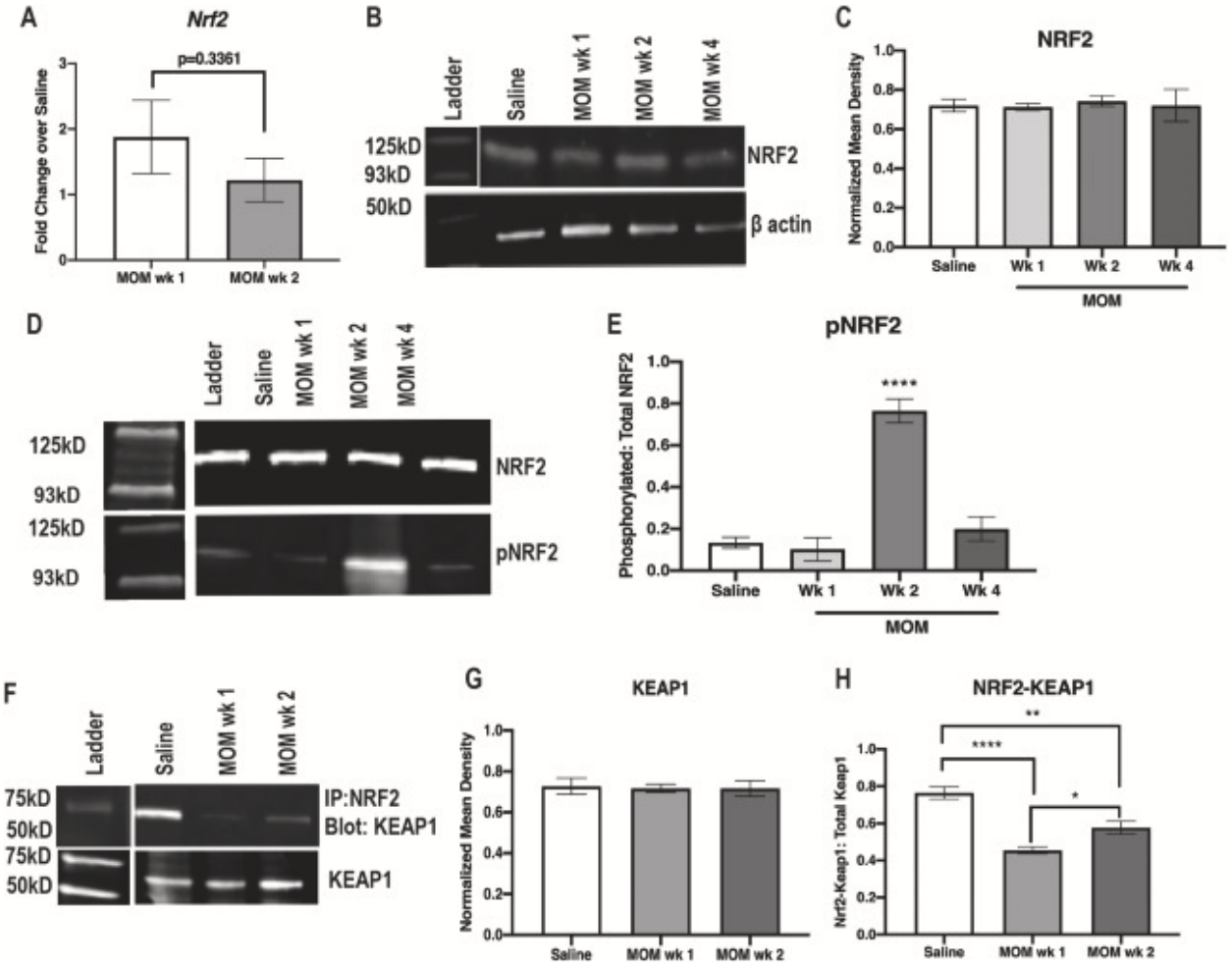

Figure 2.4. Nrf2 activation following ocular hypertension. A) Quantification of *Nrf2* mRNA. B) Representative western blots of NRF2. C) Quantification of NRF2 Western blot after normalization to β-actin. D) Representative western blots for total and phosphorylated NRF2. E) Quantification of pNRF2 after normalization to total NRF2, ****p < 0.0001. F) Representative KEAP-1 western blots with or without immunoprecipitation of NRF2. G, H) Quantification of total KEAP-1. I) Quantification of KEAP-1 that immunoprecipitated with NRF2, *p < 0.05, **p < 0.01, ****p < 0.0001.

2.4.4 NRF2 is activated by AKT/PI3K signaling

Several upstream signaling molecules can phosphorylate NRF2, including but not limited to, PI3K, AKT, JNK, GSK3b and ERK (Bryan et al., 2013; Khan et al., 2018; Niture et al., 2014; Wang et al., 2008). There were no differences in total to phosphorylated GSK3b, JNK, or ERK at 1- or 2-wks post-IOP elevation as compared to saline controls (data not shown). In contrast, phosphorylated AKT (pAKT) was significantly increased at 1- and 2-wks post-IOP elevation in comparison to saline injected controls (n=5 retinas/group, p=0.0185, F=6.416) (Figure 2.4A, B). In order to determine if NRF2 activation was dependent on phosphorylation by AKT, we treated ocular hypertensive mice with the AKT inhibitor, Ipatasertib, intraperitoneally at 7, and 10 days post-IOP elevation and collected retinas at 2-wks post-IOP elevation (n=10 mice/group) (Figure 2.4C). Ipatasertib targets the ATP-binding domain that targets active pAKT (Saura et al., 2017). Inhibition of pAKT prevented the increase in gene expression of *Gpx1* and *Txn1* (p=0.0019 and p=0.0042 respectively, Figure 2.4D). Additionally, Ipatasertib treatment reduced phosphorylation of NRF2 (p= 0.0009, Figure 2.4E, F). Further, Ipatasertib treatment prevented increases in PRDX6 (p=0.0015), GPX1 (p=0.0001) and SOD3 (p=0.0002) levels in the ocular hypertensive mice (Figure 2.4G-J).

Phosphorylation of PI3K (pPI3K) was also significantly increased at 1- and 2-wks post-IOP elevation in comparison to saline-injected controls (p<0.0001, F=130.5; Figure 2.5A, B). In order to determine if NRF2 activation following ocular hypertension is dependent on phosphorylation by PI3K, we treated with the PI3K inhibitor, Wortmannin, intravitreally at 7 and 10-days post-IOP elevation and then collected at 2-wks (Figure 2.5C). Wortmannin inactivates PI3K activity by forming a covalent adduct with Lys802 of PIK3CD (Wymann et al., 1996). The inhibitor prevented the increase in expression of *Prdx6* and *Sod3*, p=0.0397 and p=0.0105,

respectively (Figure 2.5D). NRF2 phosphorylation was also reduced in the inhibitor-treated animals as compared to vehicle controls ($p<0.0001$, Figure 2.5E, F). Further, there was a lack of increase in levels of PRDX6 ($p=0.0231$), GPX1 ($p=0.0209$) and SOD3 ($p=0.0006$) in Wortmannin injected animals (Figure 2.5G-J).

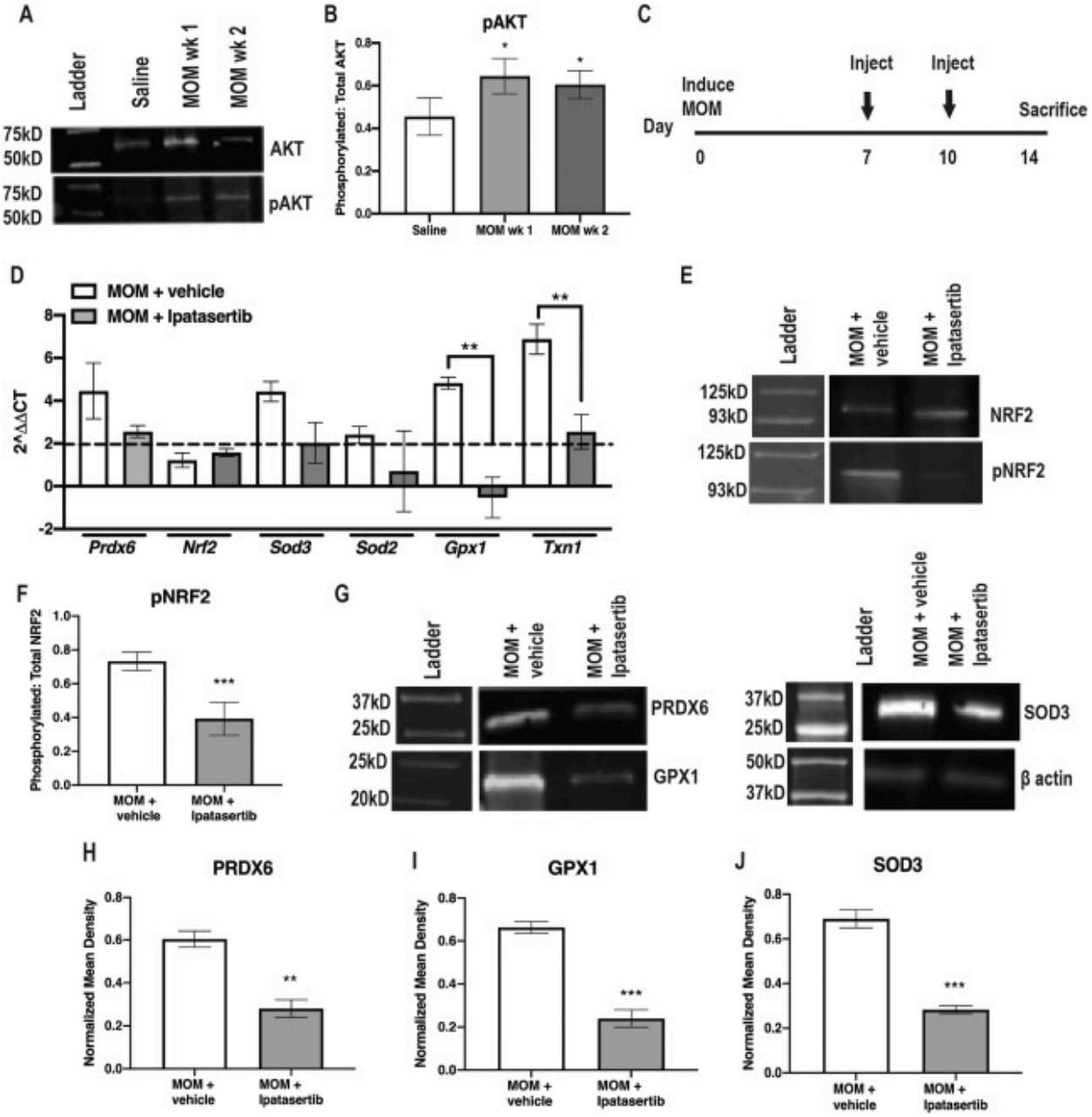

Figure 2.5. AKT-dependent NRF2 phosphorylation. A) Representative western blots of AKT and pAKT B) Quantification of pAKT to total AKT, *p < 0.05. C) Experiment timeline. D) Representative Western blot of phosphorylated NRF2 to total NRF2. E) Quantification of pNRF2 to total NRF2, ***p < 0.001. F) Quantification of antioxidant gene transcription shown as fold change over saline, **p < 0.01. G) Representative western blots for β-actin, PRDX6, SOD3 and GPX1. H-J) Quantification of PRDX6, GPX1 and SOD3, respectively, after normalization to β-actin, **p < 0.01, ***p < 0.001.

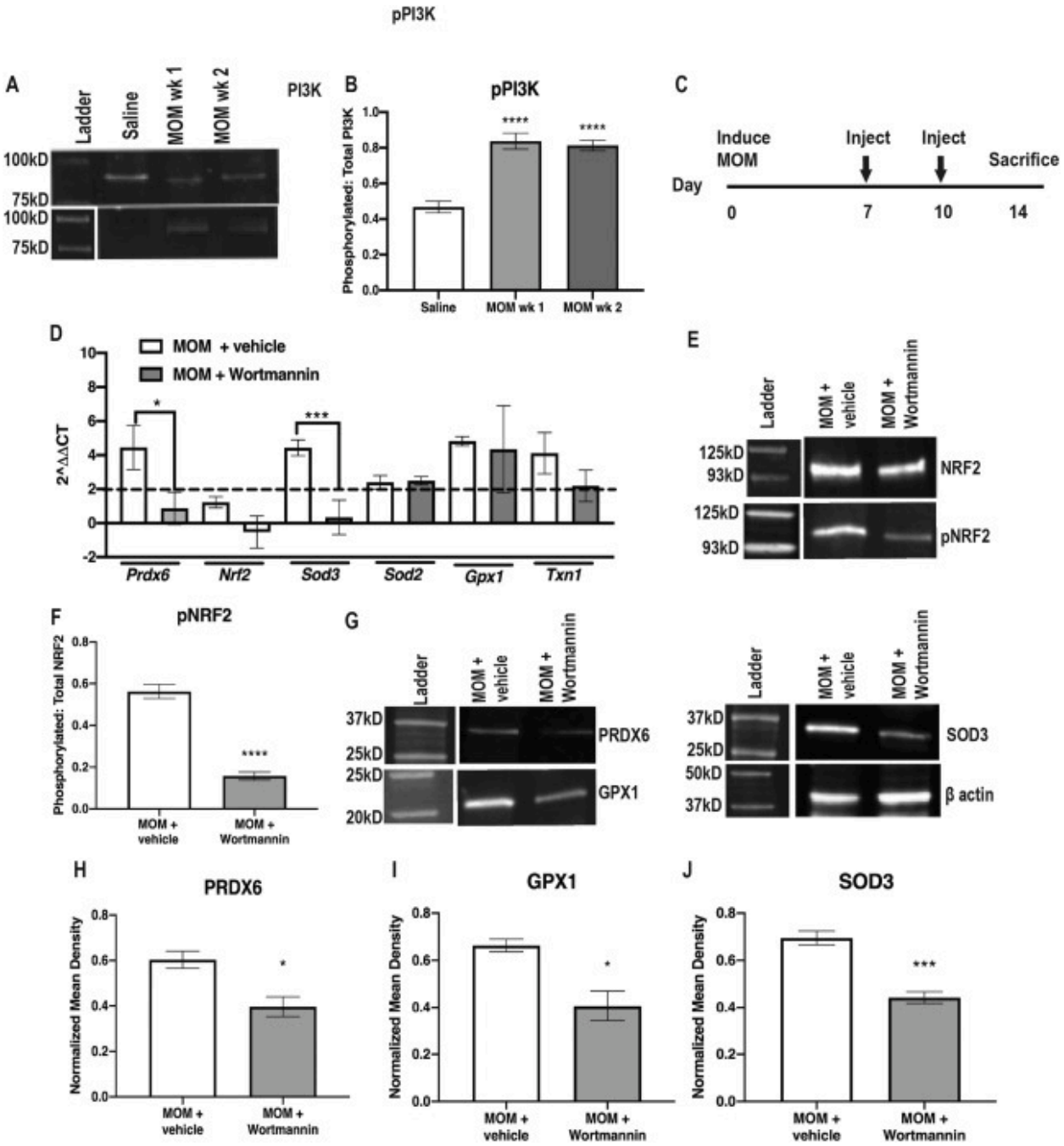

Figure 2.6. PI3K-dependent NRF2 phosphorylation. A) Representative western blots of PI3K and pPI3K B) Quantification of pPI3K to total PI3K, ****p < 0.0001. C) Experiment timeline. D) Representative western blots of pNRF2 to total NRF2. E) Quantification of pNRF2 to total NRF2, ****p < 0.0001. F) Quantification of antioxidant gene transcription shown as fold change over saline, *p < 0.05, ***p < 0.001. G) Representative western blots for β-actin, PRDX6, SOD3 and GPX1. H-J) Quantification of PRDX6, GPX1 and SOD3, respectively, after normalization to β-actin, *p < 0.05, ***p < 0.001.

2.4.5 Ocular hypertensive NRF2 KO mice have earlier onset axon degeneration

Since antioxidant protein expression can be induced through other, non-NRF2 mediated pathways, we used Nrf2 KO mice to assess the importance of this pathway on the endogenous antioxidant response of the retina. Nrf2 KO mice are highly susceptible to oxidative stress and accelerated neurodegeneration (Calkins et al., 2009; Dinkova-Kostova et al., 2018; Nakagami, 2016). In comparison to the wildtype counterparts, there was a significant increase in DHE fluorescence in the saline-injected Nrf2 KO mice, p=0.0001 (Figure 2.6A, B). Interestingly, there was no difference in the level of DHE fluorescence between the saline and microbead injected Nrf2 KO mice, p=0.1867 (Figure 2.6A, B). Out of the six antioxidant proteins we assessed, gene expression was not elevated in four of them. Further, the levels of gene expression in the Nrf2 KO retinas were statistically significantly lower than in the wild-type retinas for: *Prdx6* (p=0.0067), *Sod3* (p=0.054), *Sod2* (p=0.0220), *Gpx1* (p=0.0003) (Figure 2.6C). Expression levels of two of the antioxidant proteins, Hif1a and Sod3, were still elevated compared to the Nrf2 KO saline group. Similarly, protein levels of PRDX6, GPX1, and SOD3 were not increased in Nrf2 KO ocular hypertensive mice as compared to their saline controls, unlike in wild-type mice at 2-wks post-IOP elevation (Figure 2.6D-G). In fact, basal levels of these proteins were also reduced in the Nrf2 KO saline-injected controls compared to the saline-injected wild-type controls (p=0.0349, p=0.0312, and p=0.054 for PRDX6, GPX1, and SOD3, respectively; Figure 2.6E-G).

Next, we assessed if this lack of endogenous antioxidant response increased the susceptibility of the RGC axons to degeneration following IOP elevation. Degenerative axons were present in the optic nerves of both the saline and microbead injected Nrf2 KO mice unlike in the wild-type mice (Figure 2.6H). Quantification of the number of total optic nerve axons showed fewer axons in the microbead-injected Nrf2 KO mice in comparison to Nrf2 KO saline-injected controls, $p=0.0054$ (Figure 2.6I). There was no difference between the wildtype or Nrf2 KO saline-injected controls, $p=0.6966$ (Figure 2.6I). More degenerative axons were detected in the optic nerves of Nrf2 KO ocular hypertensive mice in comparison to the Nrf2 KO saline-injected controls, $p=0.0001$ (Figure 2.6J). Notably, there was also an increase in degenerative axons in the Nrf2 KO saline-injected mice in comparison to the wildtype saline controls, $p=0.0263$ (Figure 2.6J).

Similarly, there was a trend but no statistically significant difference in the VEP amplitude between the Nrf2 KO groups (n=14-16 eyes for wildtype groups, n=8-12 eyes for Nrf2 KO groups, $p=0.2095$) (Figure 2.6K). In contrast, the VEP amplitude of the Nrf2 KO mice was reduced in comparison to the wildtype counterparts ($p=0.0093$, saline and $p<0.0001$, microbead groups) (Figure 2.6K). We also detected a decrease in the ERG b-wave amplitude, a measure of bipolar cell function, in the Nrf2 KO mice as compared to the wild-type mice at 2-wks post-IOP elevation ($p<0.0001$ and $p=0.002$ for saline and microbead injected, respectively; data not shown). And, similar to the VEP results, there was no difference in the b-wave amplitudes between the Nrf2 KO saline-injected and microbead-injected mice ($p=0.5359$; data not shown). Since the PhNR was reduced at 2-wks after microbead-injection in wild-type mice, we expected the amplitude to be decreased in the microbead-injected Nrf2 KO mice. However, while there was a trend, there was not a statistically significant difference in the PhNR amplitude between

the Nrf2 KO saline-injected and the Nrf2 KO microbead-injected mice, p=0.1472 (Figure 2.6L). Similar to the VEP results, the Nrf2 KO saline-injected and microbead-injected mice had a significantly decreased amplitude in comparison to their respective wildtype controls ($p<0.0001$, saline and $p=0.0023$, microbead groups) (Figure 2.6L).

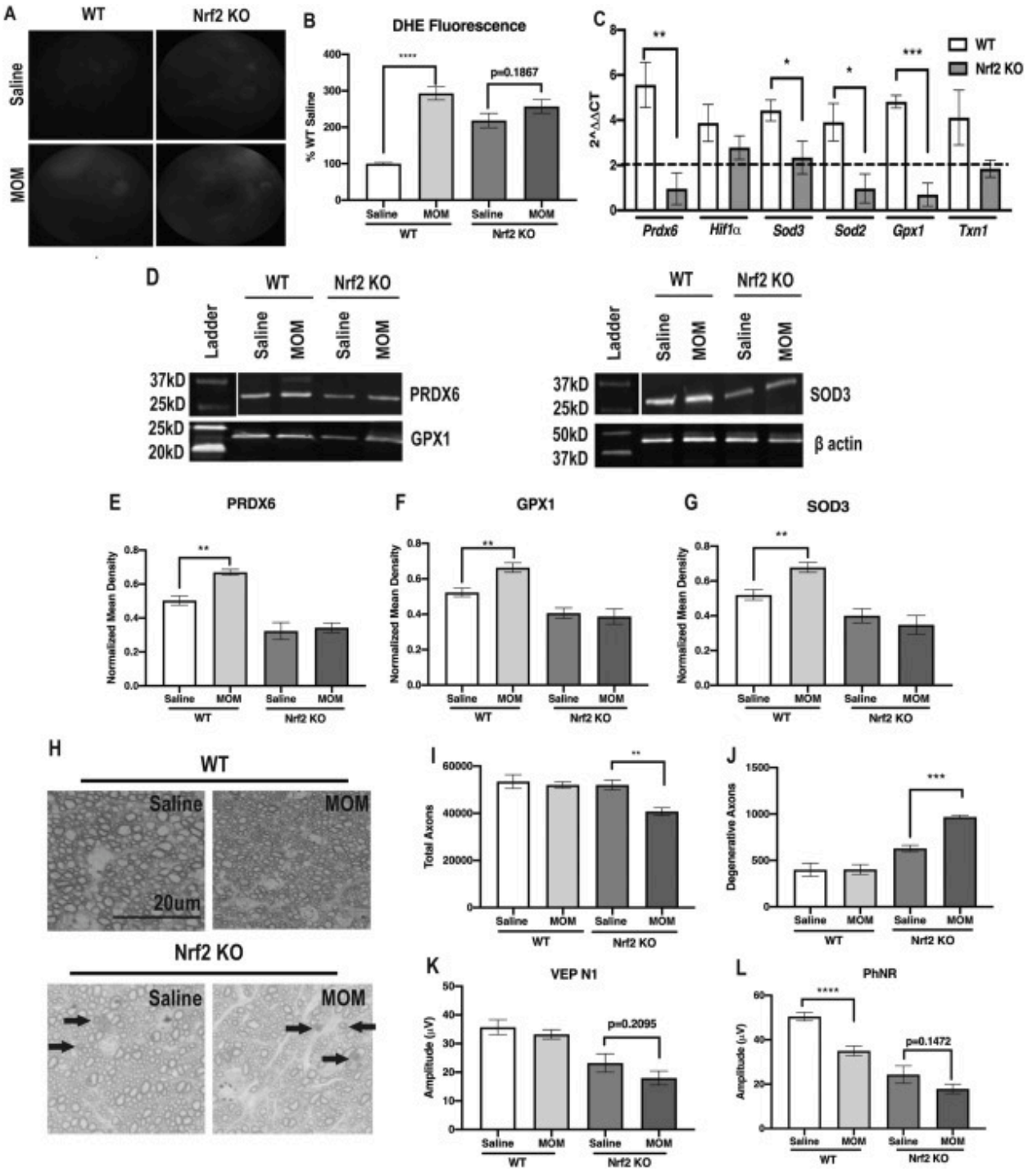

Figure 2.7. Decreased antioxidants and increased ROS, axon degeneration, and visual function deficits in ocular hypertensive Nrf2 KO mice. A) Representative fundus images of DHE fluorescence in saline and microbead-injected wildtype and Nrf2 KO mice. B) Quantification of DHE fluorescence at 2-wks post-IOP elevation in both strains of mice. C) Quantification of antioxidant gene transcription shown as fold change over respective saline groups, *$p < 0.05$, **$p < 0.01$, ***$p < 0.001$. D) Representative western blots for β-actin, PRDX6, SOD3 and GPX1. E-G) Quantification of PRDX6, GPX1 and SOD3, respectively, after normalization

to β-actin, **p < 0.01. H) Representative micrographs of wildtype and Nrf2 KO optic nerves at 2-wks post-IOP elevation. Scale bar applies to all micrographs. Arrows indicate degenerative axons. I) Quantification of total axons in the optic nerves, showing a decrease only in ocular hypertensive Nrf2 KO mice, **p < 0.01. J) Quantification of number of degenerative axons, showing an increase in ocular hypertensive Nrf2 KO mice, ***p < 0.001. K) Quantification of the N1 amplitude of the VEP. L) Quantification of the PhNR amplitude. Note: all wild-type data shown in this Figure was copied from Fig. 2.2 for purposes of comparison.

2.4.6 Role of a compensatory mechanism in Nrf2 KO mice

One possible explanation for the lack of statistically significant deficit in the PhNR in the microbead-injected Nrf2 KO mice compared to the saline-injected Nrf2 KO mice is the presence of a partially effective compensatory mechanism. The ARE can be activated independent of NRF2 (for review see Raghunath et al., 2018). For example, NRF1 can act in place of NRF2 to increase gene expression of Nqo-1 and Ho-1, among others. Additionally, HIF-1α and HIF-1β comprise a complex that, when bound, can mediate transcription of a variety of genes downstream the Hypoxia Response Element, independent of the ARE (Blancher & Harris, 1998; Dengler et al., 2014; Toth & Warfel, 2017). Similar to how NRF2 senses and responds to increases in ROS, the HIF complex can sense changes in oxygen in its environment and can upregulate transcription of genes such as erythropoietin, VEGF, iNOS and GLUT-1. We and others have previously demonstrated that erythropoietin is neuroprotective in glaucoma models (Bond et al., 2016; Ding et al., 2016; Hines-Beard et al., 2016; Resende et al., 2008; Sullivan et al., 2011; Zhong et al., 2007).

The levels of HIF-1α protein were increased in both the Nrf2 KO groups in comparison to the wildtype controls (n=5 retinas/group, p=0.0276, saline and p=0.0021 microbead groups) (Figure 2.7A, B). There was no difference between the saline and microbead-injected Nrf2 KO groups (p=0.434). The levels of NQO-1 and HO-1 were decreased in Nrf2 KO mice in comparison to wildtype controls (NQO-1: p=0.0048 saline and p=0.0085 microbead groups; HO-

1: p=0.0013 saline and p=0.0003 microbead groups) (Figure 2.7A, C). There was no significant difference in NQO-1 levels between the Nrf2 KO saline or microbead-injected groups, although levels seemed to trend up in the microbead injected mice (p=0.205).

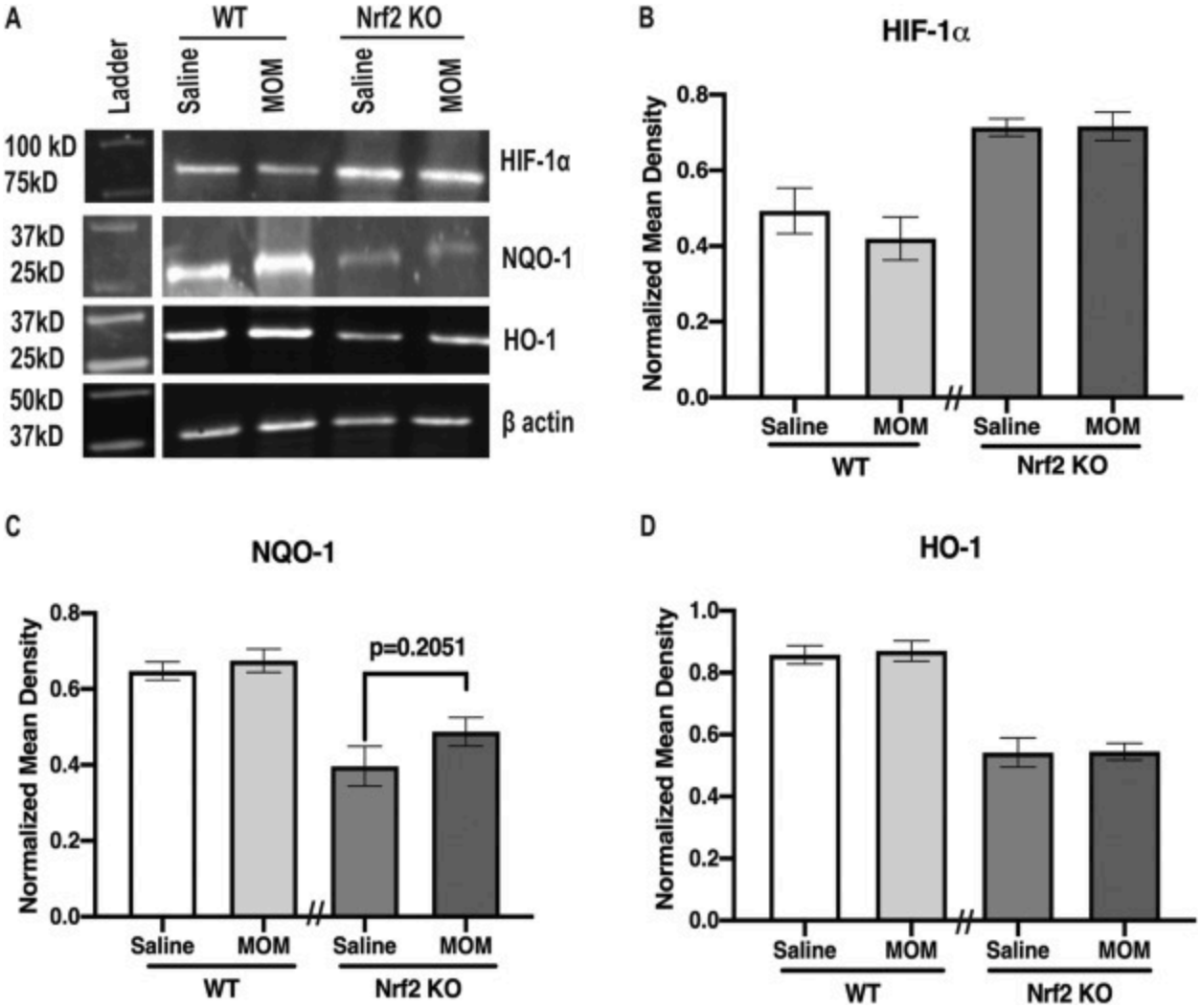

Figure 2.8. Assessment of possible compensatory pathways. A) Representative western blots of HIF-1α, NQO-1, HO-1 and β-actin. B - D) Quantification of HIF-1α, NQO-1 and HO-1 western blots, respectively, after normalization to β-actin. HIF-1α was increased in both Nrf2 KO groups in comparison to wildtypes suggesting a compensatory response to the lack of NRF2. Both NQO-1 and HO-1 were decreased in both Nrf2 KO groups in comparison to wildtypes.

2.5 Discussion

Using an inducible model of glaucoma that provides tight temporal control on the same genetic background, we have confirmed that oxidative stress is an early event in glaucoma pathogenesis and have demonstrated a robust, but transient, endogenous antioxidant response that is mediated by the NRF2/ARE pathway. We show that this pathway is activated by phosphorylation of NRF2 by the PI3K/AKT pathway. Finally, we show that lack of Nrf2 results in the earlier onset of axon degeneration after induction of ocular hypertension.

We also discovered that the amplitude of the PhNR of the ERG is decreased early after IOP elevation, prior to axon degeneration or a decrease in the VEP. The early decrease in the PhNR amplitude might be explained by dendritic pruning and reduced RGC excitability, which was reported in a recent study (Risner et al., 2018). Our data matches studies using different experimental glaucoma models, which have also shown a decrease in PhNR amplitudes in ocular hypertensive monkeys and rabbits (Elgohary & Elshazly, 2015; Machida, 2012). In addition, the diagnostic utility of the PhNR for patients who are glaucoma suspects has been demonstrated in multiple studies (Chrysostomou & Crowston, 2013; Machida, 2012; Morny et al., 2019; Porciatti, 2014; Preiser et al., 2013). While the pattern ERG has also been suggested as a preclinical diagnostic for glaucoma and other RGC-related diseases, the PhNR has the advantage of not requiring refractive correction (Preiser et al., 2013). The PhNR could potentially be used as a pre-clinical, non-invasive biomarker for glaucoma diagnosis prior to onset of neuronal degeneration as ganglion cell function is disrupted in the MOM as early as 2-wks post-IOP elevation.

Levels of ROS were elevated in the retina prior to evidence of axon degeneration and were associated with a commensurate endogenous antioxidant response driven by the NRF2-

ARE pathway. While a relationship between oxidative stress and experimental glaucoma is known (Chrysostomou et al., 2013; Ferreira et al., 2010; Moreno et al., 2004; Tezel, 2006), our findings confirm that ROS levels increase early after ocular hypertension using an inducible model, which provides tighter temporal control and allows for analysis on the same genetic background. Our results are consistent with those in the DBA/2J showing elevated *Gfap, Nos-2* and *Ho-1* levels in 3-month old mice, prior to any glaucomatous pathology, as compared to C57Bl/6 mice (Inman et al., 2013b). In a model of episcleral vein cauterization, there were increases in ROS, nitrite and lipid peroxidation levels as early as 1 day following injury (Ko et al., 2005). In another model of ocular hypertension, where hyaluronic acid injections are used to elevate IOP, SOD and catalase levels were first increased at 3-wks, with pathology worsening up to 10-wks after injection (Moreno et al., 2004). Together, these studies suggest that quantification of retinal ROS might be a useful biomarker of early glaucoma. One *in vivo* assay of ROS being developed is QUEST-MRI (QUEnch-assiSTed), which quantifies production of endogenous ROS using hydrocyanine-800CW, which is an ROS-activated fluorescent probe (Berkowitz et al., 2017; Prunty et al., 2015). Further, counteracting ROS might be an effective therapeutic strategy for early-stage glaucoma.

We detected no difference in total NRF2 at either the transcript or protein level in contrast to the decrease in NRF2 levels reported in an episcleral vein cauterization model (Arana et al., 2020). However, our detection of activation of NRF2 by PI3K and AKT is in agreement with previous findings showing that this pathway activates NRF2 in another study using the episcleral vein cauterization model of glaucoma in rats (Kanamori et al., 2004). These pathways have also been linked to protection against oxidative stress in retinal pigment epithelial cells (Faghiri & Bazan, 2010). Further, this relationship has also been reported in models of chronic

kidney disease and acute lung injury (Bryan et al., 2013; Niture et al., 2014; Sivertsen et al., 2006; Wang et al., 2008). Exploring therapeutic options that increase levels or activation of NRF2 either directly or through an upstream activator could be an effective therapeutic strategy for glaucoma.

Previous studies have shown that adult Nrf2 KO mice have the same number of ganglion cells as a wildtype mouse prior to injury (Himori et al., 2013; Liu et al., 2018; Wang et al., 2020). However, these studies did not involve an intraocular injection, nor did they assess visual function or optic nerve axons. Here, we show that Nrf2 KO mice given an intracameral injection of saline had increased levels of superoxide and greater axon degeneration and vision loss as compared to wild-type saline injected controls. This demonstrates the precarious environment in which the RGCs survive and their dependence on the NRF2/ARE pathway to remove any additional ROS insults. This result does match with our findings that an intraocular injection can be damaging to the optic nerve, particularly in the context of an ongoing insult to the optic nerve (Naguib et al., 2020) studies showed that intravitreal injection of saline one day following injury via a model of indirect traumatic optic neuropathy causes greater axon degeneration, inflammation and visual function deficits at one month in comparison to mice that were injured but did not receive an intravitreal injection.

We examined the Nrf2 KO mice at 2-wks post-IOP elevation, a time-point at which the only change detected in wildtype mice was a decrease in the amplitude of the PhNR. We detected a trend for a further decrease in both the PhNR and the VEP in the microbead-injected Nrf2 KO mice as compared to their saline controls, which were already reduced due to the injection effect. More striking, however, was the detection of fewer axons and more axon degeneration in the microbead-injected Nrf2 KO mice as compared to the saline-injected Nrf2

KO controls. This suggests an earlier onset of glaucomatous neurodegeneration when the Nrf2/ARE pathway is inactive.

We had expected a more robust deficit in the PhNR in the microbead injected Nrf2 KO mice. One rationale for the lack of a greater decrease is the presence of a partially effective compensatory, NRF2-independent, protective mechanism. We explored this by quantifying levels of antioxidant proteins whose expression levels can be increased through NRF2-independent pathways, i.e. HIF-1a, NQO-1 and HO-1 (for review see Raghunath et al., 2018). While there was less of an increase in Hif1a gene expression in the Nrf2 KO animals, there was an increase in protein levels. This suggests that there was less degradation of the HIF-1a protein in the Nrf2 KO mice, but the mechanism for this is unclear. Regardless, the increased level of HIF-1a could act on the Hypoxia Response Element and provide some protection to the retina and optic nerve. Importantly, HIF-1a was not further increased in the Nrf2 KO mice that had elevated IOP. Similarly, a previous study using Nrf2 KO mice in a model for wet age-related macular degeneration showed increased VEGF in comparison to wildtype controls suggesting increased activation of the HRE by HIF-1a (Zhao et al., 2011). In contrast, the levels of both NQO-1 and HO-1 were reduced in the Nrf2 KO mice suggesting that the associated NRF2 independent pathways were not upregulated. It is still feasible that another pathway, such as activation of AP1 on the ARE, (Nguyen et al., 2000; Soriano et al., 2009; Raghunath et al., 2018) is also increased, resulting in minimal preservation of visual function. However, our data suggests that the NRF2/ARE pathway is the primary pathway used for endogenous antioxidant defenses in the retina in this model of glaucoma. This is in agreement with studies in other models of glaucoma or RGC death showing that Nrf2 KO mice do not have the antioxidant capacity to combat neuronal injury (Inman et al., 2014; Wang & Yuan, 2019.; Xu et al., 2015)

Importantly, the results from this study provide one explanation for the delay in glaucomatous neuronal degeneration in response to ocular hypertension. The activation of an antioxidant response by the retina decreases ROS levels and, thus, limits the amount of oxidative damage that occurs. However, the effect is transient and eventually the oxidative stress and resulting inflammation accumulates to a level that is damaging to the RGCs and pathology results. The results from this study also suggest that quantification of ROS and/or the PhNR could be useful biomarkers for early-stage glaucoma and that antioxidants could be an effective therapeutic, if given early.

CHAPTER 3

Neuronal Nrf2 Modulates Glaucoma Onset and Severity

3.1 Abstract

NRF2, a transcription factor that modulates a cell's response to reactive oxygen species (ROS), has been implicated as a therapeutic target in models of neurodegeneration, including glaucoma. We used the well-characterized microbead occlusion model of glaucoma (MOM) to elevate intraocular pressure (IOP). This model causes retinal ganglion cell (RGC) degeneration and death 4-6 weeks post-IOP elevation. We previously demonstrated increased ROS at 1- and 2- weeks post-IOP elevation in this model, weeks prior to pathology. We also detected an NRF2-mediated endogenous antioxidant response at 2-weeks post-IOP elevation. The goal of this study was to determine if NRF2 activation occurred within the RGCs or glial cells, and if overexpression of NRF2 in RGCs would provide neuroprotection. We knocked down NRF2 in either RGCs or glial cells using AAVs and then elevated the IOP and assessed the endogenous antioxidant response at 2-weeks and pathology at 5-weeks post-IOP elevation. We observed that both knockdown groups had a decreased endogenous antioxidant response, further visual function deficits, and increased axon degeneration in the optic nerve. In a separate group of wildtype mice, we overexpressed *Nrf2* in ganglion cell layer neurons by intravitreal injection of AAV2/2.CMV.Nrf2. Nrf2 overexpression resulted in lower superoxide levels, preservation of the PhNR amplitude, and decreased axon degeneration. Together, these data suggest that the endogenous Nrf2/ARE-mediated protective response is driven, at least in part, by RGC-localized

NRF2 and that RGC-directed Nrf2 overexpression is a viable therapeutic approach for the treatment of glaucoma that should be explored further.

3.2 Introduction

Glaucoma is a neurodegenerative disease characterized by the progressive degeneration and eventual death of retinal ganglion cells (RGCs), the neurons necessary for the processing and transmitting of visual information from the retina to the brain (D. J. Calkins, 2012a; Greco et al., 2016; Killer & Pircher, 2018; Weinreb et al., 2014b). Glaucoma results in irreversible blindness and affects almost 80 million people worldwide, with that number projecting to increase to 111 million by 2040 (He et al., 2018; Weinreb et al., 2014b). The major risk factors for developing glaucoma are age, genetics, and sensitivity to increases in intraocular pressure (IOP).

Current treatments for glaucoma aim to decrease IOP, but these treatments are ineffective for many patients; thus, further research aimed at protecting RGCs is a better approach that needs to be explored (D. J. Calkins, 2012a; Goldberg, 2003; Killer & Pircher, 2018). While the underlying molecular cause of the RGC degeneration and death is likely complex, it is well established that accumulation of reactive oxygen species (ROS) plays a role in glaucomatous pathology in disease models as well as in patients (Chrysostomou et al., 2013; Ghanem et al., 2010; Nita & Grzybowski, 2016; J. Zhao et al., 2016). Antioxidants are therapeutic in several models of glaucoma in preventing RGC degeneration and protecting visual function (Hines-Beard et al., 2016a; Inman et al., 2013b; Kansanen et al., 2013).

One of the key ways that cells respond to oxidative stress is through activation of the transcription factor, Nuclear factor erythroid 2-related factor 2 (Nrf2). When activated, Nrf2 binds to the Antioxidant Response Element (ARE), an enhancer element that is upstream of

many antioxidant genes. Under homeostatic conditions, Nrf2 remains in the cytoplasm, where it is sequestered by its repressor protein, Kelch-like ECH associated protein 1 (Keap1) and is constantly targeted for degradation via ubiquitination. When Keap1 is oxidized, it undergoes a conformational change that releases Nrf2, allowing it to accumulate and translocate into the nucleus of the cell where it can bind to the ARE and activate antioxidant gene transcription. Nrf2 can also be released from Keap1 upon phosphorylation by upstream signaling molecules, resulting also in nuclear translocation (Kansanen et al., 2013; Nguyen et al., 2000; Raghunath et al., 2018a; Tonelli et al., 2018b).

Nrf2 plays a role in multiple models of RGC injury and glaucoma (Batliwala et al., 2017a; Cheng et al., 2017c; Himori et al., 2013a; Liu et al., 2018; Nakagami, 2016; Z. Xu et al., 2015). Nrf2 KO mice have been used in multiple models of glaucoma to show even further increased susceptibility to RGC degeneration and death, suggesting that Nrf2 plays an important role in glaucomatous pathology and RGC in the MOM (Nakagami, 2016; Z. Xu et al., 2015). In the well-characterized microbead occlusion model (MOM) of glaucoma, we have previously showed that Nrf2 is phosphorylated by the PI3K/Akt pathway at 2 weeks post-IOP elevation (S. Naguib et al., 2021). Upon phosphorylation, ARE-driven transcripts are increased to combat ocular hypertension-induced increases in ROS, showing that the retina is endogenously responding to ocular hypertension via activation of the NRF2-ARE pathway.

Because Nrf2 is expressed by multiple cell types in the retina, the cell-specific role of Nrf2 in glaucoma is unknown and is important to elucidate to develop potential therapeutics. Both astrocytes and RGCs respond to ocular hypertension. Previous studies have shown that in the glaucomatous retina, astrocytes display an increase in proliferated processes when labeled

with glial fibrillary actin protein (GFAP); additionally, astrocytes have been shown to increase following ocular hypertension (Guttenplan et al., 2020; MR, 2000).

To determine if Nrf2 is activated in RGCs or astrocytes in glaucoma, we used $Nrf2^{fl/fl}$ mice and either a vector that targets RGCs or a vector that targets astrocytes to specifically knock down Nrf2. Then, we investigated downstream functional and molecular changes when Nrf2 is decreased in both mouse types. Finally, we also used AAV.Nrf2 gene therapy to assess the efficacy of expressing Nrf2 from the RGCs either from the Nrf2 global KO background, or as over-expression in a wild-type background to assess neuroprotection.

3.3 Materials and Methods

3.3.1 ARPE-19 cells: ARPE-19 cells were purchased from ATCC (Manassas, VA) and grown as previously described (Backstrom et al. 2020). Cells in complete media were transfected with plasmid DNA mixed with FuGENE HD (Promega, Madison, WI; #E2311) at a ratio of 1:4 (1 mg DNA: 4 ml FuGENE). Eight-well chamber slides and 6-well plates were transfected with 200 ng and 1 mg DNA per well, respectively. One day after transfection, the media was replaced with serum-free (SF) medium and incubated for 24 h. Cells were treated with SF medium containing either 5 mM sulforaphane (MedChemExpress, Monmouth Junction, NJ; #HY-13755) or vehicle (0.025% DMSO) and incubated for an additional 24 h. Cells in chamber slides were fixed with Histochoice, washed with PBS, and coverslips mounted with ProLong Gold (Thermo Fisher). For immunoblots, 10 mg of PBS-soluble protein was analyzed per lane. Blots were probed with rabbit anti-RFP (Rockland Immunochemicals, Inc., Limerick, PA; #600-401-379) and mouse anti-HA (Cell Signaling Technologies, Danvers, MA; #2367).

3.3.2 Mice: C57Bl/6 J (Jackson Labs, Bar Harbor, ME), B6.129X1-*Nfe2l2*^{tm1Ywk}*/J* or C58BL/6-*Nfe2l2*$^{tm1.Sred}$*/SbisJ* mice (Jackson Labs, Bar Harbor, ME) were group-housed, maintained on a 12-h light-dark cycle, and provided food and water ad libitum. All experiments were approved by the Institutional Animal Care and Use Committee of Vanderbilt University Medical Center. An equal distribution of 2-3 month old male and female mice were used for this project.

3.3.3 Microbead Occlusion: IOP was bilaterally elevated using the well-characterized MOM (Bond et al., 2016; D. J. Calkins et al., 2018; Sappington et al., 2010). We injected 2µl of 15-µm diameter FluoSpheres polystyrene microbeads into the anterior chamber of anesthetized mice (Thermo Fisher, Waltham, MA) as previously described (Bond et al., 2016; D. J. Calkins et al., 2018; Sappington et al., 2010). Additional mice received bilateral injections of an equivalent volume of lactated Ringer's saline solution as controls. Briefly, 1.5 mm outer diameter/1.12 mm inner diameter filamented capillary tubes (World Precision Instruments, Sarasota, FL) were pulled using a P-97 horizontal puller (Sutter Instrument Company, Novato, CA), and the resulting needles were broken using forceps to an inner diameter of ~100 µm. Microbeads were loaded and injected using a microinjection pump (World Precision Instruments, Sarasota, FL). Mice were anesthetized with isoflurane and dilated using topical 1% tropicamide ophthalmic solution (Patterson Veterinary, Devens, MA), and 2 µl (~2,000 microbeads) were injected. The needle was maintained in the injection site for 20 seconds before retraction to reduce microbead efflux. Mice were given topical 0.3% tobramycin ophthalmic solution (Patterson Veterinary, Devens, MA) following injection.

3.3.4 IOP measurements: IOP was measured immediately prior to microbead injection and biweekly thereafter using the Icare TonoLab rebound tonometer (Colonial Medical Supply, Franconia, NH) as previously described(D. J. Calkins et al., 2018; Hines-Beard et al., 2016b; Sappington et al., 2010). Mice were anesthetized using isoflurane, and 10 measurements were acquired from each eye within 2 minutes of induction of anesthesia.

3.3.5 Plasmids:

Table 3.1: Plasmid information.

Plasmid Name and Nomenclature for Paper	**Plasmid Purchased from**	**AAV type/purchased from**	**Mouse injected into**
pAAV.Trx-ARE(WT)-TnSV0HA-zG referred to as AAV2/2.ARE	N/A	AAV2/2 by SignaGen	C57Bl/6
pAAV.CMV.Nrf2 referred to as AAV2/2.Nrf2	AddGene plasmid #67636	AAV2/2 by SignaGen	C57Bl/6 or Nrf KO
pAAV.CMV.eGFP referred to as AAV2/2.eGFP	AddGene plasmid #67634	AAV2/2 by SignaGen	C57Bl/6 or Nrf KO
pAAV.Ap-mSncg.Cre.IRES.tdTomato referred to as AAV.mSncg.Cre	Modified in house from Addgene plasmid #153207	AAV2/2 by Vanderbilt Eye Institute Vector Core	$Nrf2^{fl/fl}$
pAAV.Shh10.hVimentin.P2A.tdTomato referred to as AAV.Vim.Cre	N/A	AAV2/6 with a modified ShH10 with an additional Y455F mutation by Vanderbilt Eye Institute Vector Core	$Nrf2^{fl/fl}$
pAAV.Ap-mSncg.IRES.tdTomato referred to as AAV.mSncg.tdTomato	Modified in house from Addgene plasmid #153207	AAV2/2 by Vanderbilt Eye Institute Vector Core	$Nrf2^{fl/fl}$
pAAV.Shh10.hVimentin.P2A.tdTomato referred to as AAV.Vim.tdTomato	N/A	AAV2/6 with a modified ShH10 with an additional	$Nrf2^{fl}$

		Y455F mutation by Vanderbilt Eye Institute Vector Core	

For experiments with an endpoint of 5 weeks post-IOP elevation, viruses were intravitreally injected one week prior to MOM injections. For experiments with an endpoint of 2 weeks post-IOP elevation, viruses were intravitreally injected two weeks prior to MOM injections. All vectors used in this study were injected at a concentration of 1 x 10^9GC/ml.

3.3.6 *In vivo* electrophysiology: Mice were dark adapted overnight, dilated with 1% tropicamide for 10 minutes and anesthetized with 20/8/0.8 mg/kg ketamine/xylaxine/urethane according to previously published methodology (Bernardo-Colon et al., 2018; Naguib et al., 2020; Naguib et al., 2021). Mice were placed on the heated surface of the ERG system to maintain body temperature. Corneal electrodes with integrated stimulators (Celeris System, Diagnosys LLC, Lowell, MA) were placed on eyes that were lubricated with GenTeal drops. Subdermal platinum needle electrodes were placed in the snout and back of the head at the location of the visual cortex. A ground electrode was placed in the back of the mouse. For VEPs, mice were exposed to 50 flashes of 1Hz, 0.05 cd.s/m^2 white light with a pulse frequency of 1 flash. For ERGs, mice were exposed to flashes of 1 Hz, 1 cd.s/m^2 white light with a pulse frequency of 1. For photopic negative ERGs (PhNR), mice were exposed to 20 continuous flashes of white light on a green background with a pulse frequency of 2. Each experimental group had 12-16 eyes.

3.3.7 Dihydroethidum Fluorescence: A dye that fluoresces in the presence of superoxide and, to a lesser extent, hydrogen peroxide, dihydroethidum (DHE), was utilized for these studies as

previously described (Bernardo-Colon et al., 2018). Mice were anesthetized with 2.5% isofluorane and intravitreally injected with 1 µl (0.5uM) of DHE (ThermoFisher Scientific, Waltham, MA) diluted in phosphate-buffered saline (PBS) using a 30-gauge Hamilton syringe. Just prior to imaging, mice were anesthetized with ketamine/xylazine and eyes were dilated with 1% tropicamide. Thirty minutes after DHE injection, fluorescence was imaged on a Micron IV retinal imaging microscope (Phoenix Research Labs, Pleasanton, CA) using an FF02-475/50 nm excitation filter (Semrock, Inc. Rochester, NY) and ET620/60X emission filter (Chroma Technology Corp., Bellows Falls, VT). The average intensity of the fluorescence throughout the retina was quantified using ImageJ (Rasband, W.S., 2018). For each experimental group, 6-8 eyes were analyzed. For purposes of comparison, the same DHE fluorescence collected from wildtype mice at 2-weeks (wks) in Figure 2.2 was also used in Figure 2.6 compared to Nrf2 KO mice.

3.3.8 Tissue collection: For western blots and qPCR, retinas were collected and flash frozen from mice euthanized by anesthetic overdose and cervical dislocation. For immunohistochemistry and optic nerve histology, tissue was collected and incubated in 4% paraformaldehyde for until use at 4^{o}C.

3.3.9 Protein assay: Protein concentrations were determined from 10 µl of retina homogenates with the Pierce BCA Protein Assay Kit (cat#: 23225, ThermoFisher Scientific, Waltham, MA). BSA was used as the protein standard. Absorbance was measured with the plate reader POLARstar Omega (BMG Labtech, Ortenburg, Germany).

3.3.10 Western blot: Single retinas were sonicated in lysis buffer (PBS, EDTA and Halt protease inhibitor) and centrifuged for 30 minutes at 4ºC. 4x Laemmli buffer (Bio-rad, cat# 1610747) containing ß-mercaptoethanol was added to the samples and heated for 5 minutes at 95ºC. Known amounts of protein (10-20 µg/retina) or protein ladder (cat#1610375, Bio-rad, Hercules, CA) were loaded in 4-20% polyacrylamide gels (Bio-Rad #456-1095). Proteins were transferred onto nitrocellulose using the Bio-Rad trans blot turbo transfer system. Membranes were blocked in 2% BSA in TBS overnight at 4ºC. Membranes were incubated in primary antibody at room temperature with rocking for 2 hours. Membranes were incubated with secondary antibody (IRDye 800CW Donkey anti-rabbit, #926-32213 or IRDye 680CW Donkey anti-mouse, #926-68022,1:5000 in 1% BSA/TBS) at room temperature for 1 hour. After washing, blots were imaged with a Bio-Rad ChemiDoc system. Band density was quantified by scanning the blot using Adobe Photoshop. Each band was selected with the same frame and set measurements were used to obtain the gray mean value for each. Band intensity measurements from protein of interest were divided by band intensity measurements of loading control (ß-actin). Each experimental group had 5 retinas.

3.3.11 Immunohistochemistry: Eyes were embedded in paraffin and sectioned at 10 microns according to previously published methods using the Vanderbilt Vision Research Center histology core(Bricker-Anthony et al., 2014; S. Naguib et al., 2021; Sarah Naguib, Bernardo-Colón, Cencer, et al., 2020). Slides were then warmed on a slide warmer at a medium setting (about 40 ºC) for 30 min. Slides were then placed in a rack and went through a series of deparaffinization steps: xylene (10 min), 100% ethanol (10 min), 100% ethanol (5 min), 95% ethanol (5 min), 80% ethanol (5 min), 60% ethanol (5 min), 40% ethanol (5 min). Slides were

then placed in coplin jar covered with sodium citrate solution and boiled for 30 min (2.94g of tri-sodium citrate dehydrate in 1L of DI water, adjusted to pH of 6.0 and then added 0.5ml of Tween 20). Following boiling, slides were washed twice in 1x PBS for 5 min. Then, slides incubated in sodium borohydride solution (0.05g sodium borohydride dissolved in 50ml DI water, made fresh every time) at room temperature. Slides were then placed in blocking buffer (500mL 1x PBS, 1.25mL Triton-X, 1.25mL Tween 20, 0.5g sodium citrate, 11.25g glycine, 5g BSA) and 5% normal donkey serum (cat #: D9663, Millipore Sigma, Darmstadt, Germany) for 1 hr at room temperature. Slides were washed once with 1xPBS and placed in primary antibody diluted in staining buffer (500mL 1x PBS, 1.25mL Triton X, 1.25 mL Tween 20, 5g BSA) overnight at 4^{o}C in a humidified chamber. The following day, slides were twice washed with 1x PBS for 5 min each. Secondary antibody was diluted in staining buffer and was added to the slides for 2 hrs at room temperature at 1:200 dilution after spinning for 10 min at 13,000g. After 2 hrs, slides were washed twice in 1x PBS for 5 min each. Then, slides were coverslipped with Vectashield containing DAPI (cat#: H-1200-10, Vector Laboratories, Burlingame, CA) and sealed with nail polish. Slides were imaged on a Nikon Eclipse epifluorescence microscope (Nikon, Melville, NY). All images were collected from the same retinal region with identical magnification, gain and exposure settings. Fluorescence intensity was quantified via ImageJ as previously described(S. Naguib et al., 2021; Sarah Naguib, Bernardo-Colón, Cencer, et al., 2020). A rectangle was selected around the region of interest, channels were split for multiple antibodies, threshold was adjusted, noise was de-speckled and fluorescence intensity was measured. Fluorescence intensity was normalized to saline-injected mice. Each experimental group included 5 eyes.

3.3.12 Optic nerve counts: Optic nerves were post-fixed in glutaraldehyde followed by Resin 812 embedding and Araldite 502 (cat#: 14900 and 10900 respectively, Electron Microscopy Sciences, Hatfield, PA) according to previously published protocols (Naguib et al., 2020; Naguib et al., 2021; Bernardo-Colon et al., 2018). Leica EM-UC7 microtome was used to collect 1 □m thick sections of the optic nerves. Sections were then stained with 1% paraphenylenediamine and 1% toluidine blue and were imaged on a Nikon Eclipse Ni-E microscope using 100x oil immersion objective (Nikon Instruments, Melville, NY). The optic nerves were montaged into a 5 x 5 image using the Nikon Elements software to scan a large image. We used the Counting Array and Better Cell Counter plugins to ImageJ, which creates a grid of nine squares overtop the montaged optic nerve. We manually counted healthy and degenerating axons, which are color-coded by the plugins. Degenerative axon profiles were identified by dark paraphenylenediamine staining due to collapsed myelin or loose myelin (onioning) surrounding the axon. A grid was used to avoid bias, by always counting in the same squares, using a cross configuration. Twenty percent of the optic nerve cross-sectional area was counted and the total was multiplied by five to estimate total and degenerating axons within the nerve. Each experimental group included 4-5 nerves.

3.3.13 Data Analysis: All statistical analyses were performed using GraphPad Prism software (La Jolla, CA). A one-way ANOVA with a Bonferroni post hoc test ($p = 0.05$) was used to analyze western blot quantification, IHC fluorescence quantification, ON quantification data, and ERG/VEP latencies and amplitudes. A one-way ANOVA and Dunnett's multiple comparisons post hoc test ($p = 0.05$) were used to analyze the qPCR results. Means and standard deviation were calculated for each data set.

Table 3.2: Antibodies used for IHC

Antibody	**Company**	**Catalog Number**	**Species**	**Dilution for western blot**	**Dilutions for IHC**
Nrf2	Abcam	137550	Rabbit	1:1000	1:200
pNrf2	ThermoFisher	PA5-67520	Rabbit	1:1000	1:200
ß-actin	Cell Signaling	E4D9Z	Mouse	1:1000	N/A
RFP (for tdTomato)	ThermoFisher	MA5-15257	Mouse	1:200	1:200
eGFP	ThermoFisher	MA1-952	Mouse	1:100	1:100
Prdx6	Abcam	133348	Rabbit	1:1000	1:100
Gpx1	ThermoFisher	PA5-26323	Rabbit	1:500	N/A
SOD3	Abcam	80946	Rabbit	1:1000	1:200
ß-tubulin	Sigma	T8678	Mouse	N/A	1:300

3.4 Results

3.4.1 Overexpression of Nrf2 in GCL neurons in Nrf2 KO mice

To determine if Nrf2 only in the GCL neurons would be sufficient to increase retinal endogenous antioxidant response when all surrounding cell types lack Nrf2, we intravitreally injected AAV2/2.Nrf2 into total Nrf2 KO mice. Our previous studies demonstrated that ocular hypertensive Nrf2 KO mice lack an endogenous retinal antioxidant response and exhibit earlier onset axon degeneration and visual dysfunction(S. Naguib et al., 2021). In accordance with our previous findings (Naguib et al., 2021), DHE fluorescence—used as an *in vivo* superoxide marker--was equally elevated in saline and microbead injected Nrf2 KO mice ($p=0.355$, $n=3$

eyes/group, Figure 3.1A, B). We previously compared these Nrf2 KO groups to WT controls[14]. In this study, we show that the AAV2/2.Nrf2 group had 61% more DHE fluorescence as compared to the AAV2/2.eGFP group (p=0.0319, n= 3 or 4 eyes/group respectively, Figure 3.1A, B).

Similarly, we detected an increase in antioxidant protein levels in Nrf2 KO mice treated with AAV2/2.Nrf2 regardless of IOP elevation (Figure 3.1C, D). The AAV2/2.Nrf2 saline-injected mice had 44% more PRDX6 and 79% more GPX1 than the AAV2/2.eGFP controls (p=0.0276 and p=0.0141 respectively, Figure 3.1C, D). The AAV2/2.Nrf2 microbead-injected mice had 70% more PRDX6 and 67% more GPX1 than their AAV2/2.eGFP controls (p=0.0121 and p=0.1376 respectively, Figure 3.1C, D). There was no difference in SOD3 levels between the AAV2/2.Nrf2 and AAV2/2.eGFP groups (data not shown).

We have previously published that the amplitudes of the PhNR were reduced in Nrf2 KO mice in comparison to wildtype counterparts, and that there was difference in PhNR amplitude in either saline or microbead-injected Nrf2 KO mice (Naguib et al., 2021) . Here we examined if Nrf2 overexpression in GCL neurons would be sufficient to rescue visual function (Figure 3.1E, F). In the AAV2/2.Nrf2 treated, saline injected group, the PhNR amplitude was 52% greater than the AAV2/2.eGFP saline group (n=6 or 8 eyes/group respectively; p= 0.0357, Figure 3.1E, F). In the AAV2/2.Nrf2 treated, microbead injected group, PhNR amplitude was 35% greater than AAV2/2.eGFP treated, microbead injected group (n=6 or 8 eyes/group respectively; p=0.039, Figure 3.1E, F). There was no difference between saline or microbead injections in AAV.Nrf2 treated mice (n=8 eyes/group; p=0.9516, Figure 3.1E, F). Our results also showed that there was no difference in PhNR amplitude between either AAV.eGFP group matches our previous data (n=6 eyes/group; p=0.6416, Figure 3.1E, F) (Naguib et al., 2021).

We have previously published that the amplitudes of the VEP were reduced in Nrf2 KO mice at 2 weeks, 2-3 weeks earlier than VEP is normally decreased in the MOM. AAV2/2.Nrf2 preserved the VEP amplitude by 90% and 100% in Nrf2 KO mice injected with saline or microbeads, respectively ($p=0.0015$ and $p=0.0146$, respectively; n=6 or 8 eyes/group respectively; Figure 3.1E, G).

We also wanted to determine if Nrf2 overexpression only in the GCL neurons would delay axon degeneration in glaucomatous Nrf2 KO mice (Figure 3.1H-J). At 2 weeks post-IOP elevation, AAV2/2.eGFP Nrf2 KO mice have 22% fewer axons than their saline-injected controls ($p=0.0054$, n=4 nerves/group, Figure 3.1H, I), in agreement with our previous findings[14]. Further, AAV2/2.Nrf2 treatment preserved the optic nerve axons after IOP elevation. AAV2/2.Nrf2 microbead injected Nrf2 KO mice showed no additional axon loss when compared to AAV2/2.Nrf2 saline injected Nrf2 KO mice ($p=0.1304$, n=3-4 nerves/group, Figure 3.1H, I). There was a 21% decrease in total number of axons in IOP elevated AAV2/2.eGFP treated Nrf2 KO mice in comparison to AAV2/2.Nrf2 treated Nrf2 KO mice ($p=0.0263$, n=3-4 nerves/group, Figure 3.1H, I).

There were also 79% fewer degenerating axons in saline-injected AAV2/2.Nrf2 Nrf2 KO mice than their AAV2/2.eGFP injected counterparts ($p=0.009$, n=4 nerves/group, Figure 3.1H, J). The same trend occurs for the microbead-injected Nrf2 KO mice: there was 78% fewer degenerating axons in the AAV2/2.Nrf2 group in comparison to the AAV2/2.eGFP mice ($p<0.0001$, n=3-4 nerves/group, Figure 3.1H, J). AAV2/2.eGFP saline-injected Nrf2 KO mice had 35% fewer degenerative axons in comparison to their microbead-injected counterparts, in accordance with our previous findings ($p=0.0001$, n=4 nerves/group, Figure 3.1H, J). There was

no difference in the number of degenerative axons in either of the AAV2/2.Nrf2 injected groups ($p=0.2191$, n=3-4 nerves/group, Figure 3.1H, J).

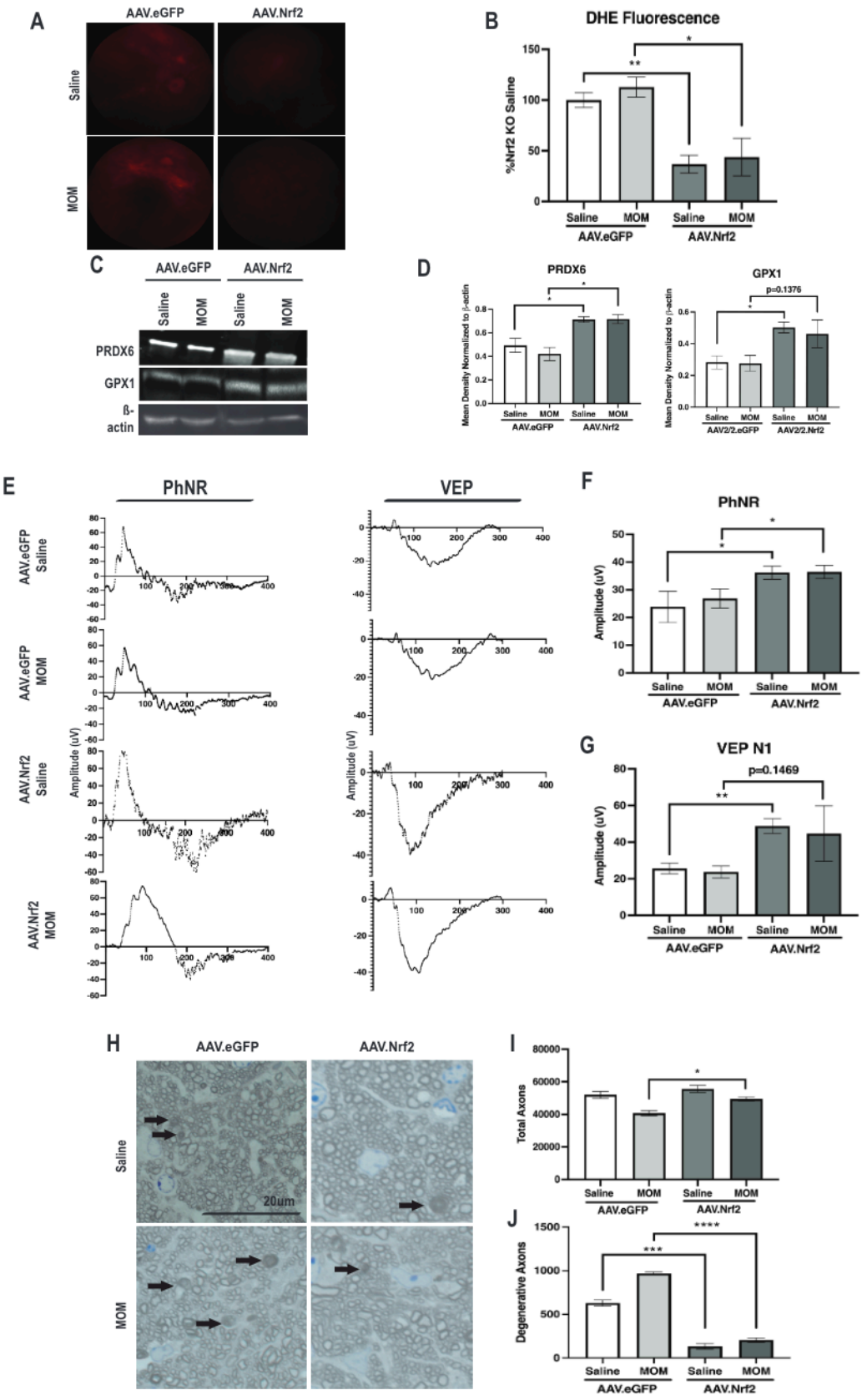
A
AAV.eGFP
AAV.Nrf2
Saline
MOM
B
DHE Fluorescence
%Nrf2 KO Saline
Saline
MOM
AAV.eGFP
AAV.Nrf2
C
PRDX6
GPX1
ß-actin
D
PRDX6
GPX1
Mean Density Normalized to β-actin
p=0.1376
AAV2/2.eGFP
AAV2/2.Nrf2
E
PhNR
VEP
Amplitude (uV)
F
PhNR
Amplitude (uV)
G
VEP N1
p=0.1469
H
20um
I
Total Axons
J
Degenerative Axons

Figure 3.1. Overexpression of Nrf2 in GCL neurons in Nrf2 KO mice decreases ROS and preserves visual function. A) Representative fundus images of DHE fluorescence in all groups. B) Quantification of DHE fluorescence in ocular hypertensive AAV.eGFP and AAV.Nrf2 injected Nrf2 KO mice at 2 weeks post-IOP elevation in comparison to respective saline-injected controls, *p<0.05, **p<0.01 C) Representative western blot of PRDX6, GPX1 and ß-actin showing increases in both antioxidant proteins in AAV.Nrf2 groups in comparison to AAV.eGFP controls. D) Quantification of PRDX6 and GPX1 levels after normalization to ß-actin, *p<0.05. E) Representative PhNR and VEP waveforms for all groups at 2 weeks post-IOP elevation F) Quantification of PhNR amplitudes in AAV.eGFP and AAV.Nrf2 groups, *p<0.05. G) Quantification of VEP N1 amplitudes in AAV.eGFP and AAV.Nrf2 groups, **p<0.01. H) Representative micrographs of optic nerves in all groups, with arrows indicating axon degeneration. Scale bar applies to all micrographs. I) Quantification of total number of axons in all groups, *p<0.05. J) Quantification of number of degenerating axons in al groups, ***p<0.001 and ****p<0.0001.

3.4.2 Activation of the ARE in RGCs at 2 weeks post-IOP elevation

We used pAAV2/2.Trx.ARE.tdTomato.SV-HA-zsGreen to quantify activation of the ARE in RGCs (Figure 3.2A). We used synthetic DNA gblocks that contained either wildtype human Trx ARE (Figure 3.2B) or mutant Trx ARE (Figure 3.2C). The mutant Trx ARE is known as M4 due to the mutation at oligonucleotide 4 positioned upstream of the mini-TK promoter, shown in red (Kim et al., 2001). The ARE promoters drove expression of nuclear-targeted tdTomato and the SV40 promoter drove expression of HA-tagged ZsGreen. We used zsGreen as a control to show that the virus has been transduced by the RGCs and tdTomato to show that the ARE is activated. We can use this fluorescent reporter to quantify Nrf2's binding to ARE as Nrf2 is the primary activator of the ARE.

We transfected this virus into ARPE19 cells and examined fluorescence (white arrows pointing to colocalization of tdTomato and ZsGreen, Figure 3.2C). In the presence of DMSO, there were basal levels of ARE activation (see white arrow) but there was increased ARE activation in the presence of sulforaphane, which has been shown to induce NRF2 (Figure 3.2C). This ARE activation is dependent on WT ARE as opposed to M4 ARE, as ARE activation in the

presence of sulforaphane in ARPE19 cells was diminished. We also quantified ARE activation via western blot analysis by probing for tdTomato and ZsGreen (110kD and 100kD, respectively; Figure 3.2D). Here, we showed that in the cells transduced with WT ARE treated with either DMSO or sulforaphane, both tdTomato and ZsGreen are present, with more intense tdTomato in the cells treated with sulforaphane (Figure 3.2D). However, in ARPE19 cells transduced with M4 ARE, there is a lack of tdTomato band altogether.

AAV2/2 has been shown to transduce RGCs when intravitreally injected (citation). We intravitreally injected the fluorescent ARE reporter into wildtype mice two weeks prior to inducing MOM to allow for ample transduction time. Then, we used an *in vivo* imaging system to quantify fluorescence in the eye. We normalized ARE fluorescence in microbead-injected mice to saline-injected controls. We found that in the 1 week post-IOP elevation group, there was a 183% increase in tdTomato fluorescence in comparison to saline-injected controls, showing that the ARE is activated as early as 1 week post-IOP elevation in RGCs ($p=0.0015$, n=4 or 5 eyes/group, Figure 3.2F). In the 2 week post-IOP elevation group, there was a 280% increase in tdTomato fluorescence in comparison to saline-injected controls ($p=0.0025$, n= 4 or 5 eyes/group, Figure 3.2F). There was also a 53% increase in tdTomato fluorescence between the 1 and 2 week post-IOP elevation groups, showing maximal ARE activation at the previously identified critical timepoint of 2 weeks post-IOP elevation ($p=0.029$, n=4 eyes/group, Figure 3.2F).

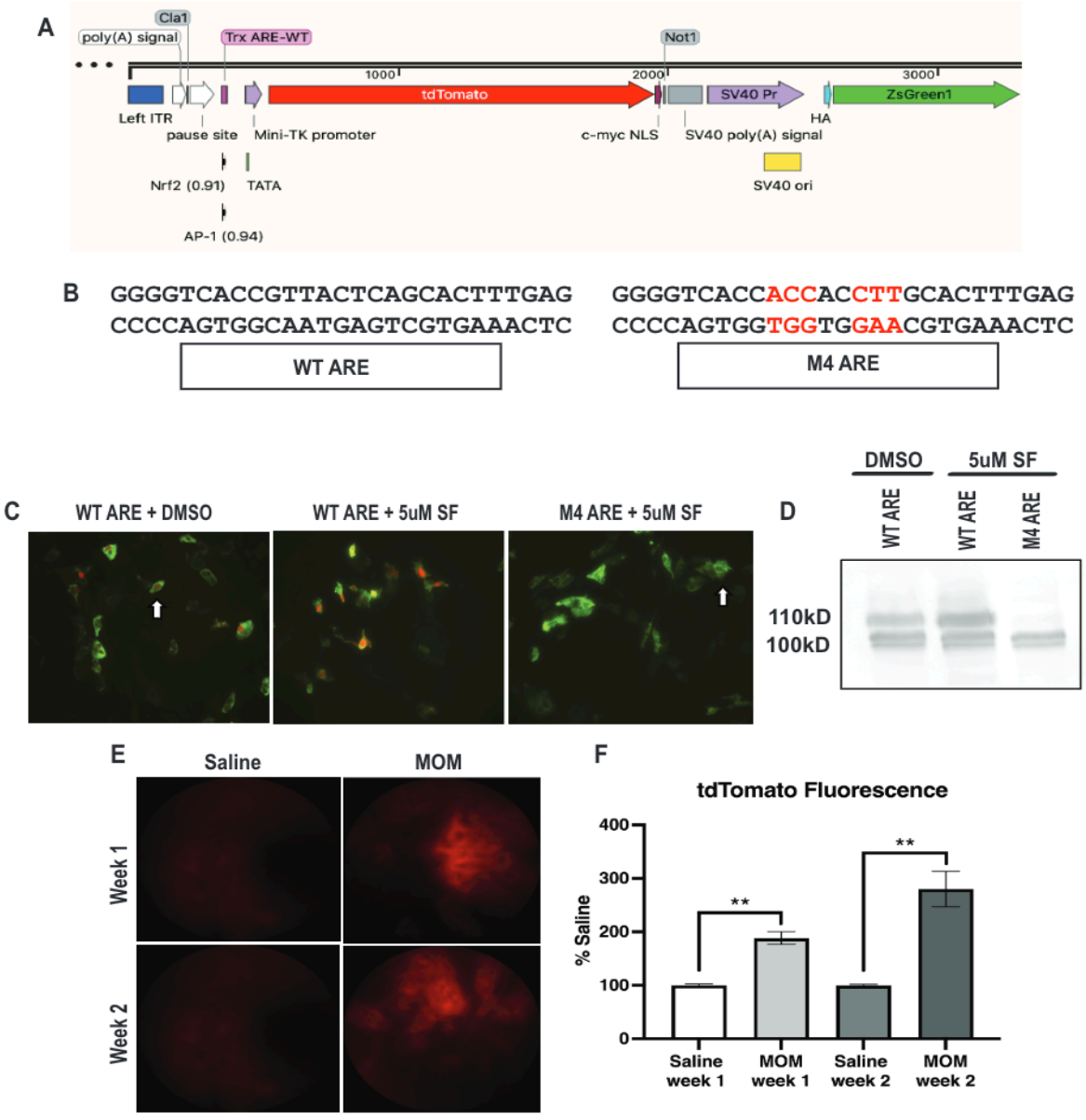

Figure 3.2. Activation of the ARE in RGCs. A) Plasmid map of pAAV2/2.Trx.ARE.tdTomato.SV-HA-zsGreen. B) Sequence of WT ARE and M4 ARE, red letters indicating the mutations made in M4 in comparison to WT ARE. C) Representative micrographs of ARPE-19 cells transfected with WT ARE or M4 ARE and treated with DMSO (control) or 5uM sulforaphane (SF), which is known to activate the ARE. White arrows indicate co-labeling of tdTomato and zsGreen. D) Representative western blot of ARPE-19 cells E) Representative fundus images of WT mice intravitreally injected with pAAV2/2.Trx.ARE.tdTomato.SV-HA-zsGreen 2 weeks prior to saline or microbead intracameral injections. F) Quantification of tdTomato fluorescence from E, showing increased tdTomato fluorescence following ocular hypertension in RGCs.

3.4.3 Knockdown of Nrf2 in either RGCs or glia can decrease endogenous antioxidant response

We used Nrf2fl/fl mice injected with AAV2/2.mSncg.Cre to specifically knockdown Nrf2 from RGCs. Gamma synuclein has been shown to be a marker for RGCs (Q et al., 2020). We validated that the AAV was transducing RGCs by labeling for tdTomato in retinal cross-sections and showed that there is positive tdTomato labeling in the RGCs (Figure 3.3A). We also showed that tdTomato co-labels with NeuN, a marker for neurons, in these cross-sections to ensure we were transducing RGCs (Figure 3.3B).

We also used Nrf2fl/fl mice injected with AAV2/6.Vim.Cre to specifically knockdown Nrf2 from astrocytes (Figure 3.3C). While vimentin is also expressed in Muller glia in the retina (Fernández-Sánchez et al., 2015; S. J et al., 1981; MJ et al., 2008; O'Leary et al., 2020), we validated that the AAV was primarily transducing astrocytes rather than Muller glia by labeling for tdTomato in retinal cross-sections. We also showed that the tdTomato co-labels with GFAP in these cross-sections to ensure that we were transducing glia (Figure 3.3D).

We also measured ARE-driven transcripts in whole retina lysates to determine if either Nrf2 knockdown would decrease antioxidant expression (Figure 3.3E). There was 195% less *Prdx6* in RGC-specific Nrf2 knockdown mice in comparison to glia-specific Nrf2 knockdown mice, where fold change was measured over respective tdTomato controls ($p=0.0294$, n=4 or 5 retinas/group respectively, Figure 3.3E). There was no difference in *Txn1, Gpx1 or Sod3* levels in either knockdown group ($p=0.0607$; $p=0.6651$; $p=0.533$; n=4 or 5 retinas/group respectively, Figure 3.3E).

We wanted to determine if knocking down NRF2 levels in either RGCs or glia would change the degree to which NRF2 is phosphorylated (Figure 3.3F, G). We used western blot to

analyze the ratio of phosphorylated to total NRF2. We found that in the AAV2/2.mSncg.Cre group, there was 25% less pNRF2 than their AAV2/2.mSncg.tdTomato controls (p=0.0233, n=5 retinas/group, Figure 3.3F, G). The same trend occurred when we knocked down NRF2 in the glia—AAV2/6.Vim.Cre mice had 31% less pNRF2 than their AAV2/6.Vim.tdTomato controls (p=0.0035, n=4 retinas/group, Figure 3.3F, G).

We assessed ARE-driven proteins as well following knockdown of NRF2 in RGCs or glia (Figure 3.3F, H-J) in comparison to housekeeping protein, ß-actin. There was 26% less PRDX6 levels in the AAV2/2.mSncg.Cre retinas in comparison to AAV2/2.mSncg.tdTomato controls (p=0.0395, n=5 retinas/group, Figure 3.3F, H). There was no significant difference in PRDX6 levels between the AAV2/6.Vim.tdTomato and AAV2/6.Vim.Cre groups (p=0.1036, n=5 retinas/group, Figure 3.3H). There was no statistically significant difference in GPX1 levels among any of the groups, however, the AAV2/2.mSncg.Cre group had trending decreases in GPX1 levels (p=0.0988, n=5 retinas/group, Figure 3.3F, I). There was 22% less SOD3 in the AAV2/2.mSncg.Cre group than their AAV2/2.mSncg.tdTomato controls (p=0.0415, n=4 retinas/group, Figure 3.3F, J). This trend also followed in the AAV2/6.Vim.Cre group where there was 20% less SOD3 in the AAV2/6.Vim.Cre group than their AAV2/6.Vim.tdTomato controls (p=0.049, n=5 retinas/group, Figure 3.3F, J).

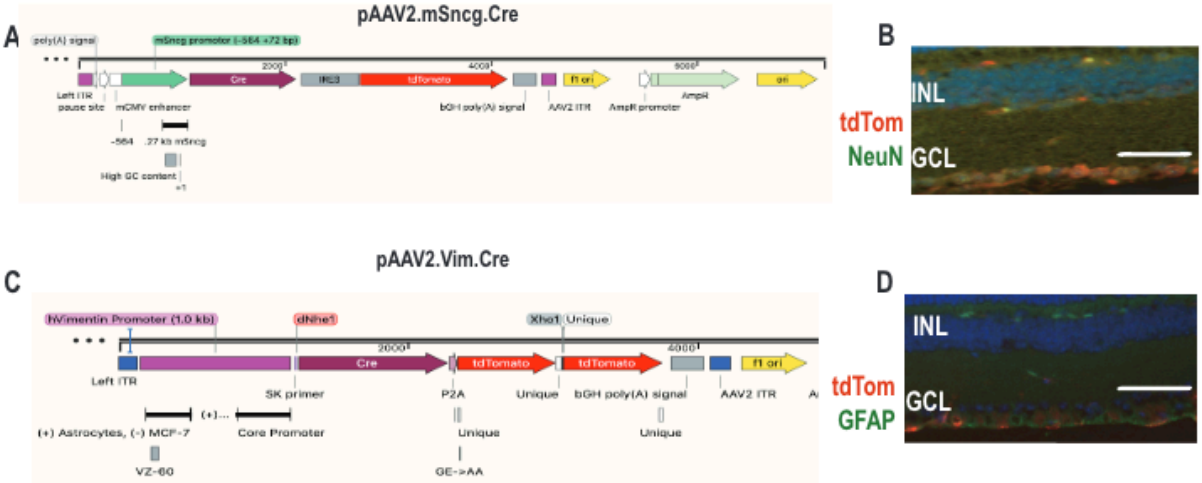
A
pAAV2.mSncg.Cre
poly(A) signal
mSncg promoter (-564..+72 bp)
Cre
tdTomato
f1 ori
ori
AmpR
Left ITR
pause site
mCMV enhancer
-564
.27 kb mSncg
High GC content
bGH poly(A) signal
AAV2 ITR
AmpR promoter
B
INL
tdTom
NeuN
GCL
C
pAAV2.Vim.Cre
hVimentin Promoter (1.0 kb)
dNhe1
Xho1 Unique
Cre
tdTomato
tdTomato
f1 ori
Left ITR
SK primer
P2A
Unique
bGH poly(A) signal
AAV2 ITR
(+) Astrocytes, (-) MCF-7
Core Promoter
Unique
Unique
VZ-60
GE->AA
D
INL
tdTom
GFAP
GCL
E
Prdx6
Gpx1
Sod3
Ho-1
Fold Change over tdTom (2^-ΔΔCT)
AAV. mSncg. Cre
AAV. Vim. Cre
F
pNRF2
PRDX6
GPX1
SOD3
AAV.mSncg.tdTom
AAV.Vim.tdTom
AAV.mSncgCre
AAV.Vim.Cre
NRF2
ß actin
G
pNRF2
Mean Density Normalized to NRF2
H
PRDX6
Mean Density Normalized to β-actin
I
GPX1
p=0.0988
Mean Density Normalized to β-actin
J
SOD3
Mean Density Normalized to β-actin
AAV. mSncg. tdTomato
AAV. Vim. tdTomato
AAV. mSncg. Cre
AAV. Vim. Cre

Figure 3.3. Knockdown of Nrf2 in either RGCs or glia can decrease endogenous antioxidant response. A) Plasmid map of pAAV2.Ap-mSncg.Cre.IRES.tdTomato. B) Representative micrograph of retina labeled with tdTomato (red) and NeuN (green) 2 weeks post-IOP elevation and four weeks after intravitreal injection of AAV2/2.mSncg.Cre. C) Plasmid map of pAAV2.Shh10.hVimentin.P2A.tdTomato. D) Representative micrograph of retina labeled with tdTomato (red) and GFAP (green) 2 weeks post-IOP elevation and four weeks after intravitreal injection of AAV2/6.Vim.Cre. E) Quantification of *Prdx6, Gpx1, Sod3* and *Ho-1,* all ARE-driven transcripts, at 2 weeks post-IOP elevation in both AAV.mSncg.Cre and AAV.Vim.Cre groups. Fold change was compared to their respective controls, AAV.mSncg.tdTom and AAV.Vim.tdTom, *p<0.05. F) Representative western blots for pNRF2, PRDX6, GPX1 and SOD3 for both knockdown groups and their respective controls, all normalized to NRF2 or ß-actin, respectively. G) Quantification of pNRF2 levels, normalized to NRF2 levels, *p<0.05, **p<0.01. H) Quantification of PRDX6 levels, normalized to ß-actin levels, *p<0.05. I) Quantification of GPX1 levels, normalized to ß-actin levels. J) Quantification of SOD3 levels, normalized to ß-actin, *p<0.05.

3.4.4 Localization of antioxidant proteins changes after Nrf2 KD in RGCs and glia

We assessed if knocking down Nrf2 in either RGCs or astrocytes would change the levels or localization of ARE-driven transcripts (Figure 3.4). We immunolabeled retina cross-sections with PRDX6 and GFAP. We found that in both AAV2/2.mSncg.tdTomato and AAV2/6.Vim.tdTomato mice, PRDX6 labeling appeared in the GCL, co-labeling with GFAP. In both knockdown groups, we a found that PRDX6 co-labeled with GFAP but instead of only in the GCL, we found PRDX6 in the inner retina where Muller cell bodies are located (Figure 3.4).

We also immunolabeled retina cross-sections with SOD3 and RBPMS. We found that in both AAV2/2.mSncg.tdTomato and AAV2/6.Vim.tdTomato mice, there was greater intensity of SOD3 than in the knockdown groups and greater overlap with SOD3 and RBPMS (Figure 3.4).

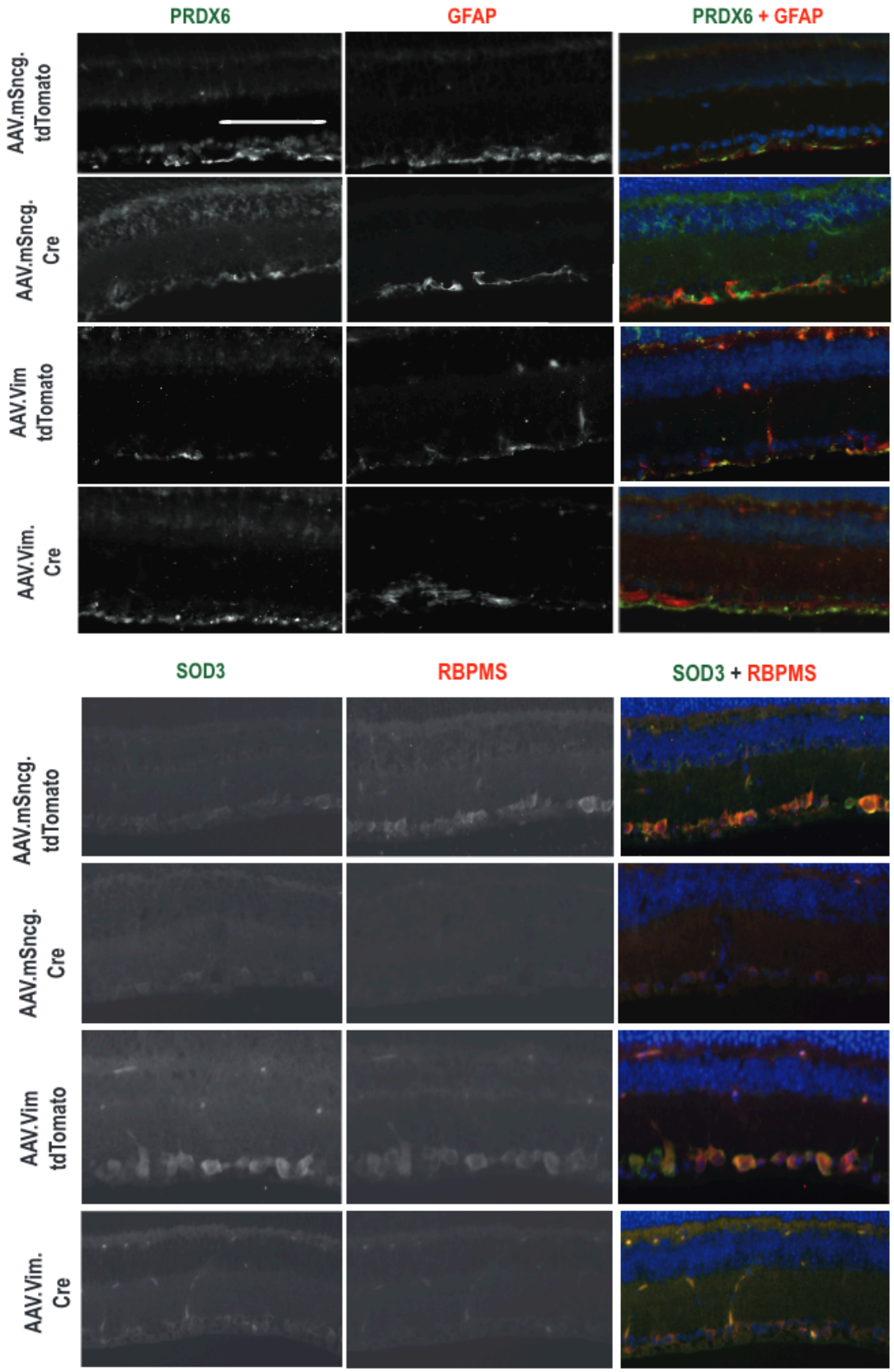
PRDX6
GFAP
PRDX6 + GFAP
AAV.mSncg. tdTomato
AAV.mSncg. Cre
AAV.Vim tdTomato
AAV.Vim. Cre
SOD3
RBPMS
SOD3 + RBPMS
AAV.mSncg. tdTomato
AAV.mSncg. Cre
AAV.Vim tdTomato
AAV.Vim. Cre

Figure 3.4. Localization of antioxidant proteins changes after Nrf2 KD in RGCs and glia. A) PRDX6 (green) and GFAP (red) in all four groups. B) SOD3 (green) and RBPMS (red) in all four groups, showing increased overlap in both AAV.tdTom controls than respective knockdown groups.

3.4.5 Knockdown of Nrf2 in either RGCs or glia decreases visual function and accelerates axon degeneration

To determine if Nrf2 is necessary for proper RGC function, we measured the PhNR of the ERG at both 2 and 5 weeks post-IOP elevation (Figure 3.5A-C, data only shown for 2 weeks post-IOP elevation). Overall, we found knocking down Nrf2 in either RGCs or astrocytes was sufficient to affect the PhNR amplitude at 2 weeks post-IOP elevation. The PhNR amplitude was 39% higher in the AAV2/2.mSncg.tdTomato group than in the AAV2/2.mSncg.Cre group ($p=0.0153$, n=16 eyes/group, Figure 3.5A, B). The PhNR amplitude was 52% higher in the AAV2/6.Vim.tdTomato group than in the AAV2/6.Vim.Cre group ($p<0.0001$, n=14 eyes/group, Figure 3.5A, B). Interestingly, there was no difference in PhNR amplitude between the two Nrf2 knockdown groups at 2 weeks post-IOP elevation ($p=0.226$, Figure 3.5A, B). At 5 weeks post-IOP elevation, there was no difference in PhNR amplitude between either AAV2/6.Vim group ($p=0.5182$, data not shown). Interestingly, by 5 weeks, the AAV2/2.mSncg.tdTomato group had a 47% higher PhNR amplitude than the AAV2/2.mSncg.Cre group ($p<0.0001$, data not shown).

At both timepoints, we also quantified the VEP amplitude (data only shown for 5 weeks post-IOP elevation). As expected, at 2 weeks post-IOP elevation there were no differences in VEP amplitude between any of the experimental groups in accordance with previously published data ($p=0.1029$, data not shown) (Bond et al., 2016; S. Naguib et al., 2021; Sappington et al., 2010). At 5 weeks post-IOP elevation, there was also no difference in VEP amplitudes between AAV2/2.mSncg.tdTomato mice and AAV2/2.mSncg.Cre mice ($p=0.8786$, n=16 eyes/group,

Figure 3.5A, C). Interestingly, there was a 37% decrease in VEP amplitude in the AAV2/6.Vim.Cre group than in comparison to the AAV2/6.Vim.tdTomato group (p=0369, n=14 eyes/group, Figure 3.5A, C).

Previous studies have shown that axon degeneration in the optic nerve does not occur in the MOM until 4-6 weeks post-IOP elevation in wildtype mice; however, axon degeneration is accelerated and exacerbated in total Nrf2 KO mice (Naguib et al., 2021). Here, we show that as early as 2 weeks post-IOP elevation, both RGC-specific and glial-specific Nrf2 knockdown groups had significantly decreased total axons and significantly increased degenerating axons in comparison to their respective tdTomato controls (Figure 3.5D-F). At 2 weeks post-IOP elevation, AAV2/2.mSncg.Cre injected mice had 35% fewer axons and 130% more degenerating axons than AAV2/2.mSncg.tdTomato controls ($p<0.0001$ and $p=0.0003$, respectively; n=5 nerves/group; Figure 3.5D-F). AAV2/6.Vim.Cre injected mice had 44% fewer axons and 260% more degenerating axons than AAV2/6.Vim.tdTomato controls ($p<0.0001$ and $p<0.0001$; n=5 nerves/group; Figure 3.5D-F). These data show that even a cell-type specific knockdown of Nrf2 in either neurons or astrocytes is sufficient to increase and accelerate axon degeneration following MOM by 2 weeks post-IOP elevation.

By 5 weeks post-IOP elevation, axon degeneration in the optic nerve in both Nrf2 KD groups is even more severe (Figure 3.5D, G-H). At 5 weeks post-IOP elevation, AAV2/2.mSncg.Cre mice had 62% fewer total axons than their AAV2/2.mSncg.tdTomato controls ($p<0.0001$, n=5 nerves/group; Figure 3.5D, G). Additionally, AAV2/2.mSncg.Cre mice had 71% more degenerative axons than AAV2/2.mSncg.tdTomato mice ($p<0.0001$, n=5 nerves/group; Figure 3.5D, H). AAV2/6.Vim.Cre mice had 24% fewer axons than their AAV2/6.Vim.tdTomato controls ($p=0.001$, n=5 nerves/group; Figure 3.5D, G). There was no

difference in the total number of axons between both knockdown groups (p=0.4538, n=5 nerves/group; Figure 3.5D, G). Similarly, AAV2/6.Vim.Cre mice had 69% more degenerative axons than their AAV2/6.Vim.tdTomato counterparts (p=0.0002, n=5 nerves/group; Figure 3.5D, H).

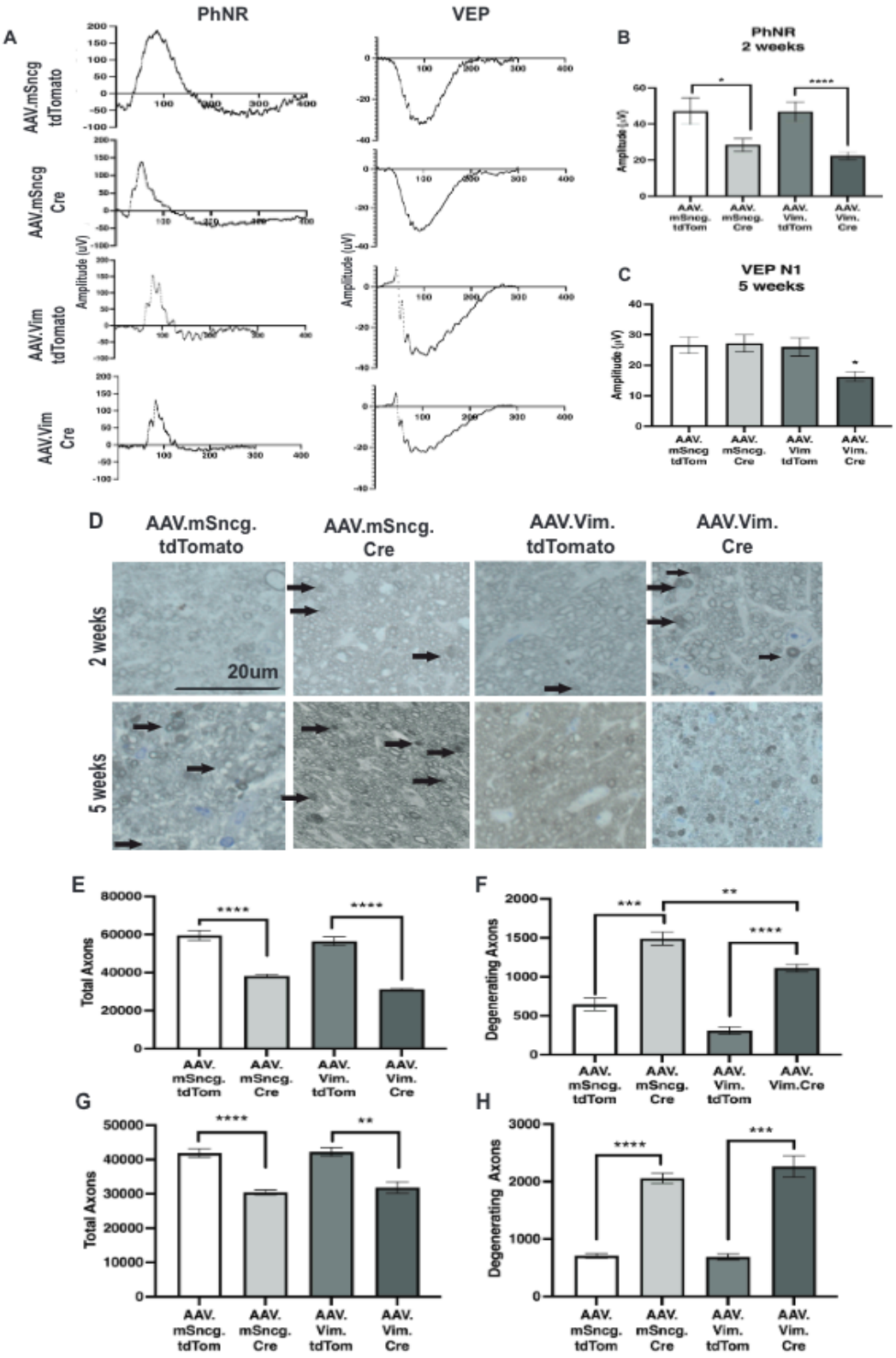
A
PhNR
VEP
AAV.mSncg tdTomato
AAV.mSncg Cre
AAV.Vim tdTomato
AAV.Vim Cre
Amplitude (uV)
B
PhNR
2 weeks
Amplitude (uV)
AAV. mSncg. tdTom
AAV. mSncg. Cre
AAV. Vim. tdTom
AAV. Vim. Cre
C
VEP N1
5 weeks
Amplitude (uV)
AAV. mSncg tdTom
AAV. mSncg. Cre
AAV. Vim tdTom
AAV. Vim. Cre
D
AAV.mSncg. tdTomato
AAV.mSncg. Cre
AAV.Vim. tdTomato
AAV.Vim. Cre
2 weeks
5 weeks
20um
E
Total Axons
AAV. mSncg. tdTom
AAV. mSncg. Cre
AAV. Vim. tdTom
AAV. Vim. Cre
F
Degenerating Axons
AAV. mSncg. tdTom
AAV. mSncg. Cre
AAV. Vim. tdTom
AAV. Vim.Cre
G
Total Axons
AAV. mSncg. tdTom
AAV. mSncg. Cre
AAV. Vim. tdTom
AAV. Vim. Cre
H
Degenerating Axons
AAV. mSncg. tdTom
AAV. mSncg. Cre
AAV. Vim. tdTom
AAV. Vim. Cre

Figure 3.5. Knockdown of Nrf2 in either RGCs or glia decreases visual function and accelerates axon degeneration. A) Representative waveforms for PhNR and VEP N1 amplitudes in all experimental groups. B) Quantification of PhNR amplitudes in all groups at 2 weeks post-IOP elevation, *p<0.05, ****p<0.0001. C) Quantification of VEP N1 amplitudes in all experimental groups at 5 weeks post-IOP elevation, *p<0.05. D) Representative micrographs of optic nerves at 2 and 5 weeks post-IOP elevation timepoints in all experimental groups, with black arrows indicating axon degeneration. Scale bar applies to all micrographs. E) Quantification of total number of axons in all experimental groups at 2 weeks post-IOP elevation, ****p<0.0001. F) Quantification of number of degenerative axons in all experimental groups, **p<0.01, ***p<0.001. G) Quantification of total number of axons in all experimental groups at 5 weeks post-IOP elevation, **p<0.01, ****p<0.0001. H) Quantification of number of degenerative axons in all experimental groups at 5 weeks post-IOP elevation, ***p<0.001, ****p<0.0001

3.4.6 Overexpression of Nrf2 in GCL neurons increases endogenous antioxidant response of the retina at 2 weeks and 5 weeks post-IOP elevation

We intravitreally injected AAV2/2.Nrf2 or AAV2/2.eGFP into C57Bl/6 (WT) mice one week prior to saline or microbead injections to allow for ample time for gene expression (Figure 3.6 and 3.7). At 2 weeks post-IOP elevation, we assessed how increased Nrf2 affected the retina's antioxidant response to ocular hypertension. While it is important that overexpression of Nrf2 in GCL neurons was protective of the PhNR as early as 2 weeks post-IOP elevation, we wanted to determine if overexpression of Nrf2 would mitigate long-term increases in ROS and protect the retina at 5 weeks. By 5 weeks, there is increased glaucomatous pathology in the MOM including axon degeneration and visual function deficits as measured visual evoked potentials (Hines-Beard et al., 2016b; S. Naguib et al., 2021; Sappington et al., 2010).

We used western blot analysis to measure NRF2 levels in whole retina lysate in saline or microbead injected AAV2/2.eGFP or AAV2/2.Nrf2 injected mice (Figure 3.6A). We quantified NRF2 levels in comparison to ß-actin and found that saline-injected AAV2/2.Nrf2 mice had increased NRF2 in comparison to saline-injected AAV2/2.eGFP mice (p=0.0028, n=5 retinas/group, Figure 3.6B). We also found that MOM-injected AAV2/2.Nrf2 mice had increased

NRF2 in comparison to MOM-injected AAV2/2.eGFP mice (p=0.0184, n=5 retinas/group, Figure 3.6B). We confirmed that there was increased NRF2 in the GCL neurons by immunohistochemical analysis of retina sections (Figure 3.6C). These sections were co-labeled with NeuN, a neuronal marker to confirm localization of vector with neurons in the GCL layer.

We intravitreally injected DHE to determine if overexpression of Nrf2 in GCL neurons would be sufficient to decrease superoxide in the retina. We found a 90% increase in DHE fluorescence in the microbead-injected AAV2/2.eGFP mice in comparison to their saline-injected controls (p=0.0012, n=5 eyes/group, Figure 3.6D, E). In microbead-injected mice that received AAV2/2.Nrf2, there was 36% less DHE fluorescence than in their AAV2/2.eGFP injected counterparts (p<0.0001, n=5 eyes/group, Figure 3.6D, E). There was no statistically significant difference in the levels of DHE fluorescence between saline and microbead injected mice in the AAV2/2.Nrf2 injected mice (p=0.7042), indicating that overexpression of Nrf2 in GCL neurons prevents ocular hypertension-induced increases in superoxide (Figure 3.6D, E). In the 5-week timepoint, in AAV2/2.eGFP mice, DHE fluorescence was increased by 90% in microbead-injected mice in comparison to saline-injected controls (p=0.0112, n=5 eyes/group, Figure 3.6I). In AAV2/2.Nrf2 mice, there was no difference in fluorescence levels between saline and microbead mice (p=0.1783; n=6 eyes/group, Figure 3.6I). Additionally, both saline and microbead injected AAV2/2.Nrf2 mice had similar DHE levels to saline-injected AAV2/2.eGFP mice at 5 weeks post-IOP elevation.

Prdx6, Nrf2, Gpx1 and *Txn1* were increased after microbead occlusion and treatment with AAV2/2.Nrf2 in comparison to the AAV2/2.eGFP controls (Figure 3.6F). Specifically, *Prdx6* was increased 198% (p<0.0001; n=5 retinas/group), *Nrf2* was increased 291% (p=0.0035; n=5 retinas/group), *Gpx1* was increased 125% (p=0.0467; n=5 retinas/group) and *Txn1* was increased

by 246% (p=0.0237; n=5 retinas/group). We previously showed an endogenous increase in these antioxidant proteins at 2 weeks post-IOP elevation(S. Naguib et al., 2021).

We also assessed antioxidants on the protein level using western blot analysis at both 2 and 5 weeks post-IOP elevation (Figure 3.6G, H). In AAV2/2.eGFP controls at 2 weeks post-IOP elevation, PRDX6 was increased by 20% in MOM mice in comparison to saline controls (p=0.0364; n=5 retinas/group), GPX1 was increased by 23% (p=0.0377; n=5 retinas/group), and SOD3 was increased by 33% (p=0.014; n=5 retinas/group; Figure 3.6G, H). This is consistent with our previous studies indicating that the retina endogenously responds to increased ROS by upregulating expression of these proteins (S. Naguib et al., 2021). Mice that received AAV2/2.Nrf2 had an exaggerated endogenous antioxidant response in both saline and microbead groups than AAV2/2.eGFP controls. In saline-injected controls, PRDX6 levels were increased in the AAV2/2.Nrf2 group by 35% in comparison to AAV2/2.eGFP controls (p=0.0043; n=5 retinas/group), GPX1 was increased by 19% (p=0.0124; n=5 retinas/group) and SOD3 was increased by 43% (p=0.0032; n=5 retinas/group). In the microbead-injected mice, PRDX6 levels were increased in the AAV2/2.Nrf2 group in comparison to AAV2/2.eGFP by 28% (p=0.0153; n=5 retinas/group), GPX1 was increased by 29% (p=0.0096; n=5 retinas/group) and SOD3 was increased by 33% (p=0.0013; n=5 retinas/group; Figure 3.6G, H).

In the 5-week post-IOP elevation group, there was no difference in GPX1 or SOD3 levels in any of the experimental groups (p=0.4761 and p=0.7226, respectively, data not shown). PRDX6 levels were increased by 45% in AAV2/2.Nrf2 saline-injected mice in comparison to AAV2/2.eGFP saline-injected mice (p=0.0276) and by 71% in the microbead mice (p=0.0121, Figure 6J, K). There was no difference in PRDX6 levels between saline or microbead AAV2/2.Nrf2 mice (n=5 retinas/all groups, Figure 3.6J, K).

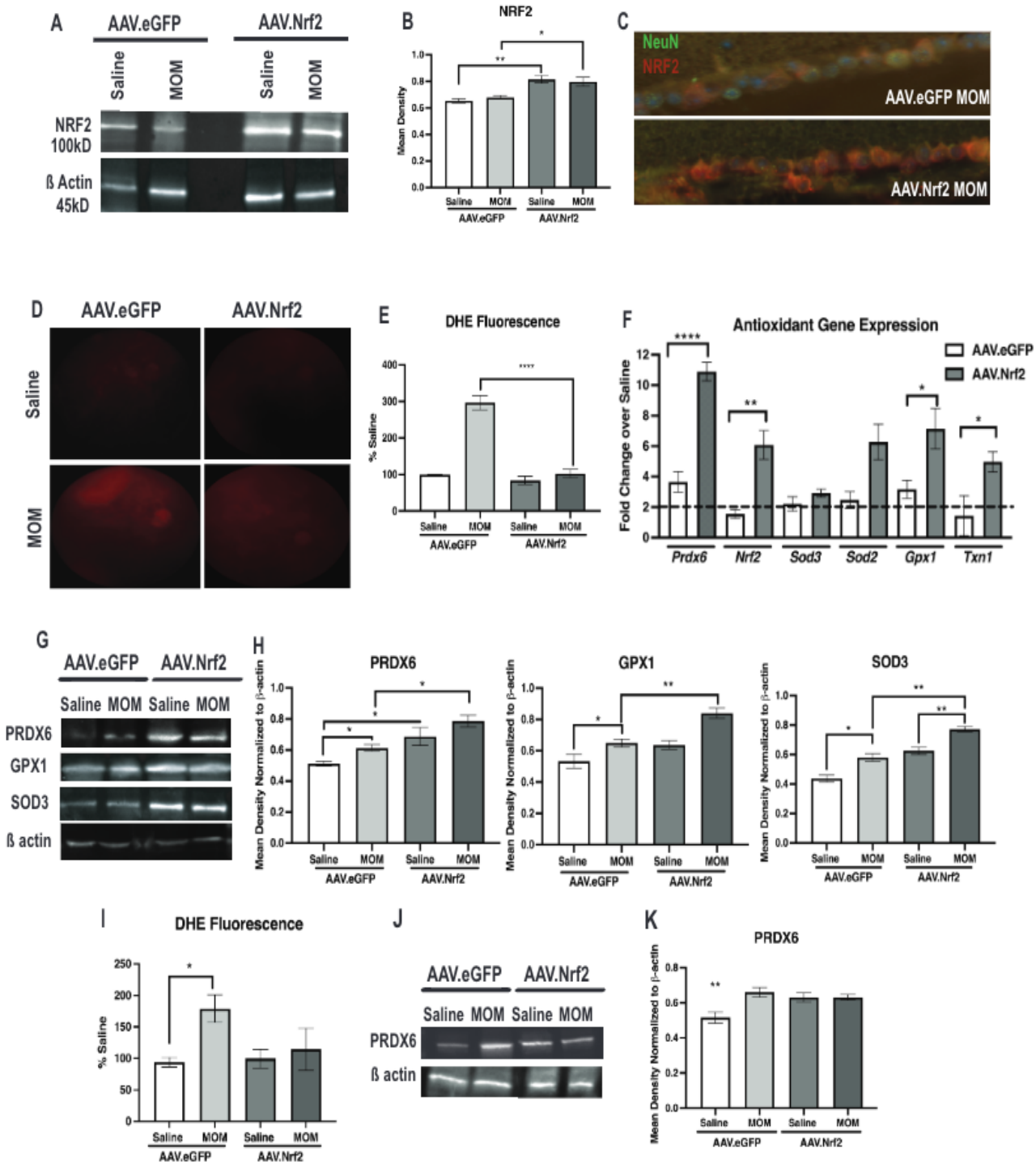
A
AAV.eGFP
AAV.Nrf2
Saline
MOM
Saline
MOM
NRF2
100kD
ß Actin
45kD
B
NRF2
Mean Density
Saline
MOM
Saline
MOM
AAV.eGFP
AAV.Nrf2
C
NeuN
NRF2
AAV.eGFP MOM
AAV.Nrf2 MOM
D
AAV.eGFP
AAV.Nrf2
Saline
MOM
E
DHE Fluorescence
% Saline
F
Antioxidant Gene Expression
AAV.eGFP
AAV.Nrf2
Fold Change over Saline
Prdx6
Nrf2
Sod3
Sod2
Gpx1
Txn1
G
AAV.eGFP
AAV.Nrf2
Saline MOM Saline MOM
PRDX6
GPX1
SOD3
ß actin
H
PRDX6
GPX1
SOD3
Mean Density Normalized to β-actin
I
DHE Fluorescence
% Saline
J
AAV.eGFP
AAV.Nrf2
Saline MOM Saline MOM
PRDX6
ß actin
K
PRDX6
Mean Density Normalized to β-actin

Figure 3.6. Overexpression of Nrf2 in GCL neurons in WT mice increases endogenous antioxidant response of the retina at 2 and 5 weeks post-IOP elevation. A) Representative western blots for ß-actin and NRF2. B) Quantification of NRF2 after normalization to ß-actin, showing increased NRF2 after intravitreal AAV.Nrf2, *p<0.05, **p<0.01. C) Representative fluorescence micrographs of GCL of retinas labeled with NRF2 (red) and NeuN (green) in AAV.eGFP and AAV.Nrf2 groups 2 weeks post-IOP elevation, showing AAV2/2.Nrf2 targets GCL neurons. D) Representative fundus images of DHE fluorescence in all groups at 2 weeks post-IOP elevation. E) Quantification of DHE fluorescence in both AAV.eGFP and AAV.Nrf2 mice at 2 weeks post-IOP elevation in comparison to saline-injected controls, ****p<0.0001. F) Quantification of antioxidant gene transcription (*Prdx6, Nrf2, Sod3, Sod2, Gpx1* and *Txn1)* shown as fold change over appropriate saline controls at 2 weeks post-IOP elevation. G) Representative western blots for PRDX6, GPX1, SOD3 and ß-actin at 2 weeks post-IOP elevation. H) Quantification of PRDX6, GPX1 and SOD3 after normalization to ß-actin at 2 weeks post-IOP elevation, *p<0.05, **p<0.01. I) Quantification of DHE fluorescence in both AAV.eGFP and AAV.Nrf2 mice at 5 weeks post-IOP elevation in comparison to saline-injected controls, *p<0.05. J) Representative western blots for PRDX6 and ß-actin at 5 weeks post-IOP elevation. K) Quantification of PRDX6 levels after normalization to ß-actin at 5 weeks post-IOP elevation, **p<0.01.

3.4.7 Overexpression of Nrf2 in GCL neurons protects against visual function deficits and slows axon degeneration at 2 and 5 weeks post-IOP elevation

We assessed visual function and axon degeneration at 2 and 5 weeks post-IOP elevation to determine if AAV2/2.Nrf2 would be sufficient to protect RGCs from ocular hypertension-induced deficits (Figure 3.7). At 2 weeks, in AAV2/2.eGFP mice, as we have previously published, the PhNR amplitude was decreased by 35% in microbead-injected mice in comparison to their saline-injected controls (p=0.0043, n=14 eyes/group, Figure 3.7A). Overexpression of Nrf2 in GCL neurons using AAV2/2.Nrf2 prevented this decrease, as there was no difference between the saline and microbead-injected mice (p=0.922, n=16 eyes/group, Figure 3.7A). There were no differences in the latency of the PhNR in any of the experimental groups (data not shown).

Previous data showed correlations between decreases in VEP N1 amplitudes and axon degeneration at 5 weeks post-IOP elevation in the MOM (Bond et al., 2016; S. Naguib et al.,

2021; Sappington et al., 2010). At earlier timepoints, we don't expect to see any differences in the total numbers of axons or the number of degenerative axons. We demonstrated, as expected with previous literature, that there were no differences in VEP N1 amplitudes at 2 weeks post-IOP elevation (p=0.9707, n=16 eyes/group, Figure 3.7B). We examined axon degeneration at 2 weeks post-IOP elevation to determine if intravitreal injection of AAV.eGFP or AAV.Nrf2 would have any deleterious effects; there was no difference in the total number of axons or the number of degenerative axons among any of the groups at 2 weeks post-IOP elevation (p=0.6754 or p=0.6079 respectively, Figure 3.7C-E).

At 5 weeks, the microbead-injected AAV2/2.eGFP mice had a 36% lower amplitude of the PhNR in comparison to their saline-injected controls (p=0.0043, n=10 eyes/group, Figure 3.7F) and microbead-injected AAV2/2.Nrf2 mice had a 30% lower amplitude than their saline-injected controls (p=0.0325; n=12 eyes/group, Figure 3.7F). However, AAV2/2.Nrf2 still preserved the amplitude of the PhNR better than AAV2/2.eGFP controls; microbead-injected AAV2/2.Nrf2 mice had a 46% greater amplitude than their AAV2/2.eGFP controls (p=0.0232, n=10 or 12 eyes/group respectively, Figure 3.7F). This pattern remained in the saline-injected controls where there was a 47% greater amplitude in the AAV2/2.Nrf2 group in comparison to the AAV2/2.eGFP group (p=0.0006; n=10 or 12 eyes/group, Figure 3.7F). There was no significant difference in the PhNR latencies of any of the four experimental groups (data not shown).

At 5 weeks post-IOP elevation, it has been previously published that microbead occlusion results in a decreased VEP N1 amplitude by 5 weeks post-IOP elevation (Bond et al., 2016; S. Naguib et al., 2021). In AAV2/2.eGFP mice, VEP N1 amplitude was decreased by 23% in the microbead-injected mice in comparison to their saline-injected controls (p=0.0007; n=10

eyes/group, Figure 3.7G), while there was no difference in VEP N1 amplitude in either group injected with AAV2/2.Nrf2 (p=0.606, n=12 eyes/group, Figure 3.7G). Additionally, the VEP N1 amplitudes of the AAV2/2.Nrf2 MOM group were 17% greater than the amplitudes of the AAV2/2.eGFP MOM group (p=0.016, n=10 or 12 eyes/group respectively, Figure 3.7G).

At 5 weeks post-IOP elevation, AAV2/2.eGFP MOM mice had 19% fewer axons than their saline-injected controls (p=0.0335, n=5 nerves/group) while AAV2/2.Nrf2 MOM had 16% fewer axons than their saline-injected controls (p=0.0011, n=5 nerves/group, Figure 3.7H-I). Still, the total number of axons in the microbead-injected AAV2/2.CMV.Nrf2 group was 20% greater than the microbead-injected AAV2/2.CMV.eGFP group (p=0.0491, n=5 nerves/group, Figure 3.7H, I). Additionally, AAV2/2.eGFP saline mice had 44% more degenerative axons than AAV2/2.Nrf2 saline mice (p=0.0316, n=5 nerves/group) and AAV2/2.eGFP MOM mice had 63% more degenerative axons than AAV2/2.Nrf2 MOM mice (p=0.0005, n=5 nerves/group, Figure 3.7H, I).

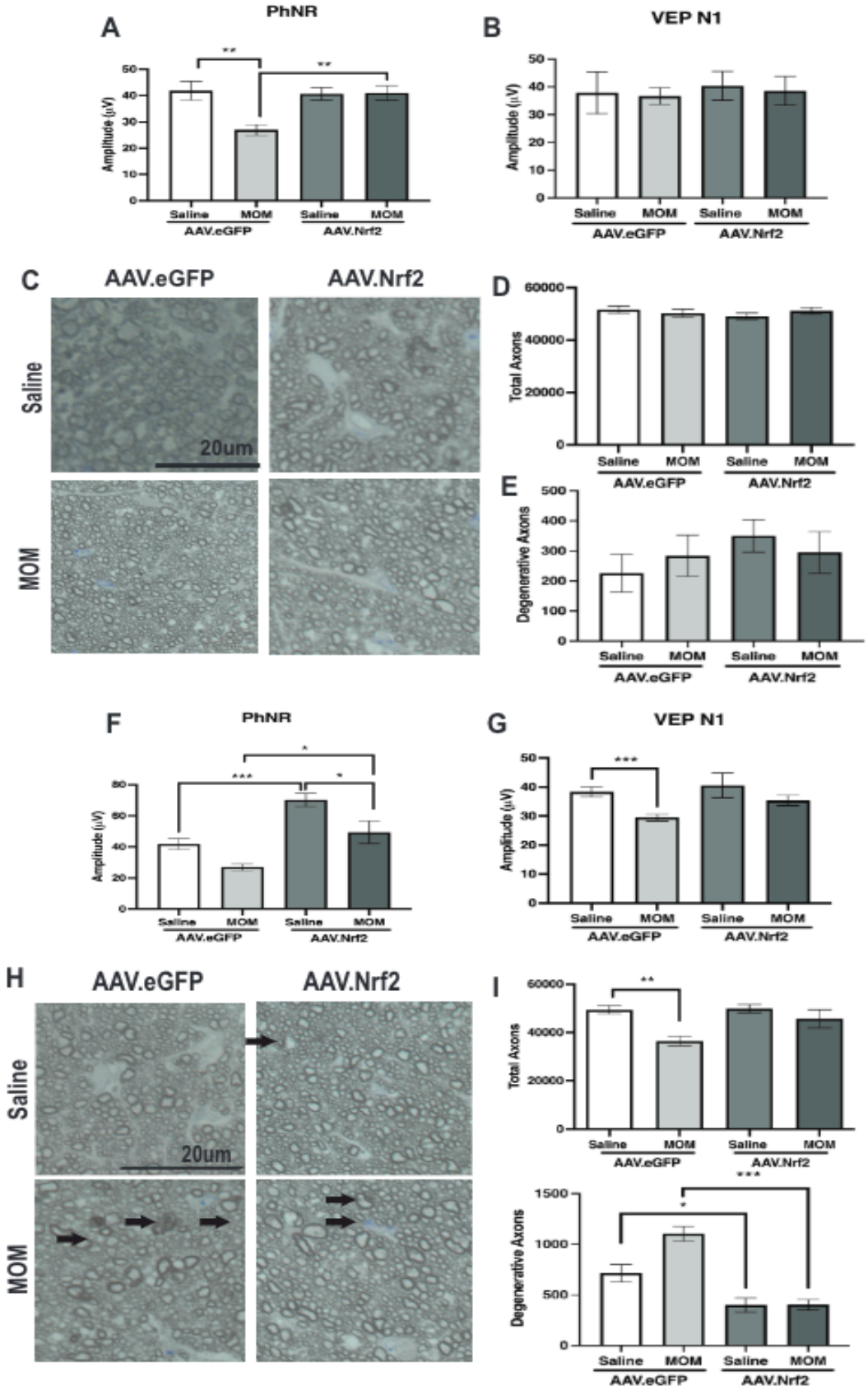
A
PhNR
Amplitude (μV)
Saline
MOM
Saline
MOM
AAV.eGFP
AAV.Nrf2
B
VEP N1
Amplitude (μV)
C
AAV.eGFP
AAV.Nrf2
Saline
MOM
20um
D
Total Axons
E
Degenerative Axons
F
PhNR
G
VEP N1
H
AAV.eGFP
AAV.Nrf2
Saline
MOM
20um
I
Total Axons
Degenerative Axons

Figure 3.7: Overexpression of Nrf2 in GCL neurons in WT mice preserves visual function and protects RGCs at 2 and 5 weeks post-IOP elevation. A) Quantification of PhNR amplitudes in AAV.eGFP and AAV.Nrf2 groups at 2 weeks post-IOP elevation, **p<0.01. B) Quantification of VEP N1 amplitudes in AAV.eGFP and AAV.Nrf2 groups at 2 weeks post-IOP elevation, showing no differences between any groups. C) Representative micrographs of AAV.eGFP and AAV.Nrf2 optic nerves at 2 weeks post-IOP elevation or post-saline injection. Scale bar applies to all micrographs. Arrows point to degenerating axons. D) Quantification of total axons in the optic nerves in all groups at 2 weeks post-IOP elevation, showing no differences in any groups. E) Quantification of degenerative axons in optic nerves in all groups at 2 weeks post-IOP elevation, showing no differences in any groups. F) Quantification of PhNR amplitudes in AAV.eGFP and AAV.Nrf2 groups at 5 weeks post-IOP elevation, *p<0.05, ***p<0.001. G) Quantification of VEP N1 amplitudes in AAV.eGFP and AAV.Nrf2 groups at 5 weeks post-IOP elevation, ***p<0.001. H) Representative micrographs of AAV.eGFP and AAV.Nrf2 optic nerves at 5 weeks post-IOP elevation or post-saline injection. Scale bar applies to all micrographs. Arrows point to degenerating axons. I) Quantification of total axons in the optic nerves in all groups at 5 weeks post-IOP elevation, **p<0.01. J) Quantification of degenerative axons in optic nerves in all groups at 5 weeks post-IOP elevation, *p<0.05, ***p<0.001.

3.5 Discussion

We have previously shown that as early as one week post-IOP elevation in the MOM, increased superoxide is detected in the retina. Then, the retina endogenously responds to ocular hypertension-induced increased ROS via phosphorylation of Nrf2 at 2 weeks post-IOP elevation, concurrent with increased antioxidant gene transcription (Naguib et al., 2021). Ultimately, the endogenous response of the retina is not sufficient to prevent downstream glaucomatous neurodegeneration, but it may be important to delay and mitigate disease progression. However, these studies pointed to Nrf2 as a potential therapeutic for glaucoma—perhaps targeting Nrf2 early in disease progression could extend and increase the retina's endogenous antioxidant response and further protect RGCs from future degeneration. We also showed that in the absence of Nrf2, the retina lacks this endogenous antioxidant response to elevated IOP and, therefore, has an exacerbated and accelerated degenerative phenotype (Naguib et al., 2021). While these findings were important, we sought in this study to elucidate the cell-type specific role of Nrf2 in glaucoma.

In this study, we demonstrate that overexpression of Nrf2 in GCL neurons in an Nrf2 KO mouse resulted in a lack of increase in superoxide levels, increased antioxidant gene expression and protection of RGC cell bodies and axons. These results identified an important role for Nrf2 specifically in RGCs for the aforementioned endogenous antioxidant response to IOP elevation to occur. We also showed that activation of the ARE, via a fluorescent reporter, occurs in RGCs at both 1 and 2 weeks post-IOP elevation in comparison to saline-injected controls; however, the reporter's fluorescence was further elevated at the aforementioned critical timepoint of 2 weeks post-IOP elevation. The increased activation of the ARE in both timepoints after ocular hypertension is important and shows that the retina is attempting to respond at 1 week but the response is increased at 2 weeks. These results could indicate a therapeutic window prior to worsened glaucomatous pathology but still when the retina is upregulating antioxidant gene transcription concurrently with Nrf2 activation as we have previously shown.

We then created cell-type specific knockdowns of Nrf2 in RGCs or astrocytes and showed that removing Nrf2 in either of these cells can result in deleterious consequences: RGC-specific KD of Nrf2 resulted in decreased PRDX6 on both the mRNA and protein level, decreased SOD3, decreased amplitude of the PhNR of the ERG, and accelerated/exacerbated axon degeneration, all at 2 weeks post-IOP elevation. Interestingly, astrocyte-specific KD of Nrf2 also resulted in decreased SOD3 as well as deficits in visual function and accelerated axon degeneration at the same timepoint. We also detected differences in localization of ARE-driven proteins in both knockdown groups; further delving into the mechanism of changes in PRDX6 and SOD3 localization and expression in both cell-specific KD of Nrf2 is outside the scope of this paper but should be explored in future studies.

We found that Nrf2 overexpression in GCL neurons, prior to IOP elevation, prevents increases in ROS and protects RGCs at both 2 and 5 weeks post-IOP elevation. These findings indicate Nrf2 in RGCs as a therapeutic for glaucoma and show that Nrf2 is necessary in RGCs in order for these neurons to mediate the retinal endogenous antioxidant response we have previously described. Our findings indicating Nrf2's importance in RGCs match with what is seen in the literature (Himori et al., 2013c; Liu et al., 2018; M. Wang et al., 2020a; Z. Xu et al., 2015). Ultimately, while our findings are certainly important for understanding neuronal Nrf2 as a therapeutic for glaucoma, we only treated with Nrf2 prior to elevating IOP. In the future, it would be interesting to dissect a time-course for efficacy in protection. Perhaps, overexpressing Nrf2 in GCL neurons past the critical timepoint of 2 weeks post-IOP elevation would render ineffective. Additionally, it could be interesting to treat with an Nrf2 activator or a Keap1 inhibitor rather than overexpressing Nrf2 in RGCs as overexpression experiments also have their own caveats. Pharmacological activation of Nrf2 has been shown to be neuroprotective in a model of ischemia/reperfusion retinal injury (Xu et al., 2015).

Our findings also identify a role for Nrf2 in astrocytes. While we did not explore the potential protective effect of overexpression of Nrf2 in astrocytes, evidence from the literature suggests we would also observe neuroprotection. Overexpression of Nrf2 in astrocytes in two models of ALS protected motor neurons via increased glutathione, secreted by the astrocytes (Vargas et al., 2008). Nrf2 is expressed at significantly higher levels in astrocytes than in neurons. If this is the case, it would make sense that if Nrf2 is knocked-down in the RGCs but not in the astrocytes, there should be some level of protection, however, our findings indicate otherwise. It could be that under normal circumstances, there is more Nrf2 in the astrocytes but it is still being targeted for degradation via Keap1. Alternatively, under homeostasis, perhaps Nrf2

is not present in its phosphorylated or active form in astrocytes, despite being present in larger quantities, and that is why we still observe deficits when Nrf2 is present in the astrocytes at normal levels but is knocked-down in the RGCs. It is also possible that if there is significantly more Nrf2 in astrocytes than in neurons, that the knockdown of Nrf2 in RGCs makes the neurons rely even more heavily on Nrf2 in astrocytes, but the astrocytes cannot compensate (Johnson et al., 2008; Vargas et al., 2008). Additionally, because astrocytes and RGCs work so closely together, it is possible that the lack of Nrf2 in one cell type can be detrimental to the other. The increased astrocytic expression of Nrf2 could be insufficient to protect the RGCs in our model. However, we can ameliorate these detriments if we overexpress Nrf2 in GCL neurons when no surrounding cells have any Nrf2.

Of course, this is not to say that if we were to overexpress Nrf2 in the astrocytes it would not also show neuroprotection. It is also not to say that overexpression or chronic activation of Nrf2 is the simple solution, as previous studies have also shown potential harmful effects. In *Drosophila*, prolonged activation of Nrf2 can actually shorten lifespan (Dengler et al., 2014). Additionally, many activators of Nrf2 work by modifying Keap1 so that it cannot degrade Nrf2 via disruption of its cysteine residues—these activators are often nonspecific and can have off-target effects. The exact mechanism by which Nrf2 overexpression or activation should be administered as a therapeutic needs to be parsed out.

There are significantly fewer studies examining the cell-type specific role of Nrf2 in glaucoma than in other neurodegenerative diseases such as Parkinson's, Alzheimer's or ALS (M. J. Calkins et al., 2009; J. A. Johnson et al., 2008; Schmidlin et al., 2019; Xiong et al., 2015). Interestingly, Nrf2's phenotype for each disease differs. In Parkinson's, Nrf2 is activated primarily in astrocytes whereas in Alzheimer's, it is expressed in astrocytes, neurons, and

potentially even microglia. In ALS, Nrf2 signaling is impaired (Bryan et al., 2013; Dinkova-Kostova et al., 2018; J. A. Johnson et al., 2008). In each of these three diseases, Nrf2 expression is most abundant in regions where pathology is most severe. Interestingly, in the MOM, we previously showed that there were no changes in total Nrf2 levels in microbead-injected mice at any timepoint in comparison to their saline-injected controls (Naguib et al., 2021). These differences could indicate a disease-specific response or even differences between Nrf2 in the retina versus the brain. Additionally, deletion of Nrf2 in each of these models, including glaucoma, as we have previously shown, enhances pathology whereas overexpression/pharmacological activation of Nrf2 is often protective (Nakagami, 2016; Nguyen et al., 2000; Z. Xu et al., 2015). These findings align with what our study shows in the MOM. Ultimately, in neurodegeneration, endogenous Nrf2 is insufficient to prevent oxidative stress and subsequent damage of neurons and it remains a potential therapeutic target for each of these diseases.

CHAPTER 4

Erythropoietin-Mediated Activation of NRF2 via MAPK Protects RGCs and Astrocytes from Glaucomatous Pathology

4.1 Abstract

Erythropoietin (EPO) has been shown to be neuroprotective in multiple neurodegenerative diseases, including glaucoma. EPO-R76E is a mutant form of EPO that has neuroprotective effects without significantly increasing hematocrit. We use PLGA microparticles to deliver EPO-R76E intravitreally in a sustained-release mechanism. Due to its pleiotropic effects, we do not know the exact mechanism by which EPO confers neuroprotection, but previous studies have pointed to the NRF2/ARE pathway. We have previously shown that NRF2 is activated earlier than glaucomatous pathology in the well-characterized microbead occlusion model (MOM) of glaucoma. In this study, we elevate intraocular pressure, the only modifiable risk factor for glaucoma, using the MOM and then delivered intravitreal PLGA.EPO-R76E one day later. We found that as early as 1 week post-IOP elevation, eyes treated with PLGA.EPO-R76E had decreased retinal superoxide levels *in vivo* in comparison to their empty PLGA particle controls. We also demonstrated that PLGA.EPO-R76E results in earlier phosphorylation of NRF2 than the endogenous antioxidant response of the retina to ocular hypertension, and that this activation of NRF2 results in differential upregulation of antioxidants than we have shown before. Additionally, we have shown that PLGA.EPO-R76E's activation of NRF2 is dependent on phosphorylation by MAPK.

4.2 Introduction

Glaucoma, a leading cause of blindness worldwide, is an age-related progressive optic neuropathy occurring from degeneration and death of retinal ganglion cells (RGCs) (D. J. Calkins & Horner, 2012; Greco et al., 2016; Weinreb et al., 2014a). A major risk factor for glaucoma is sensitivity to intraocular pressure (IOP). Current treatments for glaucoma are directed towards lowering IOP but do not always result in slower progression of the disease. Further, there are issues of poor patient compliance to administering multiple IOP-lowering drops daily (Goldberg, 2003; Nickells et al., 2012; Qu et al., 2010). A more effective long-term treatment independent of IOP lowering is needed to prevent further prevalence of this condition. In this study, we propose using a sustained release of a neuroprotective that can be delivered intravitreally through a single injection.

While the exact etiology of glaucoma is still under investigation by many labs, we know that oxidative stress significantly contributes to disease pathogenesis, and antioxidants have been shown to protect retinal neurons (Inman et al., 2013; Kimura et al., 2017; Ko et al., 2005; Naguib et al., 2021; Zhao et al., 2016). There are several endogenous antioxidant defenses against oxidative stress. One of these is via the transcription factor, NRF2, which our lab and others have implicated as a potential therapeutic target for glaucoma (Fujita et al., 2017; Himori et al., 2013c; S. Naguib et al., 2021). Under homeostatic conditions, NRF2 remains sequestered in the cytoplasm of the cell where it is constantly targeted for degradation via ubiquitination by its repressor protein, KEAP1. Under conditions of oxidative stress, Keap1 undergoes a conformational change and releases NRF2, preventing degradation. NRF2 is then able to accumulate in the cytoplasm of the cell where it can translocate into the nucleus and bind to the antioxidant response element (ARE). The ARE is a *cis*-acting enhancer region of the DNA that,

upon interaction with NRF2 and small Maf proteins, can increase transcription of antioxidant genes (Y. Huang et al., 2015; Q. Ma, 2013; Robledinos-Antón et al., 2019; Tonelli et al., 2018b; Vomhof-DeKrey & Picklo, 2012a; Vriend & Reiter, 2015). Because glaucoma is an age-related disease, it is important to note that previous studies have also shown that NRF2 nuclear translocation and interaction with the ARE decline with age (Schmidlin et al., 2019; Sykiotis et al., 2011; Zhang et al., 2015).

We and others have previously shown that overexpression of *Nrf2* can be neuroprotective in models of glaucoma (Naguib et al., 2022 *in prep;* Xu et al., 2015; Fujita et al., 2017). Additionally, activation of NRF2 by erythropoietin (EPO) has been shown to decrease oxidative stress (Genc et al., 2010; Wu et al., 2018; Zakharova et al., 2018). EPO is a cytokine that stimulates production of red blood cells through a process known as erythropoiesis. The liver secretes EPO where it can then bind and interact with its receptor (EpoR), and inhibits death of erythroid progenitor cells (Bunn, 2013; Z. Z. Chong et al., 2003; Resende et al., 2018; Rey et al., 2019; Suresh et al., 2020b). EPO and its receptor are also produced in other tissues outside of the liver, including the retina (Hernández et al., 2017b; Rey et al., 2019; Shirley Ding et al., 2016). Previous studies have shown that EPO can play a role in reducing cell death, degeneration and oxidative stress in multiple models of glaucoma (Bond et al., 2016; Hines-Beard et al., 2016b; Shirley Ding et al., 2016; T. A. Sullivan, 2011; Zhong et al., 2007).

There are challenges with EPO therapy for neurodegenerative diseases that should be considered—it has a short half-life *in vivo,* and it can increase red blood cell production (Hernández et al., 2017c; Rey et al., 2019; T. A. Sullivan et al., 2011a). Our lab has previously published using viral deliveries of a mutant form of EPO, EPO-R76E (Bond et al., 2016; Hines-Beard et al., 2016a). EPO-R76E can preserve retinal neurons and optic nerve axons in multiple

models of glaucoma, but does not induce a physiologically significant increase in hematocrit (T. A. Sullivan et al., 2011a). To allow for sustained release of EPO-R76E after a single intravitreal injection, we explored microparticle-mediated delivery of EPO-R76E. Previous studies have used the poly(lactic-co-glycolic acid)/poly(lactic acid) (PLGA/PLA) microparticle system as a way to deliver EPO in a rat model of optic nerve crush and demonstrated efficacy in protecting retinal neurons. In this model, a single injection of these microparticles sustained RGCs up to 8 weeks after injury, whereas free EPO would have had to be delivered every 2 weeks to see similar protection (Rong et al., 2012). We have also previously published using EPO-R76E formulated into microparticles containing PLGA in a model of blast-indirect traumatic optic neuropathy (DeJulius et al., 2021). In that study, we showed that a single intravitreal injection of these microparticles delivered one day after injury protected against optic nerve degeneration and visual function deficits (DeJulius et al., 2021).

In this study, we aimed to determine if EPO-R76E PLGA microparticles (PLGA.EPO-R76E) would protect against downstream neurodegeneration in the well-characterized microbead occlusion model (MOM) of glaucoma. We also sought to determine if EPO's neuroprotection is occurring via activation of the NRF2/ARE pathway. Our study demonstrates that PLGA.EPO-R76E can activate NRF2 earlier than the retina's endogenous activation of NRF2/ARE and that this activation occurs via the MAPK pathway.

4.3 Materials and Methods

4.3.1 Mice: C57Bl/6 J (Jackson Labs, Bar Harbor, ME) were group-housed, maintained on a 12-h light-dark cycle, and provided food and water ad libitum. All experiments were approved by

the Institutional Animal Care and Use Committee of Vanderbilt University. An equal distribution of male and female mice (2-3 months old) were used for this project.

4.3.2 Microbead Occlusion: We elevated IOP bilaterally using occlusion of the anterior chamber with 2 µl injections of 15-µm diameter FluoSpheres polystyrene microbeads (Thermo Fisher, Waltham, MA) as previously described(Bond et al., 2016; D. J. Calkins et al., 2018; S. Naguib et al., 2021; Sappington et al., 2010). Additional mice received bilateral injections of an equivalent volume of lactated Ringer's saline solution as controls. Briefly, 1.5 mm outer diameter/1.12 mm inner diameter filamented capillary tubes (World Precision Instruments, Sarasota, FL) were pulled using a P-97 horizontal puller (Sutter Instrument Company, Novato, CA), and the resulting needles were broken using forceps to an inner diameter of ~100 µm. Microbeads were loaded and injected using a microinjection pump (World Precision Instruments, Sarasota, FL). Mice were anesthetized with isoflurane and dilated using topical 1% tropicamide ophthalmic solution (Patterson Veterinary, Devens, MA), and 2 µl (~2,000 microbeads) were injected. The needle was maintained in the injection site for 20 seconds before retraction to reduce microbead efflux. Mice were given topical 0.3% tobramycin ophthalmic solution (Patterson Veterinary, Devens, MA) following injection.

4.3.3 IOP measurements: We measured IOP immediately prior to microbead injection and biweekly thereafter using the Icare TonoLab rebound tonometer (Colonial Medical Supply, Franconia, NH) as previously described(D. J. Calkins et al., 2018; Hines-Beard et al., 2016a). Mice were anesthetized using isoflurane, and 10 measurements were acquired from each eye within 2 minutes of induction of anesthesia.

4.3.4 Plasmids/AAV intravitreal injections:

Table 4.1. Plasmids/AAV information.

Plasmid Name and Nomenclature for Paper	Plasmid Purchased from	AAV type/purchased from	Mouse injected into
pAAV.Trx-ARE(WT)-TnSV0HA-zG referred to as AAV2/2.ARE	N/A	AAV2/2 by SignaGen	C57Bl/6

Viruses were intravitreally injected two weeks prior to MOM injections. All vectors this study were injected at a concentration of 1 x 10^9 GC/ml.

4.3.5 *In vivo* electrophysiology: Mice were dark adapted overnight, dilated with 1% tropicamide for 10 minutes and anesthetized with 20/8/0.8 mg/kg ketamine/xylaxine/urethane according to previously published methodology(Bernardo-Colon et al., 2018; S. Naguib et al., 2020, 2021). Mice were placed on heated surface of the ERG system to maintain body temperature. Corneal electrodes with integrated stimulators (Celeris System, Diagnosys LLC, Lowell, MA) were placed on eyes that were lubricated with GenTeal drops. Subdermal platinum needle electrodes were placed in the snout and back of the head at the location of the visual cortex. A ground electrode was placed in the back of the mouse. For VEPs, mice were exposed to 50 flashes of 1Hz, 0.05 cd.s/m^2 white light with a pulse frequency of 1. For ERGs, mice were exposed to flashes of 1 Hz, 1 cd.s/m^2 white light with a pulse frequency of 1. For photopic negative ERGs (PhNR), mice were exposed to 20 continuous flashes of white light on a green background with a pulse frequency of 2. Each experimental group had 12-16 eyes.

4.3.6 Dihydroethidum Fluorescence: A dye that fluoresces in the presence of superoxide and, to a lesser extent, hydrogen peroxide, dihydroethidum (DHE), was utilized for these studies as

previously described(Bernardo-Colon et al., 2018). Mice were anesthetized with 2.5% isofluorane and intravitreally injected with 1 µl (0.5uM) of DHE (ThermoFisher Scientific, Waltham, MA) diluted in phosphate-buffered saline (PBS) using a 30-gauge Hamilton syringe. Just prior to imaging, mice were anesthetized with ketamine/xylazine and eyes were dilated with 1% tropicamide. Thirty minutes after DHE injection, fluorescence was imaged on a Micron IV retinal imaging microscope (Phoenix Research Labs, Pleasanton, CA) using an FF02-475/50 nm excitation filter (Semrock, Inc. Rochester, NY) and ET620/60X emission filter (Chroma Technology Corp., Bellows Falls, VT). The average intensity of the fluorescence throughout the retina was quantified using ImageJ(Rasband, 2018). For each experimental group, 6-8 eyes were analyzed.

4.3.7 MAPK inhibitor experiments: A subset of C57 mice were intravitreally injected with a p38 inhibitor, BIRB 796 (Lambert et al., 2020). 1ul of intravitreal BIRB 796 was given one week after induction of ocular hypertension using MOM using a 3% drug suspension of 30mg BIRB 796 into 1ml buffer as previously described (Lambert et al., 2020).

4.3.8 Tissue collection: For western blots and qPCR, retinas were collected and flash frozen from mice euthanized by anesthetic overdose and cervical dislocation. For immunohistochemistry and optic nerve histology, tissue was collected and incubated in 4% paraformaldehyde for until use at 4^{o}C.

4.3.9 Protein assay: Protein concentrations were determined from 10 □l of retina homogenates with the Pierce BCA Protein Assay Kit (cat#: 23225, ThermoFisher Scientific, Waltham, MA).

BSA was used as the protein standard. Absorbance was measured with the plate reader POLARstar Omega (BMG Labtech, Ortenburg, Germany).

4.3.10 Western blot: Single retinas were sonicated in lysis buffer (PBS, EDTA and Halt protease inhibitor) and centrifuged for 30 minutes at 4ºC. 4x Laemmli buffer (Bio-rad, cat# 1610747) containing 2-ME was added to the samples and heated for 5 minutes at 95ºC. Known amounts of protein (10-20 µg/retina) or protein ladder (cat#1610375, Bio-rad, Hercules, CA) were loaded in 4-20% polyacrylamide gels (Bio-Rad #456-1095). Proteins were transferred onto nitrocellulose using the Bio-Rad trans blot turbo transfer system. Membranes were blocked in 2% BSA in TBS overnight at 4ºC. Membranes were incubated in primary antibody at room temperature with rocking for 2 hours. β-actin was usd as the loading control for all experimental groups. After washing, membranes were incubated with secondary antibody (IRDye 800CW Donkey anti-rabbit, #926-32213 or IRDye 680CW Donkey anti-mouse, #926-68022,1:5000 in 1% BSA/TBS) at room temperature for 1 hour. After washing, blots were imaged with a Bio-Rad ChemiDoc system. Band density was quantified by scanning the blot using Adobe Photoshop. Each band was selected with the same frame and set measurements were used to obtain the gray mean value for each. Band intensity measurements from protein of interest were divided by band intensity measurements of loading control (ß-actin). Each experimental group had 5 retinas.

4.3.11 EPO ELISA: EPO-R76E concentration in the cell lysates was measured by sandwich ELISA using a Quantikine Human EPO ELISA kit (R&D Systems, Minneapolis, MN) according to manufacturer directions. Samples were loaded at 10 µl per well and tested in duplicate, and the results were averaged.

4.3.12 Immunohistochemistry: Eye cups were embedded in paraffin according to previously published methods using the Vanderbilt Vision Research Center histology core and sectioned at 10um (Lambert et al., 2020). Slides were then warmed on a slide warmer at a medium setting (about 40 ºC) for 30 minutes. Slides were then placed in a rack and went through a series of deparaffinization steps: xylene (10 minutes), 100% ethanol (10 minutes), 100% ethanol (5 minutes), 95% ethanol (5 minutes), 80% ethanol (5 minutes), 60% ethanol (5 minutes), 40% ethanol (5 minutes). Slides were then placed in coplin jar covered with sodium citrate solution and boiled for 30 minutes (2.94g of tri-sodium citrate dehydrate in 1L of DI water, adjusted to pH of 6.0 and then added 0.5ml of Tween 20). Following boiling, slides were washed twice in 1x PBS for 5 minutes. Then, slides incubated in sodium borohydride solution (0.05g sodium borohydride dissolved in 50ml DI water, made fresh every time) at room temperature. Slides were then placed in blocking buffer (500mL 1x PBS, 1.25mL Triton-X, 1.25mL Tween 20, 0.5g sodium citrate, 11.25g glycine, 5g BSA) and 5% normal donkey serum (cat #: D9663, Millipore Sigma, Darmstadt, Germany) for 1 hour at room temperature. Slides were washed once with 1xPBS and placed in primary antibody diluted in staining buffer (500mL 1x PBS, 1.25mL Triton X, 1.25 mL Tween 20, 5g BSA) overnight at 4ºC in a humidified chamber. The following day, slides were twice washed with 1x PBS for 5 minutes each. Secondary antibody was diluted in staining buffer and was added to the slides for 2 hours at room temperature at 1:200 dilution after spinning for 10 minutes at 13,000g. After 2 hours, slides were washed twice in 1x PBS for 5 minutes each. Then, slides were coverslipped with Vectashield containing DAPI (cat#: H-1200-10, Vector Laboratories, Burlingame, CA) and sealed with nail polish. Slides were imaged on a Nikon Eclipse epifluorescence microscope (Nikon, Melville, NY). All images were collected from the same retinal region with identical magnification, gain and exposure settings.

Fluorescence intensity was quantified via ImageJ as previously described (Naguib et al. 2019; Naguib et al., 2021). A rectangle was selected around the region of interest, channels were split for multiple antibodies, threshold was adjusted, noise was de-speckled and fluorescence intensity was measured. Fluorescence intensity was normalized to saline-injected mice. Each experimental group included 5 eyes.

Table 4.2. Antibodies used for IHC

Antibody	**Company**	**Catalog Number**	**Species**	**Dilution for western blot**	**Dilutions for IHC**
Nrf2	Abcam	137550	Rabbit	1:1000	1:200
pNrf2	ThermoFisher	PA5-67520	Rabbit	1:1000	1:200
ß-actin	Cell Signaling	E4D9Z	Mouse	1:1000	N/A
Prdx6	Abcam	133348	Rabbit	1:1000	1:100
Gpx1	ThermoFisher	PA5-26323	Rabbit	1:500	N/A
SOD3	Abcam	80946	Rabbit	1:1000	1:200

4.3.13 Optic nerve counts: Optic nerves were post-fixed in glutaraldehyde followed by Resin 812 embedding and Araldite 502 (cat#: 14900 and 10900 respectively, Electron Microscopy Sciences, Hatfield, PA) according to previously published protocols(Bernardo-Colon et al., 2018; Hines-Beard et al., 2012; S. Naguib et al., 2021; Sarah Naguib, Bernardo-Colón, Cencer, et al., 2020). Leica EM-UC7 microtome was used to collect 1 mm thick sections of the optic nerves. Sections were then stained with 1% paraphenylenediamine and 1% toluidine blue and were imaged on a Nikon Eclipse Ni-E microscope using 100x oil immersion objective (Nikon Instruments, Melville, NY). The optic nerves were montaged into a 5 x 5 image using the Nikon

Elements software to scan a large image. We used the Counting Array and Better Cell Counter plugins to ImageJ, which creates a grid of nine squares overtop the montaged optic nerve. We manually counted healthy and degenerating axons, which are color-coded by the plugins. Degenerative axon profiles were identified by dark paraphenylenediamine staining due to collapsed myelin or loose myelin (onioning) surrounding the axon. A grid was used to avoid bias, by always counting in the same squares, using a cross configuration. Additionally, to avoid bias, Twenty percent of the optic nerve cross-sectional area was counted and the total was multiplied by five to estimate total and degenerating axons within the nerve. Each experimental group included 4-5 nerves.

4.3.14 Data Analysis: All statistical analyses were performed using GraphPad Prism software (La Jolla, CA). A one-way ANOVA with a Bonferroni post hoc test ($a = 0.05$) was used to analyze western blot quantification, IHC fluorescence quantification, ON quantification data, and ERG/VEP latencies and amplitudes. A one-way ANOVA and Dunnett's multiple comparisons post hoc test ($a = 0.05$) were used to analyze the qPCR results. Means and standard deviation were calculated for each data set.

4.4 Results

4.4.1 A single intravitreal injection of PLGA.EPO-R76E lasts up to 6 weeks

After injection of microbeads, IOP remained elevated for the duration of the study (Figure 4.1A). We calculated that we injected 1.65 U/eye of EPO-R76E in PLGA particles in accordance with our previous studies (DeJulius et al., 2021). This resulted in sustained release of 20-30 mU/ml EPO-R76E in the eye (Figure 4.1B). Low levels of endogenous EPO were present

in eyes injected with empty PLGA particles (Figure 4.1B). Release of EPO-R76E was detected out to six weeks after initial intravitreal injection without evidence of decrease (Figure 4.1B).

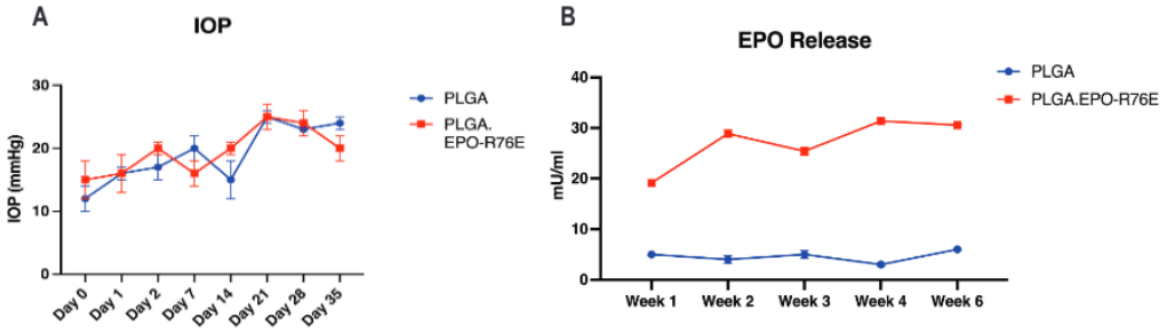

Figure 4.1. Single intravitreal injection of PLGA.EPO-R76E can last up to 6 weeks. A) IOP levels over time. B) EPO ELISA demonstrating retinal EPO levels at 1, 2, 3, 4, and 6 weeks post-IOP elevation.

4.4.2 PLGA.EPO-R76E is antioxidant and neuroprotective in the microbead occlusion model of glaucoma

We previously published that *in vivo* retinal superoxide levels are elevated as early as 1 week post-IOP elevation (Naguib et al., 2021). Here, we sought to determine if a single intravitreal injection of PLGA.EPO-R76E one day post-IOP elevation would be sufficient to reduce retinal superoxide levels. We intravitreally injected dihydroethidium (DHE), a superoxide fluorescent reporter, at 1, 2, 3 and 4 weeks post-IOP elevation and intravitreal injection with PLGA or PLGA.EPO-R76E (Figure 4.2A-B). Notably, we have previously shown that PLGA microparticles can increase ROS (DeJulius et al., 2021).

At all timepoints post-IOP elevation, PLGA.EPO-R76E treated mice had significantly reduced retinal superoxide levels than mice that received empty PLGA particles. At 1 week post-IOP elevation, PLGA.EPO-R76E treated mice had 67% less DHE fluorescence than their empty

PLGA controls (p=0.005, n=6 or 4 retinas/group respectively; Figure 4.2A-B). At 2 weeks post-IOP elevation, PLGA.EPO-R76E treated mice had 81% less DHE fluorescence than their empty PLGA controls (p=0.0422, n=6 or 4 retinas/group respectively; Figure 4.2A-B). At 3 weeks post-IOP elevation, PLGA.EPO-R76E treated mice had 37% less DHE fluorescence than their empty PLGA controls (p=0.0048, n=4 or 5 retinas/group respectively; Figure 4.2A-B). At 4 weeks post-IOP elevation, PLGA.EPO-R76E treated mice had 39% less DHE fluorescence than their empty PLGA controls (p=0.0034, n=6 or 4 retinas/group respectively; Figure 4.2A-B).

We previously published that RGC function is decreased as soon as 2 weeks post-IOP elevation in the MOM as measured by the photopic negative response (PhNR) of the ERG (Naguib et al., 2021). In this study, at 2 weeks post-IOP elevation, the PhNR amplitudes of PLGA.EPO-R76E treated mice were 50% greater than their empty PLGA counterparts (p=0.0093, n=11 or 14 eyes/group respectively; Figure 4.2C). By 5 weeks post-IOP elevation, the PhNR amplitudes of PLGA.EPO-R76E treated mice were 54% greater than their empty PLGA counterparts (p=0.0003, n=10 or 13 eyes/group, respectively; Figure 4.2C).

At later timepoints (4-6 weeks post-IOP elevation), deficits in the amplitudes of the visual evoked potential (VEP) or even the b-wave of the ERG (measuring bipolar cell function) have been reported (A. W. Kong et al., 2020; Kumar et al., 2022; Santina et al., 2013). Here, we showed that while there are no differences in the b-wave amplitudes at 2 weeks post-IOP elevation following intravitreal injection of PLGA or PLGA.EPO-R76E, at 5 weeks, the mice treated with empty PLGA particles have significantly decreased b-wave amplitude. The b-wave amplitude of the mice treated with PLGA.EPO-R76E was 42% greater than the mice that received empty PLGA particles (p=0.0079, n=6 or 7 eyes/group respectively; Figure 4.2D). Interestingly, the VEP N1 amplitude was affected by empty PLGA particles as early as 2 weeks

post-IOP elevation: the mice treated with PLGA.EPO-R76E had VEP N1 amplitudes that were 51% greater than the mice treated with empty PLGA particles ($p<0.0001$, n=8 or 14 eyes/group, respectively; Figure 4.2E). At 5 weeks post-IOP elevation, mice treated with PLGA.EPO-R76E had 41% greater VEP N1 amplitudes than their empty PLGA injected counterparts ($p=0.0004$, n=10 or 8 eyes/group, respectively; Figure 4.2E).

Axon degeneration isn't observed until 4-6 weeks post-IOP elevation in this model (Sappington et al., 2010; Hines-Beard et al., 2016; Bond et al., 2016). At 2 weeks post-IOP elevation, PLGA.EPO-R76E treated mice had 17% more total axons than their empty PLGA treated counterparts, suggesting a negative effect of PLGA alone ($p=0.0327$, n=5 nerves/group; Figure 4.2F, G). Additionally, PLGA.EPO-R76E treated mice had 82% fewer degenerative axons than their empty PLGA treated counterparts (0.0348, n=5 nerves/group; Figure 4.2F, H). At 5 weeks post-IOP elevation, PLGA.EPO-R76E treated mice had 25% more total axons and 77% fewer degenerative axons than their empty PLGA controls ($p=0.0027$ and $p=0.0071$, respectively, n=5 nerves/group; Figure 4.2F, I-J).

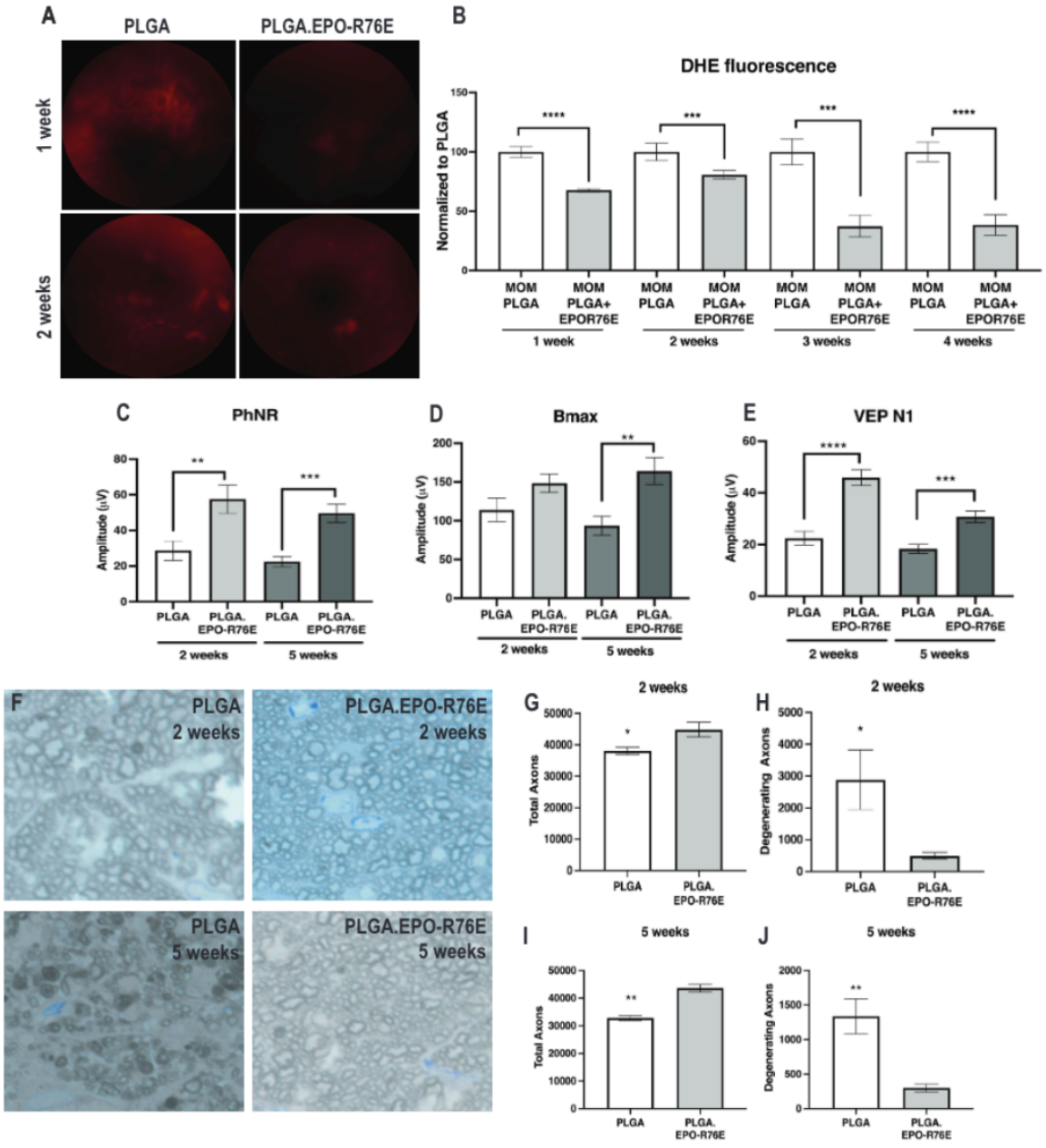

Figure 4.2. PLGA.EPO is antioxidant and neuroprotective after MOM. A) Representative fundus images of DHE fluorescence at 1 and 2 weeks post-IOP elevation in empty PLGA controls and PLGA.EPO-R76E injected mice. B) Quantification of DHE fluorescence at 1-4 weeks post-IOP elevation, ***p<0.001, ****p<0.0001. C) Quantification of PhNR of the ERG at 2 and 5 weeks post-IOP elevation, **p=0.01, ***p<0.001. D) Quantification of b-max amplitude of the ERG at 2 and 5 weeks post-IOP elevation, **p=0.01. E) Quantification of N1 amplitude of the VEP at 2 and 5 weeks post-IOP elevation, ***p<0.001, ****p<0.0001. F) Representative micrographs of optic nerves at 2 and 5 weeks post-IOP elevation. G) Quantification of total axons in the optic nerves at 2 weeks post-IOP elevation, *p<0.05. H)

Quantification of number of degenerative axons in the optic nerves at 2 weeks post-IOP elevation, *p<0.05. I) Quantification of total axons in the optic nerves at 5 weeks post-IOP elevation, **p=0.01. J) Quantification of number of degenerative axons in the optic nerves at 5 weeks post-IOP elevation, **p=0.01.

4.4.3 PLGA.EPO-R76E causes NRF2 phosphorylation

EPO has been shown to have pleiotropic effects and its mechanism of action resulting in neuroprotection is often hard to pin down. We sought to determine if PLGA.EPO-R76E could result in downstream activation of NRF2. We used western blot analysis to determine if there was a greater ratio of phosphorylated to total NRF2 in mice intravitreally injected with PLGA.EPO-R76E in comparison to their empty particle controls. We assessed total and phosphorylated NRF2 levels at 1 and 2 weeks post-IOP elevation in accordance with our previous studies, showing that NRF2 is phosphorylated in the retina at 2 weeks post-IOP elevation as a way for the retina to endogenously activate an antioxidant response (Figure 4.3A-B). We found that at 1 week post-IOP elevation, the ratio of phosphorylated to total NRF2 was 47% increased in PLGA.EPO-R76E treated mice in comparison to their PLGA particle controls (p=0.0136, n=3 retinas/group; Figure 4.3A-B), demonstrating that PLGA.EPO-R76E can accelerate NRF2 phosphorylation. At 2 weeks post-IOP elevation, the ratio of phosphorylated to total NRF2 was 41% increased in PLGA.EPO-R76E treated mice in comparison to their PLGA particle controls (p=0.0058, n=3 retinas/group; Figure 4.3A-B).

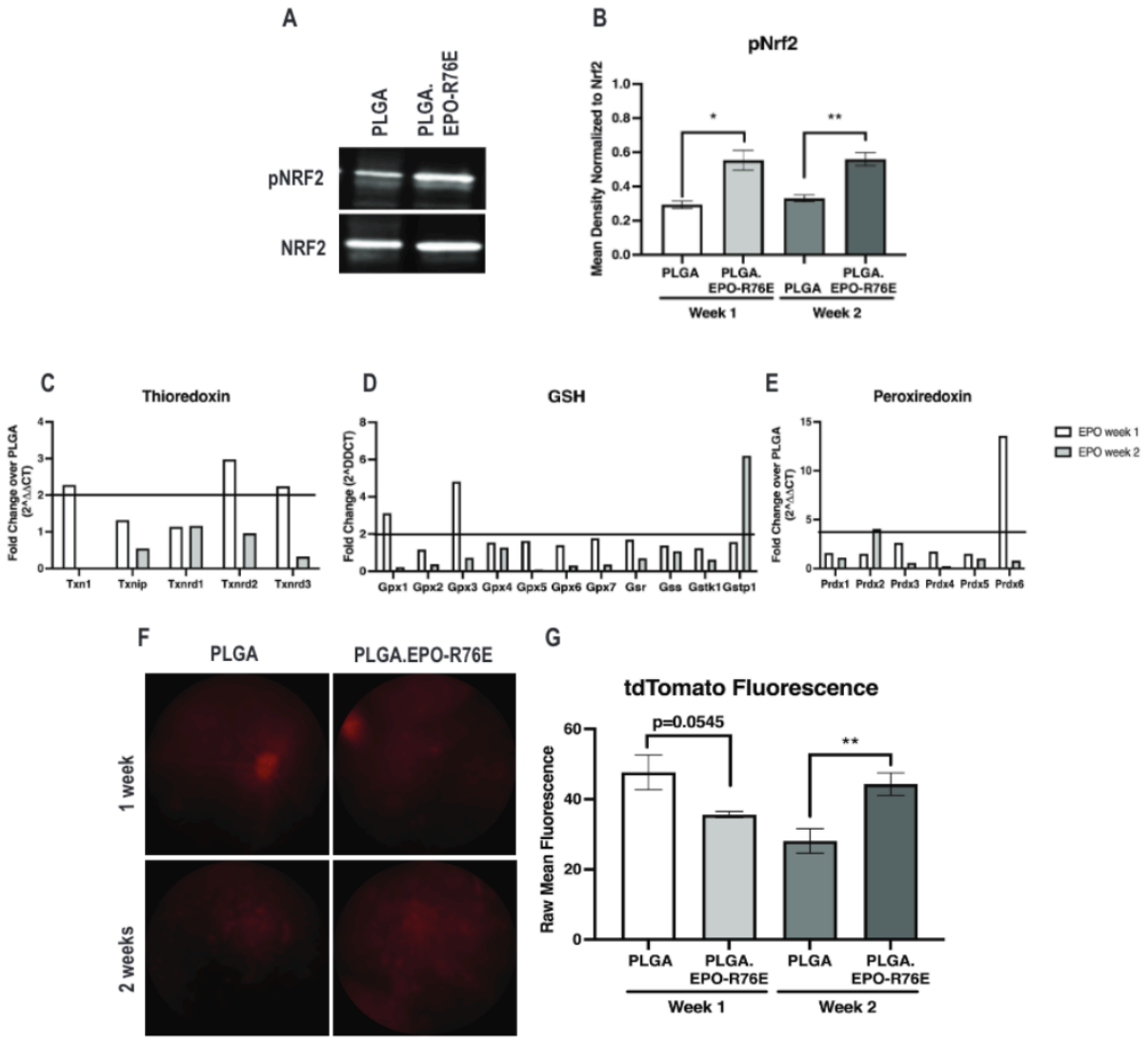

Figure 4.3. PLGA.EPO-R76E phosphorylates and activates NRF2. A) Representative western blot for pNRF2 and NRF2 in empty PLGA and PLGA.EPO-R76E at 2 weeks post-IOP elevation. B) Quantification of pNRF2 to total NRF2 in PLGA and PLGA.EPO-R76E injected mice at 1 and 2 weeks post-IOP elevation, *p<0.05, **p=0.01. C) Quantification of fold changes in PCR microarray for: C) thioredoxin-related genes; D) glutathione-related genes; and E) peroxiredoxin-related genes. E) Representative micrographs of tdTomato fluorescence in mice injected with AAV2/2.ARE and either PLGA or PLGA.EPO-R76E at 1 and 2 weeks post-IOP elevation. F) Quantification of tdTomato fluorescence in all groups, **p<0.01.

4.4.4 PLGA.EPO-R76E can activate the ARE

We sought to determine if PLGA.EPO-R76E can activate the ARE by measuring ARE-driven transcripts at 1 and 2 weeks post-IOP elevation with a PCR microarray. We found that

there were increased ARE-driven transcripts in the thioredoxin family (Figure 4.3C), glutathione family (Figure 4.3D), and peroxiredoxin family (Figure 4.3E). In contrast to our previous studies showing that the retina endogenously upregulates ARE-driven transcripts at 2 weeks post-IOP elevation, we observed that in the presence of PLGA.EPO-R76E, ARE-driven transcripts are upregulated at 1 week post-IOP elevation (Figure 4.3C-E).

To directly measure the activity of the ARE after EPO, we used a fluorescent reporter construct packaged into an AAV (AAV.ARE). We intravitreally injected AAV.ARE two weeks prior to IOP elevation via the MOM and assessed *in vivo* retinal tdTomato fluorescence at 1 and 2 weeks post-IOP elevation in eyes that received PLGA or PLGA.EPO-R76E one day post-MOM. At 1 week post-IOP elevation, there was no difference in the amount of tdTomato fluorescence in the eyes that received PLGA or PLGA.EPO-R76E ($p=0.0545$, n=5 eyes/group). By 2 weeks post-IOP elevation, however, eyes that received PLGA.EPO-R76E had 37% tdTomato fluorescence in comparison to eyes that received empty PLGA particles ($p=0.0091$, n=5 eyes/group, Figure 4.3F, G).

4.4.5 PLGA.EPO-R76E's activation of NRF2 is dependent on MAPK phosphorylation

We previously determined that after IOP elevation, NRF2 phosphorylation is dependent on the upstream phosphorylation of PI3K or Akt (Naguib et al., 2021). Here, we sought to determine if phosphorylation of NRF2 in the presence of PLGA.EPO-R76E would occur by the same mechanism. To do this, we assessed the ratio of phosphorylated to total PI3K, Akt, GSK3ß, JNK, STAT1, STAT3, and MAPK (Figure 4.4). We found that there was no difference in the ratio of phosphorylated to total PI3K, Akt, JNK, STAT1 or STAT3 between eyes that received PLGA or PLGA.EPO-R76E ($p=0.8033$, n=3 retinas/group; $p=0.7924$, n=3 retinas/group;

p=0.1145, n=3 retinas/group; p=0.1494, n=4 retinas/group; p=0.0638, n=3 retinas/group; Figure 4.4A-F). We found that there was 29% more phosphorylated to total GSK3ß in the eyes that received PLGA in comparison to the eyes that received PLGA.EPO-R76E (p=0.0139; n=3 retinas/group; Figure 4.4A, G). We also found that eyes that there was 73% more phosphorylated to total MAPK in eyes that received PLGA.EPO-R76E in comparison to eyes that received empty PLGA particles (p=0.0098; n=4 retinas/group; Figure 4.4A, H).

Because the ratio of phosphorylated to total MAPK was greatest in the mice that received PLGA.EPO-R76E at 2 weeks post-IOP elevation, we sought to determine if NRF2 phosphorylation was dependent on MAPK phosphorylation in mice. We intravitreally injected a MAPK inhibitor 1 week post-IOP elevation in mice treated with PLGA.EPO-R76E to determine if downstream NRF2 phosphorylation would be affected (Figure 4.4I-J). We used BIRB 796 because it is very potent. Previous studies applied BIRB 796 as a topical to the surface of the cornea daily, however, we chose to use an intravitreal injection as the mode of administration because it targets the retina. At 2 weeks post-IOP elevation, we collected retinas and used western blots to analyze the ratio of phosphorylated to total NRF2 following inhibition of MAPK. We found that the ratio of phosphorylated to total NRF2 was 44% greater than the MAPK-inhibitor treated group (p=0.0047, n=4 retinas/group; Figure 4.4I-J). This data suggests that PLGA.EPO-R76E's phosphorylation of NRF2 is dependent on phosphorylation and activation of MAPK.

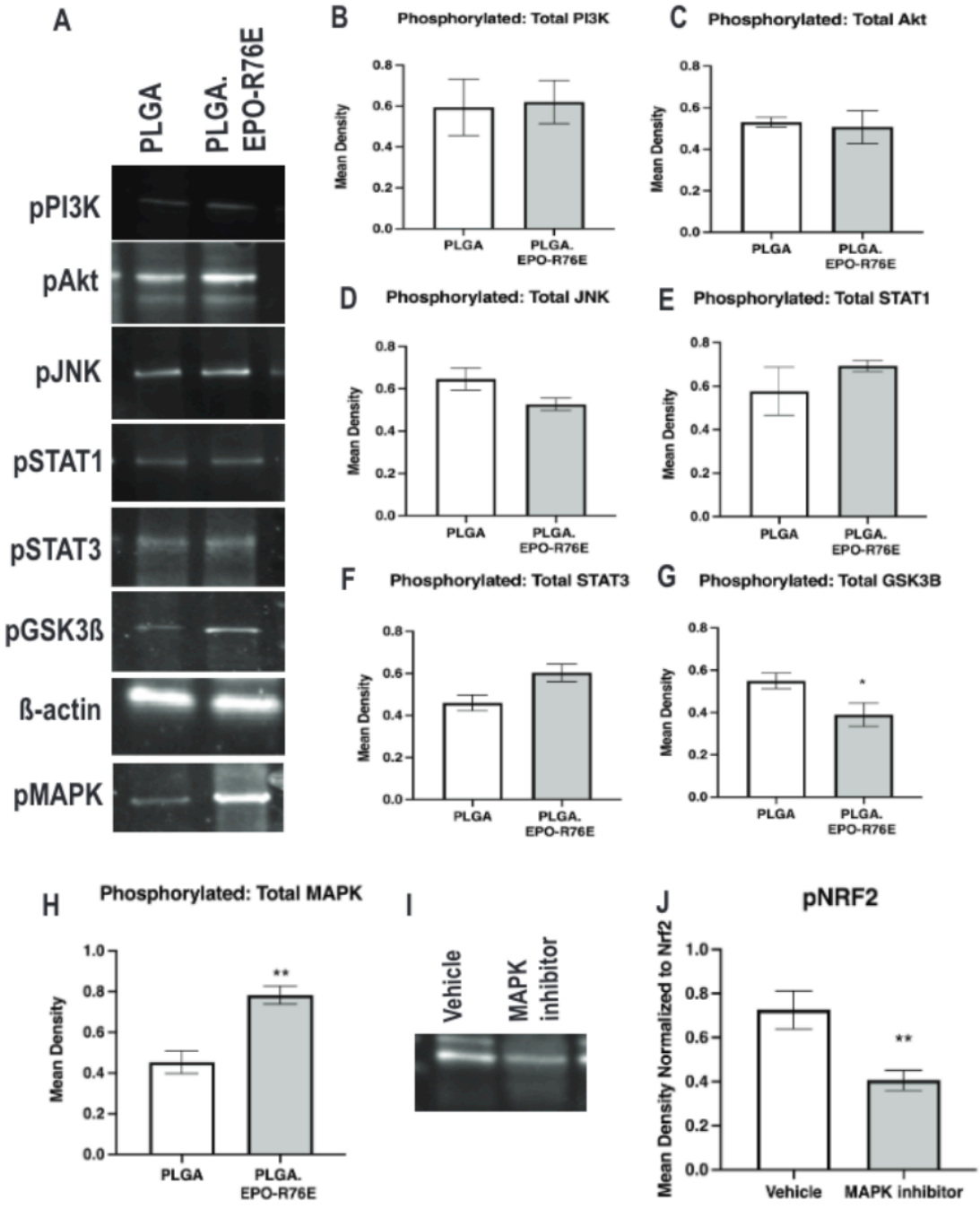

Figure 4.4. PLGA.EPO-R76E activates NRF2 in a MAPK-dependent way. A) Representative western blots for pPI3K, pAkt, pJNK, pSTAT1, pSTAT3, pGSK3B, B-actin, and pMAPK. B) Quantification of pPI3K to total PI3K. C) Quantification of pAkt to total Akt. D) Quantification of pJNK to total JNK. E) Quantification of pSTAT1 to total STAT1. F) Quantification of pSTAT3 to total STAT3. G) Quantification of pGSK3B to total GSK3B, *p<0.05. H) Quantification of pMAPK to total MAPK. I) Representative western blot of PLGA.EPO-R76E treated retinas injected with either vehicle or MAPK inhibitor, BIRB 796. J) Quantification of

pNRF2 to NRF2 in vehicle or MAPK inhibitor injected mice, both receiving PLGA.EPO-R76E at 2 weeks post-IOP elevation, **p=0.01.

4.5 Discussion

Here we demonstrated that PLGA.EPO-R76E can activate NRF2 via phosphorylation at 1 week post-IOP elevation, which is earlier than the retina's endogenous antioxidant response to ocular hypertension (Naguib et al., 2021). Previous studies have shown that EPO can activate the NRF2 pathway. Genc et al (2010) showed that EPO added to SH-SY5Y cells resulted in increased *NRF2* mRNA and induced Nrf2 nuclear translocation (K et al., 2010). In another study using a cortical lesion model, recombinant EPO treatment upregulated *NRF2* mRNA as well as *NQO1*, which is directly regulated by NRF2 (Z. J et al., 2010). Similar results were found in another study using a rat model of traumatic brain injury (H et al., 2014). Our data suggests that because EPO is able to induce NRF2 phosphorylation prior, and by a different signaling pathway, to the retina's endogenous antioxidant response, this could be a potential therapeutic target for glaucoma. The endogenous antioxidant response of the retina is mediated by PI3K/Akt pathway (Naguib et al., 2021). If we could accelerate NRF2 phosphorylation, we could also accelerate NRF2's interaction with the ARE, thereby resulting in an earlier transcription of antioxidant genes in response to high IOP-induced oxidative stress.

We also determined that the mechanism by which PLGA.EPO-R76E activates NRF2 is via a different upstream signaling molecule than what occurs endogenously. Our previous study elucidated that NRF2's phosphorylation is dependent on phosphorylation of either PI3K or Akt during the 2 week post-IOP elevation critical timepoint. Here, we found that in the presence of PLGA.EPO-R76E, NRF2's phosphorylation is dependent on MAPK's phosphorylation. Our study fits with previous literature, showing that EPO phosphorylates and activates MAPK. In a

paper studying hypoxic-ischemic encephalopathy, EPO's neuroprotective effects were modulated via the phosphorylation of MAPK (Jeong et al., 2017). In another study using a rabbit model of ischemia-reperfusion injury, EPO's activation of the Ras/Rac/MAPK pathway was necessary for its protective effects (Rafiee et al., 2005). In our study, we intravitreally injected BIRB 796 as a MAPK inhibitor to determine if NRF2's phosphorylation following treatment with PLGA.EPO-R76E was necessary. Previous studies have also administered this same MAPK inhibitor via eyedrops, which is definitely less invasive but also less specific in targeting the retina. Future studies are needed to determine if we could observe similar inhibition of NRF2 phosphorylation if we inhibit MAPK phosphorylation in another manner.

We discovered that PLGA.EPO-R76E's induced antioxidant response is different than what occurs in the retina endogenously post-IOP elevation via upregulation of different antioxidants. NRF2's activation has been shown to upregulate antioxidants including but not limited to NADPH oxidases, thioredoxins, heme oxygenase-1 and glutathione peroxidases (Tonelli et al., 2018). Interestingly, while EPO has also been shown to upregulate heme oxygenase-1 and glutathione peroxidases, we didn't observe the same upregulation of antioxidants endogenously as we did after administration of PLGA.EPO-R76E. Further quantitative PCR is needed to examine other antioxidants that EPO could be responsible for upregulating that were not included in the PCR microarray that we used in this study.

In conclusion, we demonstrated that PLGA.EPO-R76E is a viable option for the protection of RGCs' cell bodies and axons in a mouse model of glaucoma. We illustrated that this mechanism of delivery allows for sustained release of EPO up to six weeks from a single intravitreal injection given one day post-IOP elevation. Additionally, we showed that PLGA.EPO-R76E can activate NRF2 via phosphorylation and that this activation of NRF2 is

dependent on MAPK's phosphorylation. We also showed that NRF2's phosphorylation and consequential increase in ARE-driven transcripts occurs 1 week earlier than the retina's endogenous antioxidant response to ocular hypertension.

CHAPTER 5

Discussion

5.1 Summary and Conclusions

Our studies align with previous literature that shows that ROS can be a marker for glaucoma pathology (Arana et al., 2020; Prunty et al., 2015; Tezel, 2006). We showed, using an *in vivo* marker for reactive oxygen species, that oxidative stress occurs as soon as 1 week post-IOP elevation, weeks prior to glaucomatous pathology (Figure 2.2). We also showed that the photopic negative response of the ERG can be used as a potential indicator of susceptibility to future glaucomatous degeneration (Figure 2.1). The amplitude of the PhNR was decreased in the microbead-injected mice as early as 2 weeks post-IOP elevation in comparison to saline-injected controls. Previous studies have elucidated, primarily in the clinic, that the PhNR or the pattern ERG should be used as an indicator of RGC function in glaucoma suspects (Elgohary & Elshazly, 2015; Kong et al., 2020; Porciatti, 2014; Tang et al., 2020). Our studies align with others in the field showing that the 2 week post-IOP elevation period in the MOM could be a critical timepoint. Risner et al. showed that dendritic pruning of RGCs occur at 2 weeks post-IOP elevation in the MOM (2018). Interestingly, this paper showed increased RGC excitability at this timepoint, albeit transient, which doesn't translate to the PhNR data from Figure 2.1.

We found that in the well-characterized MOM of glaucoma, NRF2 is activated by phosphorylation at 2 weeks post-IOP elevation in wildtype mice, weeks before glaucomatous pathology develops. We also showed that the total amount of NRF2 does not change between saline and microbead-injected mice across any timepoints following IOP elevation (Figure 2.3). Interestingly, some prior studies have shown that NRF2 levels are upregulated following IOP

elevation in different glaucoma models, while others have shown that NRF2 levels are downregulated (Fujita et al., 2017; Wang & Yuan, 2019). We also found that activation of NRF2 occurs via phosphorylation dependent on PI3K/Akt, which aligns with previous literature showing NRF2 activation can occur exclusively by these two signaling molecules (Bryan et al., 2013; Niture et al., 2014; Sykiotis et al., 2011; Wang et al., 2008).

We showed that knocking out NRF2 results in an earlier and exacerbated onset of glaucomatous pathology in the MOM (Figure 2.6). We also demonstrated that NRF2 KO mice have their own antioxidant response, and our data suggest that this compensatory mechanism may be mediated by HIF-1 (Figure 2.7). Previous studies have illustrated that NRF2 KO mice have increased susceptibility to insult, injury, or neurodegeneration; however, they develop and grow normally, which suggests that there is a compensatory mechanism occurring that protects them to some extent (Johnson et al., 2008; Nakagami, 2016; Nguyen et al., 2000).

We sought to explore the cell-type specific role of NRF2 in glaucoma. While glaucoma is a disease that largely affects RGCs, previous work has shown activation of Müller glia, astrocytes, and microglia following increases in IOP (Chong & Martin, 2015; García-Bermúdez et al., 2021; Guttenplan et al., 2020; Tezel, 2006; Tezel et al., 2009). In this study, we overexpressed *Nrf2* only in RGCs in NRF2 KO mice to determine if that would be sufficient to elicit the endogenous retinal antioxidant response (Figure 3.1). We found that overexpression of *Nrf2* in the RGCs, when all non-transduced cells lack NRF2, is sufficient to induce the endogenous antioxidant response of the retina (Figure 3.1). We also overexpressed *Nrf2* in the RGCs of wildtype mice at both 2 and 5 weeks post-IOP elevation and found that at both timepoints, there was significantly less axon degeneration, less disruption of the PhNR of the ERG, and reduced *in vivo* reactive oxygen species (Figure 3.6-7). These studies showed that *Nrf2*

overexpression specifically in RGCs, as they are most susceptible to glaucomatous damage, could be a potential therapeutic for glaucoma. Our work aligns with others that overexpression of *Nrf2* in neurons confers neuroprotection (Calkins et al., 2009; Dinkova-Kostova et al., 2018; Johnson et al., 2008; Schmidlin et al., 2019).

To further elucidate the cell-type specific role of NRF2, we used Nrf2 floxed mice and intravitreally injected them with either a virus that targeted RGCs or a virus that targeted astrocytes (Figure 3.3-5). We found that knocking down NRF2 levels in either cell type exacerbated and accelerated the characteristic axon degeneration and visual function deficits in the MOM—we observed this worsened pathology at 2 weeks post-IOP elevation in both knockdown groups in comparison to their respective controls (Figure 3.5). It is well-known that neurons and glial cells communicate and interdepend on each other in a bidirectional manner. Additionally, knockdown of NRF2 in RGCs resulted in different reductions of downstream antioxidant proteins than knockdown of NRF2 in astrocytes (Figure 3.3-4). These data suggest that NRF2 may have a cell-type specific role in neurons and astrocytes; NRF2 may upregulate specific antioxidants in neurons and others in astrocytes. Our data also suggests that NRF2 alone cannot account for the transcriptional diversity observed in RGCs versus astrocytes in the MOM. Thus, it is likely that the NRF2 protein interactome is dynamic across time, cell type and disease model.

We previously showed in a model of indirect traumatic optic neuropathy that intravitreal injection of empty PLGA particles increased retinal oxidative stress and axon degeneration; PLGA.EPO-R76E protected against PLGA-induced damage (DeJulius et al., 2021). We found that PLGA.EPO-R76E resulted in a differential upregulation of antioxidants than the endogenous retinal antioxidant response to ocular hypertension (Figure 4.3). We also indicated that this

differential antioxidant response occurred at 1 week post-IOP elevation (Figure 4.3). We demonstrated that intravitreal injection of PLGA.EPO-R76E induced phosphorylation of NRF2 at 1 and 2 weeks post-IOP elevation in comparison to empty PLGA particles alone (Figure 4.4). The fact that treatment of PLGA.EPO-R76E resulted in earlier activation of NRF2 is suggestive of a potential therapeutic approach in glaucoma. If we can accelerate the retina's NRF2-dependent endogenous antioxidant response using EPO-R76E, upregulation of ARE-driven transcripts will occur earlier and could result in downstream neuroprotection.

We then administered a MAPK inhibitor to wildtype mice after IOP elevation and intravitreal injection of PLGA or PLGA.EPO-R76E and showed that phosphorylation of NRF2 was decreased following inhibition of MAPK (Figure 4.4). Our data aligns with previous literature showing that EPO can phosphorylate MAPK (Guillard et al., 2003; Jeong et al., 2017; Genc et al., 2010). This data suggests that PLGA.EPO-R76E activates NRF2 in a differential mechanism than the endogenous antioxidant response to ocular hypertension, as we have previously shown that endogenous NRF2 phosphorylation is regulated by PI3K/Akt (Naguib et al., 2021).

Ultimately, the work from this dissertation illuminates a cell-type specific role for NRF2 in a mouse model of glaucoma. Additionally, PLGA.EPO-R76E could be used as a neuroprotective for glaucoma via its activation of NRF2 through indirect phosphorylation. Although EPO's exact mechanism of action needs to be parsed out in future studies, EPO is a clinically relevant, and already utilized, therapeutic in other diseases that should be transitioned over to glaucoma. NRF2 should be further explored as a neuroprotective for glaucoma, though these data suggest that NRF2 therapeutics could be clinically relevant to a broader range of neurogenerative diseases. RGC protection via decreasing ROS and increasing antioxidants

through NRF2, is an incredibly important therapeutic option that should be explored in the future following the work of this dissertation. Further developing approaches to target RGCs or astrocytes specifically in non-human primates and eventually in the clinic will prove successful for treating glaucoma in the future.

5.2 Limitations and Future Directions

While this dissertation adds to the literature, there are more experiments that can be done to better understand the cell-type specific role of NRF2 in glaucoma. For example, we have not yet assessed if overexpression of NRF2 in astrocytes would induce similar, decreased or increased neuroprotection compared to overexpressing NRF2 in ganglion cell layer neurons. Previous studies using a mouse model of Parkinson's Disease overexpressed NRF2 in astrocytes and observed protection against MPTP toxicity (Chen et al., 2009). This avenue of overexpression is an option for a future study. Along the same lines, it is possible that overexpression of one of NRF2's downstream antioxidants, such as PRDX6 or SOD3, would confer similar degrees of neuroprotection as overexpression of NRF2 in either neurons or astrocytes. Overexpression of NRF2 should theoretically confer more protection, considering that its acting on the ARE would result in increased transcription of multiple antioxidants rather than just one, but it is possible that overexpression of one or more antioxidants could have a similar effect.

Notably, many of the antioxidants that are regulated by NRF2 binding to the ARE can also be regulated in NRF2-independent mechanisms. Thus, it could be that the changes that we see in overexpression studies, knockdown studies or even in the wildtype mice might not be totally dependent on NRF2's binding to the ARE. To further explore this, it would be interesting

to use an NRF2 KO mouse and then overexpress one of the antioxidants regulated by the ARE (PRDX6, for example) to see if the antioxidant's overexpression is just as neuroprotective as simply overexpressing NRF2. It is also entirely possible that there are many more antioxidants that are even further upregulated in the retina's endogenous antioxidant response to ocular hypertension but we have not detected them, due to the fact that there are so many antioxidants regulated by the ARE. Future studies could examine others of these antioxidants that were outside the scope of this project.

Also, while we did some studies on the transcript level, a lot of our analysis was done on the protein level. The ARE is responsible for upregulating antioxidants on the transcript level so it is definitely possible (and has been observed) that the transcripts of some of these antioxidants are upregulated following ocular hypertension but not translated on the protein level. We completed some immunohistochemical analysis to examine localization on the protein level, but, in the future, it would be great to use RNAscope or fluorescent in situ hybridization to examine cell-specific expression of these antioxidants on the transcript level to see if it matches with our protein data.

While our cell-type specific knockdowns of NRF2 in either RGCs or astrocytes definitely provide some insight on the cell-specific role of NRF2, there are definitely limitations to this study. First, we were not targeting every RGC or every astrocyte because we intravitreally injected our Cre rather than finding a mouse line expressing this promoter to breed with the Nrf2 floxed mice, which allowed for increased specificity but also does involve an additional intravitreal injection. Second, when we assessed for downstream antioxidants on either the transcript or protein level, we are only using whole retina lysates, which means that we are unable to conclude exactly which cell types have altered antioxidant levels after cell-type

specific knockdown of NRF2. This same sentiment occurred in our overexpression of *Nrf2* in GCL neuron studies—we don't know for sure that if we are overexpressing *Nrf2* in the GCL neurons that we were automatically getting increased antioxidant proteins in only the RGCs. To ameliorate this, it would be interesting to use fluorescent cell sorting to separate out RGCs from astrocytes/glial cells and assess antioxidant levels in each individual cell type. This could be done in knockdown and overexpression studies. To take this one step further, it would be interesting to parse out if there is one particular cell type (whether that be RGCs or astrocytes or even a subpopulation of either) that is more susceptible to upregulating specific ARE-driven transcripts versus others. To do this, after cell sorting, we could use RNA sequencing to explore even deeper into cell-type specific mechanisms of NRF2 activation.

To go even further, while our knockdown and overexpression studies point to an important role of NRF2 in RGCs, we do not know the exact cells on which NRF2's binding to the ARE is occurring. Our use of the fluorescent AAV2/2.ARE suggested that the ARE is activated, at least partially, in RGCs due to the fact that AAV2/2, when intravitreally injected, transduces the RGCs (Nickells et al., 2017). We can assume that NRF2's activation is occurring in both neurons and glial cells, but it would be interesting to delve more into the ratio of which cell types NRF2 is acting more on. Previous studies point to more of NRF2's activation occurring in astrocytes rather than neurons, but it would be ideal to be able to fluorescently label NRF2 endogenously and use high resolution imaging *in vivo* to assess nuclear translocation of NRF2 in neurons or astrocytes (Johnson et al., 2008; Vargas et al., 2008). These experiments would also elucidate how quickly NRF2 activation of the ARE is occurring following induction of ocular hypertension, as NRF2 has a very short half-life *in vivo* (Nguyen et al., 2000, 2009; Vomund et al., 2017).

While we were able to observe NRF2 phosphorylation at 2 weeks post-IOP elevation, it is possible that KEAP1 is being oxidized at earlier timepoints also leading to downstream NRF2 activation of the ARE (Naguib et al., 2021). Ultimately, we were unable to assess KEAP1 oxidation due to technical difficulties in the experiments, but using mass spectrometry as an approach in the future would be interesting. It is very possible that KEAP1 oxidation and NRF2 phosphorylation are either occurring at the same time or one occurs at one timepoint after ocular hypertension and another is occurring at another timepoint (Xu et al., 2013).

While our studies also determined that NRF2 is phosphorylated primarily by the PI3K/Akt pathway in the retina's endogenous antioxidant response to ocular hypertension, we do not know that this is the only way that NRF2 is being phosphorylated (Naguib et al., 2021). We only assessed a handful of upstream signaling molecules that could be responsible for NRF2's phosphorylation, and it is possible that there are others that could also phosphorylate NRF2. Additionally, it is also possible that the PI3K and Akt inhibitors we used were not specific enough and have too many off-target effects, especially considering that Ipatasertib was administered intraperitoneally. It would be interesting to deliver these inhibitors to either RGCs or astrocytes specifically and then see if there is a compensatory mechanism that occurs in the other cell type—for example, if we inhibited PI3K in RGCs, would we see decreased phosphorylation of NRF2 in just RGCs or in surrounding glial cells as well?

Our studies, and others in the literature, point to NRF2 phosphorylation as a potential therapeutic for glaucoma. It would be interesting if we expressed an NRF2 phosphomimetic; this would mimic NRF2 phosphorylated and we could observe if we get increased downstream antioxidant gene transcription. There are previous studies who have used a phosphomimetic NRF2 and others that have used an inhibitor of KEAP1 and have shown downstream

neuroprotection. Interestingly, knockout of KEAP1 actually has detrimental effects, so this exact mechanism is not fully teased out yet. Additionally, there are plenty of naturally occurring substances that activate NRF2 including but not limited to curcumin, resveratrol, quercetin, and sulphoraphane. It would be interesting to use these naturally occurring NRF2 activators and determine if we see similar expression of ARE-driven transcripts when compared to NRF2 overexpression or even a phosphomimetic NRF2.

One of the other limitations of our therapeutic studies is that we only overexpressed NRF2 or intravitreally injected PLGA.EPO-R76E prior to onset of degeneration. It would be interesting to determine the therapeutic window of each of these neuroprotective agents. Of course, it would be more clinically relevant if we found that we could induce overexpression of NRF2 after IOP elevation and still observe similar levels of neuroprotection. This is unlikely, however, due to the fact that it takes multiple weeks for cells to transduce AAVs. As for the PLGA.EPO-R76E studies, it would be great to be able to deliver EPO a longer time after microbead injection. It is definitely possible that the back-to-back injections, while they are not in the same location, can still induce ocular oxidative stress due to the fact that the surface of the cornea is not healed from the intracameral injection by the time that the mice receive their intravitreal injections.

We have begun some preliminary studies using different microparticles to deliver EPO-R76E after ocular hypertension. This time, we are using PPSES particles rather than PLGA particles due to the fact that the PLGA particles have inherent oxidative effects. In these preliminary studies, we are intravitreally injecting PPSES.EPO-R76E or empty PPSES particles 1 week post-IOP elevation rather than one day after. While we are still completing these studies, our preliminary data suggests that waiting 1 week after IOP elevation is still effective in

protecting the PhNR amplitude and retinal oxidative stress levels. Of course, these preliminary data cannot be used as a direct comparison as the PPSES particles are not the same as the PLGA particles used in my dissertation work—they can have their own antioxidant properties, similar to the PPS particles that we previously published using a model of indirect traumatic optic neuropathy. In our previously published work, we found that while the PPS particles have their own antioxidant effects, loading them with EPO-R76E still conferred more neuroprotective and antioxidant effects in comparison to the empty particles. We are seeing similar effects in our PPSES studies. In the future, we should perform a time-course study with either the PLGA or new PPSES particles in order to determine how far after IOP elevation we can still see neuroprotection. It would be ideal if we could use fluorescently labeled EPO for these studies so that we would be able to assess the retinal cells with which EPO interacts following release form microparticles.

While we observed NRF2 phosphorylation in the mice treated with PLGA.EPO-R76E, we do not know for sure that the neuroprotection that we observed in these mice is specifically due to EPO-R76E's activation of NRF2. To test this, we could use NRF2 KO mice and intravitreally administer PLGA.EPO-R76E at the same timepoint (one day post-IOP elevation) to determine if we still confer neuroprotection. Still, this data might not perfectly explain what EPO's mechanism of action is due to the fact that there could be some compensatory mechanisms that could take place in the absence of NRF2.

CHAPTER 6

Appendix 1: Galantamine protects against synaptic, axonal and visual deficits in experimental neurotrauma

This chapter of my thesis is published in *Neurobiology of Disease:*

Naguib S, Bernardo-Colón A, Cencer C, Gandra N, Rex TS. Galantamine protects against synaptic, axonal, and vision deficits in experimental neurotrauma. Neurobiol Dis. 2020 Feb;134:104695. doi: 10.1016/j.nbd.2019.104695. Epub 2019 Nov 25. PMID: 31778813; PMCID: PMC7769189.

6.1 Introduction

Eye injuries affect approximately 2.4 million people every year.(Feist & Farber, 1989) Between 2000 and 2010, 186,555 eye injuries occurred worldwide in military hospitals.(Andreotti et al., 2001) Further, up to 40% of monocular blindness is due to ocular trauma. (Aghadoost, 2014) Damage to the optic nerve and retina, resulting in permanent visual deficits, occurred in more than 60,000 Veterans with blast-induced traumatic brain injury (TBI) between the years of 2000-2011.(Weichel et al., n.d.) Additionally, up to 5% of patients experiencing head trauma will also develop traumatic optic neuropathy (TON).(Steinsapir & Goldberg, 2011)·(Kumaran et al., 2014) Some of the most common ocular blast injuries include, but are not limited to, hyphema, retinal detachments, retinal edema, TON, and loss of visual field. ("WHO | Priority Eye Diseases," 2018) In cases of direct TON, anatomical disruption of the optic nerve occurs from a projectile penetrating the optic nerve or avulsion. Indirect TON (ITON) results from force transmission to the optic nerve from a distant site without overt

damage to the surrounding tissue.(Singman et al., 2016; Warner & Eggenberger, 2010) Patients with ITON can experience severe vision loss, and while some experience limited recovery, they never return to baseline.(Burke et al., 2019; Singman et al., 2016) Corticosteroids or observation alone are the current standards of treatment for patients with ITON.(*Eye Health Statistics - American Academy of Ophthalmology*, n.d.)

Our lab has developed a model of blast-induced ITON (bITON), utilizing a repeat blast paradigm in order to simulate repeat injuries most often seen in military populations.(Bricker-Anthony et al., 2014; Hines-Beard et al., 2012) This model induces extensive axon degeneration in the optic nerve at two weeks after injury, as well as a decrease in the amplitude and an increase in the latency of the visual evoked potential (VEP).(Bernardo-Colon et al., 2018) It causes an increase in reactive oxygen species (ROS), and secondary activation of the IL-1 pathway, both of which contribute to axon degeneration and vision loss.(Bricker-Anthony et al., 2014; Hines-Beard et al., 2012) We have also reported that our model results in early, but not ongoing, death of retinal ganglion cells, starting two days after injury.(Bernardo-Colón et al., 2019)

Altered levels of neurotransmitters, such as acetylcholine and GABA, occur in several neurodegenerations.(McKee & Robinson, 2014) For example, in Alzheimer's Disease, decreased levels of acetylcholine correlates with disease progression.(Francis, 2005; Giacobini et al., 1989) Notably, we detected caspase-1 immunolabeling in the cholinergic amacrine cells after single blast injury.(Bricker-Anthony et al., 2014) One of the treatments for mild to moderate Alzheimer's disease, as well as other myopathies and peripheral neuropathies, is the FDA-approved compound, galantamine.(Lilienfeld, 2002) (Durães et al., 2018) Galantamine has multiple modes of actions: it increases acetylcholine via mild inhibition of acetylcholinesterase,

it increases GABA release via allosteric modulation of the nicotinic acetylcholine receptor (α7nAChR), and it has been shown to protect neurons against glutamate-induced neurotoxicity.(Santos et al., 2002) Previous studies have also shown that galantamine can have antioxidant properties; galantamine treatment reduced ROS and increased cell viability after exposure to hydrogen peroxide(Ezoulin et al., 2008; Romero et al., 2010) and protected rat cortical neurons against oxidative stress after exposure to synthetic amyloid β.(Melo et al., 2009) It also has been shown to decrease inflammation in a stroke model of rats, by preventing an increase IL-1β levels.(Furukawa et al., 2014) Additional studies have shown that galantamine can protect retinal ganglion cells in a rat model of glaucoma.(Mohammadali Almasieh et al., 2013),(M Almasieh et al., 2010)

We hypothesized that galantamine would be protective in our model of bITON. Here, we show that oral galantamine, given after bITON, mitigates visual function deficits and axon degeneration in the optic nerve, and that it does so while modulating acetylcholine, glutamate, ROS, and IL-1 levels.

6.2 Methods

6.2.1 Mice: Anesthetized C57Bl/6J mice (Jackson Labs, Bar Harbor, ME) were exposed to two repeat bursts (0.5 seconds apart) of 15psi air directed at the left eye once a day for three days in a row. Sham mice were exposed to everything except the air pressure due to a barrier placed between the eye and the barrel of the paintball marker, as previously described.[13-15] Galantamine sham and blast mice were given 120mg/L of galantamine in their water, which was changed every 72 hours (TCI America, Boston, MA). Control mice were given normal water ad libitum for one month, while galantamine-treated mice drank galantamine-containing water for one month post-injury. Average daily water intake for a laboratory mouse is 4ml, thus we estimate

that the mice consumed 480 micrograms galantamine/day for 30 days. This equates to an average dose of 15.3mg/kg for 30 days, based on the average weight of a C57Bl/6 male mouse of 31.4 grams. While previous studies administered galantamine intraperitoneally at 1-5mg/kg,(Kita et al., 2014; Noda et al., 2010; Shimizu et al., 2015) it is important to note that because galantamine is delivered orally, the dose is higher. Experimental procedures were performed in accordance with the Use of Animals in Vision and Ophthalmic research and an approved Vanderbilt University Institutional Animal Care and Use Committee protocol.

6.2.2 Electroretinograms (ERG) and VEPs: Mice were dark-adapted overnight, dilated with 1% tropicamide for 10 minutes, and anesthetized with 20/8/0.8mg/kg ketamine/xylaxine/urethane according to previously published methodology.[14] Mice were placed on the heated surface of the ERG system to maintain body temperature. Corneal electrodes with integrated stimulators were placed on eyes lubricated with Genteel drops using the Celeris system (Diagnosys LLC, Lowell, MA). Subdermal platinum needle electrodes were placed in the snout and back of the head at the location of the visual cortex. A ground electrode was placed in the back of the mouse. For VEPs, mice were exposed to 50 flashes of 1Hz, 0.5cd.s/m^2 white light. To collect ERGs, electrodes were placed on lubricated corneas were placed. Mice were then exposed to 15 flashes of 1Hz, 1cd.s/m^2.

6.2.3 Western Blot: Single retinas were homogenized and sonicated in lysis buffer and centrifuged. Sample buffer was added to the supernatant just prior to use. Known amounts of protein (10 to 20µg) or protein ladder were loaded into each well of an SDS-polyacrylamide gel. The Bio-Rad mini-trans blot cell system and mini protean pre-cast gels at 4-20% were used

(Hercules, CA). Loading control was GAPDH (rabbit; 1:1000; ab9485, Abcam, Cambridge, MA). The protein was transferred onto nitrocellulose using the Bio-Rad trans blot turbo transfer system (Hercules, CA), probed with anti-SOD2 (rabbit; 1:1000; ab13533; Abcam), probed with secondary antibody (alkaline phosphatase-conjugated AffiniPure Goat Anti-Rabbit IgG; 1:1000; cat #133466; Jackson ImmunoResearch Laboratories) and alkaline phosphatase was used for band detection. Band density was quantified by scanning the blot using an EPSON scanner and Adobe Photoshop to convert to grayscale and invert the image. Each band was selected with the same frame and set measurements were used to obtain the grey mean value for each.(Bernardo-Colon et al., 2018)

6.2.4 High-performance liquid chromatography (HPLC):

Tissue Extraction

The brain sections were homogenized, using a tissue disruptor, in 100-750 ul of 0.1M TCA, which contained 10^{-2} M sodium acetate, 10^{-4} M EDTA, and 10.5% methanol (pH 3.8). Ten microliters of homogenate was used. Then samples were spun in a microcentrifuge at 10,000g for 20 minutes. The supernatant was removed for biogenic monoamines analysis.

Biogenic Amine Analysis using HPLC-ECD

Biogenic amine concentrations were determined in the Vanderbilt University Medical Center Hormone Assay & Analytical Core utilizing an Antec Decade II (oxidation: 0.65) electrochemical detector operated at 33°C. Twenty microliter samples of the supernatant were injected using a Water 2707 autosampler onto a Phenomenex Kintex C18 HPLC column (100 x 4.60 mm, 2.6um). Biogenic amines were eluted with a mobile phase consisting of 89.5% 0.1M TCA, 10^{-}

^{2} M sodium acetate, 10^{-4} M EDTA and 10.5% methanol (pH 3.8). Solvent was delivered at 0.6 ml/min using a Waters 515 HPLC pump. HPLC control and data acquisition were managed by Empower software. Isoproterenol (5ng/mL) was included in the homogenization buffer for use as a standard to quantify the biogenic amines.

Biogenic Amine Analysis using LC/MS

Biogenic amines were determined in the Vanderbilt University Medical Center Hormone Assay & Analytical Core by a highly sensitive and specific liquid chromatography/mass spectrometry (LC/MS) methodology following derivatization of analytes with benzoyl chloride (BZC). 5µL of either tissue extract or microdialysis fluid was added to a 1.5mL microcentrifuge tube containing 20µL acetonitrile. Ten microliters each of 500mM $NaCO_3$ (aqueous) and 2% BZC in acetonitrile was added to each tube. After 2 min, the reaction was stopped by the addition of 20uL internal standard solution (in 20% acetonitrile containing 3% sulfuric acid) and 40uL water. The samples were then ready for LC/MS analysis. LC was performed on a 2.0 x 50mm, 1.7µm particle Acquity BEH C18 column (Waters Corporation, Milford, MA, USA) using a Waters Acquity UPLC. Mobile phase A was 15% aqueous formic acid and mobile phase B was acetonitrile. Samples were separated by a gradient of 98–5% of mobile phase A over 11 min at a flow rate of 600µL /min prior to delivery to a SCIEX 6500+ QTrap mass spectrometer.

6.2.5 Protein assay: Protein concentration was determined by BCA Protein Assay Kit (Thermo Scientific). Ten microliters of tissue homogenate was distributed into 96-well plate and 200 µl of mixed BCA reagent (25ml of Protein Reagent A is mixed with 500µl of Protein Reagent B) was added. The plate was incubated at room temperature for two hours for the color development. A

BSA standard curve was run at the same time. Absorbance was measured by the plate reader (POLARstar Omega), purchased from BMG Labtech Company.

6.2.6 Multiplex Cytokine ELISA: We performed a mouse multiplex mouse cytokine/chemokine magnetic bead panel for IL-1α and IL-1β, loading 25µl of sample per well. Samples were tested in duplicates and results were averaged. We performed the ELISA according to manufacturer directions (cat #: MCYTOMAG-70K, Millipore, Burlington, MA).

6.2.7 Immunohistochemistry: Eyes (n=40) were preserved in 4% paraformaldehyde, cryoprotected in 30% sucrose overnight at 4ºC and embedded in tissue freezing medium (Triangle Biomedical, Durham, NC). Ten-micron thick sections were collected in round on a cryostat (Fisher, Pittsburgh, PA). Each slide had representative sections from the entire eye. Slides were rinsed with PBS and incubated at room temperature in normal donkey serum (NDS; 0.05%) in 0.1M phosphate buffer with 0.5% bovine serum albumin and 0.1% Triton X-100 (phosphate buffer plus Triton X-100 [PBT]) for 2 hours. The slides were incubated overnight at 4ºC in primary antibody (see table below) in PBT, then rinsed with PBS and incubated with their appropriate secondary antibody (donkey anti-rabbit, donkey anti-mouse or donkey anti-goat 488 or 594; Life Technologies, Carlsbad, CA) for 2 hours at room temperature. Then, slides were rinsed in PBS, mounted in Vectashield Mounting medium with DAPI (DAPI; Vector Laboratories, Burlingame, CA) or Fluoromount-G (Southern Biotech, Birmingham, AL). Slides were imaged on a Nikon Eclipse epifluorescence microscope (Nikon, Melville, NY) or an Olympus FV-1000 confocal microscope. All images were collected from the same retinal region with identical magnification, gain and exposure settings. Fluorescence intensity was quantified

via ImageJ. A rectangle was selected around the region of interest, channels were split for multiple antibodies, threshold was adjusted, noise was de-speckled and fluorescence intensity was measured. Fluorescence intensity was normalized to sham mice. Each experimental group included 5 eyes.

Table 6.1. Antibodies Used for Immunohistochemistry

Antibody	Concentration	Animal	Catalog Number	Company
Anti-calbindin D	1:200	Mouse	126M4810V	Sigma-Aldrich, St. Louis, MO
Anti-synaptophysin	1:500	Rabbit	GR30790220	Abcam, Cambridge, MA
Anti-nitrotyrosine	1:500	Rabbit	2459610	Millipore, Burlington, MA
Anti-PKCα	1:40	Mouse	GR3164443	Abcam, Cambridge, MA

6.2.8 Optic Nerves: Optic nerves were post-fixed in glutaraldehyde followed by embedding in Resin 812 and Araldite 502 (cat # 14900 and 10900, Electron Microscopy sciences, Hatfield, PA) according to previous published protocols[13,14,28,29]. Leica EM-UC7 microtome was used to collect 1µm-thick sections. Sections were then stained with 1% paraphenylenediamine and 1% toluidine blue and were imaged on a Nikon Eclipse Ni-E microscope using a 100x oil immersion objective (Nikon Instruments Inc., Melville, NY). The optic nerves were montaged into a 5x5 image using the Nikon Elements software. We used the Counting Array and Better Cell Counter plugins to ImageJ, which creates a grid of nine squares overtop the montaged optic nerve. We manually counted healthy and degenerating axons, which are color-coded by the plugins. The grid accounts for 20% of the optic nerve cross-sectional area to avoid bias, and we multiplied these numbers by 5 to estimate total and degenerating axons within the nerve.

Acetylcholinesterase Activity Assay: Activity of AChE in the retina was measured using Acetylcholinesterase Colorimetric Assay Kit according to manufacturer's directions (ab138871, Abcam, Cambridge, MA).

6.2.9 Experimental Design and Statistical Analysis: Western blot data was normalized to loading controls. Data were analyzed using GraphPad Prism (La Jolla, CA). All experimental groups were compared to each other using a one-way ANOVA and the Tukey post-hoc test. All groups are shown (mean ± SEM).

6.3 Results

6.3.1 Oral galantamine reached bioactive levels in the mouse retina

To determine if galantamine entered the retina and was active, we quantified acetylcholinesterase activity (Figure 6.1A) and acetylcholine levels (Figure 6.1B). Interestingly, control bITON retinas had a slight, but statistically significant increase in acetylcholinesterase activity in comparison to control shams, 0.48 ± 0.03 U/mg (mean ± SEM) and 0.42 ± 0.01 U/mg, respectively ($p<0.05$; Figure 6.1A). Acetylcholinesterase activity was decreased in both galantamine sham (0.28 ± 0.01 U/mg) and galantamine bITON (0.34 ± 0.08 U/mg) groups, as compared to its control, $p < 0.001$ for both galantamine groups (Figure 6.1A). Interestingly, there is also a statistically significant increase in acetylcholinesterase activity between galantamine-sham and galantamine-bITON mice, $p<0.05$.

The levels of retinal acetylcholine in mice treated with galantamine was greater than controls (Figure 6.1B). Acetylcholine levels were 11.0 ± 1.2, 13.0 ± 3.6; 23.8 ± 10.0, and 30.0 ± 17.2 ng/mg respectively for sham, bITON, galantamine sham, and galantamine-bITON groups (Figure 6.1B). Total choline levels remained unchanged in all four experimental groups (Figure 6.1C).

Previous studies have elucidated that galantamine can modulate glutamate levels. We detected a 2.07-fold increase in glutamate levels in retinas from bITON mice as compared to those from control sham mice ($p<0.0001$; Figure 6.1D). In contrast, levels of glutamate in galantamine-treated mice were similar to control sham levels. To determine if galantamine modulated glutamate levels by affecting glutamate production or recycling, we performed immunohistochemistry and quantification of fluorescence for GLAST, a marker of glutamate synthetase, and EAAT1, glutamate transporter 1. No differences in the total fluorescence of either of these markers in the retina were detected (data not shown).

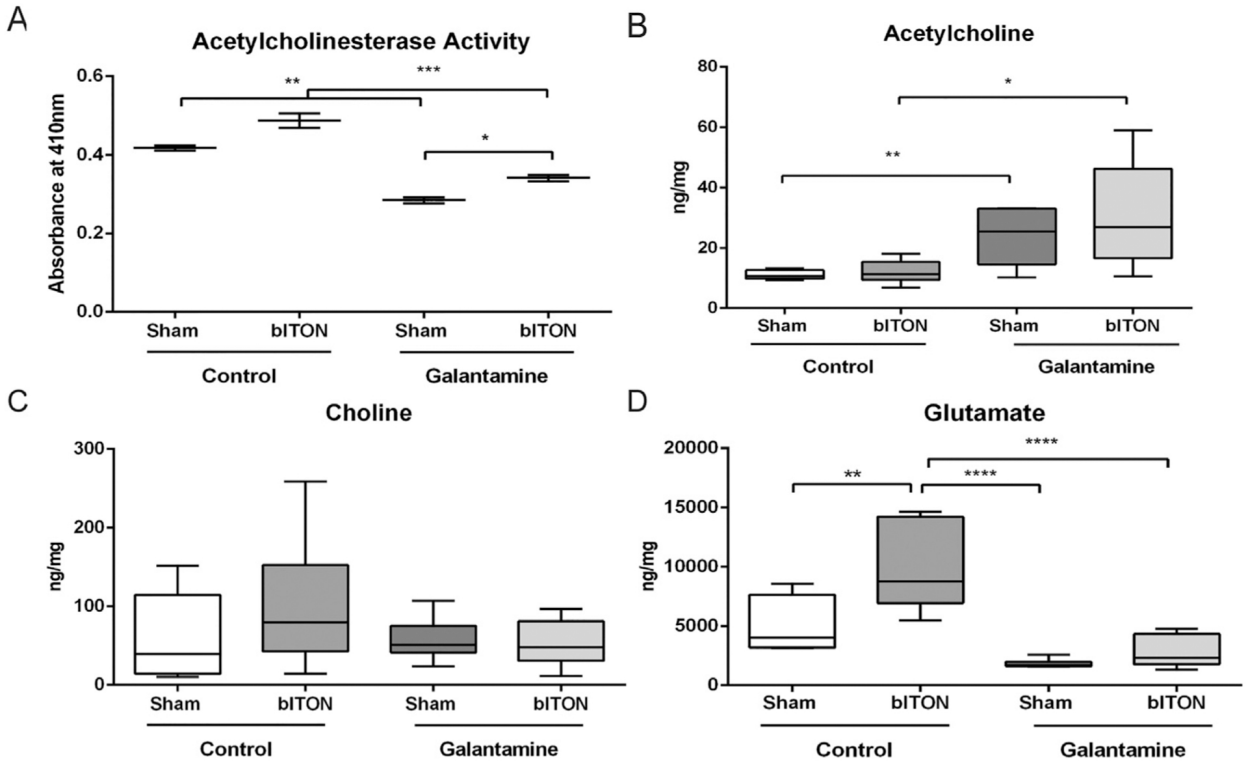

Figure 6.1. Oral galamtamine inhibited retinal acetylcholinesterase activity, increased acetylcholine and decreased glutamate. A) Acetylcholinesterase activity assay. B) Aceytlcholine levels quantified with HPLC. C) Choline levels quantified with HPLC. D) Glutamate levels quantified with HPLC. N= 5 retinas for all groups. *$p<0.05$, **$p<0.01$, ****$p<0.0001$.

6.3.2 Galantamine treatment mitigates bITON-induced reduction in the ERG

We assessed retinal function by ERG, and observed no difference in the amplitude or latency of the a-wave, indicating that our model of bITON does affect the photoreceptors (Figure 6.2A, B). However, the amplitude of the b-wave (b_{max}) of the ERG was decreased after bITON (Figure 6.2A, C). Control shams had a mean b_{max} of 203.3 ± 7.4 μV, while control bITON had a mean b_{max} of 100.6 ± 11.6μV, $p<0.001$. Additionally, bITON mice had a longer b-wave latency than the control sham mice: 41.3 ± 12.1ms as compared to 54.6 ± 9.3ms, $p<0.0001$ (Figure 6.2A, D). The b-wave is generated primarily by the rod bipolar cells, thus these data suggest that these cells are affected by bITON. Galantamine treatment after bITON partially protected the b_{max} and the b-wave latency (Figure 6.2C, D). The mean b_{max} in galantamine sham and galantamine-treated bITON mice was 190.8 ± 37.7μV and 158.8 ± 48.0μV, respectively, with $p<0.05$ between the galantamine-treated groups (Figure 6.2C). The latencies of the b-wave in galantamine sham and bITON mice were 40.5 ± 8.2ms and 45.2 ± 10.2ms, respectively, with no statistically significant difference between them (Figure 6.2D). Importantly, there was a statistically significant difference between the control bITON group and the galantamine-treated bITON groups for both b wave amplitude and latency ($p<0.001$ and $p<0.0001$, respectively).

6.3.3 Galantamine treated mice retain synaptic overlap in the OPL after bITON

We performed immunohistochemical analysis to explore the morphological basis for the ERG b-wave changes. We co-labeled retina cross-sections with anti-PKCα, a marker for rod bipolar cells, and anti-synaptophysin, a marker for the photoreceptor ribbon synapse. In control sham mice, the rod bipolar cells extend dendrites up to the photoreceptor terminals (Figure 6.2E). In contrast, in control bITON mice, the rod bipolar cell dendrites were retracted toward their cell bodies (Figure 6.2E). The rod bipolar cell dendrites of both sham and bITON mice

treated with galantamine looked similar to normal sham mouse retinas (Figure 6.2E). In an effort to quantify changes in dendritic overlap with the photoreceptor synaptic terminals, we quantified the extent of double-labeling of the two antibodies. Importantly, galantamine-treated bITON mice had a mean overlap that was comparable to the two sham groups: the mean overlap was 54 ± 2% for galantamine-bITON, sham mice, mean overlap for control-sham was 62 ± 3%, and mean overlap for galantamine-sham mice was 59 ± 3%. There was no statistically significant difference between any of the groups (Figure 6.2F). In contrast, after bITON, mean overlap of anti-PKCα and anti-synaptophysin decreased to 41 ± 5% ($p<0.05$, in comparison to either sham group or galanamine-bITON group).

In order to check the other major synapse at the outer plexiform, we also co-immunolabeled with anti-synaptophysin and anti-calbindin-D, a marker for horizontal cells (Figure 6.2G). There was a marked decrease in calbindin-D immunolabeling after bITON, which prevented visualization of changes in horizontal cell morphology. bITON mice that were treated with galantamine had preserved calbindin labeling. As expected, we quantified a significant difference in overlap in calbindin-D and synaptophysin between sham and bITON mice: sham mean overlap was 59 ± 2% and bITON mean overlap was 42 ± 4%, $p<0.05$ (Figure 6.2H). Galantamine preserved the horizontal cell and ribbon synapse double labeling: galantamine sham mean overlap was 59 ± 2%, and galantamine bITON mean overlap was 53 ± 5% (Figure 6.2H). There was no statistical difference between the either of the galantamine groups.

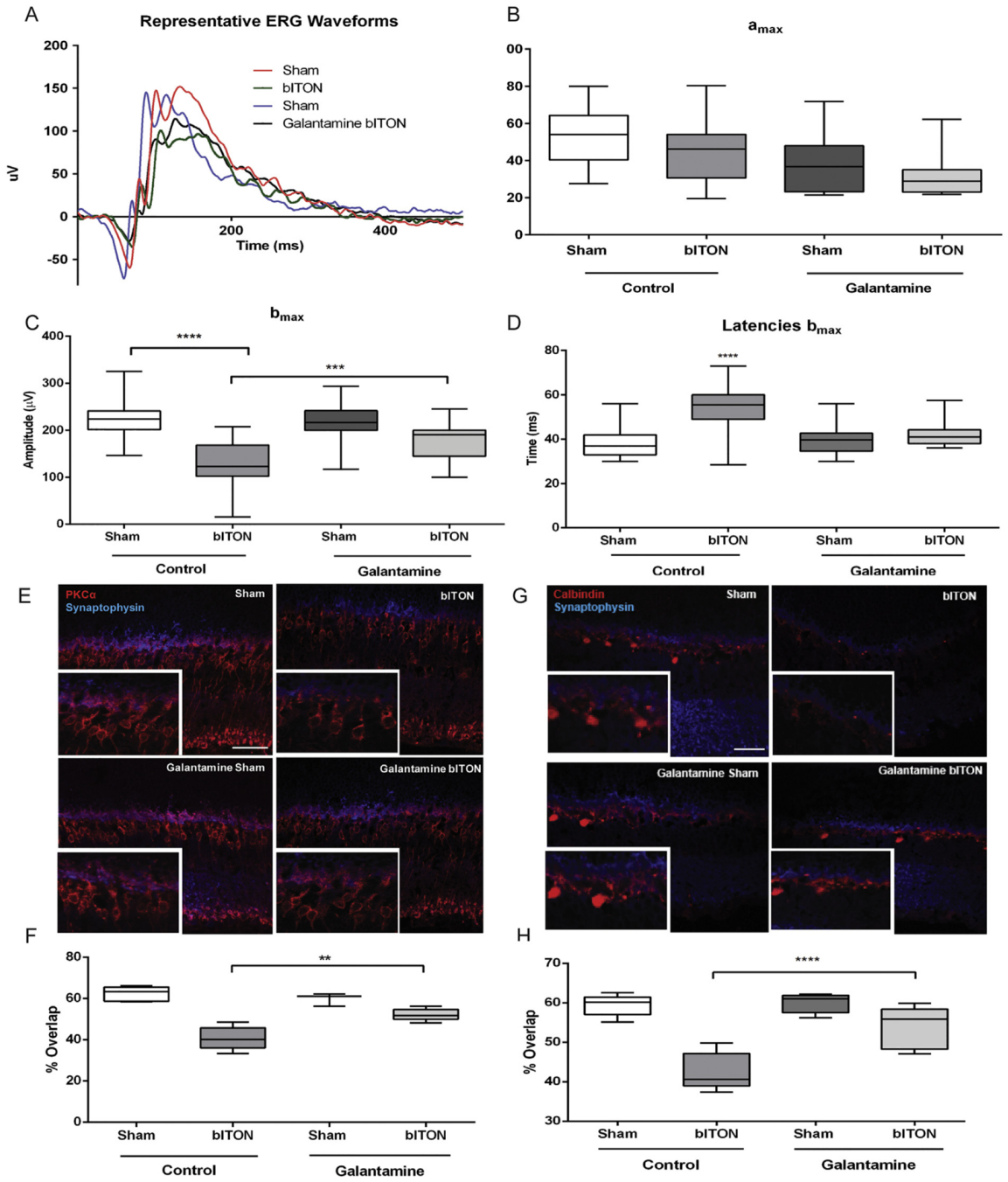

Figure 6.2. Galantamine mitigated bITON-induced the ERG b-wave deficits and rod bipolar cell dendritic retraction. A) Representative ERG waveforms. B) Graphed a-wave amplitudes. C) Graphed b-wave amplitudes. D) Graphed b-wave latencies. E) Representative fluorescent micrographs of anti-PKC-α (red) and anti-synaptophysin (blue) co-labeling in the outer plexiform layer (OPL) of retina sections. F) Quantification of co-localization of anti-PKC-α and anti-synaptophysin markers using ImageJ. G) Representative fluorescent micrographs of anti-calbindin-D (red) and anti-synaptophysin (blue) co-labeling in the OPL. H) Quantification of co-localization of anti-calbindin-D and anti-synaptophysin markers using ImageJ. For all ERG data shown, *N*=31 for control sham, 28 for control bITON, and 15 for both galantamine sham and

galantamine bITON groups. For all immunohistochemistry shown, *N*=5 retinas per group and 2 sections per retina. *p<0.05, **p<0.01, ****p<0.0001. Scale bar indicates 100um.

6.3.4 Galantamine treatment mitigated axon degeneration after bITON

Representative micrographs of optic nerve cross-sections from control sham, control bITON, and galantamine-treated bITON mice are shown. Control sham and galantamine-treated bITON nerves exhibit more axons than the control bITON nerve (Figure 6.3A-C). Similar to our previous studies, bITON mice had an average of 23,609 ± 1303 axons in the optic nerve with $p < 0.0001$ in comparison to control shams (52464 ± 4075 axons) (Ezoulin et al., 2008; Bernardo-Colon et al., 2018). Galantamine-treated shams had 52014 ± 2673 axons, and galantamine-treated bITON mice had 48,693 ± 1160 axons (Figure 6.3D), both of which were comparable to the control sham mice.

6.3.5 Galantamine treatment mitigated bITON-induced changes in the VEP

In order to assess transmission of the visual signal to the visual cortex, we performed flash VEPs (Figure 6.3E). Similar to our previously reported findings, the control sham mice had an average VEP N1 amplitude of 42.56 ± 6.78 μV while control bITON mice had an average amplitude of 21.85 ± 11.86 μV, a nearly 2-fold reduction in amplitude ($p< 0.0001$; Figure 6.3F) (Bernardo-Colon et al., 2018). The control bITON mice also had a longer VEP N1 latency than the control sham mice: 49.34 ± 11.19 ms for bITON as compared to 36.17 ± 7.30 ms ($p< 0.0001$; Figure 6.3G). Regarding the right-shifted latencies of the bITON group, these are due to a deficit in axon conductance, possibly due to changes in energetics or in myelination of the optic nerve.

Galantamine treatment after bITON resulted in partial retention of both the amplitudes and the latencies of the VEP N1 ($p<0.001$ for amplitudes and $p<0.0001$ for latencies as compared

to control bITON mice) (Figures 6.3E-G). Galantamine sham and galantamine-treated bITON mice had mean VEP N1 amplitudes of 41.98 ± 7.64 μV and 34.47 ± 8.19 μV, respectively, with no statistically significant difference between them (Figure 6.3F). Galantamine sham and bITON mean N1 latencies were 40.38 ± 5.50 ms and 45.75 ± 2.11 ms respectively, with no statistically significant difference between them (Figure 6.3G).

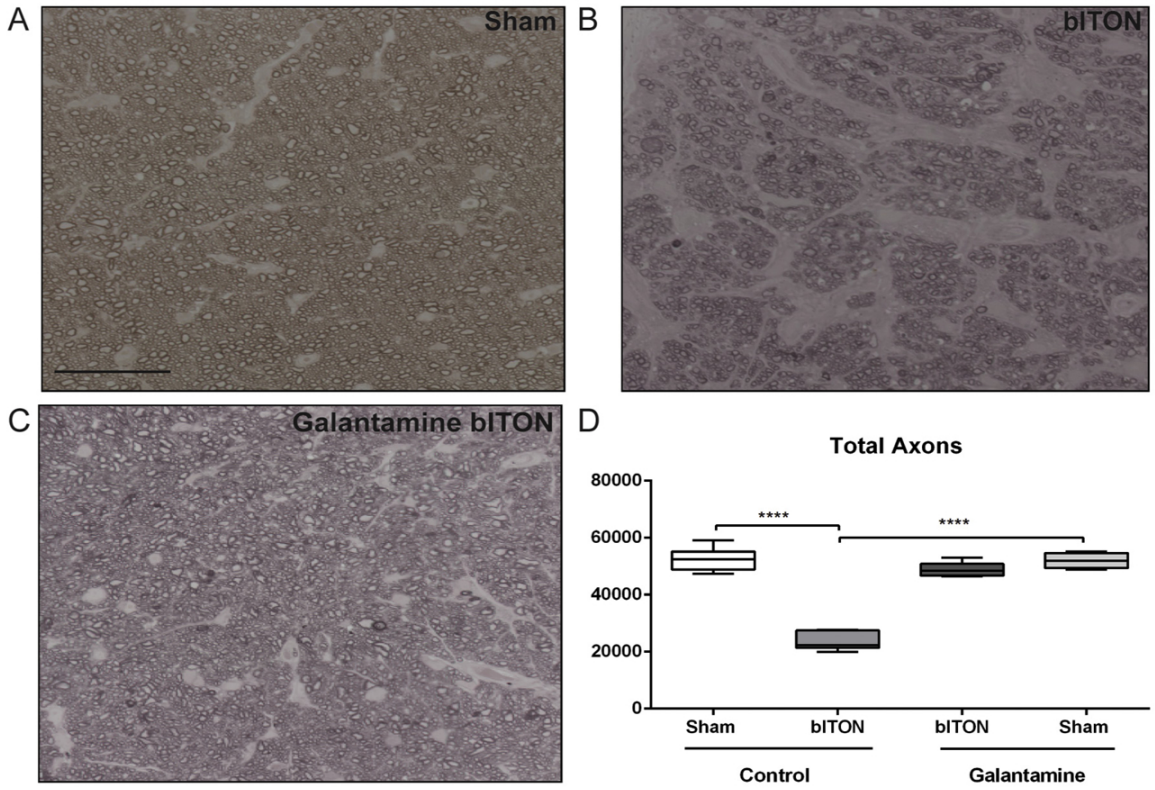
A
Sham
B
bITON
C
Galantamine bITON
D
Total Axons
80000
60000
40000
20000
0
****
****
Sham
bITON
bITON
Sham
Control
Galantamine

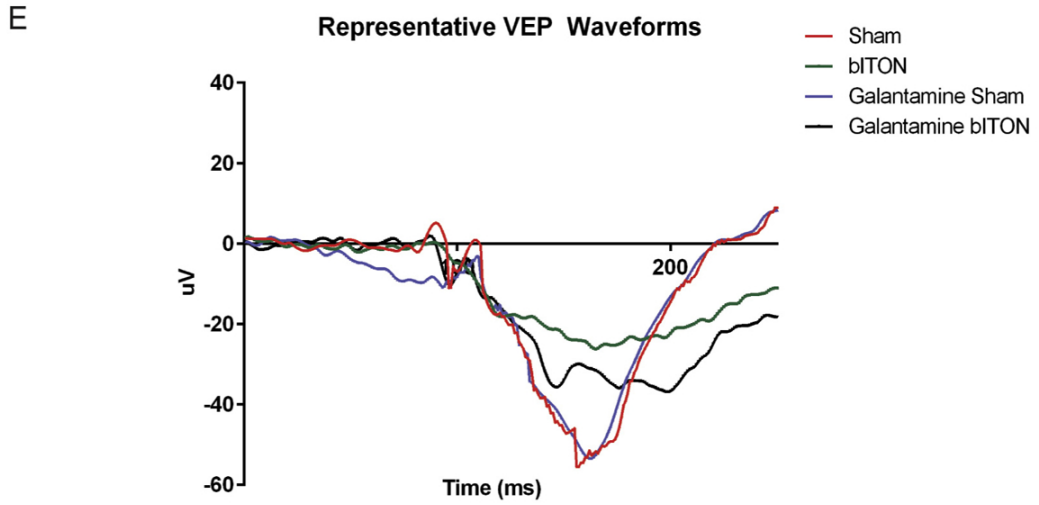
E
Representative VEP Waveforms
Sham
bITON
Galantamine Sham
Galantamine bITON
40
20
0
-20
-40
-60
uV
100
200
Time (ms)

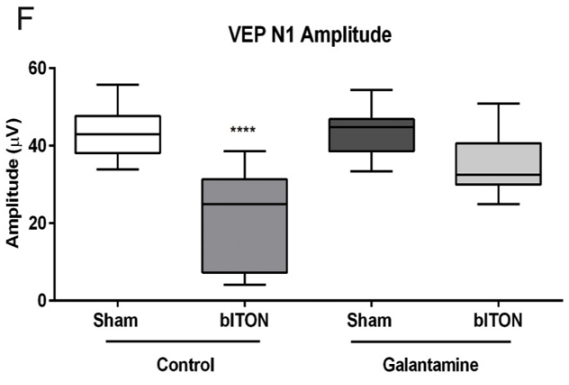
F
VEP N1 Amplitude
Amplitude (μV)
60
40
20
0
****
Sham
bITON
Sham
bITON
Control
Galantamine

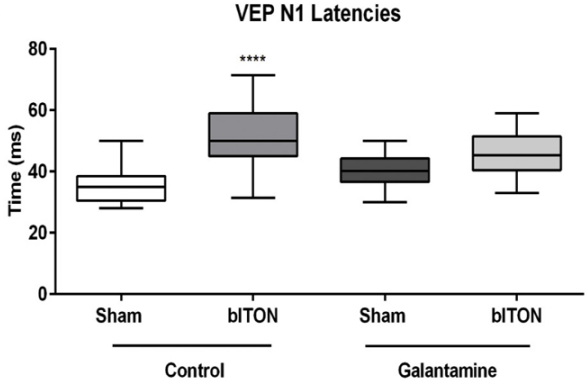
G
VEP N1 Latencies
Time (ms)
80
60
40
20
0
****
Sham
bITON
Sham
bITON
Control
Galantamine

Figure 6.3. Galantamine mitigated the VEP deficits and axon degeneration. A-C) Representative brightfield micrograph of optic nerves. Scale bar represents 20μm and applies to all micrographs. D) Quantification of total axon counts. N=5 for all groups. *p<0.05. ****p<0.00001 E) Representative VEP waveforms. F) Graphed VEP N1 amplitudes. For all VEP data, N =15 for control sham, 14 for control bITON, galantamine sham and galantamine bITON groups. G) Graphed VEP N1 latencies.

6.3.6 Galantamine mitigated bITON-induced oxidative stress and inflammation

We performed nitrotyrosine immunolabeling and quantified levels of immunofluorescence in order to assess the effect of galantamine on oxidative stress in the retina after bITON (Figure 6.4A-F). Nitrotyrosine immunolabeling was nearly absent in control sham retinas (Figure 6.4A). In the control bITON mice, nitrotyrosine immunolabeling was present specifically in the retinal ganglion cell layer (Figure 6.4B). The immunolabeling was significantly reduced in the galantamine-treated bITON retinas (Figure 6.4B, D). To determine which cell type is localized with nitrotyrosine, we co-labeled the bITON group with NeuN, which is a neuronal marker. We found that the nitrotyrosine labeling overlapped with the NeuN labeling in the ganglion cell layer (Figure 6.4E). We quantified fluorescence in the retinal ganglion cell layer of all groups (Figure 6.4F). Control bITON mice contained 174 ± 2% more fluorescence than control sham mice, $p<0.0001$, and 151 ± 5% more fluorescence than galantamine-bITON mice, $p<0.0001$ (Figure 6.4F). There was no statistically significant difference in fluorescence levels between galantamine sham mice and galantamine-treated bITON mice (Figure 6.4F).

Mitochondrial superoxide dismutase (SOD2) converts the superoxide that is formed as a metabolic by-product of oxidative phosphorylation into oxygen and thus is a critical enzyme in regulating intracellular ROS levels. Similar to our previously studies, we detected a 59 ± 4% decrease in SOD2 levels at one month after control bITON as compared to control shams (Figure

6.4G) (Bernardo-Colon et al., 2018). In contrast, SOD2 levels in galantamine-treated sham and bITON mice were comparable to control shams. We detected a statistically significant difference ($p<0.001$) between either galantamine-treated group and the control bITON group (Figure 6.4G).

We detected an increase in the pro-inflammatory cytokines, IL-1α and IL-1β in the control bITON retinas, in agreement with our previous findings (Figure 6.4H).[14,31] bITON retinas had IL-1α mean levels of 17.77 ± 6.41pg/ml in comparison to shams with mean levels of 2.26 ± 0.98pg/ml, $p<0.00001$. Average galantamine sham levels for IL-1α were 6.30 pg/ml ± 3.37 and mean galantamine bITON levels were 5.43 pg/ml ± 2.26. There was no statistically significant difference between control sham retinas, galantamine-treated sham retinas, and galantamine-treated bITON retinas. Similarly, bITON resulted in an elevation of IL-1β levels to 9.18 ± 2.4 pg/ml, compared to 4.1 ± 1.9 pg/ml detected in control sham retinas ($p<0.001$) (Figure 6.4I). In contrast, galantamine-treated sham retinas and galantamine-treated bITON retinas contained similar levels of IL-1β: 2.7 ± 1.7 pg/ml and 2.8 ± 1.4 pg/ml, respectively and were not significantly different from control sham retinas.

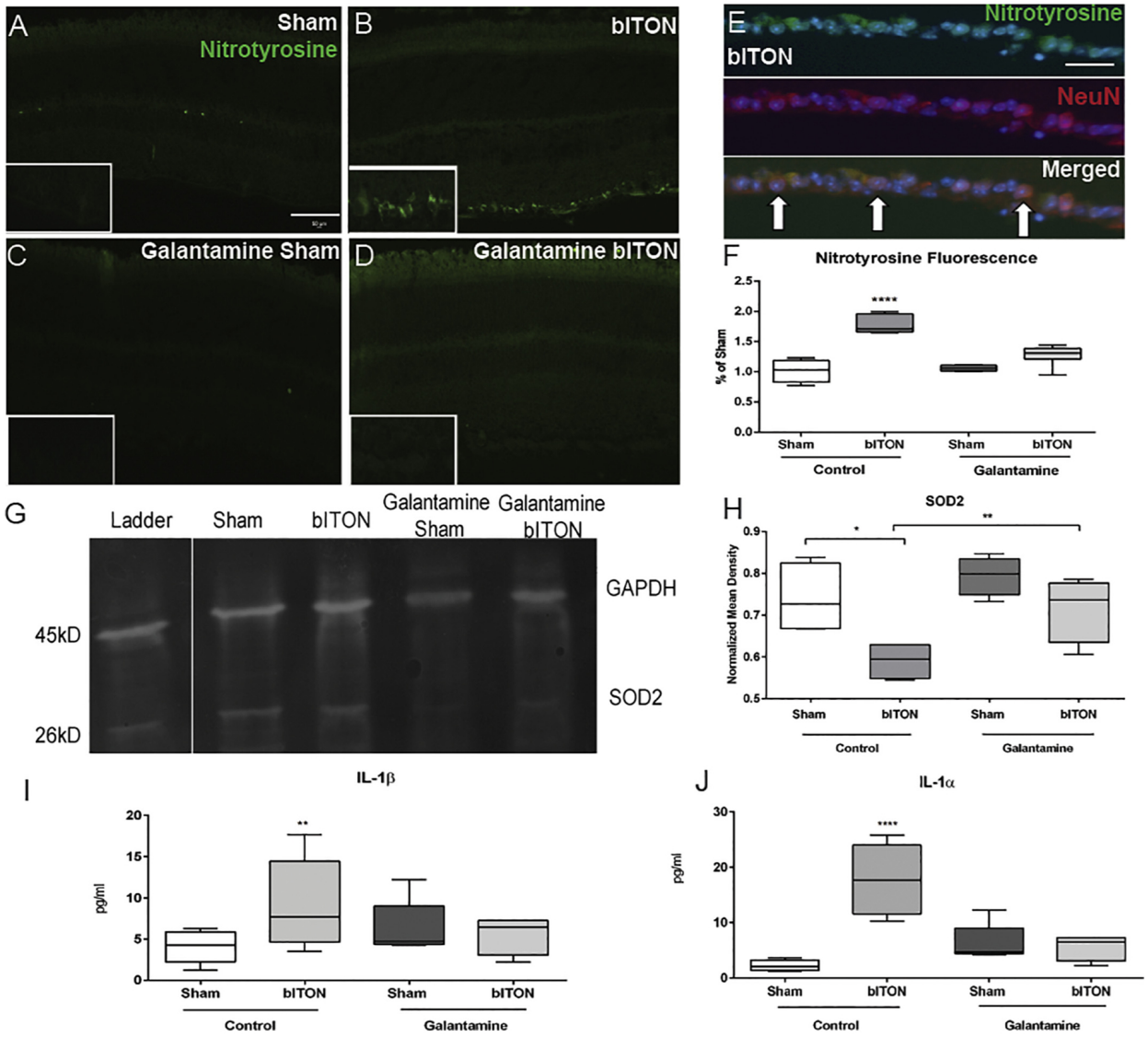

Figure 6.4. Galantamine has antioxidant and anti-inflammatory effects. A-D) Representative fluorescent micrographs of anti-nitrotyrosine labeling. Scale bar represents 50µm and applies to all images. E) Representative fluorescent micrographs of anti-nitrotyrosine labeling (green), anti-NeuN labeling (red), and DAPI (blue). Co-localization of these markers indicated with white arrows. F) Quantification of anti-nitrotyrosine fluorescence in the ganglion cell layer using ImageJ and compared as a percent of control sham mouse. G) Representative western blot of SOD2. H) Quantification of retinal SOD2 levels. *N*=5 retinas per group for all biochemical analyses. I) Quantification of retinal IL-1α levels. J) Quantification of retinal IL-1β levels. *N*=5 retinas per group and 2 sections per retina. **p*<0.05, ***p*<0.01, ****p*<0.001, *****p*<0.0001. Scale bar indicates 100um

6.4 Discussion

In this study, we initiated treatment of galantamine after the last of a 3-day series of blast exposures. We show that oral galantamine given ad libitum reached the retina, where it increased acetylcholine levels and decreased acetylcholinesterase activity. This treatment paradigm mitigated bITON-induced visual function deficits, axon degeneration in the optic nerve and rod bipolar cell dendritic retraction. Further, it moderated oxidative stress, inflammation, and glutamate levels.

It is important to note that in most cases, the treatment did not result in sham levels of protection. It may be that treating earlier could be more effective and/or that there are additional injury pathways that are activated by bITON but unaffected with galantamine treatment. The efficacy of other rational interventions should be explored. We previously demonstrated that our bITON model induces axon degeneration after only three blasts, which suggests that injury responses started prior to the last day of the blasts and the start of galantamine treatment (Bernardo-Colón et al., 2019). Further studies are also needed to elucidate if earlier treatment would be more effective and to determine how long galantamine treatment can be initiated and still be effective. It is also important to note that the retinal cells may also be modulating the oxidative stress and inflammation responses as a result of their own death or survival, separate from the effects of galantamine treatment in the system.

Based on the ERG, immunolabeling, and OCT thickness, bITON does not cause significant loss of bipolar or amacrine cells. We did find co-labeling of nitrotyrosine and NeuN in the ganglion cell layer, suggesting that these cells are primarily being affected by the oxidative stress of bITON (Figure 6.4E). Notably, we do not detect a difference in overall retinal thickness or in the thickness of any particular layer of the retina by OCT (data not shown). In addition, the

oscillatory potentials of the ERG are unaltered in our bITON model suggesting that at least the AII amacrine cells are unaffected (data not shown). Immunohistochemistry shows the presence of bipolar cells after bITON, although their dendritic branching is reduced. Finally, we have also performed TUNEL and do not detect active cell death in the retina at the time-points we have examined after bITON (data not shown). Thus, while we cannot discount some loss of amacrine or bipolar cells, it is likely minimal.

Our detection of elevated glutamate in injured retinas is consistent with reports in other models. In a rat TBI study, there was a nine-fold increase in glutamate levels in comparison to controls.(Guerriero et al., 2015) In a model of rat blast injury, glutamate was significantly increased in the retina.(Mammadova et al., 2017) Many preclinical and clinical studies have demonstrated altered glutamate production, clearance, and buffering after TBI that results in an excess of glutamate (Guerriero et al., 2015; Tehse & Taghibiglou, 2019). Glutamate may, in fact, play a large role in determining the state of the post-injury CNS. Glutamate is the most abundant excitatory neurotransmitter within the CNS and excess glutamate can lead to a massive increase in neuronal activity, increased intracellular calcium, and possibly even cell death, i.e. excitotoxicity. Retinal astrocytes and Müller glia play an important role in glutamate buffering and clearance. In a blast injury model in which altered glutamate levels were reported, the number of astrocytes containing EAAT2, one of the excitatory amino acid transporters for glutamate, was found to be down-regulated (Dorsett et al., 2017). However, in our model of bITON, we did not find a difference in the immunohistochemical labeling of GLAST, a marker for glutamate synthetase, or EAAT1, a marker for glutamate transporter, between any of our groups. The relationship between glutamate and our bITON model should be further explored outside of this study. Perhaps, other EAATs should be investigated. Additionally, galantamine

has been shown to act as a modulator of glutamate-induced excitotoxicity.(Santos et al., 2002) It is feasible that galantamine acted upstream to the mechanism that caused an increase in glutamate. This should be explored in future studies.

The positive effect of galantamine on oxidative stress and inflammation in our bITON model are in agreement with other reports showing that galantamine has antioxidant and anti-inflammatory effects on cells both in culture and *in vivo* (Melo et al., 2009; Romero et al., 2010). Galantamine treatment reduced IL-1β levels in the brain of a hypoxia-ischemic rat model, and protected cortical neurons following injury (Satapathy et al., 2011). Additionally, galantamine decreased oxidative stress and apoptosis in cortical neurons exposed to amyloid-beta peptides and in neuroblastoma cells that were treated with hydrogen peroxide (Ezoulin et al., 2008; Melo et al., 2009).

Galantamine has been utilized in a variety of neurodegenerative disease models other than Alzheimer's, and has demonstrated protection. Galantamine treatment, via modulation of the muscarinic acetylcholine receptors in the retina, has shown to be protective in multiple models of glaucoma by promoting retinal ganglion cell survival (M Almasieh et al., 2010; Di Polo, A., Almasieh, M.,; Zhou, 2006). Additionally, through its inhibition of acetylcholinesterase, galantamine treatment resulted in vaso-protection in another model of glaucoma via increasing blood flow (Mohammadali Almasieh et al., 2013). Outside the retina, efferent vagus nerve activity, via the cholinergic anti-inflammatory pathway, is responsible for regulation of cytokine production via α7nAChR-dependent signaling (Borovikova et al., 2000). Galantamine is a positive allosteric modulator of α7nAChRs, so it is feasible that the protection we detected was due to activation of this anti-inflammatory pathway (Faghih et al., 2007; Santos

et al., 2002; Texidó et al., 2005). Overall, our results are comparable with previous studies such that galantamine is antioxidant, anti-inflammatory and neuroprotective.

In conclusion, galantamine treatment given after three days of blasts, two per day, partially protected against visual function deficits, oxidative stress, inflammation and axon degeneration in a model of bITON. Future studies are needed to elucidate galantamine's therapeutic window for partial protection following bITON. Additionally, future studies should determine the exact mechanism by which galantamine exerts antioxidant and anti-inflammatory effects in our model of bITON. Since it is already FDA-approved, it has good pharmacokinetics and is safe to use, galantamine should be further studied as a potential treatment for optic neuropathies.

CHAPTER 7

Appendix 2: Intravitreal injection worsens outcomes in a mouse model of indirect traumatic optic neuropathy from closed globe injury

This chapter of my thesis is published in *Experimental Eye Research:*

Naguib S, Bernardo-Colón A, Rex TS. Intravitreal injection worsens outcomes in a mouse model of indirect traumatic optic neuropathy from closed globe injury. Exp Eye Res. 2021 Jan;202:108369. doi: 10.1016/j.exer.2020.108369. Epub 2020 Nov 22. PMID: 33238184; PMCID: PMC8117180.

7.1 Abstract

It is well established that an intravitreal needle poke or injection of buffer is protective to the retina in models of photoreceptor degeneration due to release of endogenous neurotrophic factors. Here we assess the effect of intravitreal injection of buffer in a model of closed globe trauma that causes air-blast induced indirect traumatic optic neuropathy (bITON). We injected animals 1-day after the last bITON or sham procedure and performed assessments 1-month later. Surprisingly, we detected a lower electroretinogram (ERG), greater optic nerve damage, and increased levels of pro-inflammatory cytokines in animals given an intravitreal injection. The effect was sometimes independent of bITON and sometimes exacerbated by the injury. Retina histology appeared normal, however the total number of axons in the optic nerve was lower even in uninjured animals that were injected. The number of degenerative axons was further increased in injured animals that were injected. In contrast, we detected a decrease in the ERG a wave and b wave amplitudes, but no effect on the visual evoked potential. Levels of the pro-inflammatory cytokines, IL-1α and IL-1β were elevated in the mice that received an intravitreal injection. This

increase was even greater in animals that also had a bITON. This suggests that intravitreal injections may be injurious to the optic nerve particularly during the acute stage of optic nerve injury. In addition, the data suggests a role for IL-1α and IL-1β in this response.

7.2 Manuscript

Seminal work from the laboratories of Silverman and Hughes, and LaVail and colleagues demonstrated that a needle poke or injection of saline or phosphate-buffered saline (PBS) protected the photoreceptors in inherited models of retinal degeneration (Silverman and Hughes, 1990; Faktorovich et al., 1990). LaVail and colleagues extended this work to demonstrate that an ocular needle poke or injection of buffer into the vitreous of the eye resulted in protection of photoreceptors in a light-induced injury model (Faktorovich et al., 1992). Here we report different effects in a closed globe injury model that causes optic nerve degeneration with relative sparing of the retina with the exception of outer plexiform layer synaptopathy based on histology and ERG results (Naguib et al., 2019). This is a mouse model of air-blast-induced indirect traumatic optic neuropathy (ITON). This model results in specific and robust axon degeneration in the optic nerve and a correlative decrease in the visual evoked potential (Bernardo-Colón et al., 2018, Bernardo-Colón et al., 2019).

Current clinical practice suggests that neurotrauma should be treated within 24 h. Thus, in this study we tested the effect of an intraocular injection of 1 µL of saline given 24 h after completion of the injury paradigm of two back-to-back eye-directed air blasts given once daily for 3 days straight as previously published (Bernardo-Colón et al., 2018, Bernardo-Colón et al., 2019). Sham animals were exposed to anesthesia, but the air blast was blocked. One month after injury we performed optical coherence tomography (OCT), histology, electroretinograms (ERG),

visual evoked potentials (VEP), and quantification of IL-1α, IL-1β, and caspase-1 using methods as described previously (Bernardo-Colón et al., 2018; Naguib et al., 2019) and briefly below. Eye injury was induced in C57Bl/6J mice (Jackson Labs, Bar Harbor, ME) anesthetized with 1.5% isofluorane and secured into a padded housing chamber which was slid into a pipe. The left eye of the mouse was positioned against a hole in the side, which was aligned with the barrel of a paintball marker. Mice were exposed to two 15 psi air-blasts at a 0.5 s interval per day for three days. Sham mice were anesthetized and placed in the trauma system, but the air was blocked from reaching the eye. Mice were provided gel recovery food (Clear H_2O, Portland, ME) for the first 3-days post-injury. At 1-day after the last blast exposure, mice were anesthetized with isofluorane and injected with a single 1 µl intravitreal injection of saline using a 30 gauge Hamilton syringe. All experiments were conducted in compliance with the ARVO Statement for the Use of Animals in Ophthalmic and Vision Research. This study was carried out under an animal protocol approved by the Vanderbilt University Medical Center Institutional Animal Care and Use Committee.

In vivo, just prior to euthanasia at 1-month post-injury, we performed imaging and electrophysiology. For the ERGs and VEPs, mice were dark-adapted overnight, dilated with 1% tropicamide for 10 min, and anesthetized with 20/8/0.8 mg/kg ketamine/xylaxine/urethane. Corneal electrodes with integrated stimulators were placed on eyes lubricated with Genteel drops using the Celeris system (Diagnosys LLC, Lowell, MA). Subdermal platinum needle electrodes were placed in the snout and back of the head at the location of the visual cortex. A ground electrode was placed in the back of the mouse. For ERGs, electrodes were placed on lubricated corneas. Mice were then exposed to 15 flashes of 1 Hz, 1 cd s/m^2. For VEPs, mice were exposed to 50 flashes of 1 Hz, 0.5 cd s/m^2 white light. In order to image the retina *in vivo* mice were

anesthetized with isofluorane, the eyes were dilated with 1% tropicamide, and the retinas were imaged with the Bioptigen ultra-high resolution OCT system.

Optic nerve pieces were post-fixed in glutaraldehyde followed by embedding in Resin 812 and Araldite 502 (cat # 14900 and 10900, Electron Microscopy sciences, Hatfield, PA). A Leica EM-UC7 microtome was used to collect 1 μm-thick cross-sections which were then stained with 1% paraphenylenediamine and 1% toluidine blue and imaged on a Nikon Eclipse Ni-E microscope using a 100x oil immersion objective (Nikon Instruments Inc., Melville, NY). Both total and degenerating axons were quantified using Image J. Degenerative axon profiles were identified by dark paraphenylenediamine staining due to collapsed myelin or loose myelin (onioning) surrounding the axon. A grid was used to count 20% of the optic nerve cross-sectional area in order to avoid bias.

In order to quantify IL-1α and IL-1β levels, the mouse multiplex cytokine/chemokine magnetic bead panel (cat #: MCYTOMAG-70K, Millipore, Burlington, MA) was used according to manufacturer directions. Samples were tested in duplicates and results were averaged. To quantify levels of cleaved and total caspase-1, we performed a standard western blot using anti-caspase 1 (1:1000, ab108362, Abcam, Cambridge MA) and HSP60 as loading control (1:1000, ab45134, Abcam, Cambridge MA). Band density was quantified by scanning the blot using an EPSON scanner and Adobe Photoshop to convert to grayscale and invert the image. Each band was selected with the same frame, and set measurements were used to obtain the grey mean value for each. Western blot data was normalized to loading controls. Data were analyzed using GraphPad Prism (La Jolla, CA). All experimental groups were compared to each other using a one-way ANOVA and the Tukey post-hoc test. All groups are shown as mean ± SEM.

The layers of the retina appeared normal by OCT in all experimental and sham groups regardless of injection (Fig. 7.1A). Quantification of total retina thickness showed no difference between groups (Fig. 7.1B). In contrast, representative histological optic nerve cross-sections showed few degenerative axon profiles in the sham and bITON optic nerves, but many degenerative axons in the bITON saline optic nerves (Fig. 7.1C). Quantification of total axons showed that there were fewer axons in the bITON group compared to the sham group as previously described (Bernardo-Colón et al., 2018; Naguib et al., 2019). Surprisingly, there was also a reduction in total axons in the sham saline optic nerves compared to the un-injected shams (Fig. 7.1D). There was no additional decrease in total axon numbers in the bITON saline animals as compared to uninjected bITON mice. The number of degenerative axon profiles in the optic nerve was comparable between the sham, bITON, and sham saline groups (Fig. 7.1E). This matches previous data indicating that axon degeneration in our model is completed before 1-month post-injury (Bernardo-Colón et al., 2018, Bernardo-Colón et al., 2019; Naguib et al., 2019). However, there were a large number of degenerative axon profiles in the bITON saline mice (Fig. 7.1E), suggesting either later or prolonged axon degeneration, which would likely lead to fewer total axons in this group at later time-points. Next, we assessed visual function using flash-ERG and VEP (Fig. 7.1F–H). In un-injected animals, bITON had no effect on the ERG a-wave amplitude (a_{max}) (Fig. 7.1F). However, the a_{max} was reduced equally in both the sham saline and bITON saline groups as compared to the uninjected controls ($p < 0.05$). This suggests that the intravitreal injection adversely affected the photoreceptors independent of bITON. As reported previously, bITON caused a reduction in the ERG b-wave amplitude (b_{max}) as compared to sham mice (Fig. 7.1G; Naguib et al., 2019). The sham saline group also had a lower b_{max} compared to the sham group, which is likely due to the decrease in a_{max} ($p < 0.0001$).

This was also the case when comparing the bITON group to the bITON saline group ($p < 0.01$). Finally, the VEP N1-wave amplitude showed the expected decrease in the bITON group compared to sham, regardless of intraocular injection, $p < 0.0001$ (Fig. 7.1H; Bernardo-Colón et al., 2018; Naguib et al., 2019). Surprisingly there was no additional decrease in the VEP N1 amplitude caused by the intraocular injection. This may be due to extensive redundancy in the visual system. It is possible that if we performed the VEPs at later time-points we would see a further reduction in the bITON saline group, based on the increased amount of axon degeneration detected in those animals at this time-point.

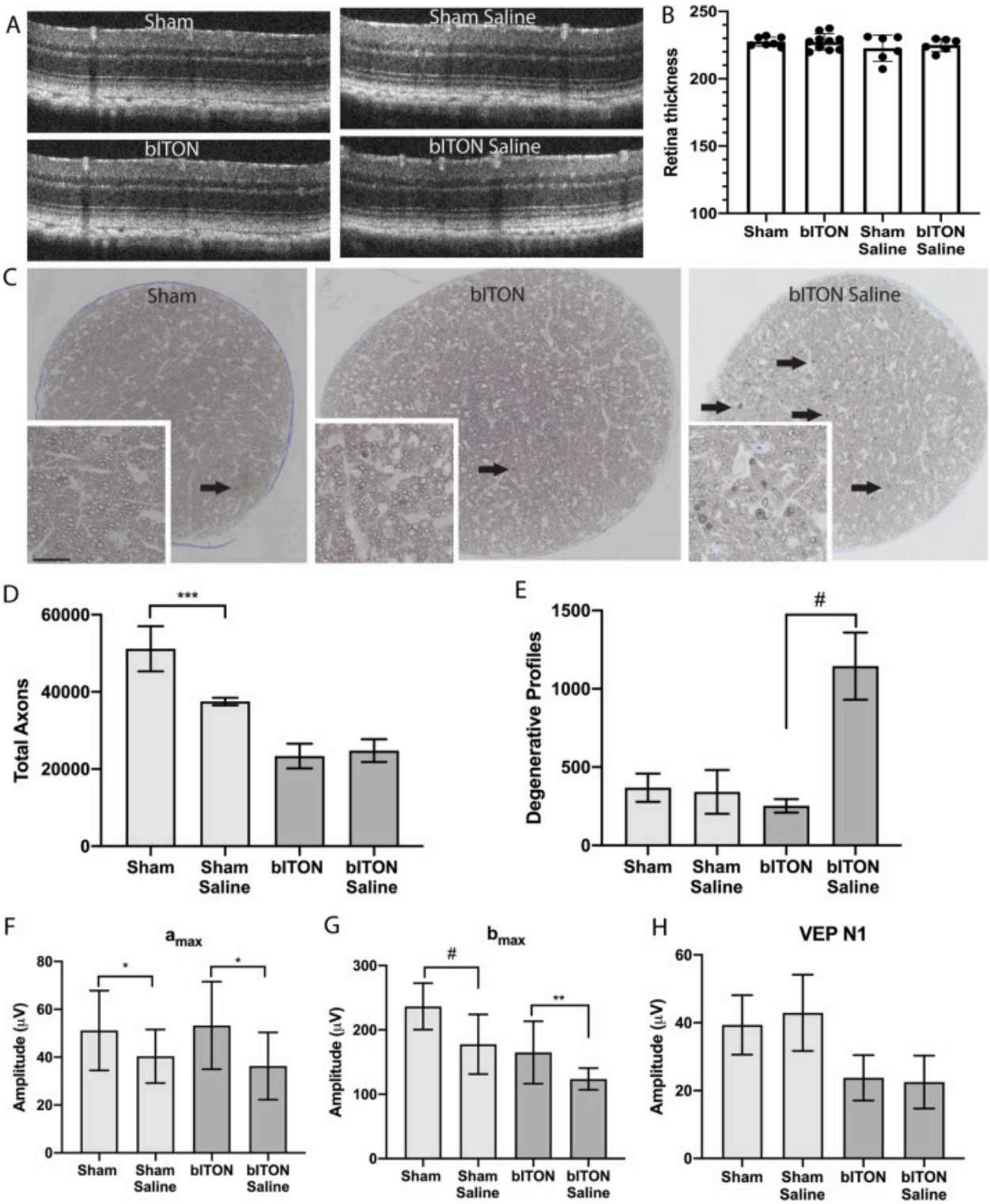

Figure 7.1. Intravitreal injection of saline affects retina function, not structure, and optic nerve structure, not function. A) Representative OCT images of retinas from all groups. B) Quantification of averaged retina thickness taken from across all collected b-scans using DIVER software (Diagnosys LLC). C) Representative brightfield micrographs of optic nerve cross-sections from sham, bITON, and bITON saline mice. Scale bar for high magnificantion insets is

20 µm. D) Quantification of degenerative axon profiles in the optic nerves of all groups. E) Quantification of total optic nerve axons in all groups. F) Quantification of the ERG a_{max} for all groups. G) Quantification of the ERG b_{max} for all groups. H) Quantification of the VEP N1 amplitude for all groups. All comparisons were made between injected and un-injected animals. *$p < 0.05$, **$p < 0.01$, ***$p < 0.001$, #$p < 0.0001$. Un-injected data was derived from Bernardo-Colón et al. (2018), 2019; Naguib et al. (2019).

We previously reported a role for the inflammasome pathway, and in particular, levels of IL-1α and IL-1β in the retina in this model (Bernardo-Colón et al., 2018). Therefore, we assessed the effect of an intravitreal injection on the levels of these pro-inflammatory cytokines in the presence or absence of bITON. We detected increases in both IL-1α and IL-1β in the retina after bITON, as previously reported (Fig. 7.2A and B; Bernardo-Colón et al., 2018). Surprisingly, an intravitreal injection of saline caused a much larger increase in both of these cytokines in both the sham and bITON groups ($p < 0.0001$; Fig. 7.2A and B). The increase was disproportionately even greater in the bITON saline group as compared to the un-injected bITON group ($p < 0.0001$). In order to determine if the increases in these pro-inflammatory cytokines resulted in activation of the inflammasome in the retina, we quantified levels of total and cleaved caspase-1 (Fig. 7.2C and D). As previously reported, bITON caused an increase in cleaved caspase-1, $p < 0.002$ sham vs bITON and $p < 0.0001$ sham saline vs bITON saline (Bernardo-Colón et al., 2018). However, there was no difference in the amount of cleaved to total caspase-1 between the uninjected and injected groups regardless if sham or bITON (Fig. 7.2D). This suggests that the injection causes priming, but not activation of the inflammasome pathway. It is feasible that pathway activation was blocked through endogenous increases in protective factors. This is something that we can explore in future studies. Certainly, it is well-known that an intravitreal injection of saline can increase release of protective factors including FGF and CNTF (Faktorovich et al., 1992; Liang et al., 2001; Ji et al., 2004; Wen et al., 2012).

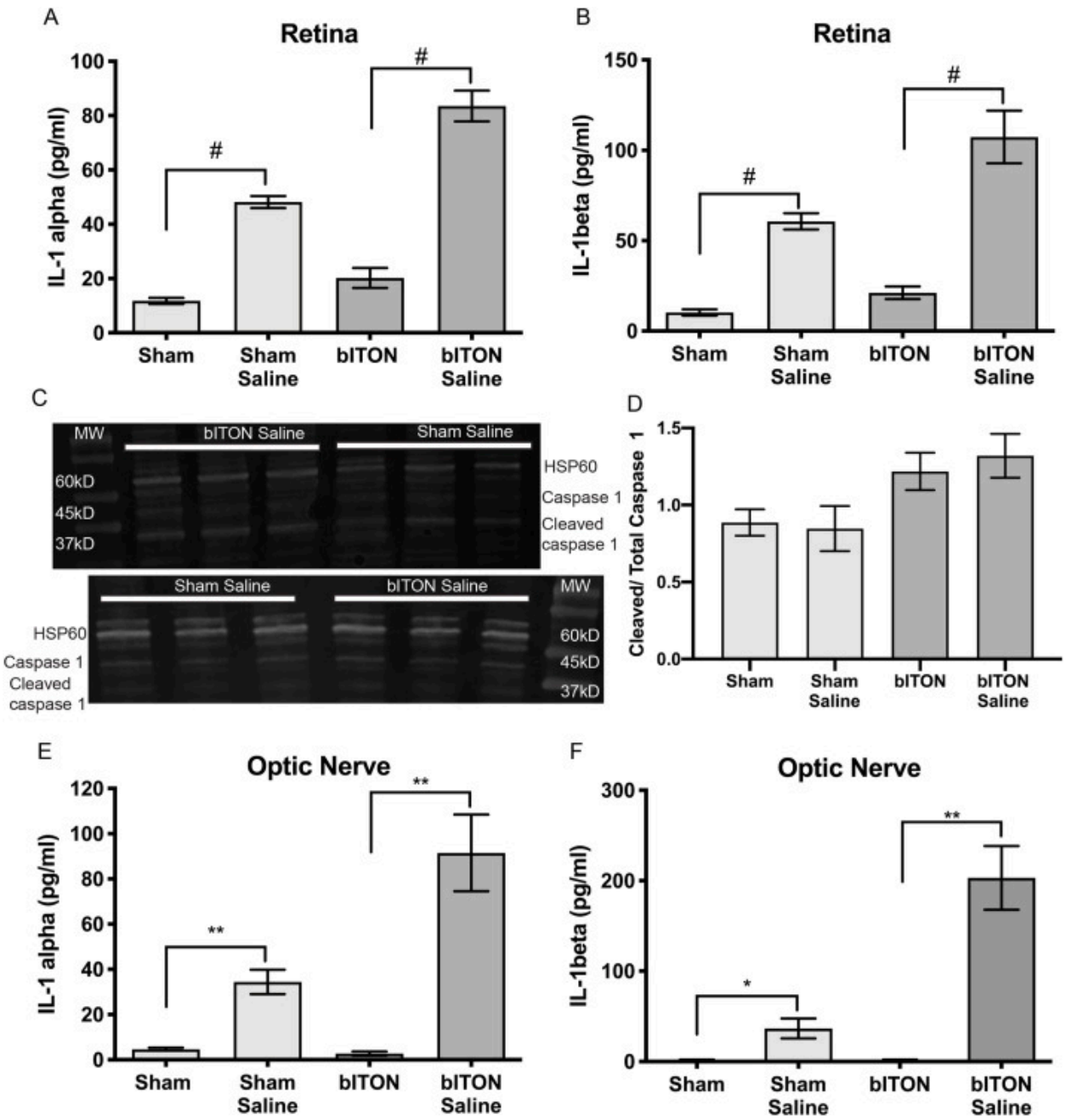

Figure 7.2. A single intravitreal injection of saline increases levels of pro-inflammatory cytokines. A) Quantification of IL-1α levels in the retina. B) Quantification of IL-1β levels in the retina. C) Representative Western blots for caspase-1 in the retina. D) Quantification of cleaved to total caspase-1 in the retina. E) Quantification of IL-1α levels in the optic nerve. F) Quantification of IL-1β levels in the optic nerve. Un-injected data was obtained from Bernardo-Colón et al. (2018), 2019; Naguib et al. (2019).

Since we detected optic nerve degeneration in the saline injected animals, we also measured levels of IL-1α and IL-1β in the optic nerve. We did not detect differences in the levels

of either cytokine in the optic nerves of uninjected sham and bITON groups (Fig. 7.2E and F). However, both IL-1α and IL-1β levels were increased in the optic nerve of saline-injected mice as compared to the uninjected mice (Fig. 7.2E and F). The increase in both cytokines was much greater in the bITON saline group than the sham saline group suggesting that bITON exacerbated the effect of the intravitreal injection. Notably, the IL-1β levels increased about two-fold more in the optic nerve than in the retina (Fig. 7.2B,F).

Together, our data show that an intravitreal injection of saline increased levels of pro-inflammatory cytokines and negatively affected photoreceptor function, but not structure, and optic nerve structure, but not function, at one-month post-injection. The ongoing axon degeneration in the saline-injected bITON group, but not the uninjected bITON group, suggests that the VEP might be decreased in the saline-injected bITON group at later time-points.

A previous study demonstrated that an intravitreal injection of saline caused temporary formation of vacuoles in the photoreceptor outer segments and RPE that resolved by 3-weeks post-injury (Hombrebueno et al., 2014). Therefore, since our assessments were performed at 4-weeks post-injection, we may have missed detection of any possible transient damage to the outer retina. Notably, they did not detect any retina damage after intravitreal injection of PBS, suggesting that this is a safer diluent than normal saline. In fact, in a light damage model, an intravitreal injection of PBS prior to light exposure showed slight, but not statistically significant protection of the outer retina (Faktorovich et al., 1990, 1992). Neither study assessed the optic nerve or ganglion cell layer. This is in contrast to our findings of retinal ganglion cell axon degeneration after injection of PBS and might represent differences between these cell types. Notably, a subretinal injection of PBS, saline, or a needle poke was more protective to the photoreceptors than was an intravitreal injection in models of photoreceptor degeneration

(Cayouette et al., 1998; Faktorovich et al., 1990, 1992; Silverman and Hughes, 1990). These studies attributed the release of cellular factors after injury as the reason for the protection.

Similar to our results, Hombrebueno et al. (2014) also detected increased inflammatory cytokines after intravitreal injection of saline. They detected increased mRNA levels of IL-1β at 1-day post-injection but did not measure levels at 3-weeks post-injection. The fact that we detected elevated IL-1β levels at 4-weeks post-injection suggests that intraocular inflammation is long-lasting after a single injection. They also reported increases in expression of TNFα, IL-6, iNOS, and VEGF at 1-day post-injection. It would be interesting to know if these cytokines are also still elevated at 4-weeks post-injection in our model. The dramatic and sustained increases in IL-1α and IL-1β that we detected in both the retina, and, even more so, in the optic nerve, suggests that this pathway may contribute to greater damage to the optic nerve axons in injected animals as compared to uninjected controls. Others have also reported evidence of inflammation in terms of leukocyte infiltration after an intravitreal injection of normal saline in rabbits (Csukas et al., 1990).

The timing of intravitreal injection could influence results. We injected after bITON and detected increased axon degeneration. In the light damage model, an intravitreal injection of saline administered prior to light exposure prevents cell loss and preserves the ERG amplitude (Belokopytov et al., 2012; Chollangi et al., 2009). However, this effect was lost when PBS was injected following light exposure (Chollangi et al., 2009). Also, there was no evidence of increased inflammation when a PBS injection was given two days prior to light damage (LaVail et al., 1992). It is feasible that administering the intravitreal injection of saline prior to injury might have resulted in protection in the bITON model. This is something that could be explored in future studies.

Interestingly, we detected a decrease in the a_{max} without obvious structural damage to the photoreceptors. This is reminiscent of the results of treatment with high levels of CNTF or LIF. Intraocular delivery of high doses of CNTF or LIF suppresses ERG amplitudes while simultaneously protecting photoreceptors, structurally (Schlichtenbrede et al., 2003; McGill et al., 2007; Chucair-Elliot et al., 2012). McGill and colleagues demonstrated that high doses of intravitreal CNTF reduced ERG amplitudes 45–70% (2007). Additionally, previous studies inducing optic nerve injury or focal mechanical damage or light damage to the rat retina resulted in endogenous upregulation of bFGF and/or CNTF (Wen et al., 1995; Gao and Hollyfield, 1995, 1996; Gargini et al., 2004). Importantly, Gargini et al., showed that optic nerve injury caused deficits in the ERG amplitudes that correlated with the timing of endogenous upregulation of CNTF (Gargini et al., 2004). If these cytokines are endogenously increased after an intravitreal saline injection and/or bITON, it might explain the suppression of the a_{max} that we detected. While no obvious structural damage was detectable in the photoreceptors it is likely that immunohistochemical approaches may show that these cells are responsive. Certainly the synaptic terminals are disconnected from their downstream targets at 1-month post-bITON, which contributes to the decrease in the ERG b-max (Naguib et al., 2019). Molecular level effects to the outer segments could be investigated in future studies. Although at least one study showed that subretinal injection of PBS did not affect ERG amplitudes in comparison to un-injected rats (Timmers et al., 2001). This should be explored in future studies.

In conclusion, the major point of this study is that an intravitreal injection of normal saline given 1-day after closed globe trauma results in sustained elevation of pro-inflammatory cytokines and is detrimental to the optic nerve. Future studies are needed to determine if there is a causative link between the elevated pro-inflammatory cytokines and axon degeneration. Our previous

study using diet to decrease oxidative stress and inflammation showed protection of the optic nerve suggesting that a link may exist (Bernardo-Colón et al., 2018). These data suggest that any treatments for traumatic optic neuropathy delivered by intravitreal injection might need to also treat the inflammation induced by the injection itself. These data also suggest that a more physiologic diluent should be used whenever possible.

REFERENCES

Abri Aghdam, K., Soltan Sanjari, M., & Ghasemi Falavarjani, K. (2016). Erythropoietin in ophthalmology: A literature review. *Journal of Current Ophthalmology*, *28*(1), 5–11. https://doi.org/10.1016/J.JOCO.2016.01.008

Aghadoost, D. (2014). A Brief Overview of Ocular Trauma. *Archives of Trauma Research*, *3*(2). https://doi.org/10.5812/atr.21639

Al-Sarraf, H., Malatiali, S., Al-Awadi, M., & Redzic, Z. (2018). Effects of erythropoietin on astrocytes and brain endothelial cells in primary culture during anoxia depend on simultaneous signaling by other cytokines and on duration of anoxia. *Neurochemistry International*. https://doi.org/10.1016/j.neuint.2017.11.014

Allen, N. J., & Lyons, D. A. (2018). Glia as Architects of Central Nervous System Formation and Function. *Science (New York, N.Y.)*, *362*(6411), 181. https://doi.org/10.1126/SCIENCE.AAT0473

Almasieh, M, Zhou, Y., Kelly, M. E., Casanova, C., & Di Polo, A. (2010). Structural and functional neuroprotection in glaucoma: role of galantamine-mediated activation of muscarinic acetylcholine receptors. *Cell Death & Disease*, *1*, e27. https://doi.org/10.1038/cddis.2009.23

Almasieh, Mohammadali, MacIntyre, J. N., Pouliot, M., Casanova, C., Vaucher, E., Kelly, M. E. M., & Di Polo, A. (2013). Acetylcholinesterase inhibition promotes retinal vasoprotection and increases ocular blood flow in experimental glaucoma. *Investigative Ophthalmology and Visual Science*, *54*(5), 3171–3183. https://doi.org/10.1167/iovs.12-11481

Andreotti, G., Lange, J. L., & Brundage, J. F. (2001). The nature, incidence, and impact of eye injuries among US military personnel: Implications for Prevention. *Archives of Ophthalmology*, *119*(11), 1693–1697. https://doi.org/10.1001/archopht.119.11.1693

Araie, M., & Mayama, C. (2011). Use of calcium channel blockers for glaucoma. *Progress in Retinal and Eye Research*, *30*(1), 54–71. https://doi.org/10.1016/J.PRETEYERES.2010.09.002

Backstrom, J. R., Sheng, J., Fischer, R. A., Sappington, R. M., & Rex, T. S. (2019). Phenotypes of primary retinal macroglia: Implications for purification and culture conditions. *Experimental Eye Research*. https://doi.org/10.1016/j.exer.2019.03.008

Banning, A., Deubel, S., Kluth, D., Zhou, Z., & Brigelius-Flohé, R. (2005). The GI-GPx Gene Is a Target for Nrf2. *Molecular and Cellular Biology*, *25*(12), 4914–4923. https://doi.org/10.1128/mcb.25.12.4914-4923.2005

Batliwala, S., Xavier, C., Liu, Y., Wu, H., & Pang, I. H. (2017a). Involvement of Nrf2 in ocular diseases. In *Oxidative Medicine and Cellular Longevity*. https://doi.org/10.1155/2017/1703810

Batliwala, S., Xavier, C., Liu, Y., Wu, H., & Pang, I. H. (2017b). Involvement of Nrf2 in Ocular Diseases. *Oxidative Medicine and Cellular Longevity*, *2017*. https://doi.org/10.1155/2017/1703810

Berkowitz, B. A., Podolsky, R. H., Lenning, J., Khetarpal, N., Tran, C., Wu, J. Y., Berri, A. M., Dernay, K., Shafie-Khorassani, F., & Roberts, R. (2017). Sodium Iodate Produces a Strain-Dependent Retinal Oxidative Stress Response Measured In Vivo Using QUEST MRI. *Investigative Ophthalmology & Visual Science*, *58*(7), 3286–3293. https://doi.org/10.1167/iovs.17-21850

Bernardo-Colon, A., Vest, V., Clark, A., Cooper, M. L., Calkins, D. J., Harrison, F. E., & Rex, T.

S. (2018). Antioxidants prevent inflammation and preserve the optic projection and visual function in experimental neurotrauma. *Cell Death and Disease*, *9*(11). https://doi.org/10.1038/s41419-018-1061-4

Bernardo-Colón, A., Vest, V., Cooper, M. L., Naguib, S. A., Calkins, D. J., & Rex, T. S. (2019). Progression and Pathology of Traumatic Optic Neuropathy From Repeated Primary Blast Exposure. *Frontiers in Neuroscience*, *13*, 719. https://doi.org/10.3389/fnins.2019.00719

Biermann, J., Grieshaber, P., Goebel, U., Martin, G., Thanos, S., Di Giovanni, S., & Lagrèze, W. A. (2010). Valproic Acid–Mediated Neuroprotection and Regeneration in Injured Retinal Ganglion Cells. *Investigative Ophthalmology & Visual Science*, *51*(1), 526–534. https://doi.org/10.1167/IOVS.09-3903

Birben, E., Sahiner, U. M., Sackesen, C., Erzurum, S., & Kalayci, O. (2012). Oxidative Stress and Antioxidant Defense. *The World Allergy Organization Journal*, *5*(1), 9. https://doi.org/10.1097/WOX.0B013E3182439613

Blancher, C., & Harris, A. L. (1998). The molecular basis of the hypoxia response pathway: Tumour hypoxia as a therapy target. In *Cancer and Metastasis Reviews* (Vol. 17, Issue 2, pp. 187–194). Springer. https://doi.org/10.1023/A:1006002419244

Bond, W. S., Hines-Beard, J., Goldenmerry, Yp. L., Davis, M., Farooque, A., Sappington, R. M., Calkins, D. J., & Rex, T. S. (2016). Virus-mediated EpoR76E therapy slows optic nerve axonopathy in experimental glaucoma. *Molecular Therapy*. https://doi.org/10.1038/mt.2015.198

Borovikova, L. V., Ivanova, S., Zhang, M., Yang, H., Botchkina, G. I., Watkins, L. R., Wang, H., Abumrad, N., Eaton, J. W., & Tracey, K. J. (2000). Vagus nerve stimulation attenuates the systemic inflammatory response to endotoxin. *Nature*, *405*(6785), 458–462. https://doi.org/10.1038/35013070

Bouhenni, R. A., Dunmire, J., Sewell, A., & Edward, D. P. (2012). Animal Models of Glaucoma. *Journal of Biomedicine and Biotechnology*, *2012*, 11. https://doi.org/10.1155/2012/692609

Bricker-Anthony, C., D'Surney, L., Lunn, B., Hines-Beard, J., Jo, M., Bernardo-Colon, A., & Rex, T. S. (2017). Erythropoietin either Prevents or Exacerbates Retinal Damage from Eye Trauma Depending on Treatment Timing. *Optometry and Vision Science*, *94*(1), 20–32. https://doi.org/10.1097/OPX.0000000000000898

Bricker-Anthony, C., Hines-Beard, J., & Rex, T. S. (2014). Molecular changes and vision loss in a mouse model of closed-globe blast trauma. *Investigative Ophthalmology and Visual Science*, *55*(8), 4853–4862. https://doi.org/10.1167/iovs.14-14353

Bryan, H. K., Olayanju, A., Goldring, C. E., & Park, B. K. (2013). The Nrf2 cell defence pathway: Keap1-dependent and -independent mechanisms of regulation. In *Biochemical Pharmacology* (Vol. 85, Issue 6, pp. 705–717). Elsevier Inc. https://doi.org/10.1016/j.bcp.2012.11.016

Bunn, H. F. (2013). Erythropoietin. *Cold Spring Harbor Perspectives in Medicine*, *3*(3). https://doi.org/10.1101/CSHPERSPECT.A011619

Burgoyne, C. F., Crawford Downs, J., Bellezza, A. J., Francis Suh, J. K., & Hart, R. T. (2005). The optic nerve head as a biomechanical structure: A new paradigm for understanding the role of IOP-related stress and strain in the pathophysiology of glaucomatous optic nerve head damage. In *Progress in Retinal and Eye Research*. https://doi.org/10.1016/j.preteyeres.2004.06.001

Burke, E. G., Cansler, S. M., & Evanson, N. K. (2019). Indirect traumatic optic neuropathy: Modeling optic nerve injury in the context of closed head trauma. In *Neural Regeneration*

Research (Vol. 14, Issue 4, pp. 593–594). Wolters Kluwer Medknow Publications. https://doi.org/10.4103/1673-5374.247463

Calkins, D. J. (2012a). Critical pathogenic events underlying progression of neurodegeneration in glaucoma. In *Progress in Retinal and Eye Research*. https://doi.org/10.1016/j.preteyeres.2012.07.001

Calkins, D. J. (2012b). Critical pathogenic events underlying progression of neurodegeneration in glaucoma. *Progress in Retinal and Eye Research*, *31*(6), 702–719. https://doi.org/10.1016/J.PRETEYERES.2012.07.001

Calkins, D. J., & Horner, P. J. (2012). The cell and molecular biology of glaucoma: Axonopathy and the brain. *Investigative Ophthalmology and Visual Science*, *53*(5), 2482–2484. https://doi.org/10.1167/iovs.12-9483i

Calkins, D. J., Lambert, W. S., Formichella, C. R., McLaughlin, W. M., & Sappington, R. M. (2018). The microbead occlusion model of ocular hypertension in mice. In *Methods in Molecular Biology* (Vol. 1695, pp. 23–39). Humana Press Inc. https://doi.org/10.1007/978-1-4939-7407-8_3

Calkins, M. J., Johnson, D. A., Townsend, J. A., Vargas, M. R., Dowell, J. A., Williamson, T. P., Kraft, A. D., Lee, J. M., Li, J., & Johnson, J. A. (2009). The Nrf2/ARE pathway as a potential therapeutic target in neurodegenerative disease. In *Antioxidants and Redox Signaling* (Vol. 11, Issue 3, pp. 497–508). Mary Ann Liebert Inc. https://doi.org/10.1089/ars.2008.2242

Cantor, L. B. (2006). Brimonidine in the treatment of glaucoma and ocular hypertension. *Therapeutics and Clinical Risk Management*, *2*(4), 337. https://doi.org/10.2147/TCRM.2006.2.4.337

Cao, Y., Lathia, J. D., Eyler, C. E., Wu, Q., Li, Z., Wang, H., McLendon, R. E., Hjelmeland, A. B., & Rich, J. N. (2010). Erythropoietin Receptor Signaling through STAT3 Is Required for Glioma Stem Cell Maintenance. *Genes & Cancer*, *1*(1), 50. https://doi.org/10.1177/1947601909356352

Chamling, X., Sluch, V. M., & Zack, D. J. (2016). The Potential of Human Stem Cells for the Study and Treatment of Glaucoma. *Investigative Ophthalmology & Visual Science*, *57*(5), ORSFi1–ORSFi6. https://doi.org/10.1167/IOVS.15-18590

Chaudhary, P., Ahmed, F., Quebada, P., & Sharma, S. C. (1999). Caspase inhibitors block the retinal ganglion cell death following optic nerve transection. *Molecular Brain Research*, *67*(1), 36–45. https://doi.org/10.1016/S0169-328X(99)00032-7

Chen, H., Wei, X., Cho, K. S., Chen, G., Sappington, R., Calkins, D. J., & Chen, D. F. (2011). Optic neuropathy due to microbead-induced elevated intraocular pressure in the mouse. *Investigative Ophthalmology and Visual Science*, *52*(1), 36–44. https://doi.org/10.1167/iovs.09-5115

Cheng, J., Liang, J., & Qi, J. (2017a). Role of nuclear factor (Erythroid-derived 2)-like 2 in the age-resistant properties of the glaucoma trabecular meshwork. *Experimental and Therapeutic Medicine*. https://doi.org/10.3892/etm.2017.4543

Cheng, J., Liang, J., & Qi, J. (2017b). Role of nuclear factor (Erythroid-derived 2)-like 2 in the age-resistant properties of the glaucoma trabecular meshwork. *Experimental and Therapeutic Medicine*, *14*(1), 791–796. https://doi.org/10.3892/ETM.2017.4543/HTML

Cheng, J., Liang, J., & Qi, J. (2017c). Role of nuclear factor (Erythroid-derived 2)-like 2 in the age-resistant properties of the glaucoma trabecular meshwork. *Experimental and Therapeutic Medicine*, *14*(1), 791–796. https://doi.org/10.3892/etm.2017.4543

Chhunchha, B., Singh, P., Stamer, W. D., & Singh, D. P. (2017). Prdx6 retards senescence and restores trabecular meshwork cell health by regulating reactive oxygen species. *Cell Death Discovery*, *3*(1). https://doi.org/10.1038/cddiscovery.2017.60

Chitranshi, N., Dheer, Y., Abbasi, M., You, Y., Graham, S. L., & Gupta, V. (2018). Glaucoma Pathogenesis and Neurotrophins: Focus on the Molecular and Genetic Basis for Therapeutic Prospects. *Current Neuropharmacology*, *16*(7), 1018–1035. https://doi.org/10.2174/1570159X16666180419121247

Cho, H., Hartsock, M. J., Xu, Z., He, M., & Duh, E. J. (2015). *Monomethyl fumarate promotes Nrf2-dependent neuroprotection in retinal ischemia-reperfusion*. https://doi.org/10.1186/s12974-015-0452-z

Chong, R. S., & Martin, K. R. (2015). Glial cell interactions and glaucoma. *Current Opinion in Ophthalmology*, *26*(2), 73. https://doi.org/10.1097/ICU.0000000000000125

Chong, Z. Z., Kang, J.-Q., & Maiese, K. (2003). Erythropoietin fosters both intrinsic and extrinsic neuronal protection through modulation of microglia, Akt1, Bad, and caspase-mediated pathways. *British Journal of Pharmacology*, *138*(6), 1107–1118. https://doi.org/10.1038/sj.bjp.0705161

Chrysostomou, V., & Crowston, J. G. (2013). The photopic negative response of the mouse electroretinogram: Reduction by acute elevation of intraocular pressure. *Investigative Ophthalmology and Visual Science*, *54*(7), 4691–4697. https://doi.org/10.1167/iovs.13-12415

Chrysostomou, V., Rezania, F., Trounce, I. A., & Crowston, J. G. (2013). Oxidative stress and mitochondrial dysfunction in glaucoma. In *Current Opinion in Pharmacology* (Vol. 13, Issue 1, pp. 12–15). Elsevier Ltd. https://doi.org/10.1016/j.coph.2012.09.008

Claes, M., Santos, J. R. F., Masin, L., Cools, L., Davis, B. M., Arckens, L., Farrow, K., Groef, L. De, & Moons, L. (2021). A Fair Assessment of Evaluation Tools for the Murine Microbead Occlusion Model of Glaucoma. *International Journal of Molecular Sciences 2021, Vol. 22, Page 5633*, *22*(11), 5633. https://doi.org/10.3390/IJMS22115633

Conlon, R., Saheb, H., & Ahmed, I. I. K. (2017). Glaucoma treatment trends: a review. *Canadian Journal of Ophthalmology. Journal Canadien d'ophtalmologie*, *52*(1), 114–124. https://doi.org/10.1016/J.JCJO.2016.07.013

Cooper, M. L., Pasini, S., Lambert, W. S., D'Alessandro, K. B., Yao, V., Risner, M. L., & Calkins, D. J. (2020). Redistribution of metabolic resources through astrocyte networks mitigates neurodegenerative stress. *Proceedings of the National Academy of Sciences of the United States of America*, *117*(31), 18810–18821. https://doi.org/10.1073/PNAS.2009425117/-/DCSUPPLEMENTAL

CR, D., A, B.-C., S, N., JR, B., T, K., MK, G., CL, D., & TS, R. (2021). Microsphere antioxidant and sustained erythropoietin-R76E release functions cooperate to reduce traumatic optic neuropathy. *Journal of Controlled Release : Official Journal of the Controlled Release Society*, *329*, 762–773. https://doi.org/10.1016/J.JCONREL.2020.10.010

Crish, S. D., Sappington, R. M., Inman, D. M., Horner, P. J., & Calkins, D. J. (2010). Distal axonopathy with structural persistence in glaucomatous neurodegeneration. *Proceedings of the National Academy of Sciences of the United States of America*, *107*(11), 5196–5201. https://doi.org/10.1073/pnas.0913141107

Cuadrado, A., Rojo, A. I., Wells, G., Hayes, J. D., Cousin, S. P., Rumsey, W. L., Attucks, O. C., Franklin, S., Levonen, A. L., Kensler, T. W., & Dinkova-Kostova, A. T. (2019). Therapeutic targeting of the NRF2 and KEAP1 partnership in chronic diseases. *Nature*

Reviews Drug Discovery 2018 18:4, *18*(4), 295–317. https://doi.org/10.1038/s41573-018-0008-x

Culbreth, M., & Aschner, M. (2018). GSK-3β, a double-edged sword in Nrf2 regulation: Implications for neurological dysfunction and disease. *F1000Research*. https://doi.org/10.12688/f1000research.15239.1

Davis, B. M., Tian, K., Pahlitzsch, M., Brenton, J., Ravindran, N., Butt, G., Malaguarnera, G., Normando, E. M., Guo, L., & Cordeiro, M. F. (2017). Topical Coenzyme Q10 demonstrates mitochondrial-mediated neuroprotection in a rodent model of ocular hypertension. *Mitochondrion*, *36*, 114–123. https://doi.org/10.1016/J.MITO.2017.05.010

Dengler, V. L., Galbraith, M. D., & Espinosa, J. M. (2014). Transcriptional regulation by hypoxia inducible factors. In *Critical Reviews in Biochemistry and Molecular Biology* (Vol. 49, Issue 1, pp. 1–15). NIH Public Access. https://doi.org/10.3109/10409238.2013.838205

Denise M. Inman; Lucy Coughlin. (2014). The role of Nrf2 transcription factor in ganglion cell survival in glaucoma. *IOVS*, *55*(2424).

Di Polo, A., Almasieh, M.,; Zhou, Y. (2006). Galantamine: A Novel Neuroprotective Strategy For Injured Retinal Ganglion Cells In Glaucoma. *IOVS*, *47*(2699).

Dinkova-Kostova, A. T., Kostov, R. V., & Kazantsev, A. G. (2018). The role of Nrf2 signaling in counteracting neurodegenerative diseases. *The FEBS Journal*, *285*(19), 3576–3590. https://doi.org/10.1111/febs.14379

Doozandeh, A., & Yazdani, S. (2016). Neuroprotection in Glaucoma. *Journal of Ophthalmic & Vision Research*, *11*(2), 209. https://doi.org/10.4103/2008-322X.183923

Dorsett, C. R., McGuire, J. L., DePasquale, E. A. K., Gardner, A. E., Floyd, C. L., & McCullumsmith, R. E. (2017). Glutamate Neurotransmission in Rodent Models of Traumatic Brain Injury. *Journal of Neurotrauma*, *34*(2), 263–272. https://doi.org/10.1089/neu.2015.4373

Dumanović, J., Nepovimova, E., Natić, M., Kuča, K., & Jaćević, V. (2021). The Significance of Reactive Oxygen Species and Antioxidant Defense System in Plants: A Concise Overview. *Frontiers in Plant Science*, *11*, 2106. https://doi.org/10.3389/FPLS.2020.552969/BIBTEX

Duncan, R. S., Goad, D. L., Grillo, M. A., Kaja, S., Payne, A. J., & Koulen, P. (2010). Control of Intracellular Calcium Signaling as a Neuroprotective Strategy. *Molecules*, *15*(3), 1168. https://doi.org/10.3390/MOLECULES15031168

Durães, F., Pinto, M., & Sousa, E. (2018). Old Drugs as New Treatments for Neurodegenerative Diseases. *Pharmaceuticals (Basel, Switzerland)*, *11*(2). https://doi.org/10.3390/ph11020044

Elgohary, A. A., & Elshazly, L. H. M. (2015). Photopic negative response in diagnosis of glaucoma: An experimental study in glaucomatous rabbit model. *International Journal of Ophthalmology*, *8*(3), 459–464. https://doi.org/10.3980/j.issn.2222-3959.2015.03.05

Espinosa-Diez, C., Miguel, V., Mennerich, D., Kietzmann, T., Sánchez-Pérez, P., Cadenas, S., & Lamas, S. (2015). Antioxidant responses and cellular adjustments to oxidative stress. *Redox Biology*, *6*, 183–197. https://doi.org/10.1016/J.REDOX.2015.07.008

Evangelho, K., Mastronardi, C. A., & De-La-Torre, A. (2019). Experimental Models of Glaucoma: A Powerful Translational Tool for the Future Development of New Therapies for Glaucoma in Humans—A Review of the Literature. *Medicina*, *55*(6). https://doi.org/10.3390/MEDICINA55060280

Eye Health Statistics - American Academy of Ophthalmology. (n.d.). Retrieved September 30, 2019, from https://www.aao.org/newsroom/eye-health-statistics

Ezoulin, M. J. M., Ombetta, J. E., Dutertre-Catella, H., Warnet, J. M., & Massicot, F. (2008).

Antioxidative properties of galantamine on neuronal damage induced by hydrogen peroxide in SK-N-SH cells. *NeuroToxicology*, *29*(2), 270–277. https://doi.org/10.1016/j.neuro.2007.11.004

Faghih, R., Gfesser, G. A., & Gopalakrishnan, M. (2007). Advances in the discovery of novel positive allosteric modulators of the alpha7 nicotinic acetylcholine receptor. *Recent Patents on CNS Drug Discovery*, *2*(2), 99–106. http://www.ncbi.nlm.nih.gov/pubmed/18221220

Faghiri, Z., & Bazan, N. G. (2010). PI3K/Akt and mTOR/p70S6K pathways mediate neuroprotectin D1-induced retinal pigment epithelial cell survival during oxidative stress-induced apoptosis. *Experimental Eye Research*, *90*(6), 718–725. https://doi.org/10.1016/j.exer.2010.03.002

Feist, R. M., & Farber, M. D. (1989). Ocular Trauma Epidemiology. *Archives of Ophthalmology*, *107*(4), 503–504. https://doi.org/10.1001/archopht.1989.01070010517021

Fernández-Sánchez, L., Lax, P., Campello, L., Pinilla, I., & Cuenca, N. (2015). Astrocytes and Müller Cell Alterations During Retinal Degeneration in a Transgenic Rat Model of Retinitis Pigmentosa. *Frontiers in Cellular Neuroscience*, *0*(DEC), 484. https://doi.org/10.3389/FNCEL.2015.00484

Ferreira, S. M., Fabián Lerner, S., Brunzini, R., Reides, C. G., Evelson, P. A., & Llesuy, S. F. (2010). Time course changes of oxidative stress markers in a rat experimental glaucoma model. *Investigative Ophthalmology and Visual Science*, *51*(9), 4635–4640. https://doi.org/10.1167/iovs.09-5044

Ferreira, S. M., Reides, C. G., Lerner, F. S., & Llesuy, S. F. (2011). Evidence of Oxidative Stress Damage in Glaucoma. *The Mystery of Glaucoma*. https://doi.org/10.5772/19194

Foldvari, M., & Chen, D. W. (2016). The intricacies of neurotrophic factor therapy for retinal ganglion cell rescue in glaucoma: a case for gene therapy. *Neural Regeneration Research*, *11*(6), 875. https://doi.org/10.4103/1673-5374.184448

Forman, H. J., & Zhang, H. (2021). Targeting oxidative stress in disease: promise and limitations of antioxidant therapy. *Nature Reviews Drug Discovery 2021 20:9*, *20*(9), 689–709. https://doi.org/10.1038/s41573-021-00233-1

Francis, P. T. (2005). The interplay of neurotransmitters in Alzheimer's disease. *CNS Spectrums*, *10*(11 Suppl 18), 6–9. https://doi.org/10.1017/s1092852900014164

Fujikawa, K., Iwata, T., Inoue, K., Akahori, M., Kadotani, H., Fukaya, M., Watanabe, M., Chang, Q., Barnett, E. M., & Swat, W. (2010). VAV2 and VAV3 as Candidate Disease Genes for Spontaneous Glaucoma in Mice and Humans. *PLoS ONE*, *5*(2). https://doi.org/10.1371/JOURNAL.PONE.0009050

Fujita, K., Nishiguchi, K. M., Shiga, Y., & Nakazawa, T. (2017). Spatially and Temporally Regulated NRF2 Gene Therapy Using Mcp-1 Promoter in Retinal Ganglion Cell Injury. *Molecular Therapy - Methods and Clinical Development*, *5*, 130–141. https://doi.org/10.1016/j.omtm.2017.04.003

Furukawa, S., Yang, L., & Sameshima, H. (2014). Galantamine, an acetylcholinesterase inhibitor, reduces brain damage induced by hypoxia-ischemia in newborn rats. *International Journal of Developmental Neuroscience : The Official Journal of the International Society for Developmental Neuroscience*, *37*, 52–57. https://doi.org/10.1016/j.ijdevneu.2014.06.011

García-Bermúdez, M. Y., Freude, K. K., Mouhammad, Z. A., van Wijngaarden, P., Martin, K. K., & Kolko, M. (2021). Glial Cells in Glaucoma: Friends, Foes, and Potential Therapeutic Targets. *Frontiers in Neurology*, *12*, 169. https://doi.org/10.3389/FNEUR.2021.624983/BIBTEX

Garcia-Medina, J. J., Rubio-Velazquez, E., Lopez-Bernal, M. D., Cobo-Martinez, A., Zanon-Moreno, V., Pinazo-Duran, M. D., & Del-Rio-Vellosillo, M. (2020). Glaucoma and Antioxidants: Review and Update. *Antioxidants*, *9*(11), 1–15. https://doi.org/10.3390/ANTIOX9111031

Ghanem, A. A., Arafa, L. F., & El-Baz, A. (2010). Oxidative Stress Markers in Patients with Primary Open-Angle Glaucoma. *Current Eye Research*, *35*(4), 295–301. https://doi.org/10.3109/02713680903548970

Gherghel, D., Griffiths, H. R., Hilton, E. J., Cunliffe, I. A., & Hosking, S. L. (2005). Systemic Reduction in Glutathione Levels Occurs in Patients with Primary Open-Angle Glaucoma. *Investigative Ophthalmology & Visual Science*, *46*(3), 877–883. https://doi.org/10.1167/IOVS.04-0777

Giacobini, E., DeSarno, P., Clark, B., & McIlhany, M. (1989). The cholinergic receptor system of the human brain: Neurochemical and pharmacological aspects in aging and Alzheimer. *Progress in Brain Research*, *79*(C), 335–343. https://doi.org/10.1016/S0079-6123(08)62493-0

Gleichmann, M., & Mattson, M. P. (2011). Neuronal calcium homeostasis and dysregulation. *Antioxidants & Redox Signaling*, *14*(7), 1261–1273. https://doi.org/10.1089/ARS.2010.3386

Goldberg, I. (2003). Relationship between intraocular pressure and preservation of visual field in glaucoma. *Survey of Ophthalmology*, *48*(2 SUPPL. 1). https://doi.org/10.1016/S0039-6257(03)00006-7

Goldman, D. (2014). Müller glial cell reprogramming and retina regeneration. *Nature Reviews Neuroscience 2014 15:7*, *15*(7), 431–442. https://doi.org/10.1038/nrn3723

Greco, A., Rizzo, M. I., De Virgilio, A., Gallo, A., Fusconi, M., & de Vincentiis, M. (2016). Emerging Concepts in Glaucoma and Review of the Literature. In *American Journal of Medicine* (Vol. 129, Issue 9). https://doi.org/10.1016/j.amjmed.2016.03.038

Guerriero, R. M., Giza, C. C., & Rotenberg, A. (2015). Glutamate and GABA imbalance following traumatic brain injury. *Current Neurology and Neuroscience Reports*, *15*(5), 27. https://doi.org/10.1007/s11910-015-0545-1

Guillard, C., Chrétien, S., Pelus, A. S., Porteu, F., Muller, O., Mayeux, P., & Duprez, V. (2003). Activation of the mitogen-activated protein kinases Erk1/2 by erythropoietin receptor via a G(i)protein beta gamma-subunit-initiated pathway. *The Journal of Biological Chemistry*, *278*(13), 11050–11056. https://doi.org/10.1074/JBC.M208834200

Guttenplan, K. A., Stafford, B. K., El-Danaf, R. N., Adler, D. I., Münch, A. E., Weigel, M. K., Huberman, A. D., & Liddelow, S. A. (2020). Neurotoxic Reactive Astrocytes Drive Neuronal Death after Retinal Injury. *Cell Reports*, *31*(12), 107776. https://doi.org/10.1016/J.CELREP.2020.107776

H, M., J, G., H, W., P, Y., X, N., & J, Z. (2014). Erythropoietin activates Keap1-Nrf2/ARE pathway in rat brain after ischemia. *The International Journal of Neuroscience*, *124*(5), 362–368. https://doi.org/10.3109/00207454.2013.848439

Hansen, J. M. (2004). Compartmentation of Nrf-2 Redox Control: Regulation of Cytoplasmic Activation by Glutathione and DNA Binding by Thioredoxin-1. *Toxicological Sciences*, *82*(1), 308–317. https://doi.org/10.1093/toxsci/kfh231

Harada, C., Kimura, A., Guo, X., Namekata, K., & Harada, T. (2019a). Recent advances in genetically modified animal models of glaucoma and their roles in drug repositioning. *British Journal of Ophthalmology*, *103*(2), 161–166. https://doi.org/10.1136/BJOPHTHALMOL-2018-312724

Harada, C., Kimura, A., Guo, X., Namekata, K., & Harada, T. (2019b). Recent advances in genetically modified animal models of glaucoma and their roles in drug repositioning. *British Journal of Ophthalmology*, *103*(2), 161–166. https://doi.org/10.1136/BJOPHTHALMOL-2018-312724

He, S., Stankowska, D. L., Ellis, D. Z., Krishnamoorthy, R. R., & Yorio, T. (2018). Targets of Neuroprotection in Glaucoma. *Journal of Ocular Pharmacology and Therapeutics*, *34*(1–2), 85–106. https://doi.org/10.1089/jop.2017.0041

Heijl, A., Leske, M. C., Bengtsson, B., Hyman, L., Bengtsson, B., & Hussein, M. (2002). Reduction of Intraocular Pressure and Glaucoma Progression: Results From the Early Manifest Glaucoma Trial. *Archives of Ophthalmology*, *120*(10), 1268–1279. https://doi.org/10.1001/ARCHOPHT.120.10.1268

Hernández, C. C., Burgos, C. F., Gajardo, A. H., Silva-Grecchi, T., Gavilan, J., Toledo, J. R., & Fuentealba, J. (2017a). Neuroprotective effects of erythropoietin on neurodegenerative and ischemic brain diseases: The role of erythropoietin receptor. In *Neural Regeneration Research*. https://doi.org/10.4103/1673-5374.215240

Hernández, C. C., Burgos, C. F., Gajardo, A. H., Silva-Grecchi, T., Gavilan, J., Toledo, J. R., & Fuentealba, J. (2017b). Neuroprotective effects of erythropoietin on neurodegenerative and ischemic brain diseases: the role of erythropoietin receptor. *Neural Regeneration Research*, *12*(9), 1381. https://doi.org/10.4103/1673-5374.215240

Hernández, C. C., Burgos, C. F., Gajardo, A. H., Silva-Grecchi, T., Gavilan, J., Toledo, J. R., & Fuentealba, J. (2017c). Neuroprotective effects of erythropoietin on neurodegenerative and ischemic brain diseases: the role of erythropoietin receptor. *Neural Regeneration Research*, *12*(9), 1381. https://doi.org/10.4103/1673-5374.215240

Himori, N., Yamamoto, K., Maruyama, K., Ryu, M., Taguchi, K., Yamamoto, M., & Nakazawa, T. (2013a). Critical role of Nrf2 in oxidative stress-induced retinal ganglion cell death. *Journal of Neurochemistry*, *127*(5), 669–680. https://doi.org/10.1111/jnc.12325

Himori, N., Yamamoto, K., Maruyama, K., Ryu, M., Taguchi, K., Yamamoto, M., & Nakazawa, T. (2013b). Critical role of Nrf2 in oxidative stress-induced retinal ganglion cell death. *Journal of Neurochemistry*, *127*(5), 669–680. https://doi.org/10.1111/JNC.12325

Himori, N., Yamamoto, K., Maruyama, K., Ryu, M., Taguchi, K., Yamamoto, M., & Nakazawa, T. (2013c). Critical role of Nrf2 in oxidative stress-induced retinal ganglion cell death. *Journal of Neurochemistry*, *127*(5), 669–680. https://doi.org/10.1111/jnc.12325

Hines-Beard, J., Bond, W. S., Backstrom, J. R., & Rex, T. S. (2016a). Virus-mediated EpoR76E gene therapy preserves vision in a glaucoma model by modulating neuroinflammation and decreasing oxidative stress. *Journal of Neuroinflammation*. https://doi.org/10.1186/s12974-016-0499-5

Hines-Beard, J., Bond, W. S., Backstrom, J. R., & Rex, T. S. (2016b). Virus-mediated EpoR76E gene therapy preserves vision in a glaucoma model by modulating neuroinflammation and decreasing oxidative stress. *Journal of Neuroinflammation*, *13*, 39. https://doi.org/10.1186/s12974-016-0499-5

Hines-Beard, J., Marchetta, J., Gordon, S., Chaum, E., Geisert, E. E., & Rex, T. S. (2012). A mouse model of ocular blast injury that induces closed globe anterior and posterior pole damage. *Experimental Eye Research*, *99*, 63–70. https://doi.org/10.1016/j.exer.2012.03.013

Huang, W., Fileta, J. B., Filippopoulos, T., Ray, A., Dobberfuhl, A., & Grosskreutz, C. L. (2007). Hsp27 phosphorylation in experimental glaucoma. *Investigative Ophthalmology and Visual Science*, *48*(9), 4129–4135. https://doi.org/10.1167/iovs.06-0606

Huang, Y., Li, W., Su, Z. yuan, & Kong, A. N. T. (2015). The complexity of the Nrf2 pathway: Beyond the antioxidant response. In *Journal of Nutritional Biochemistry* (Vol. 26, Issue 12, pp. 1401–1413). Elsevier Inc. https://doi.org/10.1016/j.jnutbio.2015.08.001

Hui, F., Tang, J., Williams, P. A., McGuinness, M. B., Hadoux, X., Casson, R. J., Coote, M., Trounce, I. A., Martin, K. R., van Wijngaarden, P., & Crowston, J. G. (2020). Improvement in inner retinal function in glaucoma with nicotinamide (vitamin B3) supplementation: A crossover randomized clinical trial. *Clinical & Experimental Ophthalmology*, *48*(7), 903–914. https://doi.org/10.1111/CEO.13818

Hvozda Arana, A. G., Lasagni Vitar, R. M., Reides, C. G., Lerner, S. F., & Ferreira, S. M. (2020). Glaucoma causes redox imbalance in the primary visual cortex by modulating NADPH oxidase-4, iNOS, and Nrf2 pathway in a rat experimental model. *Experimental Eye Research*, *200*. https://doi.org/10.1016/j.exer.2020.108225

Inman, D. M., Lambert, W. S., Calkins, D. J., & Horner, P. J. (2013a). α-Lipoic Acid Antioxidant Treatment Limits Glaucoma-Related Retinal Ganglion Cell Death and Dysfunction. *PLoS ONE*, *8*(6). https://doi.org/10.1371/JOURNAL.PONE.0065389

Inman, D. M., Lambert, W. S., Calkins, D. J., & Horner, P. J. (2013b). α-Lipoic Acid Antioxidant Treatment Limits Glaucoma-Related Retinal Ganglion Cell Death and Dysfunction. *PLoS ONE*, *8*(6), e65389. https://doi.org/10.1371/journal.pone.0065389

Ishikawa, M., Yoshitomi, T., Zorumski, C. F., & Izumi, Y. (2015). Experimentally Induced Mammalian Models of Glaucoma. *BioMed Research International*, *2015*. https://doi.org/10.1155/2015/281214

Ito, Y. A., & Di Polo, A. (2017). Mitochondrial dynamics, transport, and quality control: A bottleneck for retinal ganglion cell viability in optic neuropathies. *Mitochondrion*. https://doi.org/10.1016/j.mito.2017.08.014

Izzotti, A., Bagnis, A., & Saccà, S. C. (2006). The role of oxidative stress in glaucoma. *Mutation Research/Reviews in Mutation Research*, *612*(2), 105–114. https://doi.org/10.1016/J.MRREV.2005.11.001

J, S., WW, F., & M, S. (1981). Immunocytochemical demonstration of vimentin in astrocytes and ependymal cells of developing and adult mouse nervous system. *The Journal of Cell Biology*, *90*(2), 435–447. https://doi.org/10.1083/JCB.90.2.435

J, Z., Y, Z., D, Z., Z, W., & G, C. (2010). Recombinant human erythropoietin (rhEPO) alleviates early brain injury following subarachnoid hemorrhage in rats: possible involvement of Nrf2-ARE pathway. *Cytokine*, *52*(3), 252–257. https://doi.org/10.1016/J.CYTO.2010.08.011

Jäkel, S., & Dimou, L. (2017). Glial Cells and Their Function in the Adult Brain: A Journey through the History of Their Ablation. *Frontiers in Cellular Neuroscience*, *11*. https://doi.org/10.3389/FNCEL.2017.00024

Jayaram, H. (2020). Intraocular pressure reduction in glaucoma: Does every mmHg count? *Taiwan Journal of Ophthalmology*, *10*(4), 255. https://doi.org/10.4103/TJO.TJO_63_20

Jeong, J. E., Park, J. H., Kim, C. S., Lee, S. L., Chung, H. L., Kim, W. T., & Lee, E. J. (2017). Neuroprotective effects of erythropoietin against hypoxic injury via modulation of the mitogen-activated protein kinase pathway and apoptosis. *Korean Journal of Pediatrics*, *60*(6), 181. https://doi.org/10.3345/KJP.2017.60.6.181

Jiang, C., Gui, C. Y., Fan, J., Tang, X. Da, & Qiao, R. L. (1998). STAT1 is involved in signal transduction in the EPO induced HEL cells. *Cell Research*, *8*(2), 106–117. https://doi.org/10.1038/CR.1998.11

Johnson, J. A., Johnson, D. A., Kraft, A. D., Calkins, M. J., Jakel, R. J., Vargas, M. R., & Chen, P. C. (2008). The Nrf2-ARE pathway: An indicator and modulator of oxidative stress in neurodegeneration. *Annals of the New York Academy of Sciences*, *1147*, 61–69. https://doi.org/10.1196/annals.1427.036

Johnson, T. V., Bull, N. D., & Martin, K. R. (2011). Stem cell therapy for glaucoma: possibilities and practicalities. *Expert Review of Ophthalmology*, *6*(2), 165. https://doi.org/10.1586/EOP.11.3

K, G., MY, E., & S, G. (2010). Erythropoietin induces nuclear translocation of Nrf2 and heme oxygenase-1 expression in SH-SY5Y cells. *Cell Biochemistry and Function*, *28*(3), 197–201. https://doi.org/10.1002/CBF.1639

Kanamori, A., Nakamura, M., Nakanishi, Y., Nagai, A., Mukuno, H., Yamada, Y., & Negi, A. (2004). Akt is activated via insulin/IGF-1 receptor in rat retina with episcleral vein cauterization. *Brain Research*, *1022*(1–2), 195–204. https://doi.org/10.1016/j.brainres.2004.06.077

Kansanen, E., Kuosmanen, S. M., Leinonen, H., & Levonen, A.-L. (2013). *The Keap1-Nrf2 pathway: Mechanisms of activation and dysregulation in cancer $*. https://doi.org/10.1016/j.redox.2012.10.001

Khazaeni, B., & Khazaeni, L. (2022). Acute Closed Angle Glaucoma. *StatPearls*. https://www.ncbi.nlm.nih.gov/books/NBK430857/

Killer, H. E., & Pircher, A. (2018). Normal tension glaucoma: Review of current understanding and mechanisms of the pathogenesis /692/699/3161/3169/3170 /692/699/3161 review-article. In *Eye (Basingstoke)*. https://doi.org/10.1038/s41433-018-0042-2

Kim, U. S., Mahroo, O. A., Mollon, J. D., & Yu-Wai-Man, P. (2021). Retinal Ganglion Cells—Diversity of Cell Types and Clinical Relevance. *Frontiers in Neurology*, *12*, 635. https://doi.org/10.3389/FNEUR.2021.661938/BIBTEX

Kimura, A., Guo, X., Noro, T., Harada, C., Tanaka, K., Namekata, K., & Harada, T. (2015). Valproic acid prevents retinal degeneration in a murine model of normal tension glaucoma. *Neuroscience Letters*, *588*, 108–113. https://doi.org/10.1016/j.neulet.2014.12.054

Kimura, A., Namekata, K., Guo, X., Noro, T., Harada, C., & Harada, T. (2017a). *Targeting Oxidative Stress for Treatment of Glaucoma and Optic Neuritis*. https://doi.org/10.1155/2017/2817252

Kimura, A., Namekata, K., Guo, X., Noro, T., Harada, C., & Harada, T. (2017b). Targeting Oxidative Stress for Treatment of Glaucoma and Optic Neuritis. *Oxidative Medicine and Cellular Longevity*, *2017*. https://doi.org/10.1155/2017/2817252

Kita, Y., Ago, Y., Higashino, K., Asada, K., Takano, E., Takuma, K., & Matsuda, T. (2014). Galantamine promotes adult hippocampal neurogenesis via M<inf>1</inf> muscarinic and α7 nicotinic receptors in mice. *International Journal of Neuropsychopharmacology*, *17*(12), 1957–1968. https://doi.org/10.1017/S1461145714000613

Ko, M. L., Peng, P. H., Ma, M. C., Ritch, R., & Chen, C. F. (2005a). Dynamic changes in reactive oxygen species and antioxidant levels in retinas in experimental glaucoma. *Free Radical Biology and Medicine*, *39*(3), 365–373. https://doi.org/10.1016/j.freeradbiomed.2005.03.025

Ko, M. L., Peng, P. H., Ma, M. C., Ritch, R., & Chen, C. F. (2005b). Dynamic changes in reactive oxygen species and antioxidant levels in retinas in experimental glaucoma. *Free Radical Biology and Medicine*, *39*(3), 365–373. https://doi.org/10.1016/j.freeradbiomed.2005.03.025

Kolb, H. (2007). Gross Anatomy of the Eye. *Webvision: The Organization of the Retina and Visual System*. https://www.ncbi.nlm.nih.gov/books/NBK11534/

Kolb, H. (2012). Simple Anatomy of the Retina. *Webvision: The Organization of the Retina and Visual System*. https://www.ncbi.nlm.nih.gov/books/NBK11533/

Kong, A. W., Della Santina, L., & Ou, Y. (2020). Probing ON and OFF Retinal Pathways in Glaucoma Using Electroretinography. *Translational Vision Science & Technology*, *9*(11), 1–14. https://doi.org/10.1167/TVST.9.11.14

Kong, G. Y. X., Van Bergen, N. J., Trounce, I. A., & Crowston, J. G. (2009). Mitochondrial dysfunction and glaucoma. *Journal of Glaucoma*, *18*(2), 93–100. https://doi.org/10.1097/IJG.0B013E318181284F

Koriyama, Y., Chiba, K., Yamazaki, M., Suzuki, H., Ichiro Muramoto, K., & Kato, S. (2010). Long-acting genipin derivative protects retinal ganglion cells from oxidative stress models in vitro and in vivo through the Nrf2/antioxidant response element signaling pathway. *Journal of Neurochemistry*, *115*(1), 79–91. https://doi.org/10.1111/j.1471-4159.2010.06903.x

Koriyama, Y., Nakayama, Y., Matsugo, S., & Kato, S. (2013). Protective effect of lipoic acid against oxidative stress is mediated by Keap1/Nrf2-dependent heme oxygenase-1 induction in the RGC-5 cellline. *Brain Research*, *1499*, 145–157. https://doi.org/10.1016/j.brainres.2012.12.041

Kumar, S., Benavente-Perez, A., Ablordeppey, R., Lin, C., Viswanathan, S., Akopian, A., & Bloomfield, S. A. (2022). A Robust Microbead Occlusion Model of Glaucoma for the Common Marmoset. *Translational Vision Science & Technology*, *11*(1), 14–14. https://doi.org/10.1167/TVST.11.1.14

Kumaran, A., Sundar, G., & Chye, L. (2014). Traumatic Optic Neuropathy: A Review. *Craniomaxillofacial Trauma and Reconstruction*, *08*(01), 031–041. https://doi.org/10.1055/s-0034-1393734

Lacher, S. E., Levings, D. C., Freeman, S., & Slattery, M. (2018). Identification of a functional antioxidant response element at the HIF1A locus. *Redox Biology*, *19*, 401–411. https://doi.org/10.1016/j.redox.2018.08.014

Lambert, W. S., Carlson, B. J., Ghose, P., Vest, V. D., Yao, V., & Calkins, D. J. (2019). Towards A Microbead Occlusion Model of Glaucoma for a Non-Human Primate. *Scientific Reports 2019 9:1*, *9*(1), 1–15. https://doi.org/10.1038/s41598-019-48054-y

Lambert, W. S., Pasini, S., Collyer, J. W., Formichella, C. R., Ghose, P., Carlson, B. J., & Calkins, D. J. (2020). Of Mice and Monkeys: Neuroprotective Efficacy of the p38 Inhibitor BIRB 796 Depends on Model Duration in Experimental Glaucoma. *Scientific Reports 2020 10:1*, *10*(1), 1–20. https://doi.org/10.1038/s41598-020-65374-6

Lambert, W. S., Ruiz, L., Crish, S. D., Wheeler, L. A., & Calkins, D. J. (2011). Brimonidine prevents axonal and somatic degeneration of retinal ganglion cell neurons. *Molecular Neurodegeneration*, *6*(1), 4. https://doi.org/10.1186/1750-1326-6-4

Lee, D. A., & Higginbotham, E. J. (2005). Glaucoma and its treatment: A review. *American Journal of Health-System Pharmacy*, *62*(7), 691–699. https://doi.org/10.1093/AJHP/62.7.691

Leung, L., Kwong, M., Hou, S., Lee, C., & Chan, J. Y. (2003). Deficiency of the Nrf1 and Nrf2 Transcription Factors Results in Early Embryonic Lethality and Severe Oxidative Stress. *Journal of Biological Chemistry*. https://doi.org/10.1074/jbc.M308439200

Levin, L. A., Schlamp, C. L., Spieldoch, R. L., Geszvain, K. M., & Nickells, R. W. (1997).

Identification of the bcl-2 family of genes in the rat retina. Investigative Ophthalmology and Visual Science. https://iovs.arvojournals.org/article.aspx?articleid=2180650

Li, B., Zhang, T., Liu, W., Wang, Y., Xu, R., Zeng, S., Zhang, R., Zhu, S., Gillies, M. C., Zhu, L., & Du, J. (2020). Metabolic Features of Mouse and Human Retinas: Rods versus Cones, Macula versus Periphery, Retina versus RPE. *IScience*, *23*(11), 101672. https://doi.org/10.1016/J.ISCI.2020.101672

Li, Y., Wang, Q., Chu, C., & Liu, S. (2020). Astaxanthin protects retinal ganglion cells from acute glaucoma via the Nrf2/HO-1 pathway. *Journal of Chemical Neuroanatomy*, *110*, 101876. https://doi.org/10.1016/J.JCHEMNEU.2020.101876

Liguori, I., Russo, G., Curcio, F., Bulli, G., Aran, L., Della-Morte, D., Gargiulo, G., Testa, G., Cacciatore, F., Bonaduce, D., & Abete, P. (2018). Oxidative stress, aging, and diseases. *Clinical Interventions in Aging*, *13*, 757. https://doi.org/10.2147/CIA.S158513

Lilienfeld, S. (2002). Galantamine--a novel cholinergic drug with a unique dual mode of action for the treatment of patients with Alzheimer's disease. *CNS Drug Reviews*, *8*(2), 159–176. http://www.ncbi.nlm.nih.gov/pubmed/12177686

Liu, X. F., Zhou, D. D., Xie, T., Hao, J. L., Malik, T. H., Lu, C. B., Qi, J., Pant, O. P., & Lu, C. W. (2018). The Nrf2 signaling in retinal ganglion cells under oxidative stress in ocular neurodegenerative diseases. In *International Journal of Biological Sciences* (Vol. 14, Issue 9, pp. 1090–1098). Ivyspring International Publisher. https://doi.org/10.7150/ijbs.25996

Ma, L., Liu, J., Zhang, X., Qi, J., Yu, W., & Gu, Y. (2015). p38 MAPK-dependent Nrf2 induction enhances the resistance of glioma cells against TMZ. *Medical Oncology (Northwood, London, England)*, *32*(3), 69. https://doi.org/10.1007/s12032-015-0517-y

Ma, Q. (2013). Role of Nrf2 in Oxidative Stress and Toxicity. *Annual Review of Pharmacology and Toxicology*. https://doi.org/10.1146/annurev-pharmtox-011112-140320

Machida, S. (2012). Clinical applications of the photopic negative response to optic nerve and retinal diseases. In *Journal of Ophthalmology* (Vol. 2012). https://doi.org/10.1155/2012/397178

Mallick, J., Devi, L., Malik, P. K., & Mallick, J. (2016). Update on normal tension glaucoma. In *Journal of Ophthalmic and Vision Research*. https://doi.org/10.4103/2008-322X.183914

Malone, P. E., & Hernandez, M. R. (2007). 4-Hydroxynonenal, a product of oxidative stress, leads to an antioxidant response in optic nerve head astrocytes. *Experimental Eye Research*, *84*(3), 444–454. https://doi.org/10.1016/J.EXER.2006.10.020

Mammadova, N., Ghaisas, S., Zenitsky, G., Sakaguchi, D. S., Kanthasamy, A. G., Greenlee, J. J., & West Greenlee, M. H. (2017). Lasting Retinal Injury in a Mouse Model of Blast-Induced Trauma. *American Journal of Pathology*, *187*(7), 1459–1472. https://doi.org/10.1016/j.ajpath.2017.03.005

Martucci, A., & Nucci, C. (2019). Evidence on neuroprotective properties of coenzyme Q10 in the treatment of glaucoma. *Neural Regeneration Research*, *14*(2), 197. https://doi.org/10.4103/1673-5374.244781

McCarty, D. M., Monahan, P. E., & Samulski, R. J. (2001). Self-complementary recombinant adeno-associated virus (scAAV) vectors promote efficient transduction independently of DNA synthesis. *Gene Therapy 2001 8:16*, *8*(16), 1248–1254. https://doi.org/10.1038/sj.gt.3301514

McKee, A. C., & Robinson, M. E. (2014). Military-related traumatic brain injury and neurodegeneration. *Alzheimer's and Dementia*, *10*(3 SUPPL.). https://doi.org/10.1016/j.jalz.2014.04.003

Melo, J. B., Sousa, C., Garção, P., Oliveira, C. R., & Agostinho, P. (2009). Galantamine protects against oxidative stress induced by amyloid-beta peptide in cortical neurons. *The European Journal of Neuroscience*, *29*(3), 455–464. https://doi.org/10.1111/j.1460-9568.2009.06612.x

MJ, P.-A., C, I., C, S., JJ, S., AI, R., A, T., JM, R., JP, A., EJ, de la R., & C, P. (2008). Vimentin isoform expression in the human retina characterized with the monoclonal antibody 3CB2. *Journal of Neuroscience Research*, *86*(8), 1871–1883. https://doi.org/10.1002/JNR.21623

Moreno, M. C., Campanelli, J., Sande, P., Sáenz, D. A., Keller Sarmiento, M. I., & Rosenstein, R. E. (2004). Retinal oxidative stress induced by high intraocular pressure. *Free Radical Biology and Medicine*, *37*(6), 803–812. https://doi.org/10.1016/j.freeradbiomed.2004.06.001

Morgan, J. E. (2012). Retina ganglion cell degeneration in glaucoma: An opportunity missed? A review. In *Clinical and Experimental Ophthalmology* (Vol. 40, Issue 4, pp. 364–368). Clin Exp Ophthalmol. https://doi.org/10.1111/j.1442-9071.2012.02789.x

Morny, E. K. A., Patel, K., Votruba, M., Binns, A. M., & Margrain, T. H. (2019). The relationship between the photopic negative response and retinal ganglion cell topography. *Investigative Ophthalmology and Visual Science*, *60*(6), 1879–1887. https://doi.org/10.1167/iovs.18-25272

MR, H. (2000). The optic nerve head in glaucoma: role of astrocytes in tissue remodeling. *Progress in Retinal and Eye Research*, *19*(3), 297–321. https://doi.org/10.1016/S1350-9462(99)00017-8

Mukai, R., Park, D. H., Okunuki, Y., Hasegawa, E., Klokman, G., Kim, C. B., Krishnan, A., Gregory-Ksander, M., Husain, D., Miller, J. W., & Connor, K. M. (2019). Mouse model of ocular hypertension with retinal ganglion cell degeneration. *PLOS ONE*, *14*(1), e0208713. https://doi.org/10.1371/JOURNAL.PONE.0208713

Myklebust, J. H., Blomhoff, H. K., Rusten, L. S., Stokke, T., & Smeland, E. B. (2002). Activation of phosphatidylinositol 3-kinase is important for erythropoietin-induced erythropoiesis from CD34+ hematopoietic progenitor cells. *Experimental Hematology*, *30*(9), 990–1000. https://doi.org/10.1016/S0301-472X(02)00868-8

Naguib, S., Backstrom, J. R., Gil, M., Calkins, D. J., & Rex, T. S. (2021). Retinal oxidative stress activates the NRF2/ARE pathway: An early endogenous protective response to ocular hypertension. *Redox Biology*. https://doi.org/10.1016/j.redox.2021.101883

Naguib, S., Bernardo-Colón, A., Cencer, C., Gandra, N., & Rex, T. S. (2020). Galantamine protects against synaptic, axonal, and vision deficits in experimental neurotrauma. *Neurobiology of Disease*, *134*. https://doi.org/10.1016/j.nbd.2019.104695

Naguib, Sarah, Bernardo-Colón, A., Cencer, C., Gandra, N., & Rex, T. S. (2020). Galantamine protects against synaptic, axonal, and vision deficits in experimental neurotrauma. *Neurobiology of Disease*, *134*. https://doi.org/10.1016/j.nbd.2019.104695

Naguib, Sarah, Bernardo-Colón, A., & Rex, T. S. (2020). Intravitreal injection worsens outcomes in a mouse model of indirect traumatic optic neuropathy from closed globe injury. *Experimental Eye Research*. https://doi.org/10.1016/j.exer.2020.108369

Naik, S., Pandey, A., Lewis, S. A., Rao, B. S. S., & Mutalik, S. (2020). Neuroprotection: A versatile approach to combat glaucoma. *European Journal of Pharmacology*, *881*, 173208. https://doi.org/10.1016/J.EJPHAR.2020.173208

Nakagami, Y. (2016). *Nrf2 Is an Attractive Therapeutic Target for Retinal Diseases*. https://doi.org/10.1155/2016/7469326

Naso, M. F., Tomkowicz, B., Perry, W. L., & Strohl, W. R. (2017). Adeno-Associated Virus (AAV) as a Vector for Gene Therapy. *Biodrugs*, *31*(4), 317. https://doi.org/10.1007/S40259-017-0234-5

Nguyen, T., Huang, H. C., & Pickett, C. B. (2000). Transcriptional regulation of the antioxidant response element. Activation by Nrf2 and repression by MafK. *Journal of Biological Chemistry*, *275*(20), 15466–15473. https://doi.org/10.1074/jbc.M000361200

Nguyen, T., Nioi, P., & Pickett, C. B. (2009a). *The Nrf2-Antioxidant Response Element Signaling Pathway and Its Activation by Oxidative Stress * ARE-mediated Pathway*. https://doi.org/10.1074/jbc.R900010200

Nguyen, T., Nioi, P., & Pickett, C. B. (2009b). The Nrf2-Antioxidant Response Element Signaling Pathway and Its Activation by Oxidative Stress. *The Journal of Biological Chemistry*, *284*(20), 13291. https://doi.org/10.1074/JBC.R900010200

Nickells, R. W. (2002). Apoptosis of Retinal Ganglion Cells in Glaucoma. *Survey of Ophthalmology*. https://doi.org/10.1016/s0039-6257(99)00029-6

Nickells, R. W. (2012). The cell and molecular biology of glaucoma: Mechanisms of retinal ganglion cell death. *Investigative Ophthalmology and Visual Science*, *53*(5), 2476–2481. https://doi.org/10.1167/iovs.12-9483h

Nickells, R. W., Howell, G. R., Soto, I., & John, S. W. M. (2012). Under Pressure: Cellular and Molecular Responses During Glaucoma, a Common Neurodegeneration with Axonopathy. *Annual Review of Neuroscience*. https://doi.org/10.1146/annurev.neuro.051508.135728

Nickells, R. W., Schmitt, H. M., Maes, M. E., & Schlamp, C. L. (2017). AAV2-Mediated Transduction of the Mouse Retina After Optic Nerve Injury. *Investigative Ophthalmology & Visual Science*, *58*(14), 6091. https://doi.org/10.1167/IOVS.17-22634

Nita, M., & Grzybowski, A. (2016). The Role of the Reactive Oxygen Species and Oxidative Stress in the Pathomechanism of the Age-Related Ocular Diseases and Other Pathologies of the Anterior and Posterior Eye Segments in Adults. In *Oxidative Medicine and Cellular Longevity*. https://doi.org/10.1155/2016/3164734

Niture, S. K., Khatri, R., & Jaiswal, A. K. (2014). Regulation of Nrf2 - An update. In *Free Radical Biology and Medicine*. https://doi.org/10.1016/j.freeradbiomed.2013.02.008

Noda, Y., Mouri, A., Ando, Y., Waki, Y., Yamada, S. N., Yoshimi, A., Yamada, K., Ozaki, N., Wang, D., & Nabeshima, T. (2010). Galantamine ameliorates the impairment of recognition memory in mice repeatedly treated with methamphetamine: Involvement of allosteric potentiation of nicotinic acetylcholine receptors and dopaminergic-ERK1/2 systems. *International Journal of Neuropsychopharmacology*, *13*(10), 1343–1354. https://doi.org/10.1017/S1461145710000222

O'Leary, L. A., Davoli, M. A., Belliveau, C., Tanti, A., Ma, J. C., Farmer, W. T., Turecki, G., Murai, K. K., & Mechawar, N. (2020). Characterization of Vimentin-Immunoreactive Astrocytes in the Human Brain. *Frontiers in Neuroanatomy*, *0*, 31. https://doi.org/10.3389/FNANA.2020.00031

Oddone, F., Roberti, G., Micera, A., Busanello, A., Bonini, S., Quaranta, L., Agnifili, L., & Manni, G. (2017). Exploring Serum Levels of Brain Derived Neurotrophic Factor and Nerve Growth Factor Across Glaucoma Stages. *PloS One*, *12*(1). https://doi.org/10.1371/JOURNAL.PONE.0168565

Oh, D. J., Chen, J. L., Vajaranant, T. S., & Dikopf, M. S. (2019). Brimonidine tartrate for the treatment of glaucoma. *Expert Opinion on Pharmacotherapy*, *20*(1), 115–122. https://doi.org/10.1080/14656566.2018.1544241

Oliveira-Valença, V. M., Bosco, A., Vetter, M. L., & Silveira, M. S. (2020). On the Generation and Regeneration of Retinal Ganglion Cells. *Frontiers in Cell and Developmental Biology*, *8*, 970. https://doi.org/10.3389/FCELL.2020.581136/BIBTEX

Osborne, N. N., & Del Olmo-Aguado, S. (2013). Maintenance of retinal ganglion cell mitochondrial functions as a neuroprotective strategy in glaucoma. In *Current Opinion in Pharmacology*. https://doi.org/10.1016/j.coph.2012.09.002

Pamplona, R., & Costantini, D. (2011). Molecular and structural antioxidant defenses against oxidative stress in animals. *American Journal of Physiology - Regulatory Integrative and Comparative Physiology*, *301*(4), 843–863. https://doi.org/10.1152/AJPREGU.00034.2011/ASSET/IMAGES/LARGE/ZH601011770600004.JPEG

Peng, B., Kong, G., Yang, C., & Ming, Y. (n.d.). *Erythropoietin and its derivatives: from tissue protection to immune regulation*. https://doi.org/10.1038/s41419-020-2276-8

Peng, B., Kong, G., Yang, C., & Ming, Y. (2020). Erythropoietin and its derivatives: from tissue protection to immune regulation. *Cell Death & Disease 2020 11:2*, *11*(2), 1–12. https://doi.org/10.1038/s41419-020-2276-8

Peng, M., Qiang, L., Xu, Y., Li, C., Li, T., & Wang, J. (2019). Inhibition of JNK and activation of the AMPK-Nrf2 axis by corosolic acid suppress osteolysis and oxidative stress. *Nitric Oxide - Biology and Chemistry*. https://doi.org/10.1016/j.niox.2018.11.002

Pizzino, G., Irrera, N., Cucinotta, M., Pallio, G., Mannino, F., Arcoraci, V., Squadrito, F., Altavilla, D., & Bitto, A. (2017). Oxidative Stress: Harms and Benefits for Human Health. *Oxidative Medicine and Cellular Longevity*, *2017*. https://doi.org/10.1155/2017/8416763

Ponce, L. L., Navarro, J. C., Ahmed, O., & Robertson, C. S. (2013). Erythropoietin neuroprotection with traumatic brain injury. *Pathophysiology : The Official Journal of the International Society for Pathophysiology*, *20*(1), 31–38. https://doi.org/10.1016/j.pathophys.2012.02.005

Porciatti, V. (2014). Electrophysiological assessment of retinal ganglion cell function. In *Experimental Eye Research* (Vol. 141, pp. 164–170). Academic Press. https://doi.org/10.1016/j.exer.2015.05.008

Preiser, D., Lagrèze, W. A., Bach, M., & Poloschek, C. M. (2013). Photopic negative response versus pattern electroretinogram in early glaucoma. *Investigative Ophthalmology and Visual Science*, *54*(2), 1182–1191. https://doi.org/10.1167/iovs.12-11201

Prunty, M. C., Aung, M. H., Hanif, A. M., Allen, R. S., Chrenek, M. A., Boatright, J. H., Thule, P. M., Kundu, K., Murthy, N., & Pardue, M. T. (2015). In vivo imaging of retinal oxidative stress using a reactive oxygen species-activated fluorescent probe. *Investigative Ophthalmology and Visual Science*, *56*(10), 5862–5870. https://doi.org/10.1167/iovs.15-16810

Q, W., P, Z., H, H., L, L., L, L., HC, W., R, D., L, S., CM, F., KC, C., M, N., A, K., Y, S., JS, M., JL, G., & Y, H. (2020). Mouse γ-Synuclein Promoter-Mediated Gene Expression and Editing in Mammalian Retinal Ganglion Cells. *The Journal of Neuroscience : The Official Journal of the Society for Neuroscience*, *40*(20). https://doi.org/10.1523/JNEUROSCI.0102-20.2020

Qi Cui 1, Louisa S Tang, Bing Hu, Kwok-Fai So, H. K. Y. (n.d.). *Expression of trkA, trkB, and trkC in injured and regenerating retinal ganglion cells of adult rats - PubMed*. Retrieved August 20, 2020, from https://pubmed.ncbi.nlm.nih.gov/12037005/

Qu, J., Wang, D., & Grosskreutz, C. L. (2010). Mechanisms of retinal ganglion cell injury and

defense in glaucoma. *Experimental Eye Research*, *91*(1), 48–53. https://doi.org/10.1016/j.exer.2010.04.002

Quigley, H. A., & Addicks, E. M. (1981). Regional Differences in the Structure of the Lamina Cribrosa and Their Relation to Glaucomatous Optic Nerve Damage. *Archives of Ophthalmology*, *99*(1), 137–143. https://doi.org/10.1001/ARCHOPHT.1981.03930010139020

Quigley, H. A., Hohman, R. M., Addicks, E. M., Massof, R. W., & Richard Green, W. (1983). Morphologic Changes in the Lamina Cribrosa Correlated with Neural Loss in Open-Angle Glaucoma. *American Journal of Ophthalmology*, *95*(5), 673–691. https://doi.org/10.1016/0002-9394(83)90389-6

Quillen, S., Schaub, J., Quigley, H., Pease, M., Korneva, A., & Kimball, E. (2020). Astrocyte responses to experimental glaucoma in mouse optic nerve head. *PLOS ONE*, *15*(8), e0238104. https://doi.org/10.1371/JOURNAL.PONE.0238104

Raghunath, A., Sundarraj, K., Nagarajan, R., Arfuso, F., Bian, J., Kumar, A. P., Sethi, G., & Perumal, E. (2018a). Antioxidant response elements: Discovery, classes, regulation and potential applications. In *Redox Biology* (Vol. 17, pp. 297–314). Elsevier B.V. https://doi.org/10.1016/j.redox.2018.05.002

Raghunath, A., Sundarraj, K., Nagarajan, R., Arfuso, F., Bian, J., Kumar, A. P., Sethi, G., & Perumal, E. (2018b). Antioxidant response elements: Discovery, classes, regulation and potential applications. In *Redox Biology* (Vol. 17, pp. 297–314). Elsevier B.V. https://doi.org/10.1016/j.redox.2018.05.002

Raghunath, A., Sundarraj, K., Nagarajan, R., Arfuso, F., Bian, J., Kumar, A. P., Sethi, G., & Perumal, E. (2018c). Antioxidant response elements: Discovery, classes, regulation and potential applications. *Redox Biology*, *17*, 297–314. https://doi.org/10.1016/J.REDOX.2018.05.002

Rasband, W. S. (2018). ImageJ. *U.S. National Institutes of Health, Bethesda, Maryland*.

Reichenbach, A., & Bringmann, A. (2013). New functions of Müller cells. *Glia*, *61*(5), 651–678. https://doi.org/10.1002/GLIA.22477

Reichenbach, A., & Bringmann, A. (2020). Glia of the human retina. *Glia*, *68*(4), 768–796. https://doi.org/10.1002/GLIA.23727

Resende, A. P., Rosolen, S. G., Nunes, T., Braz, B. S., & Delgado, E. (2018). Functional and Structural Effects of Erythropoietin Subconjunctival Administration in Glaucomatous Animals. *Biomedicine Hub*, *3*(2), 1–11. https://doi.org/10.1159/000488970

Rex, T. S., Wong, Y., Kodali, K., & Merry, S. (2009). Neuroprotection of photoreceptors by direct delivery of erythropoietin to the retina of the retinal degeneration slow mouse. *Experimental Eye Research*, *89*(5), 735–740. https://doi.org/10.1016/J.EXER.2009.06.017

Rey, F., Balsari, A., Giallongo, T., Ottolenghi, S., Giulio, A. M. Di, Samaja, M., & Carelli, S. (2019). Erythropoietin as a Neuroprotective Molecule: An Overview of Its Therapeutic Potential in Neurodegenerative Diseases. *ASN NEURO*, *11*. https://doi.org/10.1177/1759091419871420

Risner, M. L., Pasini, S., Cooper, M. L., Lambert, W. S., & Calkins, D. J. (2018). Axogenic mechanism enhances retinal ganglion cell excitability during early progression in glaucoma. *Proceedings of the National Academy of Sciences of the United States of America*, *115*(10), E2393–E2402. https://doi.org/10.1073/pnas.1714888115

Robledinos-Antón, N., Fernández-Ginés, R., Manda, G., & Cuadrado, A. (2019). Activators and Inhibitors of NRF2: A Review of Their Potential for Clinical Development. In *Oxidative*

medicine and cellular longevity (Vol. 2019, p. 9372182). NLM (Medline). https://doi.org/10.1155/2019/9372182

Romero, A., Egea, J., García, A. G., & López, M. G. (2010). Synergistic neuroprotective effect of combined low concentrations of galantamine and melatonin against oxidative stress in SH-SY5Y neuroblastoma cells. *Journal of Pineal Research*, *49*(2), 141–148. https://doi.org/10.1111/j.1600-079X.2010.00778.x

Rusciano, D., Pezzino, S., Mutolo, M. G., Giannotti, R., Librando, A., & Pescosolido, N. (2017). Neuroprotection in glaucoma: Old and new promising treatments. *Advances in Pharmacological Sciences*, *2017*. https://doi.org/10.1155/2017/4320408

Saccà, S. C., & Izzotti, A. (2008). Oxidative stress and glaucoma: injury in the anterior segment of the eye. *Progress in Brain Research*, *173*, 385–407. https://doi.org/10.1016/S0079-6123(08)01127-8

Santina, L. Della, Inman, D. M., Lupien, C. B., Horner, P. J., & Wong, R. O. L. (2013). Differential Progression of Structural and Functional Alterations in Distinct Retinal Ganglion Cell Types in a Mouse Model of Glaucoma. *Journal of Neuroscience*, *33*(44), 17444–17457. https://doi.org/10.1523/JNEUROSCI.5461-12.2013

Santos, M. D., Alkondon, M., Pereira, E. F. R., Aracava, Y., Eisenberg, H. M., Maelicke, A., & Albuquerque, E. X. (2002). The nicotinic allosteric potentiating ligand galantamine facilitates synaptic transmission in the mammalian central nervous system. *Molecular Pharmacology*, *61*(5), 1222–1234. https://doi.org/10.1124/mol.61.5.1222

Sappington, R. M., Carlson, B. J., Crish, S. D., & Calkins, D. J. (2010). The microbead occlusion model: A paradigm for induced ocular hypertension in rats and mice. *Investigative Ophthalmology and Visual Science*. https://doi.org/10.1167/iovs.09-3947

Satapathy, S. K., Ochani, M., Dancho, M., Hudson, L. K., Rosas-Ballina, M., Valdes-Ferrer, S. I., Olofsson, P. S., Harris, Y. T., Roth, J., Chavan, S., Tracey, K. J., & Pavlov, V. A. (2011). Galantamine alleviates inflammation and other obesity-associated complications in high-fat diet-fed mice. *Molecular Medicine (Cambridge, Mass.)*, *17*(7–8), 599–606. https://doi.org/10.2119/molmed.2011.00083

Saura, C., Roda, D., Roselló, S., Oliveira, M., Macarulla, T., Pérez-Fidalgo, J. A., Morales-Barrera, R., Sanchis-García, J. M., Musib, L., Budha, N., Zhu, J., Nannini, M., Chan, W. Y., Sanabria Bohórquez, S. M., Meng, R. D., Lin, K., Yan, Y., Patel, P., Baselga, J., … Cervantes, A. (2017). A first-in-human phase I study of the ATP-competitive AKT inhibitor Ipatasertib demonstrates Robust and safe targeting of AKT in patients with solid tumors. *Cancer Discovery*, *7*(1), 102–113. https://doi.org/10.1158/2159-8290.CD-16-0512

Schmidlin, C. J., Dodson, M. B., Madhavan, L., & Zhang, D. D. (2019). Redox Regulation by NRF2 in Aging and Disease. *Free Radical Biology & Medicine*, *134*, 702. https://doi.org/10.1016/J.FREERADBIOMED.2019.01.016

Schuster, A. K., Erb, C., Hoffmann, E. M., Dietlein, T., & Pfeiffer, N. (2020). The Diagnosis and Treatment of Glaucoma. *Deutsches Ärzteblatt International*, *117*(13), 225. https://doi.org/10.3238/ARZTEBL.2020.0225

Sharifi-Rad, M., Anil Kumar, N. V., Zucca, P., Varoni, E. M., Dini, L., Panzarini, E., Rajkovic, J., Tsouh Fokou, P. V., Azzini, E., Peluso, I., Prakash Mishra, A., Nigam, M., El Rayess, Y., Beyrouthy, M. El, Polito, L., Iriti, M., Martins, N., Martorell, M., Docea, A. O., … Sharifi-Rad, J. (2020). Lifestyle, Oxidative Stress, and Antioxidants: Back and Forth in the Pathophysiology of Chronic Diseases. *Frontiers in Physiology*, *11*, 694. https://doi.org/10.3389/FPHYS.2020.00694/BIBTEX

Shi, Z., Hodges, V. M., Dunlop, E. A., Percy, M. J., Maxwell, A. P., El-Tanani, M., & Lappin, T. R. J. (2010). Erythropoietin-induced activation of the JAK2/STAT5, PI3K/Akt, and Ras/ERK pathways promotes malignant cell behavior in a modified breast cancer cell line. *Molecular Cancer Research : MCR*, *8*(4), 615–626. https://doi.org/10.1158/1541-7786.MCR-09-0264

Shimizu, S., Mizuguchi, Y., Sobue, A., Fujiwara, M., Morimoto, T., & Ohno, Y. (2015). Interaction between anti-Alzheimer and antipsychotic drugs in modulating extrapyramidal motor disorders in mice. *Journal of Pharmacological Sciences*, *127*(4), 439–445. https://doi.org/10.1016/j.jphs.2015.03.004

Shin, J. H., Yue, Y., & Duan, D. (2012). Recombinant Adeno-Associated Viral Vector Production and Purification. *Methods in Molecular Biology (Clifton, N.J.)*, *798*, 267. https://doi.org/10.1007/978-1-61779-343-1_15

Shirley Ding, S. L., Leow, S. N., Munisvaradass, R., Koh, E. H., Bastion, M. L. C., Then, K. Y., Kumar, S., & Mok, P. L. (2016). Revisiting the role of erythropoietin for treatment of ocular disorders. *Eye 2016 30:10*, *30*(10), 1293–1309. https://doi.org/10.1038/eye.2016.94

Shpak, A. A., Guekht, A. B., Druzhkova, T. A., Kozlova, K. I., & Gulyaeva, N. V. (2017). Ciliary neurotrophic factor in patients with primary open-angle glaucoma and age-related cataract. *Molecular Vision*, *23*, 799. /pmc/articles/PMC5710971/

SIES, H. (1993). Strategies of antioxidant defense. *European Journal of Biochemistry*, *215*(2), 213–219. https://doi.org/10.1111/J.1432-1033.1993.TB18025.X

Sies, H., Berndt, C., & Jones, D. P. (2017). Oxidative Stress. *Https://Doi.Org/10.1146/Annurev-Biochem-061516-045037*, *86*, 715–748. https://doi.org/10.1146/ANNUREV-BIOCHEM-061516-045037

Singman, E. L., Daphalapurkar, N., White, H., Nguyen, T. D., Panghat, L., Chang, J., & McCulley, T. (2016). Indirect traumatic optic neuropathy. In *Military Medical Research* (Vol. 3, Issue 1). BioMed Central Ltd. https://doi.org/10.1186/s40779-016-0069-2

Sivertsen, E. A., Hystad, M. E., Gutzkow, K. B., Døsen, G., Smeland, E. B., Blomhoff, H. K., & Myklebust, J. H. (2006). PI3K/Akt-dependent Epo-induced signalling and target genes in human early erythroid progenitor cells. *British Journal of Haematology*, *135*(1), 117–128. https://doi.org/10.1111/j.1365-2141.2006.06252.x

Song, M., Bode, A. M., Dong, Z., & Lee, M. H. (2019). AKt as a therapeutic target for cancer. In *Cancer Research* (Vol. 79, Issue 6, pp. 1019–1031). American Association for Cancer Research Inc. https://doi.org/10.1158/0008-5472.CAN-18-2738

Soriano, F. X., Baxter, P., Murray, L. M., Sporn, M. B., Gillingwater, T. H., & Hardingham, G. E. (2009). Transcriptional regulation of the AP-1 and Nrf2 target gene sulfiredoxin. In *Molecules and Cells* (Vol. 27, Issue 3, pp. 279–282). Mol Cells. https://doi.org/10.1007/s10059-009-0050-y

Stein, J. D., Khawaja, A. P., & Weizer, J. S. (2021). Glaucoma in Adults—Screening, Diagnosis, and Management: A Review. *JAMA*, *325*(2), 164–174. https://doi.org/10.1001/JAMA.2020.21899

Steinsapir, K. D., & Goldberg, R. A. (2011). Traumatic optic neuropathy: an evolving understanding. *American Journal of Ophthalmology*, *151*(6), 928-933.e2. https://doi.org/10.1016/j.ajo.2011.02.007

Strauss, O. (2005). The retinal pigment epithelium in visual function. *Physiological Reviews*, *85*(3), 845–881. https://doi.org/10.1152/PHYSREV.00021.2004/ASSET/IMAGES/LARGE/Z9J0030503690

006.JPEG
Subiras, N., Del Barco, D. G., & Coro Antich, R. M. (2012). Erythropoietin: Still on the neuroprotection road. In *Therapeutic Advances in Neurological Disorders*. https://doi.org/10.1177/1756285611434926
Sullivan, T. A. (2011). Systemic AAV-Mediated Gene Therapy Using Epo-R76E to Protect Retinal Ganglion Cells from Optic Nerve Injury and Disease. *Theses and Dissertations (ETD)*. https://doi.org/10.21007/etd.cghs.2011.0389
Sullivan, T. A., Geisert, E. E., Hines-Beard, J., & Rex, T. S. (2011a). Systemic Adeno-Associated Virus-Mediated Gene Therapy Preserves Retinal Ganglion Cells and Visual Function in DBA/2J Glaucomatous Mice. *Human Gene Therapy*. https://doi.org/10.1089/hum.2011.052
Sullivan, T. A., Geisert, E. E., Hines-Beard, J., & Rex, T. S. (2011b). Systemic Adeno-Associated Virus-Mediated Gene Therapy Preserves Retinal Ganglion Cells and Visual Function in DBA/2J Glaucomatous Mice. *Human Gene Therapy*, *22*(10), 1191. https://doi.org/10.1089/HUM.2011.052
Sullivan, T., Kodali, K., & Rex, T. S. (2011). Systemic gene delivery protects the photoreceptors in the retinal degeneration slow mouse. *Neurochemical Research*, *36*(4), 613–618. https://doi.org/10.1007/S11064-010-0272-6
Sun, D., Lye-Barthel, M., Masland, R. H., & Jakobs, T. C. (2009). The morphology and spatial arrangement of astrocytes in the optic nerve head of the mouse. *Journal of Comparative Neurology*, *516*(1), 1–19. https://doi.org/10.1002/CNE.22058
Sun, J., Lei, Y., Dai, Z., Liu, X., Huang, T., Wu, J., Xu, Z. P., & Sun, X. (2017). Sustained Release of Brimonidine from a New Composite Drug Delivery System for Treatment of Glaucoma. *ACS Applied Materials and Interfaces*, *9*(9), 7990–7999. https://doi.org/10.1021/ACSAMI.6B16509/SUPPL_FILE/AM6B16509_SI_001.PDF
Sun, Z., Huang, Z., & Zhang, D. D. (2009). Phosphorylation of Nrf2 at multiple sites by MAP kinases has a limited contribution in modulating the Nrf2-dependent antioxidant response. *PLoS ONE*, *4*(8), 6588. https://doi.org/10.1371/journal.pone.0006588
Suresh, S., Rajvanshi, P. K., & Noguchi, C. T. (2020a). The Many Facets of Erythropoietin Physiologic and Metabolic Response. *Frontiers in Physiology*, *0*, 1534. https://doi.org/10.3389/FPHYS.2019.01534
Suresh, S., Rajvanshi, P. K., & Noguchi, C. T. (2020b). The Many Facets of Erythropoietin Physiologic and Metabolic Response. *Frontiers in Physiology*, *10*, 1534. https://doi.org/10.3389/FPHYS.2019.01534/BIBTEX
Sykiotis, G. P., Habeos, I. G., Samuelson, A. V., & Bohmann, D. (2011). The role of the antioxidant and longevity-promoting Nrf2 pathway in metabolic regulation. *Current Opinion in Clinical Nutrition and Metabolic Care*, *14*(1), 41–48. https://doi.org/10.1097/MCO.0b013e32834136f2
Tang, J., Hui, F., Hadoux, X., Soares, B., Jamieson, M., van Wijngaarden, P., Coote, M., & Crowston, J. G. (2020). Short-Term Changes in the Photopic Negative Response Following Intraocular Pressure Lowering in Glaucoma. *Investigative Opthalmology & Visual Science*, *61*(10), 16. https://doi.org/10.1167/iovs.61.10.16
Tehse, J., & Taghibiglou, C. (2019). The overlooked aspect of excitotoxicity: Glutamate-independent excitotoxicity in traumatic brain injuries. *The European Journal of Neuroscience*, *49*(9), 1157–1170. https://doi.org/10.1111/ejn.14307
Texidó, L., Ros, E., Martín-Satué, M., López, S., Aleu, J., Marsal, J., & Solsona, C. (2005).

Effect of galantamine on the human α7 neuronal nicotinic acetylcholine receptor, the Torpedo nicotinic acetylcholine receptor and spontaneous cholinergic synaptic activity. *British Journal of Pharmacology*, *145*(5), 672–678. https://doi.org/10.1038/sj.bjp.0706221

Tezel, G. (2006). Oxidative stress in glaucomatous neurodegeneration: Mechanisms and consequences. In *Progress in Retinal and Eye Research*. https://doi.org/10.1016/j.preteyeres.2006.07.003

Tezel, G., Ben-Hur, T., Gibson, G. E., Stevens, B., Streit, W. J., Wekerle, H., Bhattacharya, S. K., Borras, T., Burgoyne, C. F., Caspi, R. R., Chauhan, B. C., Clark, A. F., Crowston, J., Danias, J., Dick, A. D., Flammer, J., Foster, C. S., Grosskreutz, C. L., Grus, F. H., … Zimmerman, T. J. (2009). The Role of Glia, Mitochondria, and the Immune System in Glaucoma. *Investigative Ophthalmology & Visual Science*, *50*(3), 1001–1012. https://doi.org/10.1167/IOVS.08-2717

Tham, Y. C., Li, X., Wong, T. Y., Quigley, H. A., Aung, T., & Cheng, C. Y. (2014). Global prevalence of glaucoma and projections of glaucoma burden through 2040: A systematic review and meta-analysis. *Ophthalmology*. https://doi.org/10.1016/j.ophtha.2014.05.013

Tonelli, C., Chio, I. I. C., & Tuveson, D. A. (2017). Transcriptional Regulation by Nrf2. *Antioxidants & Redox Signaling*. https://doi.org/10.1089/ars.2017.7342

Tonelli, C., Chio, I. I. C., & Tuveson, D. A. (2018a). Transcriptional Regulation by Nrf2. *Antioxidants and Redox Signaling*, *29*(17), 1727–1745. https://doi.org/10.1089/ARS.2017.7342/ASSET/IMAGES/LARGE/FIGURE6.JPEG

Tonelli, C., Chio, I. I. C., & Tuveson, D. A. (2018b). Transcriptional Regulation by Nrf2. *Antioxidants & Redox Signaling*, *29*(17), 1727–1745. https://doi.org/10.1089/ars.2017.7342

Tonelli, C., Chio, I. I. C., & Tuveson, D. A. (2018c). Transcriptional Regulation by Nrf2. In *Antioxidants and Redox Signaling* (Vol. 29, Issue 17, pp. 1727–1745). Mary Ann Liebert Inc. https://doi.org/10.1089/ars.2017.7342

Toth, R. K., & Warfel, N. A. (2017). Strange bedfellows: Nuclear factor, erythroid 2-Like 2 (Nrf2) and hypoxia-inducible factor 1 (HIF-1) in tumor hypoxia. In *Antioxidants* (Vol. 6, Issue 2). MDPI AG. https://doi.org/10.3390/antiox6020027

Tóthová, Z., Šemeláková, M., Solárová, Z., Tomc, J., Debeljak, N., & Solár, P. (2021). The Role of PI3K/AKT and MAPK Signaling Pathways in Erythropoietin Signalization. *International Journal of Molecular Sciences*, *22*(14). https://doi.org/10.3390/IJMS22147682

Tsiftsoglou, A. S., & Kalyuzhny, A. E. (2021). Erythropoietin (EPO) as a Key Regulator of Erythropoiesis, Bone Remodeling and Endothelial Transdifferentiation of Multipotent Mesenchymal Stem Cells (MSCs): Implications in Regenerative Medicine. *Cells 2021, Vol. 10, Page 2140*, *10*(8), 2140. https://doi.org/10.3390/CELLS10082140

Tsuji-Takayama, K., Otani, T., Inoue, T., Nakamura, S., Motoda, R., Kibata, M., & Orita, K. (2006). Erythropoietin induces sustained phosphorylation of STAT5 in primitive but not definitive erythrocytes generated from mouse embryonic stem cells. *Experimental Hematology*, *34*(10), 1323–1332. https://doi.org/10.1016/J.EXPHEM.2006.06.004

Vargas, M. R., Johnson, D. A., Sirkis, D. W., Messing, A., & Johnson, J. A. (2008). Nrf2 Activation in Astrocytes Protects against Neurodegeneration in Mouse Models of Familial Amyotrophic Lateral Sclerosis. *The Journal of Neuroscience*, *28*(50), 13574. https://doi.org/10.1523/JNEUROSCI.4099-08.2008

Vasudevan, S. K., Gupta, V., & Crowston, J. G. (2011). Neuroprotection in glaucoma. *Indian Journal of Ophthalmology*, *59*(SUPPL. 1). https://doi.org/10.4103/0301-4738.73700

Vecino, E., Rodriguez, F. D., Ruzafa, N., Pereiro, X., & Sharma, S. C. (2016a). Glia-neuron

interactions in the mammalian retina. In *Progress in Retinal and Eye Research* (Vol. 51, pp. 1–40). https://doi.org/10.1016/j.preteyeres.2015.06.003

Vecino, E., Rodriguez, F. D., Ruzafa, N., Pereiro, X., & Sharma, S. C. (2016b). Glia-neuron interactions in the mammalian retina. *Progress in Retinal and Eye Research*, *51*, 1–40. https://doi.org/10.1016/J.PRETEYERES.2015.06.003

Volland, S., Esteve-Rudd, J., Hoo, J., Yee, C., & Williams, D. S. (2015). A Comparison of Some Organizational Characteristics of the Mouse Central Retina and the Human Macula. *PLoS ONE*, *10*(4). https://doi.org/10.1371/JOURNAL.PONE.0125631

Vomhof-DeKrey, E. E., & Picklo, M. J. (2012a). The Nrf2-antioxidant response element pathway: A target for regulating energy metabolism. In *Journal of Nutritional Biochemistry* (Vol. 23, Issue 10, pp. 1201–1206). J Nutr Biochem. https://doi.org/10.1016/j.jnutbio.2012.03.005

Vomhof-DeKrey, E. E., & Picklo, M. J. (2012b). The Nrf2-antioxidant response element pathway: A target for regulating energy metabolism. In *Journal of Nutritional Biochemistry* (Vol. 23, Issue 10, pp. 1201–1206). Elsevier. https://doi.org/10.1016/j.jnutbio.2012.03.005

Vomund, S., Schäfer, A., Parnham, M. J., Brüne, B., & Von Knethen, A. (2017). Nrf2, the master regulator of anti-oxidative responses. In *International Journal of Molecular Sciences* (Vol. 18, Issue 12). MDPI AG. https://doi.org/10.3390/ijms18122772

Von Lindern, M., Parren-Van Amelsvoort, M., Van Dijk, T., Deiner, E., Van Den Akker, E., Van Emst-De Vriesi, S., Willems, P., Beug, H., & Löwenberg, B. (2000). Protein kinase C alpha controls erythropoietin receptor signaling. *The Journal of Biological Chemistry*, *275*(44), 34719–34727. https://doi.org/10.1074/JBC.M007042200

Vriend, J., & Reiter, R. J. (2015). The Keap1-Nrf2-antioxidant response element pathway: A review of its regulation by melatonin and the proteasome. In *Molecular and Cellular Endocrinology* (Vol. 401, pp. 213–220). Elsevier Ireland Ltd. https://doi.org/10.1016/j.mce.2014.12.013

W, Z., G, Z., Y, G., Y, Z., J, L., L, Z., A, L., L, Z., & P, T. (2017). A sequential delivery system employing the synergism of EPO and NGF promotes sciatic nerve repair. *Colloids and Surfaces. B, Biointerfaces*, *159*, 327–336. https://doi.org/10.1016/J.COLSURFB.2017.07.088

Wang, D. Y., Ray, A., Rodgers, K., Ergorul, C., Hyman, B. T., Huang, W., & Grosskreutz, C. L. (2010). Global gene expression changes in rat retinal ganglion cells in experimental glaucoma. *Investigative Ophthalmology and Visual Science*, *51*(8), 4084–4095. https://doi.org/10.1167/iovs.09-4864

Wang, L., Chen, Y., Sternberg, P., & Cai, J. (2008). Essential roles of the PI3 kinase/Akt pathway in regulating Nrf2-dependent antioxidant functions in the RPE. *Investigative Ophthalmology and Visual Science*. https://doi.org/10.1167/iovs.07-1099

Wang, M., Li, J., & Zheng, Y. (2020a). The potential role of nuclear factor erythroid 2-related factor 2 (Nrf2) in glaucoma: A review. In *Medical Science Monitor* (Vol. 26, pp. e921514-1). International Scientific Information, Inc. https://doi.org/10.12659/MSM.921514

Wang, M., Li, J., & Zheng, Y. (2020b). The Potential Role of Nuclear Factor Erythroid 2-Related Factor 2 (Nrf2) in Glaucoma: A Review. *Medical Science Monitor : International Medical Journal of Experimental and Clinical Research*, *26*, e921514-1. https://doi.org/10.12659/MSM.921514

Wang, X., & Yuan, Z. lan. (2019). Activation of Nrf2/HO-1 pathway protects retinal ganglion cells from a rat chronic ocular hypertension model of glaucoma. *International*

Ophthalmology, *39*(10), 2303–2312. https://doi.org/10.1007/S10792-018-01071-8/FIGURES/5

Wang Zhi-lan Yuan, X. (n.d.). *Activation of Nrf2/HO-1 pathway protects retinal ganglion cells from a rat chronic ocular hypertension model of glaucoma*. https://doi.org/10.1007/s10792-018-01071-8

Wareham, L. K., Risner, M. L., & Calkins, D. J. (n.d.). *Protect, Repair, and Regenerate: Towards Restoring Vision in Glaucoma*. https://doi.org/10.1007/s40135-020-00259-5/Published

Warner, N., & Eggenberger, E. (2010). Traumatic optic neuropathy: a review of the current literature. *Current Opinion in Ophthalmology*, *21*(6), 459–462. https://doi.org/10.1097/ICU.0b013e32833f00c9

Weichel, E. D., Colyer, M. H., Bautista, C., Bower, K. S., & French, L. M. (n.d.). Traumatic brain injury associated with combat ocular trauma. *The Journal of Head Trauma Rehabilitation*, *24*(1), 41–50. https://doi.org/10.1097/HTR.0b013e3181956ffd

Weinreb, R. N., Aung, T., & Medeiros, F. A. (2014a). The pathophysiology and treatment of glaucoma: A review. In *JAMA - Journal of the American Medical Association* (Vol. 311, Issue 18, pp. 1901–1911). American Medical Association. https://doi.org/10.1001/jama.2014.3192

Weinreb, R. N., Aung, T., & Medeiros, F. A. (2014b). The pathophysiology and treatment of glaucoma: A review. In *JAMA - Journal of the American Medical Association*. https://doi.org/10.1001/jama.2014.3192

Weinreb, R. N., Aung, T., & Medeiros, F. A. (2014c). The Pathophysiology and Treatment of Glaucoma: A Review. *JAMA*, *311*(18), 1901. https://doi.org/10.1001/JAMA.2014.3192

Weinreb, R. N., & Levin, L. A. (1999). Is Neuroprotection a Viable Therapy for Glaucoma? *Archives of Ophthalmology*, *117*(11), 1540–1544. https://doi.org/10.1001/ARCHOPHT.117.11.1540

Weinreb, R. N., Liebmann, J. M., Cioffi, G. A., Goldberg, I., Brandt, J. D., Johnson, C. A., Zangwill, L. M., Schneider, S., Badger, H., & Bejanian, M. (2018). Oral Memantine for the Treatment of Glaucoma: Design and Results of 2 Randomized, Placebo-Controlled, Phase 3 Studies. *Ophthalmology*, *125*(12), 1874–1885. https://doi.org/10.1016/J.OPHTHA.2018.06.017

WHO | Priority eye diseases. (2018). *WHO*.

Wiggs, J. L., & Pasquale, L. R. (2017). Genetics of glaucoma. *Human Molecular Genetics*, *26*(R1), R21. https://doi.org/10.1093/HMG/DDX184

Wu, H., Chen, M., Yan, P., Yao, Q., Fan, J., Gao, Z., & Wang, H. (2018). Erythropoietin suppresses D-galactose-induced aging of rats via the PI3K/Akt/Nrf2-ARE pathway. *International Journal of Clinical and Experimental Pathology*, *11*(4), 2227. /pmc/articles/PMC6958193/

Wymann, M. P., Bulgarelli-Leva, G., Zvelebil, M. J., Pirola, L., Vanhaesebroeck, B., Waterfield, M. D., & Panayotou, G. (1996). Wortmannin inactivates phosphoinositide 3-kinase by covalent modification of Lys-802, a residue involved in the phosphate transfer reaction. *Molecular and Cellular Biology*, *16*(4), 1722–1733. https://doi.org/10.1128/mcb.16.4.1722

X, R., S, Y., H, M., T, G., Z, W., W, S., X, M., W, Y., & T, J. (2012). Effects of erythropoietin-dextran microparticle-based PLGA/PLA microspheres on RGCs. *Investigative Ophthalmology & Visual Science*, *53*(10), 6025–6034. https://doi.org/10.1167/IOVS.12-9898

Xiong, W., Garfinkel, A. E. M. C., Li, Y., Benowitz, L. I., & Cepko, C. L. (2015). NRF2 promotes neuronal survival in neurodegeneration and acute nerve damage. *Journal of Clinical Investigation*. https://doi.org/10.1172/JCI79735

Xu, Y., Fang, F., Miriyala, S., Crooks, P. A., Oberley, T. D., Chaiswing, L., Noel, T., Holley, A. K., Zhao, Y., Kiningham, K. K., Clair, D. K. S., & Clair, W. H. S. (2013). KEAP1 is a redox sensitive target that arbitrates the opposing radiosensitive effects of parthenolide in normal and cancer cells. *Cancer Research*. https://doi.org/10.1158/0008-5472.CAN-12-4297

Xu, Z., Cho, H., Hartsock, M. J., Mitchell, K. L., Gong, J., Wu, L., Wei, Y., Wang, S., Thimmulappa, R. K., Sporn, M. B., Biswal, S., Welsbie, D. S., & Duh, E. J. (2015). Neuroprotective role of Nrf2 for retinal ganglion cells in ischemia-reperfusion. *Journal of Neurochemistry*, *133*(2), 233–241. https://doi.org/10.1111/jnc.13064

Xu, Z., Wei, Y., Gong, J., Cho, H., Park, J. K., Sung, E. R., Huang, H., Wu, L., Eberhart, C., Handa, J. T., Du, Y., Kern, T. S., Thimmulappa, R., Barber, A. J., Biswal, S., & Duh, E. J. (2014). NRF2 plays a protective role in diabetic retinopathy in mice. *Diabetologia*, *57*(1), 204–213. https://doi.org/10.1007/s00125-013-3093-8

Yabana, T., Sato, K., Shiga, Y., Himori, N., Omodaka, K., & Nakazawa, T. (2019). The relationship between glutathione levels in leukocytes and ocular clinical parameters in glaucoma. *PLOS ONE*, *14*(12), e0227078. https://doi.org/10.1371/JOURNAL.PONE.0227078

Yang, S., Zhou, J., & Li, D. (2021). Functions and Diseases of the Retinal Pigment Epithelium. *Frontiers in Pharmacology*, *12*, 1976. https://doi.org/10.3389/FPHAR.2021.727870/BIBTEX

Yang, X., Hondur, G., & Tezel, G. (2016a). Antioxidant treatment limits neuroinflammation in experimental glaucoma. *Investigative Ophthalmology and Visual Science*, *57*(4). https://doi.org/10.1167/IOVS.16-19153

Yang, X., Hondur, G., & Tezel, G. (2016b). Antioxidant treatment limits neuroinflammation in experimental glaucoma. *Investigative Ophthalmology and Visual Science*, *57*(4), 2344–2354. https://doi.org/10.1167/IOVS.16-19153

Yun, H., Lathrop, K. L., Yang, E., Sun, M., Kagemann, L., Fu, V., Stolz, D. B., Schuman, J. S., & Du, Y. (2014). A laser-induced mouse model with long-term intraocular pressure elevation. *PLoS ONE*, *9*(9). https://doi.org/10.1371/journal.pone.0107446

Zakharova, E. T., Sokolov, A. V., Pavlichenko, N. N., Kostevich, V. A., Abdurasulova, I. N., Chechushkov, A. V., Voynova, I. V., Elizarova, A. Y., Kolmakov, N. N., Bass, M. G., Semak, I. V., Budevich, A. I., Kozhin, P. M., Zenkov, N. K., Klimenko, V. M., Kirik, O. V., Korzhevskii, D. E., Menshchikova, E. B., & Vasilyev, V. B. (2018). Erythropoietin and Nrf2: key factors in the neuroprotection provided by apo-lactoferrin. *Biometals : An International Journal on the Role of Metal Ions in Biology, Biochemistry, and Medicine*, *31*(3), 425–443. https://doi.org/10.1007/S10534-018-0111-9

Zhang, H., Davies, K. J. A., & Forman, H. J. (2015). Oxidative stress response and Nrf2 signaling in aging. *Free Radical Biology and Medicine*, *88*(Part B), 314–336. https://doi.org/10.1016/J.FREERADBIOMED.2015.05.036

Zhao, J., Wang, S., Zhong, W., Yang, B., Sun, L., & Zheng, Y. (2016). Oxidative stress in the trabecular meshwork (Review). In *International Journal of Molecular Medicine*. https://doi.org/10.3892/ijmm.2016.2714

Zhao, Z., Chen, Y., Wang, J., Sternberg, P., Freeman, M. L., Grossniklaus, H. E., & Cai, J.

(2011). Age-Related Retinopathy in NRF2-Deficient Mice. *PLoS ONE*, *6*(4), e19456. https://doi.org/10.1371/journal.pone.0019456

Zhong, L., Bradley, J., Schubert, W., Ahmed, E., Adamis, A. P., Shima, D. T., Robinson, G. S., & Ng, Y. S. (2007). Erythropoietin Promotes Survival of Retinal Ganglion Cells in DBA/2J Glaucoma Mice. *Investigative Ophthalmology & Visual Science*, *48*(3), 1212–1218. https://doi.org/10.1167/IOVS.06-0757